Transported emissions from the Indo-Gangetic Plain dominate Air pollution and Climatic impacts over North East India during Pre-monsoon season

A Thesis

Submitted in Partial Fulfillment of the Requirements

for the award of the Degree of

Doctor of Philosophy

by

Neeldip Barman

Department of Civil Engineering

Indian Institute of Technology Guwahati

Guwahati- 781039, Assam, India

March 2024

DEDICATED TO

All the creations of
The Almighty

Declaration

I hereby declare that the research incorporated in this thesis entitled "**Transported emissions from the Indo-Gangetic Plain dominate Air pollution and Climatic impacts over North East India during Pre-monsoon season**" has been carried out by me in the Department of Civil Engineering, Indian Institute of Technology Guwahati, Assam, India under the guidance of Prof. Sharad Gokhale. Wherever I have referred to the research work of others in creating this work, I have given due citation in the text and provided their details in the references.

Neeldip Barman

Roll No: 186104022

Department of Civil Engineering

Indian Institute of Technology Guwahati

Guwahati – 781039, Assam, India

Date: March 2024

Place: Guwahati

Certificate

This is to certify that the work described in this thesis entitled "**Transported emissions from the Indo-Gangetic Plain dominate Air pollution and Climatic impacts over North East India during Pre-monsoon season**" submitted by Neeldip Barman (Roll No. 186104022) is an authentic record of the results obtained from research work carried out under my supervision in the Department of Civil Engineering, Indian Institute of Technology Guwahati, Assam, India. I certify that he has fulfilled all the requirements according to the rules of this institute regarding the research incorporated in his thesis, and this work has not been submitted elsewhere for a degree.

Dr. Sharad Gokhale

Professor

Department of Civil Engineering

Indian Institute of Technology Guwahati

Guwahati – 781039, Assam, India

Date: March 2024

Place: Guwahati

Acknowledgements

“You have a right to perform your prescribed duties, but you are not entitled to the fruits of your actions.” – Bhagavad Gita: Chapter 2, Verse 47

“Keep away from people who try to belittle your ambitions. Small people always do that, but the really great make you feel that you, too, can become great” – Mark Twain

My foremost heartfelt gratitude goes to the **Almighty**, who gave me the courage to do the arduous task of pursuing a doctorate degree, and who accompanied me through the thick and thin as a guiding light, providing me the strength to not give up. These efforts of mine were always supported and encouraged by my mentor and supervisor, **Prof. Sharad Gokhale** without whom this work would have not been possible. He always supported me with any research idea I go to discuss with him and gave me the freedom to do my research work. I cherish my relationship with him as co-researchers rather than only a supervisor-student relationship. To this Great, I express my sincere gratitude.

I would also like to express my gratitude to the Chairman of my doctoral committee: **Prof. Subashisa Dutta**, Department of Civil Engineering, IIT Guwahati and the members of the doctoral committee: **Prof. Bulu Pradhan**, Department of Civil Engineering, IIT Guwahati and **Prof. Mahuya De**, Department of Chemical Engineering, IIT Guwahati for sharing their valuable time and suggestions at different stages of the research to improve my work.

I would also like to thank the technical and administrative staff members of the Department of Civil Engineering, IIT Guwahati: **Ms. Jonali Saikia**, Mr. Chitta R. Medhi, Mr. Payodhar Pathak, **Mr. Susanta K. Sarma**, **Mrs. Juri Hazarika** for their valuable cooperation in different works. I had a wonderful time with the friends and colleagues of research group of Air, Noise and Climate Research Laboratory, Department of Civil

Engineering, IIT Guwahati: Nikhil V. A, Dr. Mitali Sahu, Ardhendu Shekhar Chaudhary, **Dr. Sameer Singh**, Argha Kamal Guha, Rahul Choudhury, **Rajib Das**, Rajarshi Sharma, Mukesh Tiwari, Himanshu Gupta and **Himangshu Pratim Bhattacharyya** with whom I could discuss and share research and off-research topics. I would also like to acknowledge IIT Guwahati for providing the high-performance computing facilities. I also thank **Kelly Werner, Ming Chen, Neelam Dale, Rajesh Kumar, Mary Birth, Gabriele Pfiester, Stacy Walters, Shovan Sahu, Caterina Mogno, Jordan Schnell** and Prerita Agarwal belonging to different institutions who helped me immensely in setting up my model and diagnosis of model errors.

The journey would not have been possible without my parents, **Mr. Narayan Barman** and **Mrs. Dipali Barman**, my brother **Mr. Hriday Barman** who always supported my pursuits and encouraged me to do better.

Neeldip Barman

March 2024

Guwahati

Table of Contents

Abstract

Aerosols are suspended particles that can significantly impact air quality as well as weather through their different effects. Among the aerosol species, black carbon is known to have a significant climate impact due to its strong sunlight absorption capability. Indo-Gangetic Plain is a distinguished hotspot of diverse aerosols and the largest source of black carbon in India. The westerlies carry emissions from the Indo-Gangetic Plain towards North-East India through atmospheric transport along the southern slope of the Himalayas and contribute to the aerosol burden over North-East India. The pre-monsoon season is a period of high aerosol loading over North-East India, with the highest atmospheric heating and aerosol optical depth with an increasing trend. An increase in direct radiative forcing over the region has also been reported. Moreover, studies have also reported a declining rainfall trend and an increasing rainfall intensity over this region.

This study first investigated the direct and semi-direct radiative effect of atmospheric aerosols and black carbon, specifically on the rainfall mechanisms responsible for the pre-monsoon rainfall over North-East India with the WRF-Chem model. Aerosol radiative effects affected rainfall according to the height of the terrain in the North-East India region. Aerosol effects, in general, tended to increase total rainfall over lower-terrain areas, whereas moisture reduced between 2-3 km, which decreased total rainfall over high-terrain areas. However, irrespective of the increase in total rainfall, aerosol effects suppressed rainfall for more duration than it caused enhancement. The semi-direct effect was found to be responsible for cloud reduction below 2 km altitude, thus affecting mainly lower-level clouds, which reduced rainfall formation. The study also differentiated the impacts of aerosols emitted locally within the NE India region and those transported from outside this region to ascertain whether local or transported aerosols were more impactful in influencing this region's rainfall during this season. The role of different aerosol effects on radiative forcing and rainfall was also studied.

Results show that aerosols transported primarily from the Indo-Gangetic Plain were responsible for about 94% of the PM_{10} mass over North-East India's atmosphere and 64% of near-surface PM_{10} concentration. Transported aerosols contributed >50 % of black carbon, organic carbon, sulfate, nitrate, ammonium and dust aerosol concentration and hence a major contributor to air pollution. Hence, the effects were much greater with transported aerosols. The indirect aerosol effect was found to be the major effect and more impactful with transported aerosols that dominated both rainfall and radiative forcing and suppressed rainfall significantly than the direct and semi-direct effect. Thus, this study found that emission control policies implemented in Indo-Gangetic Plain will reduce air pollution as well as the climatic impacts of aerosols over the North-East India region. Moreover, black carbon was also found to be responsible for suppression of lower intensity and enhancement of higher intensity rainfall may also contribute to the observed increase in higher intensity rainfall. These results provide insights into the effects of aerosols on pre-monsoon rainfall patterns and the mechanisms involved.

The study also compared the performance of planetary boundary layer parametrization schemes to select a suitable scheme to accurately predict meteorological parameters during the pre-monsoon and monsoon season with the WRF model at an enhanced resolution of 3 km grid size compared to the 10 km used in WRF-Chem. The study found that the enhancement in resolution showed significant improvement in prediction performance. The HONG scheme was found to be suitable for the region.

Keywords: Semi-direct effect; North-East India; Black carbon; Aerosol radiative feedback; Rainfall; Pre-monsoon; planetary boundary layer

List of Figures

List of Tables

List of Abbreviations

BC	Black carbon
CAIPEEX	Cloud Aerosol Interaction and Rainfall Enhancement Experiment
CCN	Cloud condensation nuclei
CDNC	Cloud droplet number concentration
CF	Cloud fraction
CLWP	Cloud liquid water path
COT	Cloud optical thickness
GCM	General circulation model
GISS	Goddard Institute for Space Studies
IGP	Indo-Gangetic Plain
IMD	India Meteorological Department
LES	Large eddy simulation
LW	Long-wave
NCAR	National Center for Atmospheric Research
NE	North-East
NESAC	North-East Space Application Center
NOAA	National Oceanic and Atmospheric Administration
OC	Organic carbon
PBL	Planetary boundary layer
PBLH	Planetary boundary layer height
PM_{10}	Particulate matter with aerodynamic diameter less than 10 µm
$PM_{2.5}$	Particulate matter with aerodynamic diameter less than 2.5 µm
RF	Radiative forcing
SW	Short-wave
TKE	Turbulent kinetic energy
TOA	Top-of-the-atmosphere
WRF	Weather Research and Forecasting
WRF-Chem	Weather Research and Forecasting with chemistry

Chapter 1

1. Introduction

1.1 General

The atmosphere is a combination of several gases along with tiny specs of suspended solid and liquid particles known as aerosols. These particulates not only impacts air quality and health but are indispensable with respect to the effects on local, regional and even global weather patterns (Rosenfeld, 2012; Lohmann and Feichter, 2005; Manoj et al., 2012; Menon et al., 2002; Ackerman et al., 2000; Fan et al., 2008; Choudhury et al., 2020). They vary significantly in their sizes, ranging from nanometres to 100 μm depending upon the source and method of formation (Wallace and Hobbs, 2006). They even vary considerably in number concentration and chemical constitution, both spatially and temporally. Aerosols have both natural and anthropogenic sources. They are released from sea sprays, dust emissions, forest fires or anthropogenic sources as primary particles; or may be formed in the atmosphere from gas-to-particle conversion processes of both natural and anthropogenic gas emissions known as secondary particles; each source having their distinct physical and chemical characteristics (Wallace and Hobbs, 2006). While the proportion of natural emissions greatly exceeds the latter, there is a growing imbalance due to the increasing anthropogenic emissions, such that the natural balance of the aerosols in the atmosphere is disturbed.

The climate effects of aerosols are well recognized though not sufficiently quantified. These effects are broadly recognized as four different types: direct, semi-direct, first indirect and second indirect (Baklanov et al., 2014a). The scattering and absorption of solar radiation by aerosols is termed direct effect (Mitchell, 1971). This affects the amount of solar radiation reaching the Earth's surface which further affects the stability of the underlying atmosphere. The absorption and heating are done by light-absorbing aerosols such as BC, dust and organic carbon (Ramachandran et al., 2020). The heating increases the atmospheric temperature, which increases the saturation vapour pressure of cloud droplets which evaporates them, thus reducing cloud cover (Koch and Del Genio, 2010a). This is known as semi-direct effect. Aerosols are also a critical requirement in the cloud formation process and take part as CCN for cloud droplet formation. However, the presence of a greater quantity of aerosols affects this process and the subsequent impacts are known as aerosol indirect effect. Indirect effect causes the formation of a larger number but smaller cloud droplets (Braham, 1974). This increases the reflectivity of clouds, causing an increase in cloud albedo, a decrease in surface radiation and an increase in the reflected radiation. This is known as the first indirect effect (Twomey, 1977). The increase in the droplet number and decrease in droplet radius affect cloud life time, rainfall and rainfall intensity, known as the second indirect effect (Albrecht, 1989). The indirect and direct effects of aerosols act in competition with each other and the indirect effects are found to be dominant (Makar et al., 2015). Bauer and Menon (2012) has defined the total aerosol forcing as the summation of direct, semi-direct and indirect forcing. The graphical representation of different aerosol effects is shown in Figure 1.1. The first figure in Figure 1.1 shows the direct effect as explained in the second paragraph of section 1.1. The subsequent figure shows a cloud which is unperturbed by any aerosol effect and the figures after this shows the different consequences of semi-direct, first indirect and second indirect effect.

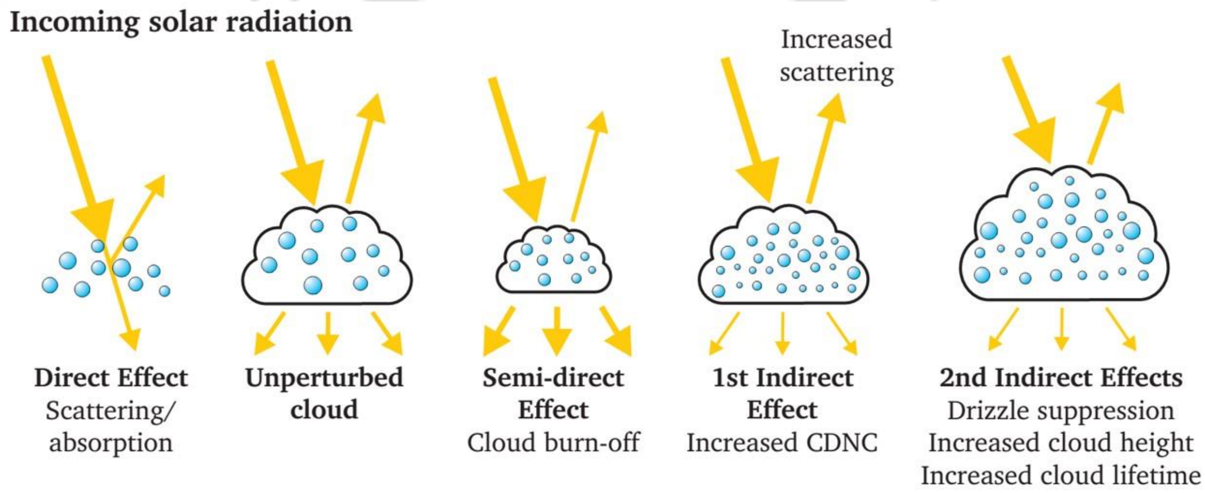

Figure 1.1: Different effects of aerosols (Source: Davies (2014))

Thus, aerosols interact with the atmosphere in numerous ways. Radiation and water, both key elements to our survival, are largely regulated by these microscopic and sub-microscopic particles. Thus, aerosols regulate the Earth's energy budget and hydrological cycle. These effects are of prime importance to the beings of the biosphere, as they determine the nature of the environment around them. However, the aerosol effects differ spatially depending on the constituents of aerosols, their physical and chemical properties as well as the quantity. Ambient aerosols are generally composed of species such as inorganic ions, organic compounds, BC, and mineral dust. Inorganics mainly contain sulfate, nitrate, and ammonium, while organic aerosols consist of a large number of chemicals (Wallace and Hobbs, 2006). Some of these aerosol compositions are inherited during their formation, while some aerosols undergo further chemical modifications after release with respect to their mixing state and chemical composition due to numerous chemical reactions and mechanisms in the atmosphere. The mechanisms include processes like condensation, coalescence, homogenous nucleation and heterogenous nucleation. Cloud condensation nuclei are a subset of these aerosols that can form and activate as cloud droplets when the ambient water vapour pressure is greater than the saturation vapour pressure (Wallace and Hobbs, 2006). This composition and mixing state modify the aerosols' properties both physically and chemically. The physical properties include light extinction, refractivity, aerosol size mode and aerosol size distribution, while hygroscopicity is the primary relevant chemical property. These new properties of the aerosols have significant impacts on its ability to interact with direct and indirect effect processes like cloud droplet formation, cloud droplet size, CDNC and cloud albedo (Koch et al., 2011). Wang (2013) observed that the radiative and microphysical effects of aerosols are determined primarily by the particles' size and chemical composition. The chemical composition also defines the hygroscopicity of the particles and along with size, it determines the activation probability to act as a CCN. The presence of sulfate and nitrate in the mixture makes the particle more hygroscopic and makes it more susceptible to act as CCN.

BC is the light-absorbing component of carbonaceous aerosol. It is a constituent of soot which is a combustion product (Andreae and Crutzen, 1997). BC is formed from incomplete combustion processes. They form by the condensation of intermediate combustion products like benzene and pyrene. Sources of BC include the burning of fossil fuels and biomass such as wood and crop residue. Black carbon aerosols are expected to remain in an internally mixed state due to the presence of sulfates and other organics at the source of formation (Lesins et al., 2002). Bond et al. (2013) found that BC strongly absorbs visible light with a mass absorption cross-section of at least 5 m^2 g^{-1} at 550 nm wavelength as compared to other absorbing aerosols like dust and brown carbon with a mass absorption cross-section of 0.009 and 1 m^2 g^{-1} respectively. Bond and Bergstrom (2006) found BC absorption refractive index to be the highest amongst all the aerosol species with a reported refractive index is 1.95-0.79i, the imaginary part representing the index of absorption. Mixing of BC with other aerosol components is found to further enhance the absorbing capacity (Moffet and Prather (2009). The process involves conversion of fresh fractal forms of soot into internal mixtures of soot, sulfate, organics, nitrate, ammonium and water, which enhances its absorption capacity further (Liu et al., 2015).

The climate effects of BC are many. BC being a constituent of aerosols, is involved in interactions with the clouds and radiation like most other aerosols such as sulfate, nitrate, and mineral dust, but the absorbing nature of BC is what makes it stand out from the others with respect to its climate effects as an aerosol. BC can also alter atmospheric circulation (Zanis, 2009) by changing the atmospheric heating and stability to affect monsoon (Lau et al., 2006) and severe storms (Rosenfeld, 2006). Strongly absorbing aerosols have been found to invigorate and restructure convective clouds due to solar heating and induced convection by these aerosols (Koren et al., 2005), thus enhancing precipitation.

North-East India is a region located in the easternmost part of India. Geographically, it is characterized by its hilly terrain, dense forests, and numerous rivers. It is blessed with abundant rainfall, resulting in a diverse range of flora and fauna, making it a biodiversity hotspot. The North-Eastern region of India is one of the highest rainfall regions in the world (Jain et al. 2013), with most of the rainfall in pre-monsoon and monsoon seasons. The region is known for its rich cultural diversity, with a vibrant mix of ethnicities, languages, and traditions. Northeast India has significant historical and strategic importance. It shares borders with Bhutan, China, Myanmar, and Bangladesh, making it a crucial gateway for trade and cultural exchanges. The economy of Northeast India is primarily agrarian, with agriculture and allied activities being the mainstay of livelihood for the majority of the population. The Indo-Gangetic Plains, also known as the Indus-Ganga Plain, is a vast region in the northern and eastern parts of the Indian subcontinent. It stretches across several countries, including India, Pakistan, Nepal, and Bangladesh, and covers an area of approximately 2.5 million square kilometres. The region has a predominantly flat terrain with a gradual slope from the Himalayas in the north to the Thar Desert in the west. The plains are crisscrossed by numerous rivers and their tributaries, forming an intricate network of water bodies that provide irrigation for agriculture and support a diverse ecosystem. The plains are formed by the alluvial deposits brought by the mighty rivers Ganges, Brahmaputra, and their tributaries, as well as the Indus River in the western part. The fertile soil, enriched by centuries of sedimentation, makes the Indo-Gangetic Plains one of the most agriculturally productive regions in the world. However, the Indo-Gangetic Plains also face challenges such as overpopulation, rapid urbanization, and water scarcity. The IGP is a global source of diverse aerosols (Ojha et al., 2020; Kumar et al.,

2018) that impacts regional and global climate (Ramanathan et al., 2005; Tripathi et al., 2005; Sarangi et al., 2015).

Atmospheric transport also plays an important role which extends the climatic impacts to the transported region from the source region (Lee et al., 2022). Air masses transport aerosols from the IGP to nearby regions, which also impacts air quality (Bhat et al., 2022; Ojha et al., 2012). Bonasoni et al. (2010) showed that pollutants from the IGP follow the southern slope of the Himalayas as a path into the Bay of Bengal and NE India and similar observations were made by Gogoi et al. (2017). The Indian region experiences westerly wind flows during the pre-monsoon (Kant et al., 2019), during which, along with local emissions, long-range transport of dust from Thar desert also takes place (Sarkar et al., 2019), which ultimately flows into the NE India. This flow also transports the high amount of aerosols generated in the IGP into the NE region. Among the aerosols, BC is a high climate-influencing aerosol component due to its strong absorption capability (Bond et al., 2013; Nenes et al., 2002; Koch and Del Genio, 2010) and IGP is the largest source region of it in India (Rana et al., 2019). Several studies (Guha et al., 2015; Sarkar et al., 2019; Chatterjee et al., 2010) found BC, among other aerosols measured at sites in NE India to be transported from the IGP. Moreover, in the NE India region, an increase in BC emissions was observed along with high BC concentrations near the surface level (Chaudhury et al., 2022; Singh and Gokhale, 2021). Tiwari et al. (2016) and Dhar et al. (2017) observed maximum BC concentration during this season in this region, along with the highest surface RF. As a result high dust and black carbon concentration is observed in this region with aerosol optical depth also being maximum during this period with an increasing trend (Dahutia et al., 2018; Dahutia et al., 2019; Gogoi et al., 2017; Pathak et al., 2010 ; Pathak et al., 2016). Thus, the aerosols in pre-monsoon are more absorptive which contributes to highest heating rate during this season (Nair et al., 2017) and strong vertical transport leads to having surface black carbon concentration same as at 850 hPa over NE (P.

Singh et al., 2020). Pathak et al. (2016) had observed elevated aerosol layers over NE. Dust is a major aerosol in this season transported from the Thar desert (Gogoi et al., 2009). Hence, the presence of high quantities of both BC and dust causes high atmospheric warming. A recent study (Subba et al., 2023) showed also gave similar conclusions and reported an increase in direct radiative forcing over NE India.

The pre-monsoon rainfall not only provides respite to the summer heat but is also an important source of water for the preparation of land for crop-related activities (Sinha et al., 2019) and with NE India being an agrarian economy. However, several studies show a decreasing trend of pre-monsoon rainfall in NE India (Mondal et al., 2018; Kumar et al., 2010; Mondal et al., 2015; Dash et al., 2007; Jain et al., 2013). Dahutia et al. (2018) also observed a decreasing trend of cloud droplet radius over different locations in NE. Also, it was said that the decreasing trend of precipitable water vapor led to a lesser probability of cloud formation. The lower moisture content, along with the increase in CCN, leads to a reduction in cloud droplet radius, which ultimately affected rainfall. Panicker et al. (2014) observed semi-direct effects over Guwahati in an experimental study, while Panicker et al. (2016) observed indirect effects showing the prevalence of both effects in the region.

Since the NE region becomes a hotbed of absorptive aerosols during pre-monsoon, there is a possibility of existence of semi-direct effect on the rainfall and may explain or add to the already available mechanisms in literature. The indirect effect may further complement the semi-direct effect. Moreover, how much is the contribution of transported aerosols to air pollution and climatic effects compared to those emitted within NE India region? What is the role of different aerosol effects on the rainfall mechanisms? The effect of transported aerosols on different regions of the world has been studied (Krishnamohan et al., 2021; Wang et al., 2020; Bagtasa et al., 2019) but none of them covered the IGP and its climatic impact on a nearby region. Moreover, the direct and indirect effect was found to be involved in large-scale suppression as well as catastrophic floods (Wang et al., 2022), which show the involvement of aerosols in extreme weather events. Choudhury et al. (2020b) also found aerosols to be responsible for high rainfall events near the Himalayan foothills. A recent report (Vinay Kumar and Venkateswara Naidu, 2020) showed an increase in higher-intensity rainfall during pre-monsoon over NE India. Studies have shown an increase in BC emissions over India and over NE India (PTI, 2022).This provides an opportunity to understand whether BC impacts rainfall intensity and whether it may have any role in the increase in extreme rainfall events over NE India.

The PBL, the lowermost layer of the atmosphere is directly influenced by the Earth's surface and responds to forcing within a period of one hour or less (Stull 1988). Turbulences within the PBL are responsible for distributing heat, momentum, moisture into the upper atmosphere (Boadh et al., 2016; Shi et al., 2021). Hence, its realistic reproduction is vital for forecasting weather through numerical simulation (Xie et al. 2012) as well as air quality. Turbulent mixing through eddies is needed to accurately represent the atmosphere's vertical thermodynamic and kinematic structure (Cohen et al. 2015). However, these turbulent eddies have such temporal and spatial scales that mesoscale models cannot resolve them and hence are required to be parametrized. The accuracy of turbulence parametrization is also critical for predicting and initiating the development of clouds. It is also crucial for accurate prediction of the planetary boundary layer processes, moisture, wind speed, and wind direction required for predicting convective clouds and precipitation (Cohen et al. 2015; Shin and Hong 2015; Xie et al. 2012). Parametrization involves relating the unresolved turbulent components of moisture, heat and momentum with the known variables. However, depending on whether the unresolved components at a grid point are defined in terms of known quantities at the adjacent grid points or many grid points in the vertical, PBL parametrization schemes are divided into two classes: local and non-local (Warner 2011). Within this classification, the PBL schemes differ according to the orders of closure, which represents the highest order of the prognostic equations for turbulent components. Higher-order closure schemes involve lesser approximation and more predicted components. Moreover, turbulence also plays an important role in the atmospheric distribution of air pollutants (Chen et al., 2022). Climate models such as WRF and WRF-Chem use parametrizations to predict meteorological parameters as well as chemical species of air pollutants. Thus, the evaluation of these parametrizations is necessary for accurate prediction of the state of the atmosphere.

WRF and WRF-Chem are state-of-the-art regional climate models developed by NCAR and NOAA, along with the collaboration of other organisations. WRF is mainly used for atmospheric research and forecasting, while WRF-Chem is mainly used for the study of air quality and climatic impacts of chemical species. WRF uses several integrated models to predict radiation, boundary layer, precipitation, heat and moisture fluxes from the land surface, together which predicts the overall state of the atmosphere. The radiation schemes involve the radiative transfer equation, which calculates the quantity of solar radiation reaching the earth's surface. Friction velocities and exchange coefficients for moisture and heat are estimated by the surface layer schemes. The land surface model then estimates the heat and moisture fluxes from the land surface. The boundary layer parametrizations predict the turbulent mixing of heat, moisture and momentum and define the state of the atmosphere nearer to the surface. Cumulus parametrizations are responsible for sub-grid scale convective transport of moisture and heat and sub-grid scale rainfall, while grid-resolved rainfall processes are simulated by the microphysics scheme. In addition, the parametrizations used in WRF, WRF-Chem includes additional chemistry schemes which simulate the chemical state of the atmosphere and affect the predicted meteorology to give the climatic impacts.

1.2 Scope and objective

The primary objective of the study is to investigate the role of aerosols on the rainfall mechanisms that affect the pre-monsoon rainfall, which may be responsible for the decreasing pre-monsoon rainfall trend over NE India, using the WRF-Chem model. BC primarily being a product of anthropogenic activities and having significant climatic impact, its role in such climatic effects was specifically investigated. Moreover, through qualitative and quantitative comparison of the impacts of local and transported aerosols, the study also tried to find the source region of aerosols that has a greater impact on the atmosphere over NE India during the pre-monsoon season. However, the conclusions from the simulations with WRF-Chem are based on simulation period of 10 days and hence does not account for long-term climatic changes and their impacts. In addition, the suitability of the planetary boundary layer parametrization schemes over NE India was checked using the WRF model. The results of this research can add to the understanding of the working of the pre-monsoon atmosphere over NE India and thus be helpful for policy formation w.r.t selection of emission control region and weather forecasting. Key tasks to fulfill the objectives are:

1. Setting up the model – selection of study period, model domain and model configuration
2. Development of model inputs – selection of meteorological initial and boundary conditions and preparation of inputs, preparation of chemical initial and boundary conditions, selection of emission inventories and development of emission files
3. Designing simulations – editing chemical initial and boundary condition and emission files
4. Performing simulations and model validation by comparison with observed data
5. Analysis, post-processing and interpretation of outputs

1.3 Novelty statement

This the first detailed study of the aerosol effects on the pre-monsoon atmosphere over NE India, using a state-of-the-art regional climate chemistry and regional climate model.

1. The different aerosol effects' roles on radiative forcing and rainfall over NE India have been investigated.
2. The separate impacts of local and transported aerosols on air pollution and climatic impacts over NE India have been identified.
3. The critical mechanism which may be responsible for the decline of rainfall trend over NE India has been identified.
4. The direct effect of BC on rainfall intensity has been studied.
5. A comparative study to identify the planetary boundary layer parametrizations using the WRF model, suitable for the NE India region.

1.4 Thesis outline

The thesis is divided into seven chapters. A brief description of them is given below.

Chapter 1: Introduction – highlights the importance of the topic and the requirement for the study of the North-East India region. It describes the main aim, objectives, scope, novelty statement and organization of the thesis.

Chapter 2: Literature Review – reviews the literature on the observed aerosol effects and their impacts, methods of study as well as modelling of the aerosol effects with WRF-Chem model. Focus is given to NE India. The chapter also reviews the literature regarding the evaluation of planetary boundary layer parametrizations with the WRF and WRF-Chem model.

Chapter 3: Pre-monsoon aerosol flow and its direct and semi-direct effect on rainfall - discusses how the pre-monsoon aerosol flow from the IGP influences the rainfall over the NE India region through aerosol direct and semi-direct effects.

Chapter 4: Comparison of climatic effects of local and transported aerosols - compares the impacts of different aerosol effects on the atmosphere over NE India during pre-monsoon season. Also, it compared the contributions of transported aerosols and locally emitted aerosols within NE India on the climatic impacts to ascertain their importance.

Chapter 5: Direct aerosol effect of black carbon on rainfall intensity – describes how the increase in black carbon emissions can cause changes to rainfall intensity over NE India through direct aerosol effects. Also, it discusses the decrease of rainfall amount with a continuous increase in black carbon emissions.

Chapter 6: Comparison and evaluation of planetary boundary layer parametrization schemes – explores the suitability of different planetary boundary layer schemes for better prediction of meteorological parameters at a finer resolution and suggests better-performing schemes.

Chapter 7: Findings and Conclusions – outlines the findings and conclusions from the entire research work, limitations and future scope. The key findings are highlighted.

Chapter 2

2. Literature review

The literature study has been carried out pertaining to the topics relevant to the aims and objectives of the study. The review has been focussed mainly on the following topics:

1. Trends in rainfall and rainfall characteristics over India
2. Sources of pollutants in NE India during pre-monsoon
3. Observational studies on aerosols effects
4. Quantification of aerosol effects and impacts through models
5. Parametrization of planetary boundary layer in WRF and WRF-Chem

2.1 Trends in rainfall and rainfall characteristics over India

This section describes the prevailing atmospheric condition during the pre-monsoon season over NE India and the climatic issues observed during this period.

Mondal et al. (2018) established a decreasing rainfall trend over central and eastern parts of India through statistical methods using different rainfall datasets from 1998 to 2015 on annual scale. Similar kind of observations were also made by Mondal et al. (2015) and Kumar et al. (2010). Dash et al. (2007) had also reported the highest decline in rainfall to be occurring over several states of NE India, namely Tripura, Nagaland, Mizoram and Manipur. In case of seasonal trends, Jain and Kumar (2012) had reported negative rainfall trends over several basins in NE India which was also further verified by Mondal et al. (2015) and Mondal et al. (2018). Konwar et al. (2012) had studied the regional trends of monsoon rainfall in India from 1979 to 2010. They observed that low to medium intensity (5-100 mm day^{-1}) rainfall was decreasing in the Eastern region of India due to decreasing trend of vertical moisture transport. In contrast to this, a recent study, Vinay Kumar and Venkateswara Naidu (2020) reported that the frequency of heavy rain, very heavy rain and extremely heavy rain days has increased over

NE India during pre-monsoon. The enhanced rainfall activity was related to increase in higher water vapor at surface and convective available potential energy. This is further supported by Chaudhuri and Middey (2013), who also observed an increasing trend of convective available potential energy during over NE India during this season. These studies, thus indicate a decreasing rainfall trend but increase in frequency of higher intensity rainfall during the pre-monsoon season, both of which indicate a problem. The long-term rainfall decrease may lead to water scarcity, while the increase in rainfall intensity leads to flash floods. Thus, several studies have identified the presence of a climatic issue over this region, which may be purely natural or contributed by anthropogenic factors, or a combination of both. Dahutia et al. (2018) however had attributed the decreasing pre-monsoon rainfall trend to different effects of aerosols through an observational study. They had observed an increasing trend of aerosol optical depth over NE India, with highest values during pre-monsoon. The study attributed the declining rainfall trend to decreasing precipitable water vapor and cloud droplet radius. The lower moisture content was reported to be caused by decrease in surface radiation by the increasing aerosol loading (indicated by increasing AOD trend), which reduced surface evaporation. The increasing aerosol mass also led to the increase in CCN, leading to a reduction in cloud droplet radius., Both of these factors reduced the possibility of rain droplet formation, which ultimately affected rainfall. This identifies as an anthropogenic factor to explain the negative rainfall trend. Moreover, Wang et al. (2022) also explains that although higher amount of aerosols in stratiform clouds can cause rainfall suppressions, aerosol invigoration can cause catastrophic floods in localized areas. The observations made by Koren et al. (2005) that strongly absorbing aerosols can enhance precipitation by invigorating clouds also calls for investigation for possible role of BC in causing increasing rainfall intensity.

While other factors may have also contributions on the negative rainfall trend and increasing rainfall intensity, the anthropogenic aerosol aspect is worth investigating, as its emissions can be controlled to a greater extent through policies and interventions to reduce its negative effects. Hence, the sources of these aerosols, their characteristics and their effects need to be ascertained.

2.2 Sources of pollutants in NE India during pre-monsoon

NE India is located to in close proximity to the eastern side of the IGP, which is recognised as pollution hotspot in India and the world (Chawala et al., 2023) due to its high population density. It is a source of diverse aerosols (Ojha et al., 2020) which has been found to impact regional as well as global climate (Ramanathan et al., 2005; Tripathi et al., 2005; Sarangi et al., 2015). This diversity is reported by Brooks et al. (2019) which found organic matter to dominate the submicron aerosol mass (43 %), followed by sulfate (29 %), ammonium (14 %), nitrate (7 %) and black carbon (7 %) inside the IGP. However, sulfate was the dominant species (44%), followed by organic matter (30 %), ammonium (14 %), nitrate (6 %) and black carbon (6 %) outside the IGP. However, within India, IGP is the largest source of BC (Rana et al., 2019) which has numerous climate impacts, as described before. Additionally, Brooks et al. (2019a) studied the BC physical and optical properties over IGP, north-west and NE India. BC concentration was highest in IGP during pre-monsoon. Moreover, the mass absorption cross section was higher (8.08 m^2 g^{-1}) for NE India than over IGP (6.76 m^2 g^{-1}) with mass absorption cross-section of BC aloft higher than those at the surface. This suggests that BC particles go transformation due to aging by long-range transport from IGP to NE in pre-monsoon.

India being one of the fastest developing economies and accounts for a bulk of the BC emissions. Solutions (2010) suggests that the bulk (25-35%) of the world's BC emissions are from India and China. These emissions of BC along with other pollutants were seen to be increasing from the past few decades. Several studies (Sadavarte and Venkataraman, 2014; Bond and Bergstrom, 2006; Sindhwani and Goyal, 2014; Lu et al, 2011; Singh et al, 2020;

Kumar et al, 2023) have indicated increasing BC emissions over last two decades in India. Moreover, estimates of BC emissions from 1990 to 2030 by GAINS model (http://gains.iiasa.ac.at) also show an increasing value, mostly contribute by the residential sector, as shown in Table 2.1.

Table 2.1: BC emissions from India (Gg)

Sector	1990	1995	2000	2005	2010	2015	2020	2025	2030
Combustion-energy	2	3	2	2	1	1	1	1	1
Residential	471	498	511	590	628	623	616	610	604
Manufacturing industry	82	109	145	231	255	297	331	354	381
Production processes	7	7	5	5	5	5	5	5	5
Road transport	33	44	62	78	78	31	31	34	37
Other mobile sources and machinery	16	23	32	44	58	71	86	102	120
Waste treatment and Disposal	18	13	14	15	16	16	16	17	18
Agriculture	69	70	69	64	65	63	62	60	59
Total	**698**	**766**	**842**	**1029**	**1104**	**1107**	**1149**	**1184**	**1227**

However, as already discussed in Section 1.1, emissions from the IGP are also transported by the Westerlies from the IGP to NE India and hence the pollution and the climatic impacts may be a combination of the local emissions within NE India and those transported from the IGP. Interestingly, Tiwari et al. (2016) had estimated that the annual BC emissions from Guwahati, the largest city in NE India and the emissions were found to be highest in the pre-monsoon season contributing to highest BC concentration in this season. BC concentrations were found to increase near the surface level in different studies over Guwahati (Chaudhury et al., 2022; Singh and Gokhale, 2021). Moreover, many studies (Dahutia et al., 2018; Dahutia et al., 2019; Gogoi et al., 2017; Pathak et al., 2010 ; Pathak et al., 2016) report highest aerosol concentration and highest aerosol optical depth in this period with contributions of dust from the Thar Desert (Gogoi et al., 2009). Dahutia et al. (2019) and Pathak et al. (2016) observed that dust and carbonaceous aerosols were predominant in the vertical column during pre-monsoon over NE India, which is explained by Singh et al. (2020) to be due to strong vertical transport from the IGP.

2.3 Observational studies on aerosols effects

This section gives an account of the effects from aerosols from different observational studies mostly over different locations in India including NE India to justify its occurrence in the atmosphere.

Tiwari et al. (2016) did a year-long study on the radiative effects of BC in Guwahati in 2013-2014. The annual mean atmospheric radiative forcing was found to be +30.16 W $m^{-2,}$ with annual mean atmospheric heating rate by BC was 0.86 K day^{-1}, indicating atmospheric heating by the absorbing aerosols in the region. Moreover, the annual mean radiative forcing at the surface was -21.1 W m^{-2}, indicating cooling at the surface. Similar observations were reported by Pathak et al. (2010) over Dibrugarh in NE India with surface cooling observed at the surface but with highest forcing efficacy and heating rates during winter and pre-monsoon, respectively. Chakrabarty et al. (2012) also reported BC induced radiative forcing of -63.4 and +11.1 W m^{-2} at the surface and TOA, respectively over Guwahati. The lower atmospheric heating rate was found to be 2 K day^{-1}. Talukdar et al. (2019) explains the consequence of direct effect on atmospheric stability. They found that an increase in the surface concentration of BC causes a significant decrease in convective available potential energy over Gadanki, India. BC caused a decrease in the lapse rate which reduced buoyancy for air parcels, thus increasing atmospheric stability.

In addition to direct radiative forcing, Panicker et al. (2014) studied the semi-direct effect of BC aerosols over Guwahati. BC was observed to cause significant heating in the clouds and reducing the cloud liquid water content and cloud fraction thus inducing a cloud-burning effect over the region. They suggested that this might reduce the rainfall over the region. Heating rates in the range of 1.5-2.5 K day^{-1} were observed which correlated negatively with liquid water content. The heating was also found to be responsible for reducing the cloud effective radius by 1.07- 1.63 μm. Negative correlations were also obtained between cloud fraction and heating rate, as shown in Figure 2.1.

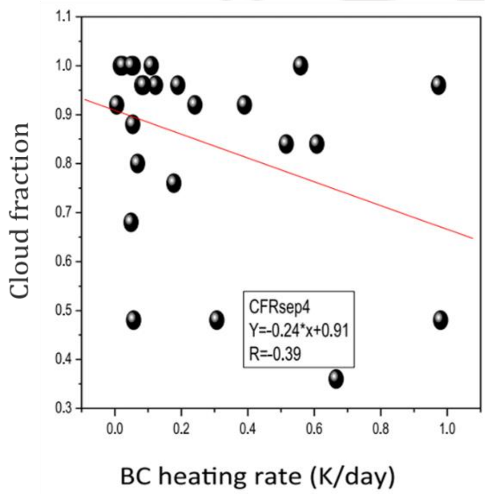

Figure 2.1: BC induced cloud heating rate vs Cloud fraction (Source: Panicker et al. (2014))

The above study also reports the presence of elevated BC concentrations, caused by strong vertical transport, which were also observed by Rahul et al. (2014). They had carried out 3-day aircraft observations of vertical profiles of BC over Guwahati during CAIPEEX in 2009. The mean 3-day profile above ground level is shown in Figure 2.2.

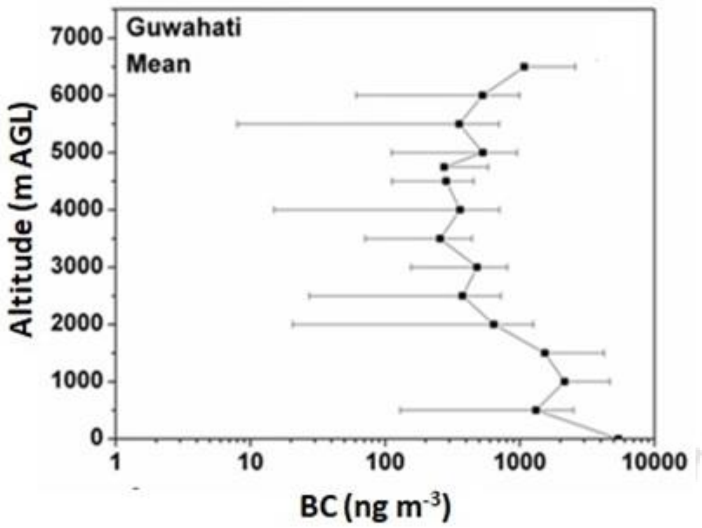

Figure 2.2: BC vertical profile over Guwahati (Source: Rahul et al. (2014))

They also observed that apart from heating induced near the surface due to anthropogenic surface loading of BC, a second layer was also formed in the upper atmosphere, which led to a heating rate of 2 K day^{-1}. This verifies that presence of elevated BC concentrations over NE India.

However, such profiles are also observed by Babu et al. (2011) who had carried out an in-situ measurement of the atmospheric BC profile over central India. They found two peaks of BC concentration one at 4.5 km and the other at 8 km above ground level. They observed a large decrease in environmental lapse rate and an increase in stability, caused by the heating induced by BC. The profile and lapse rate are shown in Figure 2.3.

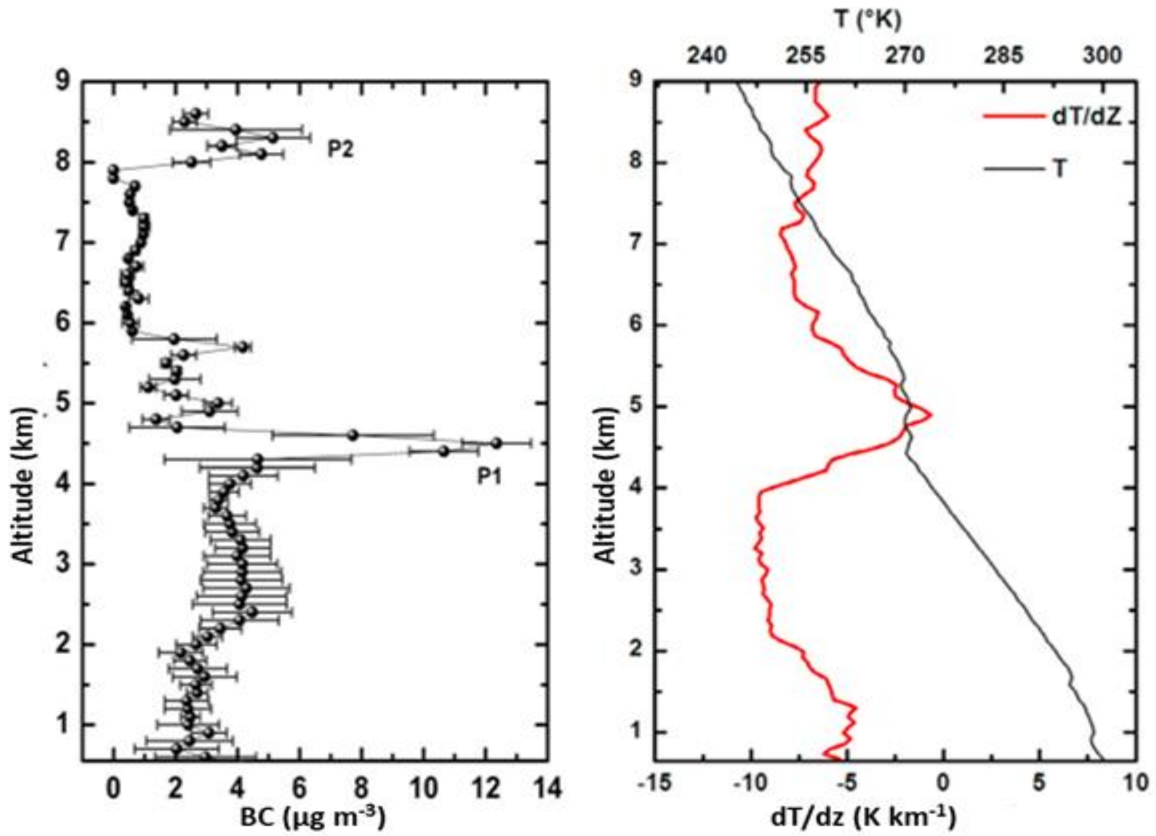

Figure 2.3: Vertical profile of BC (left) and lapse rate, ambient temperature (right) with altitude (Source: Babu et al. (2011))

Nair et al. (2016) carried out aircraft measurements of aerosol absorption over IGP during November-December 2012 and April-May 2013 and enhanced absorption was observed in spring in the lower free troposphere while it decreased near the surface. Increasing absorbing aerosol optical depth gradient from west to east IGP was observed. This also supports and complements the findings of Brooks et al. (2019a). Direct radiative forcing increased from winter at 24.9 W m^{-2} to spring at 34.0 W m^{-2}, indicating the presence of more absorptive aerosols. Hence, Nair et al. (2017) found the aerosols in pre-monsoon to be more absorptive with highest heating rate during this season.

However, in contrast to rainfall decrease mechanism suggested by Panicker et al. (2014) due to semi-direct effect, Devara and Manoj (2013) suggested that increased heating by the BC aerosols over Central India could cause a low-pressure uplift and cause a large-scale convergence of moisture from the surrounding area leading to increased rainfall. This suggests that, aerosol heating can cause increase or decrease in rainfall through different mechanisms.

In addition to the direct and semi-direct effects, Panicker et al. (2016) had studied the BC-induced indirect radiative forcing over NE India by doing in-cloud measurements of BC concentration and other cloud parameters. BC aerosols were also found to reduce the cloud albedo by 1.5-2.0% over the region and were also responsible for the reduction of droplet radius. The indirect forcing due to BC was -24 to -37.1 W m^{-2} at the surface and +2.5 to +14.8 W m^{-2} at TOA.

2.4 Quantification of aerosol effects and impacts through models

The above literature indicates the presence of different aerosol effects over different locations including NE India. These effects are simulated by climate models to quantify their impacts and mechanisms. Lohmann and Feichter (2005) suggested that aerosols affect the climate by changing the cloud characteristics in different ways. A brief description is given in Table 2.2, which would be helpful in understanding the subsequent literature.

Table 2.2: Overview of different aerosol effects on clouds

Effect	Description
Cloud albedo or Twomey effect (1st indirect effect)	More numerous smaller cloud particles reflect more solar radiation
Cloud lifetime effect (2nd indirect effect)	Smaller cloud droplets decrease the rainfall efficiency, thereby increasing cloud lifetime
Semi-direct effect	Absorption of solar radiation by soot may cause evaporation of cloud droplets
Surface energy budget effect (direct + indirect effect)	Increased aerosol and cloud optical thickness decrease the net surface solar radiation

2.4.1 Aerosol effects and their quantification

Bauer and Menon (2012) had studied the aerosol direct, semi-direct and indirect effects between pre-industrial emissions in 1850 and emissions in 2000 using the GISS Model. The total aerosol effect was considered as the sum of direct, semi-direct and indirect effects. This is also followed by Ghan et al. (2012a) using the Community Atmosphere Model v5.1.. They had decomposed the total anthropogenic aerosol radiative forcing into direct, indirect and semi-direct effect between 1850 and 2000 emissions. The following methodology was used to estimate the different effects:

$$\Delta S = S_{2000} - S_{1850} \quad (1)$$

$$Direct = \Delta(S - S_{clean}) \quad (2)$$

$$Indirect = \Delta S_{noanthrad,\ clean} \quad (3)$$

$$Semi\text{-}direct = \Delta S - Direct - Indirect \quad (4)$$

Where S = Total forcing, including clouds and aerosols

S_{clean} = Total aerosol forcing, including clouds but excluding aerosols

$S_{noanthrad,\ clean}$ = Total forcing excluding scattering absorption and scattering by aerosols

The results showed that cloud-borne aerosols showed a significant semi-direct effect. Indirect effects were found to be the most dominant.

Similar approach is used by Nabat et al. (2014) for estimation of direct and semi-direct radiative forcings.

Ackerman et al. (2000) did a study in the northern Indian Ocean during February-March of 1998 and 1999 on semi-direct effects of soot, and found that soot particles significantly reduce areal coverage of clouds. They suggested that soot-induced solar absorption amplifies the reduction in cloud cover and liquid water path. The semi-direct effect increased the aerosol forcing by 7.5 W m^{-2}. Modelling results showed that soot reduced daytime cloud fraction by 25-40%. Similar studied with different models were performed by other studies (Hill and Dobbie, 2008; McFarquhar and Wang, 2006; Johnson et al., 2004; Fan et al., 2008) which reported absorbing aerosols to evaporate cloud droplets and decrease cloud LWP and reduced rainfall. Lindeman et al. (2011) had examined the semi-direct effect of BC with WRF-Chem in Barrow, Alaska during a campaign study. It was seen that the atmosphere was affected by BC aerosols even if it is present in small quantities in the atmosphere. BC by its semi-direct effect, heated the lower troposphere by 0.15 K. In order to separate the semi-direct effect, four scenarios were created. One scenario contained no BC while the others contained different levels of BC. Semi-direct effects were estimated by comparing the results from the different scenarios. In a more recent study, Wang et al. (2018) had studied the radiative effects of BC and sulfate on cloud properties with the WRF-Chem and found semi-direct effects of BC on cloud droplets where a significant reduction in cloud droplet mass is found. On the contrary, Takemura and Uchida (2011) had reported contrasting results. They did global simulations with BC and without BC conditions to assess the semi-direct effects of BC on parameters: cloud droplet effective radius, rainfall and liquid water path. In East and South Asia, it was observed that there was an increase in all the aforementioned parameters. The reason behind this was observed to be the increased heating near the surface which caused increased evaporation and atmospheric instability leading to enhanced parameters.

Baklanov et al. (2014) stated that aerosols are necessary for cloud formation and the aerosol influence cloud properties such as cloud droplet radius, CDNC and cloud albedo. Modelling-wise this is verified by Yang et al. (2011), who found that the simulation of aerosol number, aerosol composition and optical properties and coupling these with clouds can lead to significant improvements in simulated stratocumulus cloud's optical and microphysical properties such as cloud top effective radius, cloud water path, and cloud optical thickness compared to when such couplings were turned off and hence suggested for its use. Chapman et al. (2009) shows the impact of this coupling by comparing the impacts of point emission sources on aerosol-cloud-radiative processes with the WRF-Chem model by including and not including them in separate scenarios. The additional aerosols from these sources scattered incoming solar radiation. Moreover, the additional aerosols caused the clouds to be more optically thick and caused lesser rainfall compared to when point sources were not included. Thus, indirect aerosol effect was found to be involved. Over the Unites States of America Wang et al. (2015) studied the impacts of the direct and indirect effects of aerosols over the with the WRF-Chem model. The indirect aerosol effect was found to be dominant with net surface radiation reduction by 12 W m^{-2} due to aerosol indirect effects compared to 4 W m^{-2} due to direct aerosol effect. CCN, CDNC, COT and CF greatly increased by a domain-wide mean of 0.9×10^{10} cm^{-2}, 1.2 and 0.01, respectively, causing a significant reduction of the shortwave radiation. Aerosol indirect effects suppressed the precipitation with a region average of 0.12 mm day^{-1} due to the formation of small-size CCNs. The areas with a large decrease of precipitation corresponded well with the increase of cloud liquid water path. Over the same domain with WRF-Chem, Zhang et al. (2010) found that aerosols reduced incoming by up to 11.3 W m^{-2} in January and 39.5 W m^{-2} in July which decreased 2-m temperature by 0.16 °C and 0.37 °C in January and July, respectively. Total column CDNC increased by up to 4×10^6 cm^{-2} in January and up to 11.8×10^6 cm^{-2} in July, with higher values over regions where CCN concentrations and cloud fractions were high. Liu et al. (2016) checked the climatic impacts of anthropogenic aerosols over East Asia with the WRF-Chem model. Anthropogenic aerosols reduced net shortwave flux at the surface by up to 40.5-57.2 W m^{-2}, 2-m temperature by up to 0.5-0.8 °C., NO_2 photolytic rates by up to 0.06-0.1 min^{-1} and the planetary boundary layer height by up to 83.6-130.4 m. Anthropogenic aerosols increased the column cloud droplet number concentrations by 3.6-11.7×10^8 cm^{-2} and cloud optical thickness by 19.8-33.2 which indicated the effect of indirect aerosol effect. Anthropogenic aerosols decreased precipitation in most areas by up to 3.9-18.6 mm during the study period of 4 months. The impact on radiation was more due to indirect effect than direct effect.

2.4.2 Aerosol effects on rainfall

The literature covered in this section with focus on the aerosol effects on rainfall, as it is the primary meteorological parameter under study in this thesis.

Soni et al. (2018) studied the direct radiative effect of BC aerosols on the Indian monsoon by using WRF-Chem. It was observed that during the pre-monsoon season, lower-troposphere heating led to increased instability and convection over India, which brought moist air from the Bay of Bengal which led to an increase in rainfall in NE India. Gogoi et al. (2017), through model simulations with WRF-Chem found that this atmospheric heating was highest in the western part of the NE India, mainly attributed to fossil fuel. A recent study (Subba et al., 2023) reported 43% increase in direct radiative forcing over NE India from -11.2 Wm^{-2} to -16.0 Wm^{-2} from 2001 to 2020.

With respect to monsoon rainfall, Kedia et al. (2016) used the WRF-Chem model to study the aerosol effects on monsoon rainfall in July 2010 over India. The aerosol effects exerted a strong influence on the rainfall magnitude and spatial distribution. Rainfall increased over central and eastern IGP due to an increase in moisture transported from the Bay of Bengal.

Adding to the above study, Kedia et al. (2019) had studied the specie-wise effect of different aerosols on convective and non-convective rainfall with WRF-Chem during a normal monsoon year 2010 in June – September. The effect of aerosols was found to be non-negligible. Dust increased non-convective rainfall in NE and rainfall decreased when dust was removed. Similar effects were seen for BC. Biomass burning reduced both convective and non-convective rainfall over NE, but the effect was stronger on convective rainfall. Sea salt emissions were found to decrease rainfall.

On the other hand, Fadnavis et al. (2019) observed that the presence of an Asian tropopause aerosol layer reduces rainfall during monsoon in India. This is amplified during the El-Nino year, when the aerosol contribution is more from East Asia, which makes the aerosol layer thicker which enhances droughts during monsoon season, by reducing surface evaporation. Manoj et al. (2012) had related the aberrant break of the Indian Monsoon in 2009, during which Central and North India received deficient rainfall which caused droughts to indirect aerosol effect. Thus, the reduction in rainfall due to decrease in surface evaporation is further worsened by indirect aerosol effects. Cherian et al.(2017) studied the effect of BC on indirect effect with a general circulation model. BC enhanced CDNC by 10-15% in BC emission regions which resulted in higher cloud water due to lower cloud water to rain water conversion and lower rainfall. In contrast, Kant et al. (2021) observed studied the aerosol-climate interaction of a certain wintertime hot weather event. Enhancement in rainfall through cloud invigoration was suggested due to the positive AOD and rainfall relationship. Moreover, Lau et al. (2006) with the help of GCM augmented with aerosol optical depth from the GOCART model studied the effect of dust and BC on the Indian monsoon. They observed that during the pre-monsoon season aerosols accumulated in the Tibetan Plateau and created a heated region. This created low-pressure areas and draws in more moisture from the Indian Ocean leading to the intensification of the Indian monsoon.

Ramanathan et al. (2005) did a climate simulation of the South Asian region from 1930-2000 to understand the climate effects of brown carbon containing BC on the observed trends. A strong correlation was found between the increasing emissions and the atmospheric forcing and decreasing surface forcing, shown in Figure 2.4. The surface dimming led to decreased evaporation levels reducing sea surface temperature which is required for cloud formation and rainfall. A reduction of monsoon rainfall of ~5% (±3%) from 1930 to 2000 was seen and was consistent with observed monsoon rainfall data. This is further supported by Shiogama et al. (2010) and Ming et al. (2010).

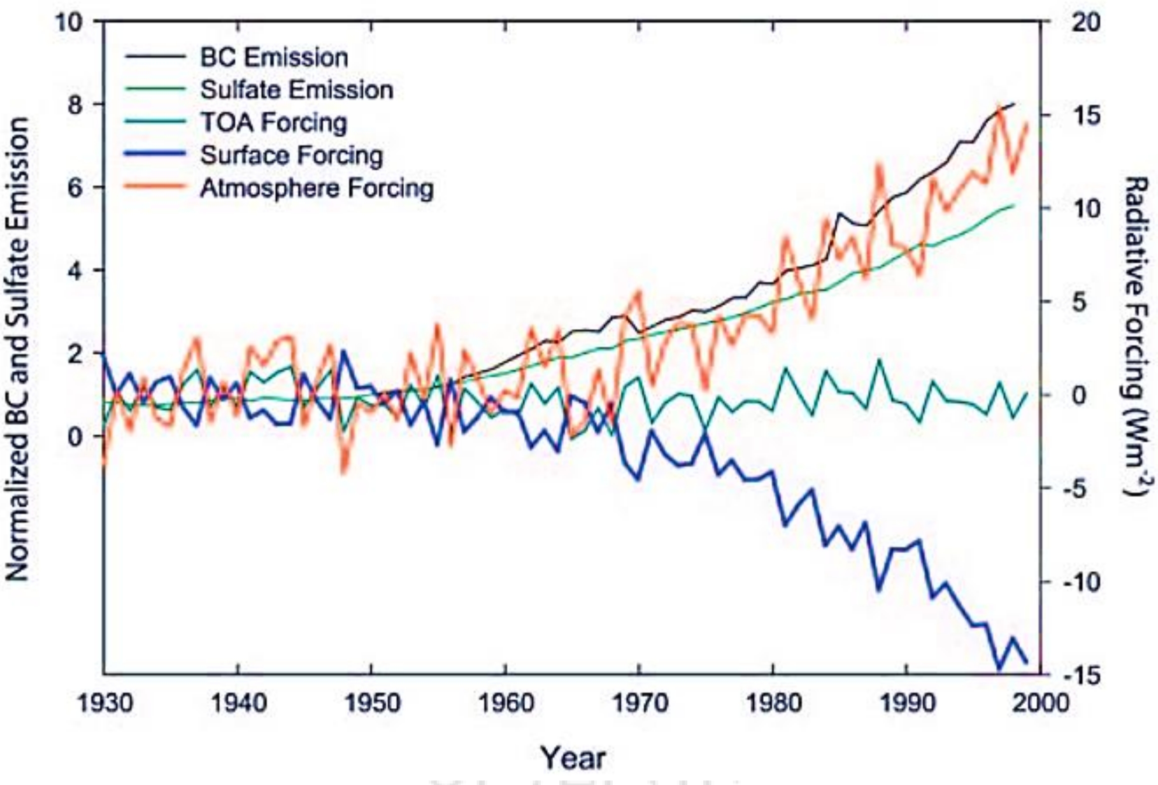

Figure 2.4: Change in emissions and radiative forcing (Source: Ramanathan et al. (2005b))

Moreover, Menon et al. (2002) studied the climate effects of BC in India and China with a global climate model. They found that BC may be responsible for altering the vertical motions of air and altering the hydrological cycle. It was suggested that BC may be responsible for the increased rainfall in southern China and drought-like conditions in the northern areas of both

India and China. Ramanathan and Carmichael (2008) however, suggested that it is difficult to predict the net effect of black carbon on global rainfall and suggested investigating rainfall at regional scales.

2.5 Planetary boundary layer parametrizations in WRF and WRF-Chem

The PBL parameterizations are responsible for modelling the processes in the lowest levels of the troposphere, such as aerosol transport and dispersion as well as the meteorology within it and hence for the air quality and regional weather. Hence, the testing of different parametrizations is an important exercise to judge its suitability in the study domain and study period. A brief description of the mostly used PBL parametrizations found in the literature is provided below.

1. YSU scheme (Hong et al., 2006): It is a first-order, non-local scheme with an explicit entrainment layer and a parabolic eddy-diffusivity profile in an unstable mixed layer. PBLH is defined on the basis of bulk Richardson number calculated starting from the surface. For stable cases, the threshold value is 0 and 0.25 for unstable cases.

2. ACM2 scheme (Pleim, 2007): It is a first-order, non-local scheme with non-local upward mixing and local downward mixing.

3. MYJ scheme (Janjić, 2001): It is a local, 1.5-order prognostic TKE scheme. PBLH is defined as the height where TKE decreases to 0.2 $m^2\,s^{-2}$.

4. MYNN3 scheme (Nakanishi and Niino, 2006): It is a second-order, local closure scheme. PBLH is defined as the height at which TKE falls below $1 \times 10^{-6}\,m^2\,s^{-2}$. It is necessary to note that the MYNN or MYNN2 scheme mentioned hereafter is the lower or one and half order version of MYNN3.

5. QNSE scheme (Sukoriansky et al., 2005): It is similar to MYJ. PBLH is defined as the height where TKE decreases to 0.01 $m^2 s^{-2}$.

6. HONG scheme (Shin and Hong, 2015): It is based on TKE and is scale dependent for vertical transport.

2.5.1 For predicting air quality with WRF-Chem

Shi et al. (2021) found the MYNN scheme to be suitable for the prediction of $PM_{2.5}$ and NO_2, while YSU for O_3 in the Yangtze River Delta, China, among the four tested schemes of YSU, ACM2, MYNN and MYJ, carried out during July and November. Similarly, Cuchiara et al. (2014) found YSU to show the highest agreement with observations for the prediction of O_3 over Houston, Texas among YSU, ACM2, MYJ and QNSE. Among similar studies in India, only two studies are found in the literature: Mohan and Gupta (2018) and Gunwani et al. (2023). Mohan and Gupta (2018) tested ACM2 and YSU schemes over Delhi, India to predict air quality during June 2015. ACM2 was reported to be more appropriate for prediction of O_3 and PM_{10}. In addition, Gunwani et al. (2023) reported MYNN and MYJ to more accurately predict $PM_{2.5}$ concentration over the IGP during the winter season on 2017-2018. This shows that, the performance of schemes may vary location-wise, as Delhi is also within the IGP, and season-wise. The above two studies carried out in India also shows that different schemes give better performances with different chemical species.

2.5.2 For predicting meteorology with WRF

Non-local schemes are found to be more appropriate for unstable atmospheric conditions while stable atmosphere by local schemes. Cohen et al. (2015) had studied the effect of several local and non-local PBL schemes with WRF to simulate severe cold events in the United States. They observed that non-local schemes inducing non-local mixing is necessary to predict the lower tropospheric lapse rates. Banks et al. (2016) had carried out a similar as a part of the

Hygra-CD campaign over Athens. The non-local schemes consisting of YSU, ACM2 and TEMF were found to give the best results when compared with the observations. Xie et al. (2012) carried out a similar study over Hong Kong at 27 km, 9 km and 3 km resolution with local and non-local schemes and found the non-local scheme, ACM2 to be the best performing. Moya-Álvarez et al. (2020) had carried out a sensitivity analysis of PBL schemes in a mountainous region in the central Andes of Peru for forecasting of rainfall between 2009 and 2012 in the months of January, February and March. The schemes producing more unstable conditions in the boundary layer with weaker winds were found to be producing more rainfall. MYNN3 scheme was adjudged to be the overall best for rainfall forecasting in the region, but is a local scheme. These studies thus, generally recommends the use of a non-local scheme. Moreover, the Table 2.3 lists similar studies carried out for regions in India.

Table 2.3: PBL sensitivity studies carried out in India

Study	**Study location, season**	**Recommended schemes for meteorological parameters**
Gunwani and Mohan (2017)	India, Winter and pre-monsoon	Temperature: ACM2 Relative humidity: QNSE Wind Speed: ACM2 and MYNN
Boadh et al. (2016)	Nagpur, winter and summer	All parameter: YSU and MYNN
Mohan and Bhati (2011)	Delhi, winter and summer	Temperature and relative humidity: ACM2
Hariprasad et al. (2014)	Kalpakkam, monsoon,	All parameter: YSU and MYNN
Panda and Sharan (2012)	Ahmedabad-Delhi-Jodhpur, summer and winter	All parameter: MYJ
Madala et al. (2014)	Gadanki, pre-monsoon	Rainfall: MYJ
Madala et al. (2015)	Ranchi, all seasons	All parameter: ACM2
Rai and Pattnaik (2019)	India, monsoon	Rainfall: YSU and ACM2
Gunwani et al. 2020	Delhi, pre-monsoon	All parameter: TEMF (Angevine, 2005)

There have been few studies in India in the last decade which evaluated the performances of PBL schemes with WRF model. Among the studies in India, only one study (Gunwani and Mohan 2017) covered India's NE region, which was limited to evaluation of the meteorological parameters during December (winter) and May (pre-monsoon) at 10 km grid grids size for all of India.

2.6 Summary of literature review

The review finds the presence of a negative rainfall over NE India during the pre-monsoon season trend but also an increase in frequency of higher intensity rainfall, both of which indicate a problem for the inhabitants of the biosphere. Negative rainfall trend might reduce the availability of water while increase in frequency of higher intensity rainfall indicates a health hazard through occurrence of floods. Due to being in close proximity, the region also observes emission transport by the Westerlies during this season from the IGP, which is considered as one of the pollution hotspots of the world and the largest source of BC in India. Hence, a mixture of different pollutants is transported from the IGP during this season. The literature also shows that the absorption capability of BC increases during its transport from the IGP to NE India and coincidentally, the region observes the highest atmospheric heating during this period. Moreover, the aerosol mass loading over this region has seen an increasing trend along with the BC concentration. This gives possible hints that links different aerosol effects and rainfall trend. In addition, the literature also finds the occurrence of different aerosol effects over NE India through observational studies which verifies its presence in the region. Direct and semi-direct effect was found to cause surface cooling, atmospheric heating and evaporation of clouds. Moreover, indirect effect was also found to affect clouds. Hence, the aerosol-cloud-radiation-rainfall processes need to be studied owing to the coincidence of high aerosol loading and negative rainfall trend over NE India during the pre-monsoon season. The seasonal rainfall pattern during pre-monsoon is shown in Figure 3.3.2 and which mainly due the westerly and southerly wind flow moisture transport from other regions outside NE India, as described in Section 3.3.2.

BC aerosols through its atmospheric warming creates instability over NE India which enhance this southerly wind flow and causing more rainfall (Soni et al., 2018) and is the only literature found for aerosol effect on pre-monsoon rainfall. The literature review finds modelling studies are more focussed on aerosols effects on monsoon rainfall. Moreover, several studies showed an increase in BC emissions in the last two decades. Global scale studies carried out by different models (Menon et al., 2002; Ramanathan et al., 2005; Lau et al., 2006) in different regions of the world shows different nature of results and may be a function of the region, which needs to be studied on a regional scale (Ramanathan and Carmichael, 2008) as its effects vary regionally. Hence, the effect of BC on rainfall was found to be uncertain with its increase in emissions and is required to be studied on a regional scale.

The two important studies giving directions to the objectives of this thesis as well as showing the research gap are Dahutia et al. (2018) and Soni et al. (2018). Dahutia et al. (2018) has added tried to explain the decreasing rainfall trend as a result of aerosol effects while the modelling study (Soni et al., 2018) explained the direct effect of BC on the wind flow causing increased rainfall. However, none of the studies quantify the roles of different aerosol effects and their mechanisms on the established wind flow responsible for causing rainfall. Indirect effect is generally found to be a dominant mechanism in literature but not covered in this study (Soni et al., 2018). Moreover, these studies did not distinguish between the quantity of transported aerosols and aerosols generated within NE India and their impacts, which would be helpful to identify the region of influence. Overall, none of the studies quantify the influence of the emissions in IGP over the climatic effects observed over NE India. Thus, this study can shed light on the declining rainfall trend in a detailed manner, taking into account the role of all aerosols in general and BC specifically. Also, the literature also show enhancement in BC emissions in last decades but does not show whether and how this can impact rainfall quantity and intensity over NE India and whether it has any relation on the increasing rainfall frequency.

The literature also finds that PBL parametrization to be an important aspect for modelling dispersion of air pollutants as well as modelling of meteorology. Also, most of the studies have suggested the use of non-local schemes to simulate the boundary layer as they ensure better mixing within the layer. However, the performance of schemes varied from region to region and season depending on the prevailing weather conditions. Hence, it is suitable to test different PBL schemes to judge their suitability in the modelling domain. The review did not find any PBL parametrization sensitivity study with WRF-Chem for dispersion chemical species over NE India in pre-monsoon season. The literature shows that ACM2, YSU, MYJ and MYNN schemes are generally tested and used for air quality modelling with WRF-Chem. Hence, these schemes were tested with WRF-Chem for finding a suitable PBL scheme for pollutant dispersion in the study period. Additionally, there is no study to date which evaluates the PBL schemes' performance with the WRF model in NE India during pre-monsoon and monsoon for prediction of meteorology. Hence, PBL schemes were tested with the WRF model for meteorology prediction at a higher grid resolution. The study is extended to the monsoon season to check whether similar or different PBL schemes are suitable as both these seasons are rainfall periods for this region.

Chapter 3

3. Pre-monsoon aerosol flow and its direct and semi-direct effect on rainfall

3.1 General

The chapter analyses the flow pattern of aerosols during the pre-monsoon season and its direct and semi-direct radiative effect on the rainfall over NE India during this period. The study first makes a comparative analysis between different planetary boundary layer parametrization schemes w.r.t prediction of different chemical species. The best-performing scheme is then utilized for aerosol flow analysis and assessing the influence of direct and semi-direct effects of aerosols on the pre-monsoon rainfall mechanisms. The pre-monsoon season is a transition period from the dry and colder winter (December – February) towards the hotter and wetter monsoon (June – September). The pre-monsoon period is marked by moderate to high temperatures, Westerlies, and initiation of rainfall in this region, whereas the monsoon season is characterized by high rainfall from the South-West monsoon and high temperatures.

3.2 Methodology

3.2.1 Model domain

The study used version 4.2.1 of the WRF-Chem model (Grell et al., 2005). Being an online coupled two-way model, both atmospheric chemistry and meteorology affect each other. The model domain for the simulations is shown in Figure 3.1, which also shows the terrain height in the domain. The domain covers the IGP, NE India, along with other regions of the Indian subcontinent. The domain is selected based on a preliminary investigation that showed NE India to be receiving air flows from the western and southern directions. The northern boundary of the IGP and NE India is bounded by the Himalayas. The NE India region is bounded by the black lines within the red box, which consists of hilly terrain, with hill ranges in the south and mountain ranges in the north, forming the narrow region of Brahmaputra River valley along the east-west direction. The domain extended from 10.64 to 31.22 °N and 71.67 to 100.43 °E with 300 (east-west) × 232 (north-south) grid points at 10 km resolution. The model extended from the surface up to a height of 17 km, divided into 45 levels. The level spacing between the surface and the next level is 40 m. The dashed lines indicate the location of the vertical cross-sections in Figure 3.7.

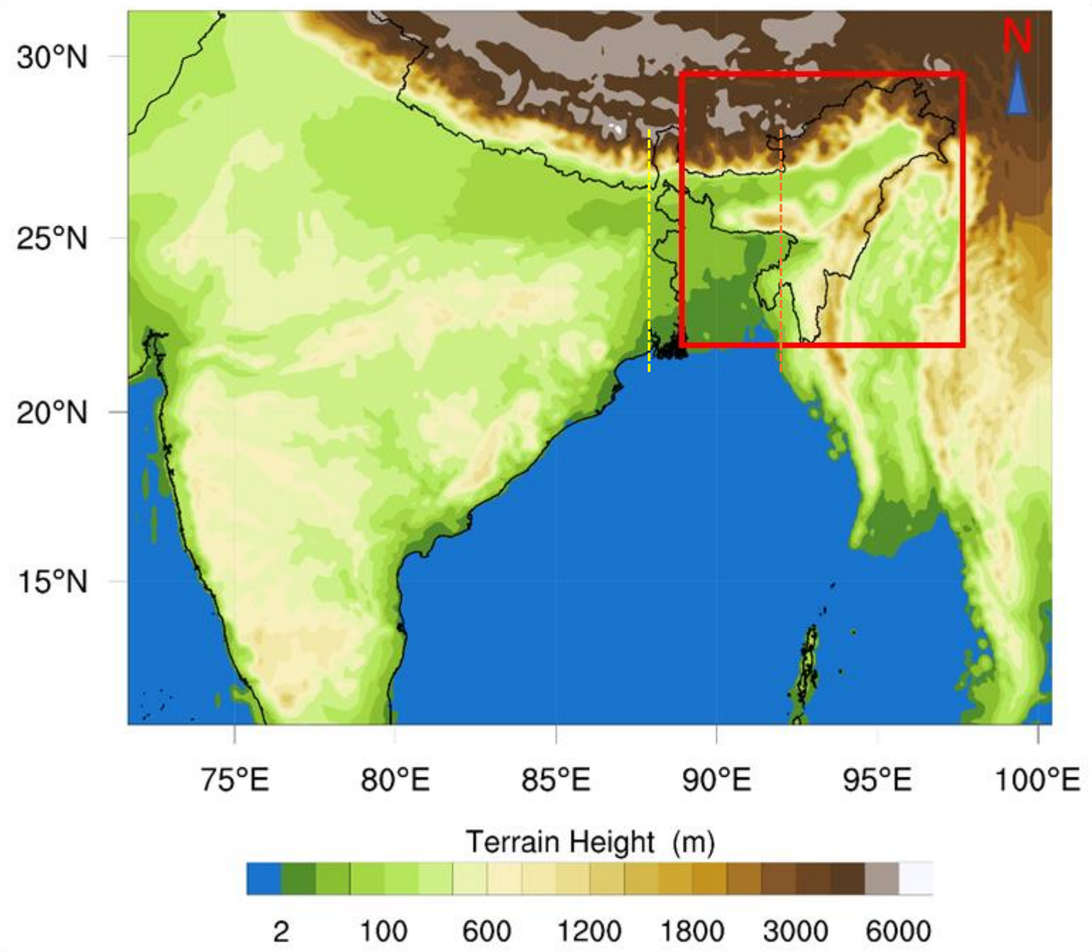

Figure 3.1: Domain used in WRF-Chem model simulations with the red box showing the location of NE India region within the modelling domain

3.2.2 Model inputs and configuration

ERA5 reanalysis datasets (Hersbach et al., 2020) were used for meteorological initial and boundary conditions. The dataset consists of hourly analysis at 30 km spatial resolution up to a height of 80 km.

The chemical initial and boundary conditions were developed from CAM-Chem output data (Lamarque et al., 2012). Anthropogenic emissions at 0.1°×0.1° were taken from the CAMS emission inventory (Granier et al., 2019). The inventory is based on the EDGARv4.3.2 inventory (Crippa et al., 2018) for 2010, extended to subsequent years based on the trends in CEDS inventory (Hoesly et al., 2018). Fire emissions were taken from the FINN inventory (Wiedinmyer et al., 2010), which estimates fire emissions of gases and aerosols from open burning sources based on satellite observations. Biogenic emissions from the terrestrial ecosystem were estimated online with the MEGAN model v2.04 (Guenther et al., 2006). The MOZART chemistry model (Emmons et al., 2010) and the MOSAIC (Zaveri et al., 2008) aerosol model simulated atmospheric chemistry. MOZART includes 85 chemical species and 196 chemical reactions. MOSAIC (Zaveri et al., 2008) is a sectional aerosol model with 4 bins that assumes the aerosols to be internally mixed. At a point in space, within a particular bin, all the aerosols present at that point are mixed together so that all the particles have the same composition, while the other bin might have a different composition. Bin sizes range from 39.0625-156.25 nm, 156.25-625 nm, 625-1250 nm, and 1250-10000 nm dry diameters. The model considers 12 aerosols such as sulfate, methanosulfonate, nitrate, chloride, carbonate, ammonium, sodium, calcium, BC, organic carbon, liquid water and other inorganic species such as silica, trace metals, minerals, all together specified as "other inorganic mass", which is considered as dust aerosol. In contrast to the other aerosols, dust aerosols are simulated online that depend on the land use category and wind speed among other factors, described in Zhao et al. (2010). The change in composition and number concentration of aerosols between different bins occurs due to different aerosol processes such as gas-particle partitioning, homogenous nucleation, coagulation, dry removal, wet removal, heterogeneous chemistry and acting as nucleation sites for cloud droplets and ice particles. The estimation of aerosol optical properties in WRF-Chem is described in Fast et al. (2006).

The physics parametrization schemes that were used included the RRTMG scheme (Iacono et al., 2008) for both short-wave and long-wave radiation, NOAH land surface model (Tewari et al., 2004), Grell-Freitas cumulus scheme (Grell and Freitas, 2014) for sub-grid scale convective transport of moisture, heat, gases and aerosols and Morrison microphysics scheme (Morrison et al., 2009). MOSIAC is coupled with the Morrison microphysics scheme for CCN activation into cloud droplets. However, the MOZART-MOSAIC scheme in this study does not support cloud droplet activation of aerosols and hence only the direct and semi-direct effects are analysed. Only the wind components above the boundary layer were nudged using spectral nudging. Four planetary boundary layer schemes were evaluated and details regarding it is provided in the next section.

3.2.3 Simulation details

Rainfall over the NE India region increases continuously from March to May, which may be verified from observed rainfall in Figure 3.2, sourced from IMD (https://www.imdpune.gov.in/cmpg/Griddata/Rainfall_25_Bin.html.) by Pai et al. (2014). The data consists of daily rainfall data at 0.25° × 0.25°. Hence, the mid-season period of 10 days from 10th to 19th April 2018 was used for the study. A period of 13 days from 7th to 19th April 2018 was simulated. However, the period of 3 days from 7th to 9th was taken as model spin-up. Model outputs from 10th to 19th were used for analysis. Moreover, April 2018 period was also an El-Nino Southern Oscillation and Indian Ocean Dipole neutral period and hence was suitable for rainfall analysis with aerosols. The months of March and May were also simulated for the same duration as April but only used for aerosol flow analysis.

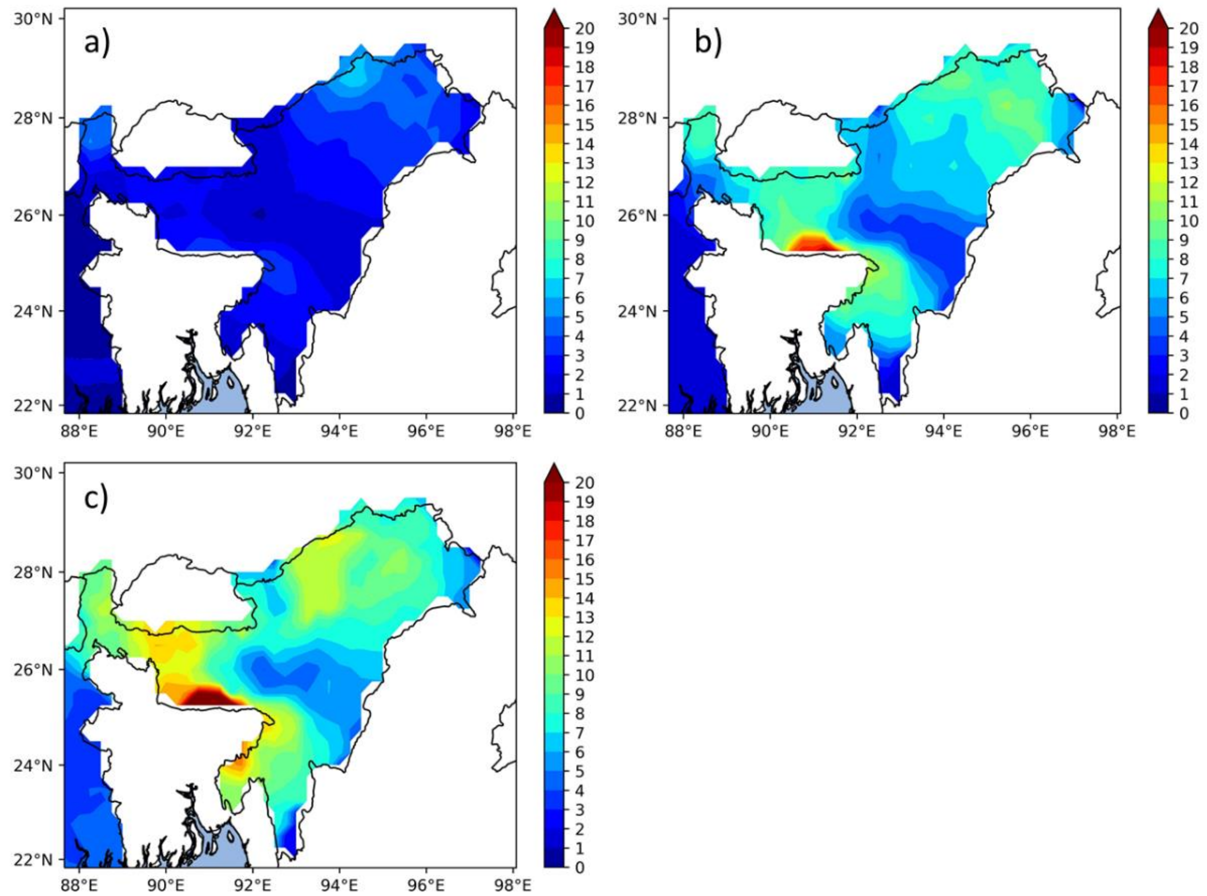

Figure 3.2: Mean daily observed rainfall (mm day^{-1}) from 2001-2020 in a) March b) April c) May

Table 3.1: Description of simulations

	Simulation name	**Description of simulation**
1.	NOR	With standard emissions and aerosol radiative effects turned on
2.	NOFEED	Same as NOR but with aerosol radiative effects turned off
3.	NO_BC_ABS	Same as NOR but with absorption by BC disabled
4.	2NOR	Same as NOR but with 2×BC emissions
5.	4NOR	Same as NOR but with 4×BC emissions

A brief description of the simulations carried out for this study is provided in Table 3.1. NOR simulation represents the normal atmospheric scenario with standard emissions from CAMS emission inventory and with aerosol radiative feedbacks turned on in the model. The NOR simulation was conducted separately with different planetary boundary layer (PBL) schemes to evaluate and compare which scheme best predicts chemical species. Four PBL schemes were tested: YSU scheme (Hong et al., 2006), ACM2 scheme (Pleim, 2007), MYJ scheme (Janjić, 2001), MYNN3 scheme (Nakanishi and Niino, 2006). These schemes were selected based on their frequent use with the model available in literature as well as on suggestions from the modelling community. The chemical species outputs of these four simulations were evaluated and the best performing PBL scheme was used for the remaining simulations in Table 3.1, as well for simulations in Chapter 4 and 5. The same PBL scheme was also used for the simulations of March and May.

NOFEED is similar to NOR, except with aerosol radiative feedbacks turned off. Hence, the difference between the NOR and NOFFED scenarios gives the effect of aerosol radiative feedback due to all aerosols, or called as aerosol direct effect and described in the Section 1.1. A similar approach has been used before in Wang et al. (2015). 2NOR and 4NOR, respectively, have twice and four times the standard BC emissions compared to NOR. NO_BC_ABS is similar to NOR but with no solar radiation absorption by BC and hence no atmospheric heating by BC. Thus, the difference between NOR, 2NOR, 4NOR and NO_BC_ABS help to study the influence of changing atmospheric heating due to BC on radiation, clouds and rainfall and rainfall characteristics, called as the semi-direct effect, as described in Section 1.1. The process of changing emissions also helps to bridge the uncertainty with emission inventories, as Gadhavi et al. (2015) found emission underestimation in BC emission rates to be the primary reason behind model underestimation of BC concentration. The approach of finding the BC semi-direct effects by changing emissions is taken from Lindeman et al. (2011), but in this study, the absorption due to BC is disabled instead of turning off the emissions. This allowed only the absorptive component of the BC refractive index to be turned off while allowing scattering. A similar approach was used by Ghan et al. (2012).

3.2.4 Model evaluation

The NOR simulations with the four different PBL schemes were first evaluated against MERRA-2 global model dataset for comparison of predicted chemical species. Furthermore, evaluation of meteorology was also carried out against surface station and gridded dataset. Mean error (ME), root mean square error (RMSE) and index of agreement (IOA) were used as statistical parameters.

3.2.4.1 Evaluation of chemical species

The M2T1NXAER_5.12.4 dataset from the MERRA-2 global model (GMAO, 2015) provides one-day averaged surface level concentrations of organic carbon, BC, sulfate and dust (https://disc.gsfc.nasa.gov/datasets/M2T1NXAER_5.12.4/summary). MERRA-2 model is run at 0.625° × 0.5° spatial resolution. Hence, the M2T1NXAER_5.12.4 is regrided to match the WRF-Chem model output resolution. The statistical evaluation of MYNN3, ACM2, YSU and MYJJ over the whole modelling domain and NE India using this MERRA-2 dataset is provided in Table 3.2.

Table 3.2: Statistical evaluation of chemical species. RMSE and ME in µg m^{-3}

		NOR-MYNN3		NOR-ACM2		NOR-YSU		NOR-MYJ	
		Whole domain	NE India	Whole domain	NE India	Whole domain	NE India	Whole domain	NE India
BC	RMSE	**0.70**	**0.64**	1.09	0.89	0.67	0.77	**0.70**	0.66
	IOA	**0.51**	**0.53**	0.50	0.52	0.50	0.50	0.49	0.52
	ME	0.21	-0.13	0.40	**-0.01**	**-0.19**	-0.48	**0.19**	-0.14
Organic carbon	RMSE	4.60	5.44	5.77	6.61	**4.51**	**5.29**	4.70	5.36
	IOA	0.49	0.47	0.49	**0.48**	**0.51**	**0.48**	0.49	**0.48**
	ME	-0.45	-2.99	0.22	-2.13	-0.62	-3.01	-0.28	-2.67
DUST	RMSE	**38.62**	**23.90**	41.63	28.40	53.04	41.63	39.77	25.86
	IOA	**0.39**	**0.37**	0.35	0.33	0.33	0.26	0.35	0.33
	ME	**-16.25**	**-16.75**	-22.57	-21.34	-45.23	-39.03	-17.91	-20.15
sulfate	RMSE	2.47	2.88	**2.39**	**2.82**	2.45	2.86	2.48	3.02
	IOA	**0.40**	**0.46**	**0.40**	**0.46**	0.39	0.42	0.37	0.41
	ME	1.39	-1.01	1.29	**-0.58**	1.30	-0.43	**1.22**	-0.70
Mean of all species	RMSE	**11.60**	**8.22**	12.72	9.68	15.17	12.64	11.91	8.72
	IOA	**0.45**	**0.46**	0.44	0.45	0.43	0.41	0.42	0.44
	ME	**-3.78**	**-5.22**	-5.16	-6.01	-11.18	-10.74	-4.19	-5.92

The best statistical values are represented by bold letters. The results show that MYNN3 performed the best among all the schemes, with most of the chemical species, including BC, and dust, both throughout the domain as well as over NE India. ACM2 performed the best with sulfate while YSU simulated OC better. Overall, it was observed that MYNN3 had the least RMSE (whole domain: 11.60 µg m^{-3}, NE India: 8.22 µg m^{-3}), highest IOA (whole domain: 0.45, NE India: 0.46) and least ME (whole domain: -3.78 µg m^{-3}, NE India: -5.22 µg m^{-3}) considering all the chemical species. Hereafter, the NOR-MYNN3 simulation is called as

‘NOR’ simulation and is used for the subsequent evaluation in this study and simulations in Chapters 4 and 5.

3.2.4.2 Evaluation of meteorology

Surface station datasets (https://mesonet.agron.iastate.edu/sites/locate.php) from IMD were used to evaluate meteorological parameters of 2m temperature, 2m relative humidity, 10 m wind speed and wind direction at Bangalore (13.20 °N, 77.70 °E), Delhi (28.56 °N, 77.11 °E), Kolkata (22.65 °N, 88.45 °E), Mumbai (19.10 °N, 72.86 °E), Patna (25.59 °N, 85.08 °E) and Guwahati (26.10 °N, 91.58 °E) against the NOR simulation. IMD gridded rainfall dataset by Pai et al. (2014) as mentioned before was used to evaluate rainfall. This dataset was regrided to match model output resolution for comparison.

The meteorological performance statistics are shown in Table 3.3. According to Emery et al. (2001), RMSE value of 2.0 K, IOA > 0.7 and ME ±0.5 K was proposed for temperature and the acceptance criteria of IOA > 0.7, RMSE < 20%, and ME < 10% were considered for relative humidity as used by Gunwani and Mohan (2017). Also, according to Emery et al. (2001), ME should be ±0.5 m/s, IOA > 0.6 and RMSE should be within 2.0 m/s for wind speed. Considering these criteria, the model under-predicts temperature and performs well with relative humidity and wind speed. In the case of wind direction model shows a large RMSE, which may also be related to slow wind speeds as under-prediction is observed (Carvalho et al., 2014).

Statistically, over the NE India region, rainfall in NOR has an RMSE of 21.26 mm/day, IOA of 0.40 and ME of 9.22 mm/day. Overestimated rainfall may also be due to the non-inclusion of indirect effects in this high aerosol loading region. In terms of rainfall performance, the model overestimates rainfall but the spatial distribution is similar shown in Figure 3.3. Rainfall overestimation with the same model was also observed in Kumar et al.

(2015). The overestimated rainfall, especially over higher terrain, may be a feature of the model as seen in the same study and also in Soni et al. (2018). However, the objective of this study to analyse the response of the meteorological parameters and rainfall to different emission scenarios and to aerosol effects and hence their accurate prediction is not necessary.

Table 3.3: Performance statistics of meteorological parameters

	Temperature (K)			Relative humidity (%)			Wind speed (m/s)			Wind direction (°)		
	ME	RMSE	IOA	ME	RMSE	IOA	ME	RMSE	IOA	ME	RMSE	IOA
Bangalore	-1.99	2.25	0.93	2.10	10.39	0.96	0.00	1.15	0.56	-15.82	44.95	0.81
Delhi	-0.72	1.84	0.96	2.45	7.75	0.94	-0.73	1.74	0.62	6.98	91.65	0.80
Kolkata	-2.87	3.86	0.79	14.08	16.94	0.78	-0.21	1.81	0.57	11.81	59.59	0.50
Mumbai	-1.95	2.48	0.82	1.69	10.60	0.85	-1.17	1.58	0.78	10.41	81.42	0.63
Patna	-0.16	1.86	0.95	1.54	10.87	0.92	0.27	1.48	0.65	1.57	85.49	0.82
Guwahati	-1.45	2.59	0.78	5.03	11.99	0.76	-0.47	1.85	0.37	36.35	137.46	0.58
Mean	**-1.54**	**2.46**	**0.89**	**4.37**	**11.31**	**0.89**	**-0.37**	**1.55**	**0.63**	**2.99**	**72.62**	**0.71**

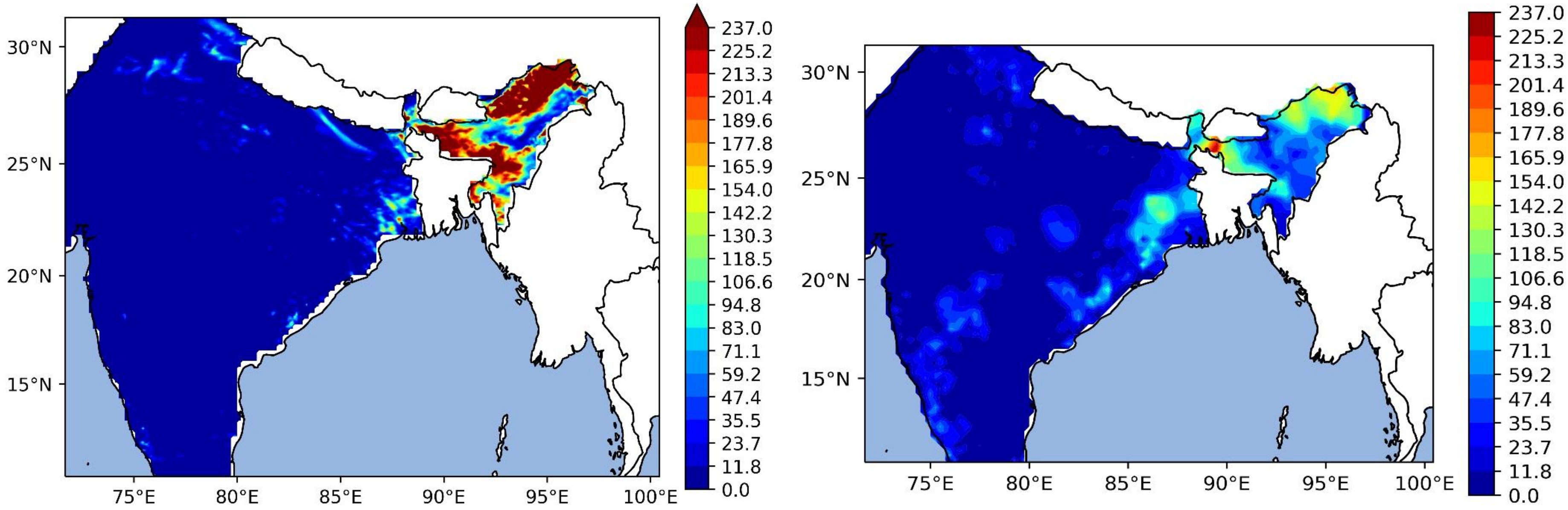

Figure 3.3: Spatial distributions of total rainfall (mm) in WRF-Chem (left) and IMD (right)

3.3 Results and discussions

3.3.1 Aerosol flow analysis

The product of air velocity and aerosol concentration at a point shows the flux at that point and the path shown by the streamline shows the path of instantaneous direction of air flow. If the wind components are averaged, the streamlines show the prevailing direction of flow. The streamline plots are shown for multiple model levels, which are the model outputs at multiple heights from the surface.

Figures 3.4, 3.5 and 3.6 show the PM_{10} aerosol mass flux at 20, 160, 520, 1330, 2340 and 4850 m above ground level, respectively for March, April and May. The direction of the arrow represents the direction in which the aerosol at a point will be carried to. Higher flux at any location is also an indication of higher aerosol concentration at that point. At lower levels (20 m, 160 m), incoming aerosol flow is from the south and south-west side over the Bay of Bengal. At these heights, the airflow diverts to the west due to obstruction by the Khasi hills in Meghalaya. The influx from the IGP is not seen at these heights. As we go to higher heights, there is a change in the wind direction and along with it the direction of influx. At 520 m and higher, the direction of influx gradually changes to the west, with contribution from the IGP. In March at 520, 1330 and 2340 m, the maximum flux values occur within NE, while for April and May, it is over IGP. This can lead to higher aerosol influxes from IGP in April and May. Thus, the IGP acts as a source of emissions to be transported to the NE Indian region during the pre-monsoon season. Also, it is seen that, fluxes near the surface levels are relatively less, which increases with an increase in height at 520, 1150 and 2340m. Thus, the mid-level heights are more involved in aerosol transport, which causes elevated aerosol layers in NE India during pre-monsoon season. This is verified in Figure 3.7.

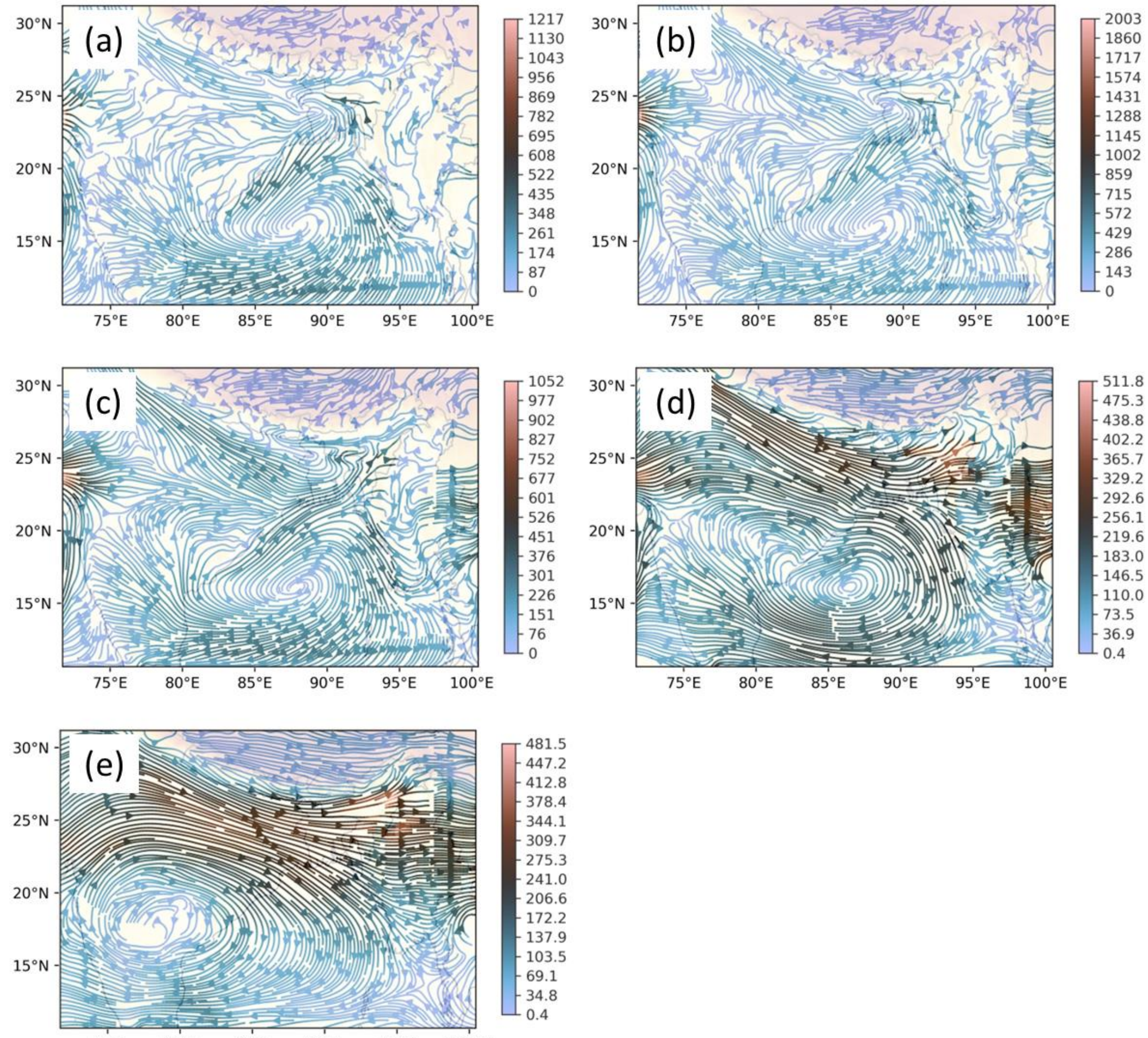

Figure 3.4: Wind flow streamlines and aerosol mass flux (µg m^2 s^{-1}) at a) 20 m b) 160 m c) 520 m d) 1330 m e) 2340 m in March

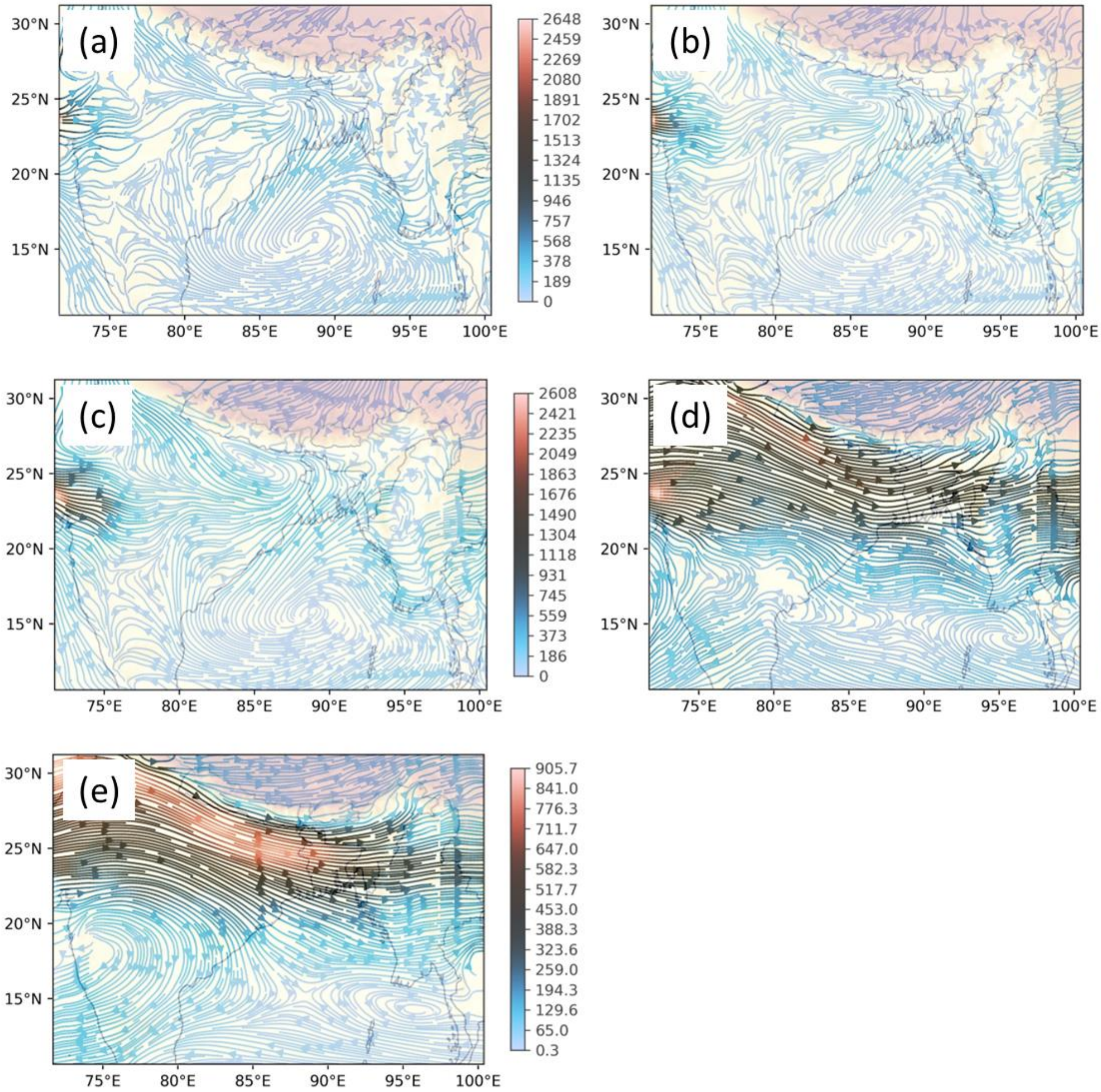

Figure 3.5: Wind flow streamlines and aerosol mass flux (µg m^2 s^{-1}) at a) 20 m b) 160 m c) 520 m d) 1330 m e) 2340 m in April

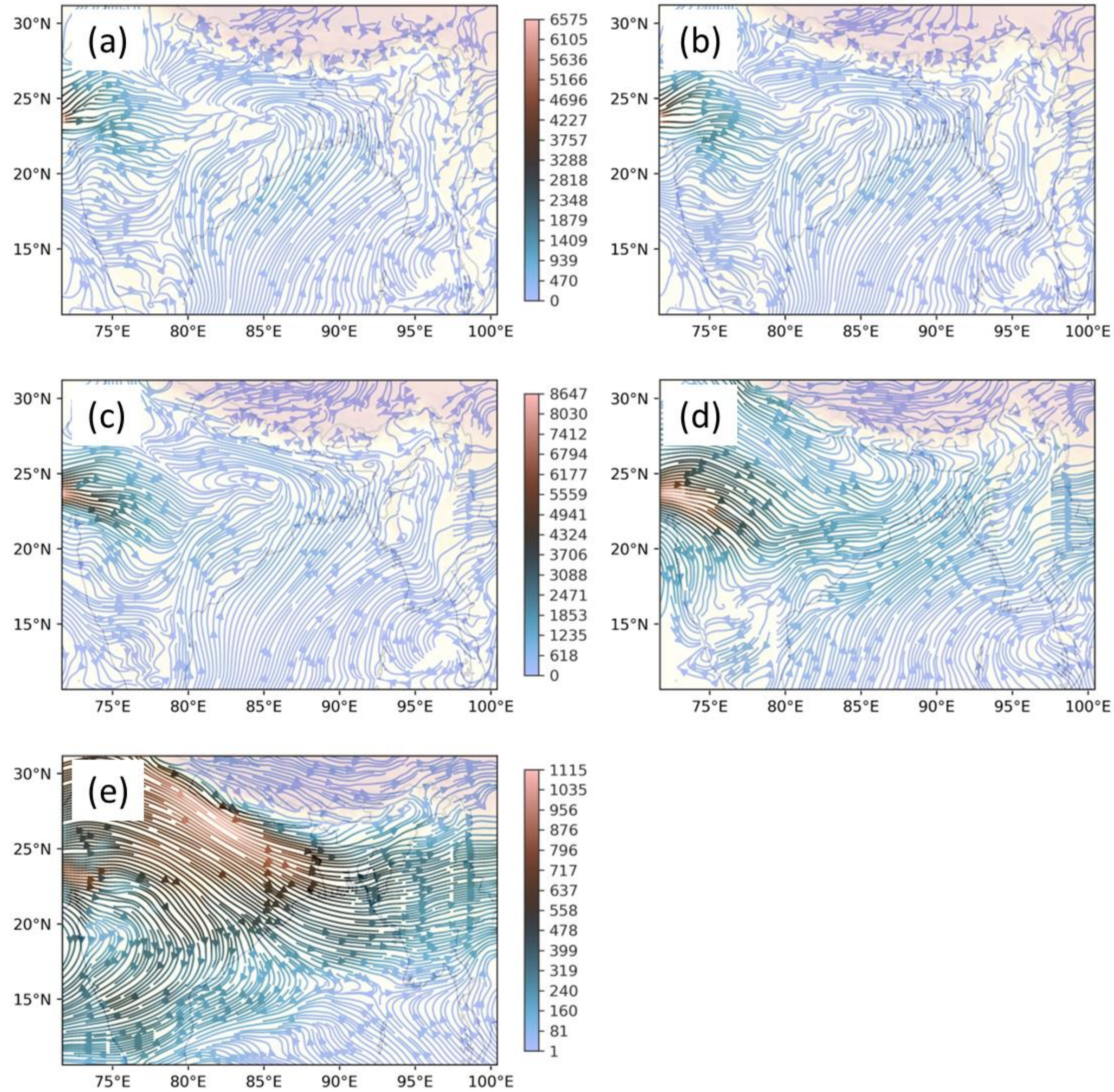

Figure 3.6: Wind flow streamlines and aerosol mass flux (μg m^2 s^{-1}) at a) 20 m b) 160 m c) 520 m d) 1330 m e) 2340 m in May

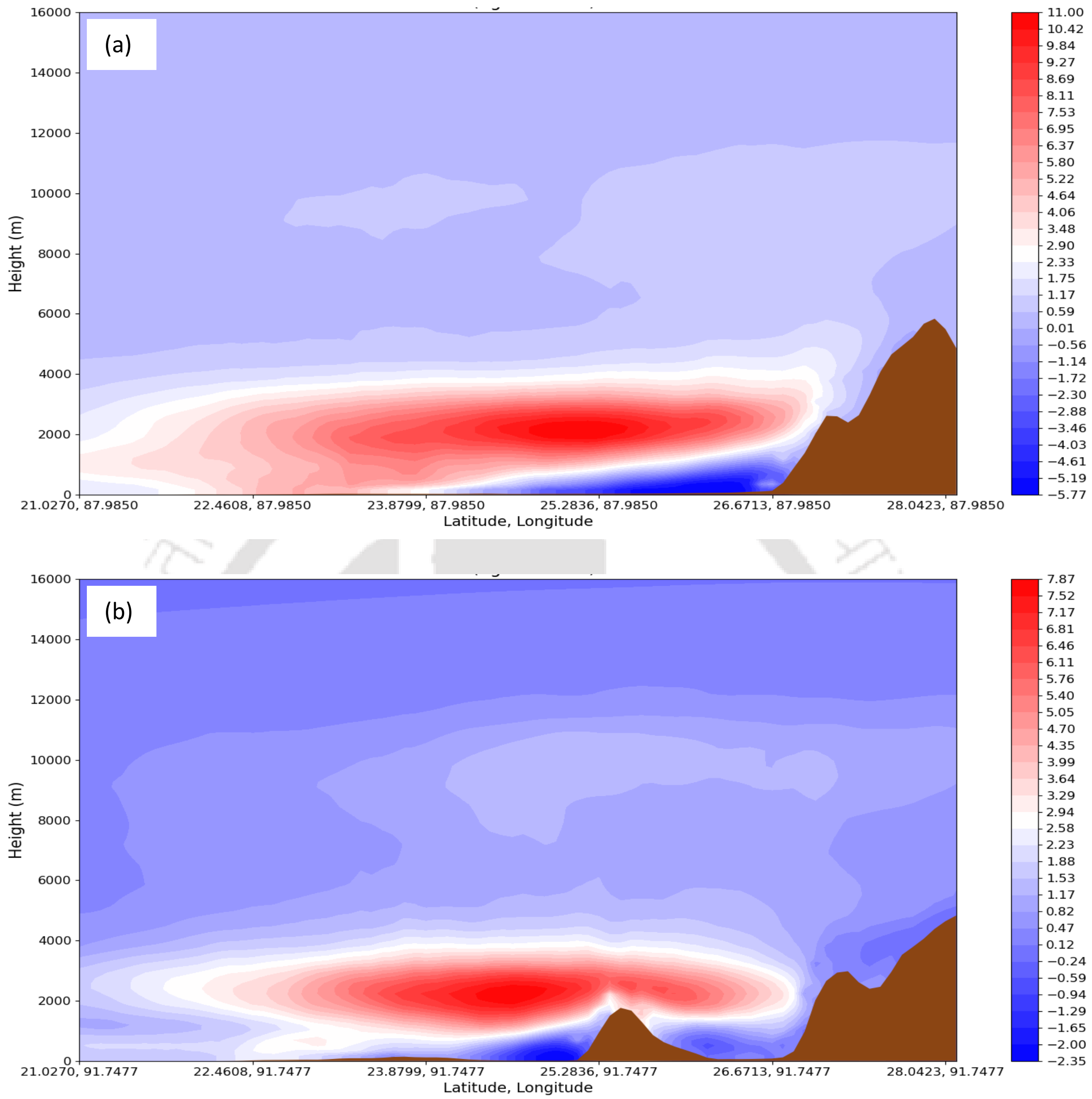

Figure 3.7: Vertical cross-sectional flux profile (µg m^2 s^{-1}) of black carbon between 21° and 28° N latitude and along a) 88° E longitude and b) 91.74° E longitude in April

The vertical cross-sectional flux profiles of black carbon, which is one of the components of PM_{10}, are shown in Figure 3.7. These cross-sections are also indicated by yellow (88° E) and orange (91.74° E) dashed lines in Figure 3.1. The profiles indicate west-east component of fluxes and hence, positive values indicate inflow into NE India from IGP and negative values indicate the outflow from NE India to IGP. These plots confirm the aerosol flow direction shown before. Positive influx exists at multiple levels, the major being at around 2000-4000 m and also at around 10000 m. Outflow is observed near the surface. Hence different natures of aerosol flow are observed at different heights.

3.3.2 Aerosol radiative effect on rainfall

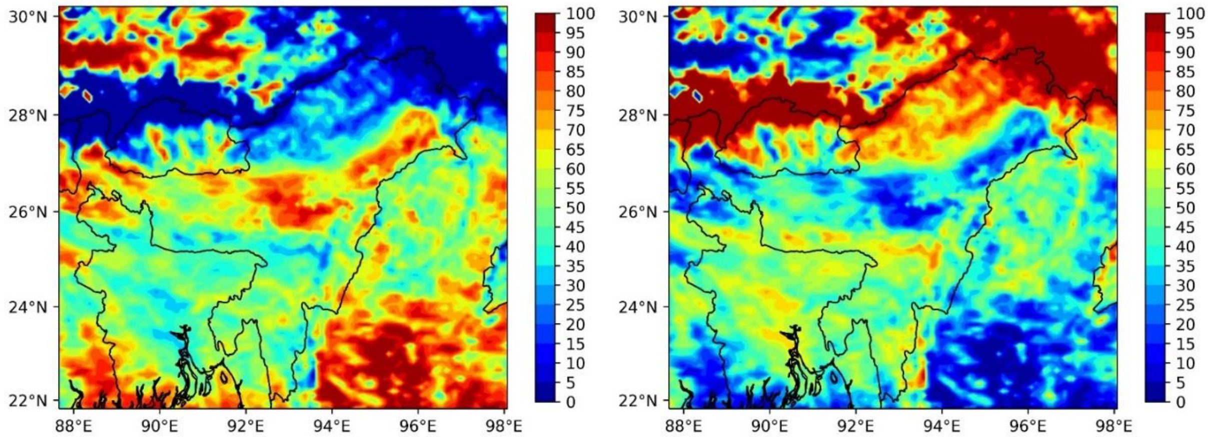

Figure 3.8: Spatial distributions showing contribution (%) of CR (left) and NCR (right) in total rainfall

This section discusses the radiative effect of the aerosols on the pre-monsoon rainfall in the NE India region. In WRF and WRF-Chem, rainfall is divided into sub-grid or convective rainfall (CR) and grid-scale/microphysical or non-convective (NCR) rainfall. NCR rainfall is contributed by stratiform-type clouds, controlled by the microphysics scheme. CR, controlled by the cumulus scheme, is contributed by cumulus-type clouds formed due to rising thermals. The contribution of grid-scale rainfall with NOR was more area-wise (Figure 3.8). NCR was found to be more spatially dominant in the region, also reported by Romatschke and Houze (2011). CR rainfall was seen to be dominant mostly along the Brahmaputra River Valley.

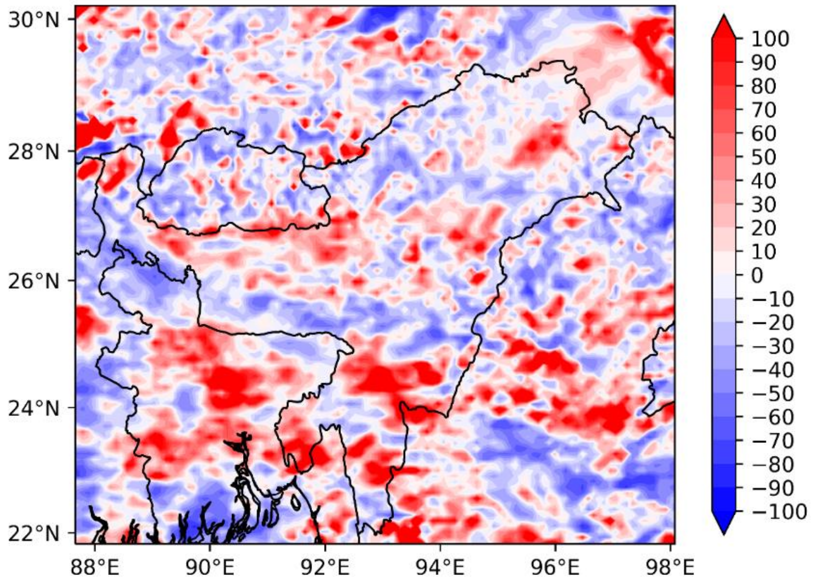

Figure 3.9: Spatial distribution of percentage change in total rainfall between NOR and NOFEED simulations

Figure 3.9 shows the percentage change in 10-day total rainfall over NE India due to aerosol radiative effects, estimated from NOR-NOFEED. The figure shows regions containing concentrated regions of total rainfall changes. However, every grid point includes both periods of rainfall enhancement and suppression, as seen in Figure 3.10, which shows the spatial distribution of the percentage of simulation time aerosols increase or decrease rainfall.

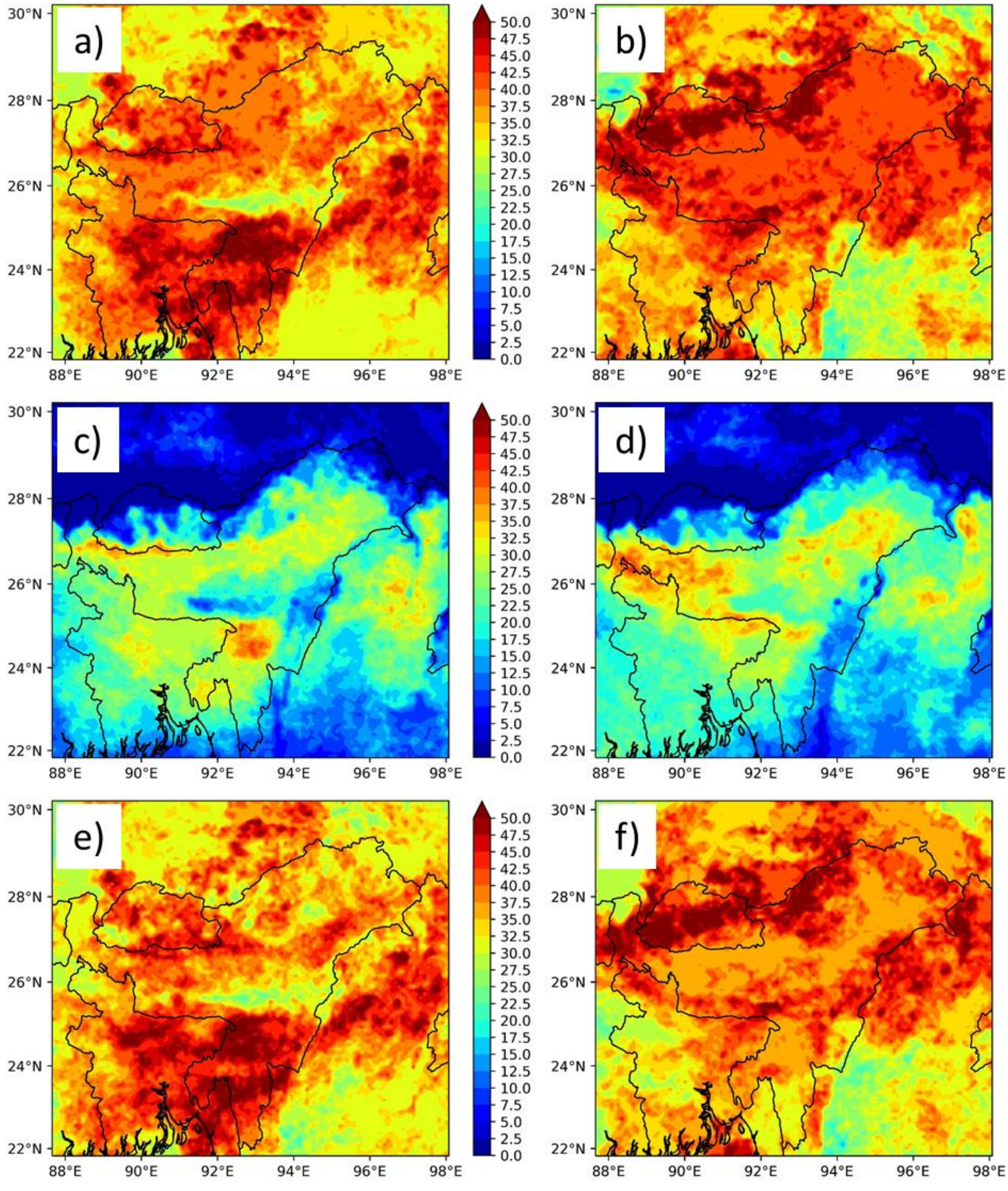

Figure 3.10: Spatial distributions of percentage of time (a) total rainfall increases, (b) total rainfall decreases, (c) CR increases, (d) CR decreases, (e) NCR increases and (f) NCR decrease

The regional mean within NE India for Figures 3.10(a) and 3.10(b) is 39.16% and 40.89%, respectively, the value of 39.16% mostly contributed by the southern region, while it is more homogenously contributed by the entire region for the 40.89%. If the southern region is not considered, the regional mean changes to 37.24% and 41.73%. Moreover, since the model overestimated rainfall, suppression might be even more temporally and spatially dominant. Most of the total rainfall changes, both increase and decrease, were induced by changes in NCR, as seen by comparing Figures 3.10(c), 3.10(d), 3.10(e) and 3.10(f). The decrease in CR was more in the western region of NE India and mostly lay on the low terrains along the valley, in contrast to the NCR, which showed more suppression along the higher terrains. In both cases of CR and NCR, suppression was more dominant than enhancement and hence, was mostly affected by aerosol radiative feedback. Both suppression and enhancement occurred due to changes in low-intensity rainfall followed by high-intensity rainfall, shown in Figure 3.11.

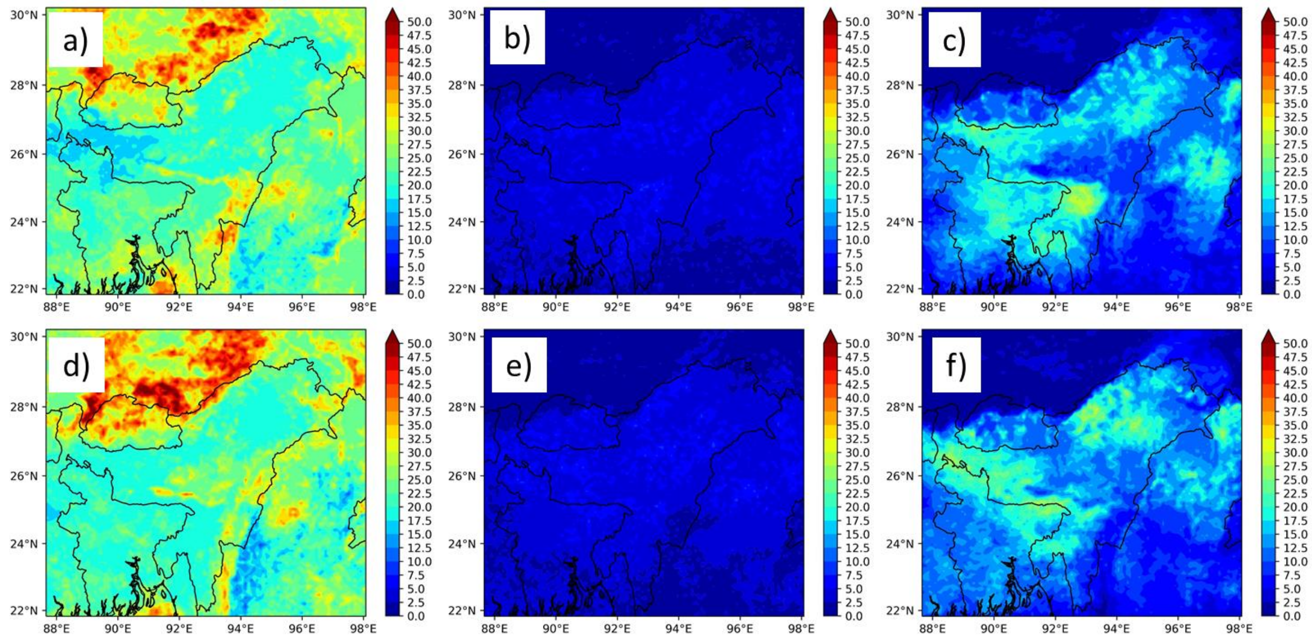

Figure 3.11: Spatial distributions of percentage of time aerosols increase a) low b) medium c) high-intensity rainfall and decrease d) low e) medium f) high-intensity rainfall

Moderate-intensity rainfall was the least affected. The definition of low (<5 mm day^{-1}), medium (5-10 mm day^{-1}) and high-intensity (≥ 10 mm day^{-1}) rainfall are based on Raju et al. (2015). The regional average across all intensities implied suppression to be dominating. The regional average across intensities of suppression: 22.25% (low), 4.00% (medium) and 14.63% (high) and enhancement: 21.05% (low), 3.79% (medium) and 14.32% (high). Thus, rainfall suppression occurred more amount of the time compared to enhancement in most of the region across all rainfall intensities.

3.3.3 Comparison with observations

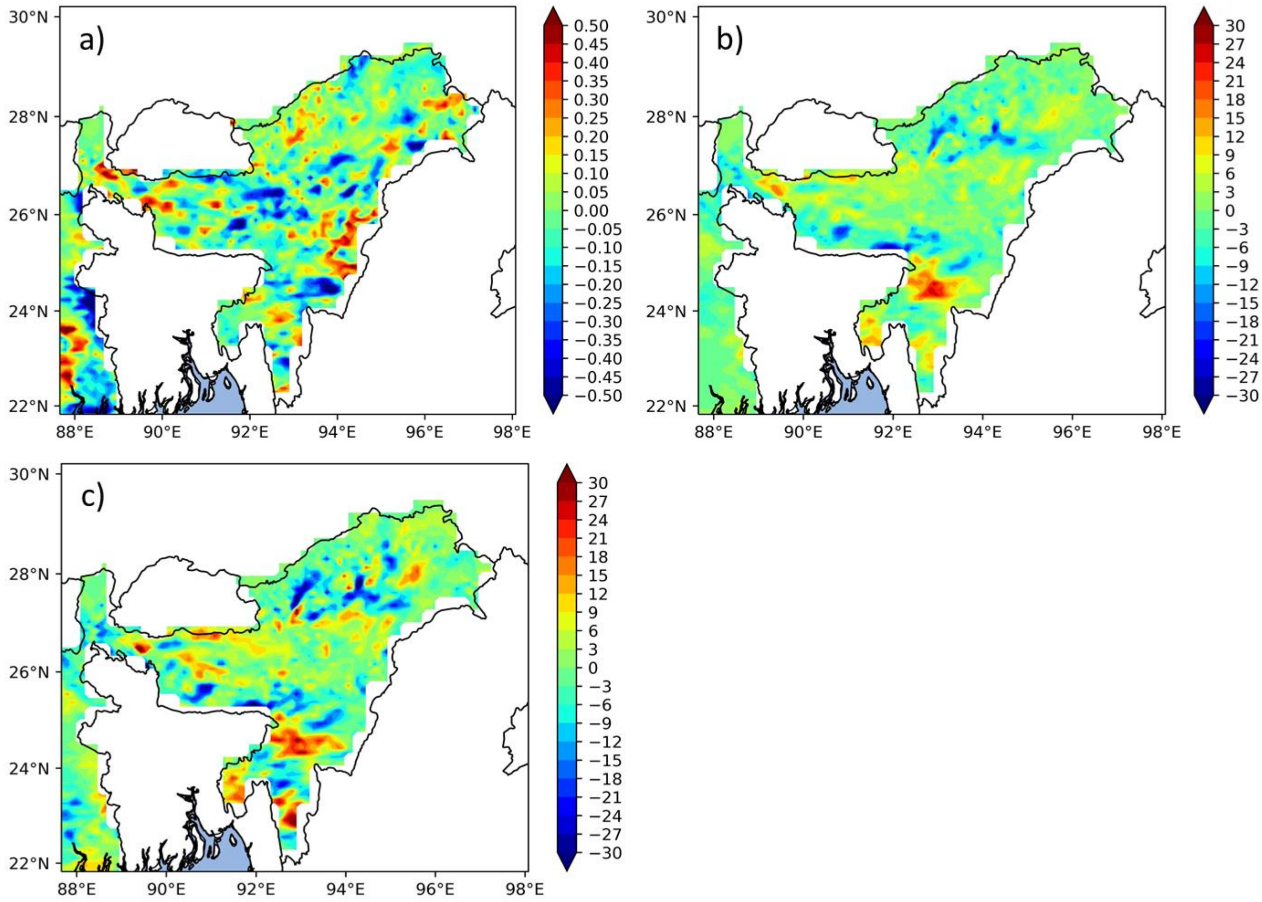

Figure 3.12: Spatial differences of (a) IOA (b) ME (mm day^{-1}) and (c) RMSE (mm day^{-1}), estimated from the difference in model performance statistics of NOR and NOFEED simulations

But was the rainfall enhancement or suppression due to aerosol feedback an actual process, or was it just a model-simulated outcome? Figure 3.12 shows the difference in performance statistics of IOA, ME and RMSE. These statistics were estimated for both NOR and NOFEED simulations by comparing against the IMD dataset and then spatially subtracting them (NOR statistics -NOFEED statistics) over the region shown in the figure. At the locations where performance had improved (IOA change >0 and RMSE change <0), the mean difference from these locations (negative at 829 and positive at 190 grid points) came out as -3.88 mm day^{-1} per grid point. Similarly, at the locations where performance had reduced (IOA change <0 and RMSE change >0), the calculated mean difference from these locations (negative at 245 and positive at 929 grid points) came out as 3.63 mm day^{-1} per grid point. This shows that aerosol feedback in the NOR simulation, which represents the natural atmospheric state suppressed rainfall at locations with improved performance but overestimated rainfall at locations with degraded performance. For further verification, grid points were selected based on 50th, 75th, 90th and 95th percentile criteria values of IOA and 50th, 25th, 10th and 5th percentile values of RMSE. Table 3.4 shows the number of grid points that fulfil both the criteria and where the difference between NOR-NOFEED rainfall is >0 or <0. Values in brackets show criteria RMSE percentile values.

Table 3.4: Rainfall difference and grid points based on criteria

Percentile	**50(50)**		**75(25)**		**90(10)**		**95(5)**	
	NOR	NOFEED	NOR	NOFEED	NOR	NOFEED	NOR	NOFEED
No. of grid points with difference >0	388	630	123	243	23	74	9	31
No. of grid points with difference <0	531	430	196	83	51	16	23	6
Difference (mm day^{-1})	-0.97	1.99	-1.27	2.45	-1.40	3.12	-1.92	3.15

For the NOR column, percentile values were first estimated from evaluated statistics for NOR rainfall (IOA and RMSE). Then the rainfall data from the corresponding grid points of NOR and NOFEED qualifying the percentile criteria (IOA and RMSE should be higher and lower, respectively than the corresponding percentile value) were extracted and mean rainfall difference from those selected grid points data were estimated. A similar procedure for NOFEED column, but evaluated statistics were read from NOFEED. The number of selected grid points is small as it must satisfy both the IOA and RMSE criteria simultaneously. The mean rainfall differences for NOR with respect to 50^{th}, 75^{th}, 90^{th} and 95^{th} percentile is -0.97, -1.27, -1.40 and -1.92 mm day^{-1}, shown in Table 3.4. Thus, out of the grid points falling into the criteria, rainfall suppression was seen at most of them for NOR, which contributes to the overall difference and this is the same among all the criteria. It is seen that aerosol feedback mostly suppressed rainfall on average. However, this does not mean that rainfall suppression or enhancement may not have occurred at other locations, but the model was unable to simulate rainfall with adequate accuracy at those locations with aerosol feedbacks incorporated, which is the natural and real atmospheric condition. It is seen that the number of grid points with a difference >0 was more in NOFEED in all criteria and the rainfall difference was positive. Thus, NOR overestimated rainfall at poorly performing locations. With the increase in the strictness of criteria from 50^{th} to 95^{th} percentile, the mean rainfall difference in NOR consistently increased, which verified that better-performing locations indeed had rainfall suppression. Thus, this analysis supports what was observed in the previous analysis that aerosols suppress rainfall at most of the region since most of the grid points qualifying the criteria show suppression. This also shows that depending on the location, aerosol feedback may induce errors by high-intensity rainfall. Figure 3.12 also shows that large rainfall errors may be involved in the southern region and hence rainfall suppression may be even more dominant.

3.3.4 Rainfall suppression and enhancement analysis

The NE India region has been divided into four regions for analysis: west (region 1), east (region 2), north and north-east (region 3) and south (region 4), which is shown in Figure 3.13(e). Figure 3.13 shows the changes in cloud fraction, cloud droplet number and water vapor mixing ratio due to radiative effects, estimated from NOR-NOFEED.

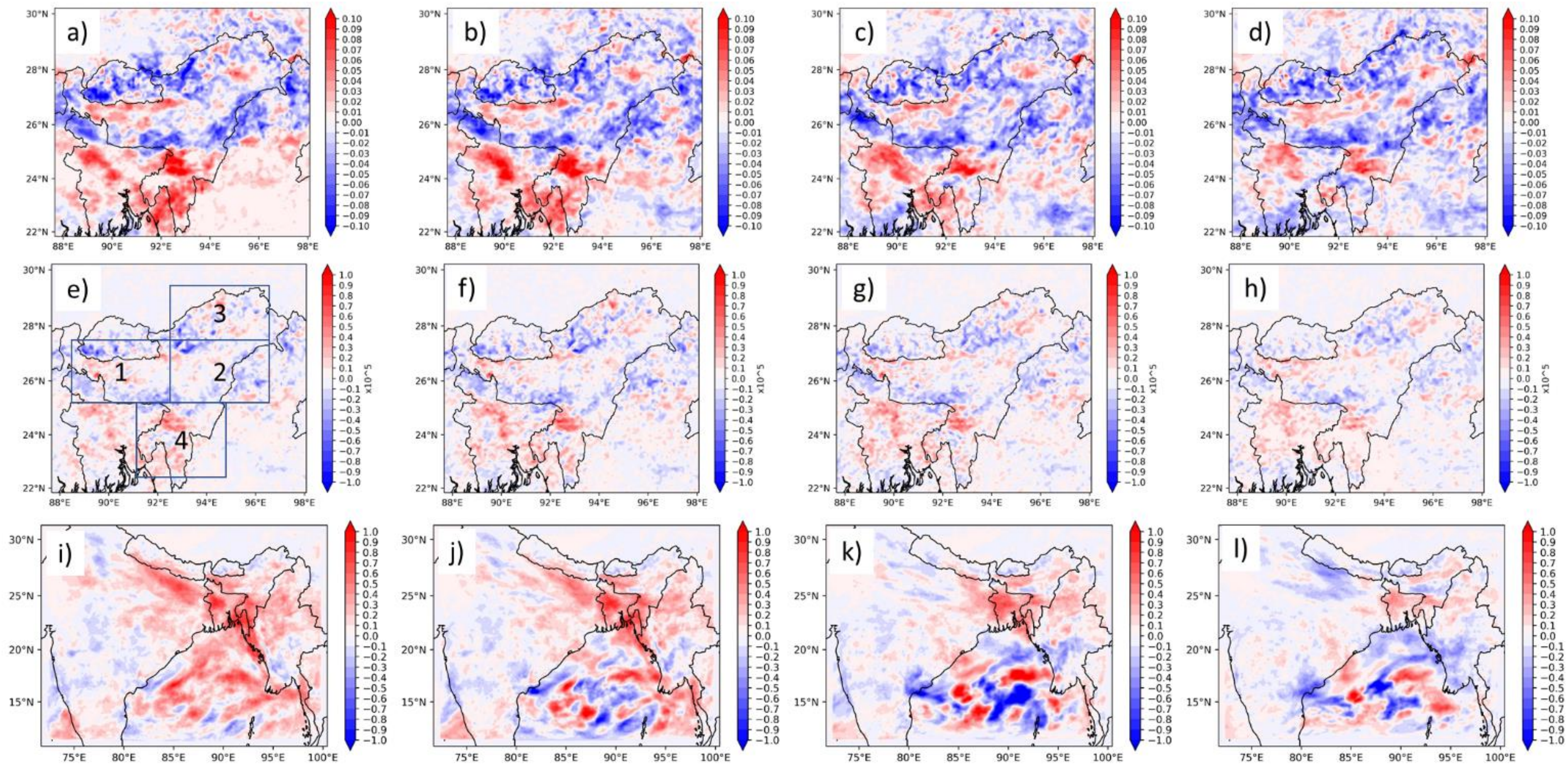

Figure 3.13: Spatial distributions of difference in cloud fraction (a, b, c, d), cloud droplet number (e, f, g, h) in # kg^{-1} and water vapor mixing ratio (i, j, k, l) in g kg^{-1} between NOR and NOFEED simulations. Figures in each column are at the same model. Height increases from left to right in each row, given in Figure 3.14.

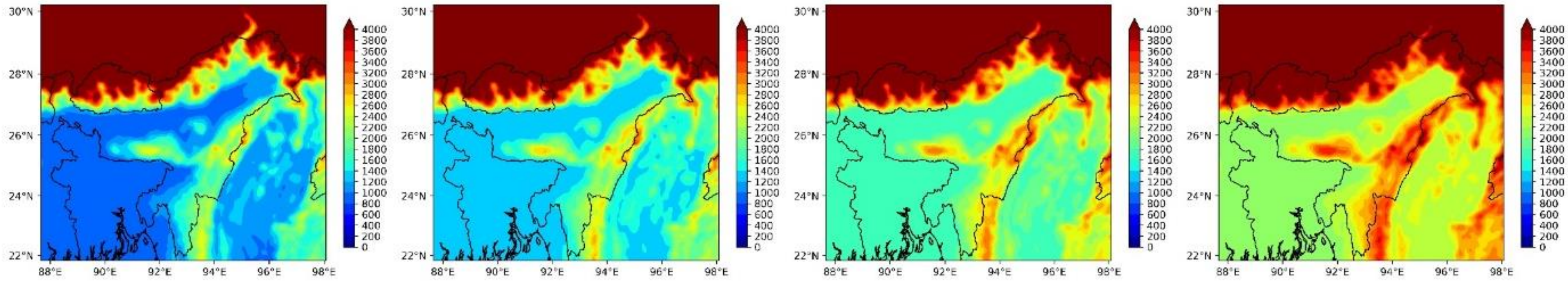

Figure 3.14: Spatial distributions of geopotential heights (m) of model levels at levels =11, 13, 15 and 17 (from left to right)

The spatial distributions of increase and decrease in cloud fraction matched the spatial distribution of total rainfall in Figure 3.10. This shows that rainfall changes are related to cloud cover changes. This is further verified by the spatial distribution of cloud droplet number concentration changes, matching with rainfall and cloud fraction distributions. Thus, the aerosol radiative feedback influenced the cloud microphysical processes. The southern region shows large increases in water vapor, cloud fraction and cloud droplets which also relates to the large increase in rainfall of 26.47%. A decrease in water vapor is seen over the higher terrain areas, which also shows a decrease in clouds, rainfall and cloud droplets. This relates water vapor changes to cloud and rainfall changes. The wind flow pattern has been discussed in Section 3.3.1, in which near-surface winds flow from over the Bay of Bengal but gradually change to the west with increasing height. Aerosols effects cause more moisture inflow at lower heights into NE India from the Bay of Bengal, causing an increase in moisture, while moisture decreases with increasing height and at higher terrain, as seen from Figures 3.13(i, j, k, l). This may again be verified from the cross-sectional profiles of water vapor mixing ratio change in Figure 3.15, which shows moisture increase below 2000 m and decrease above it. Thus, these changes in moisture w.r.t altitude explain the terrain-wise changes in cloud cover and rainfall. Soni et al. (2018) observed that atmospheric heating due to BC leads to stronger meridional winds, which bring more moisture from the Bay of Bengal during pre-monsoon. Dahutia et al. (2018) also observed that there had been a decrease in moisture in the region, which has led to cloud reduction.

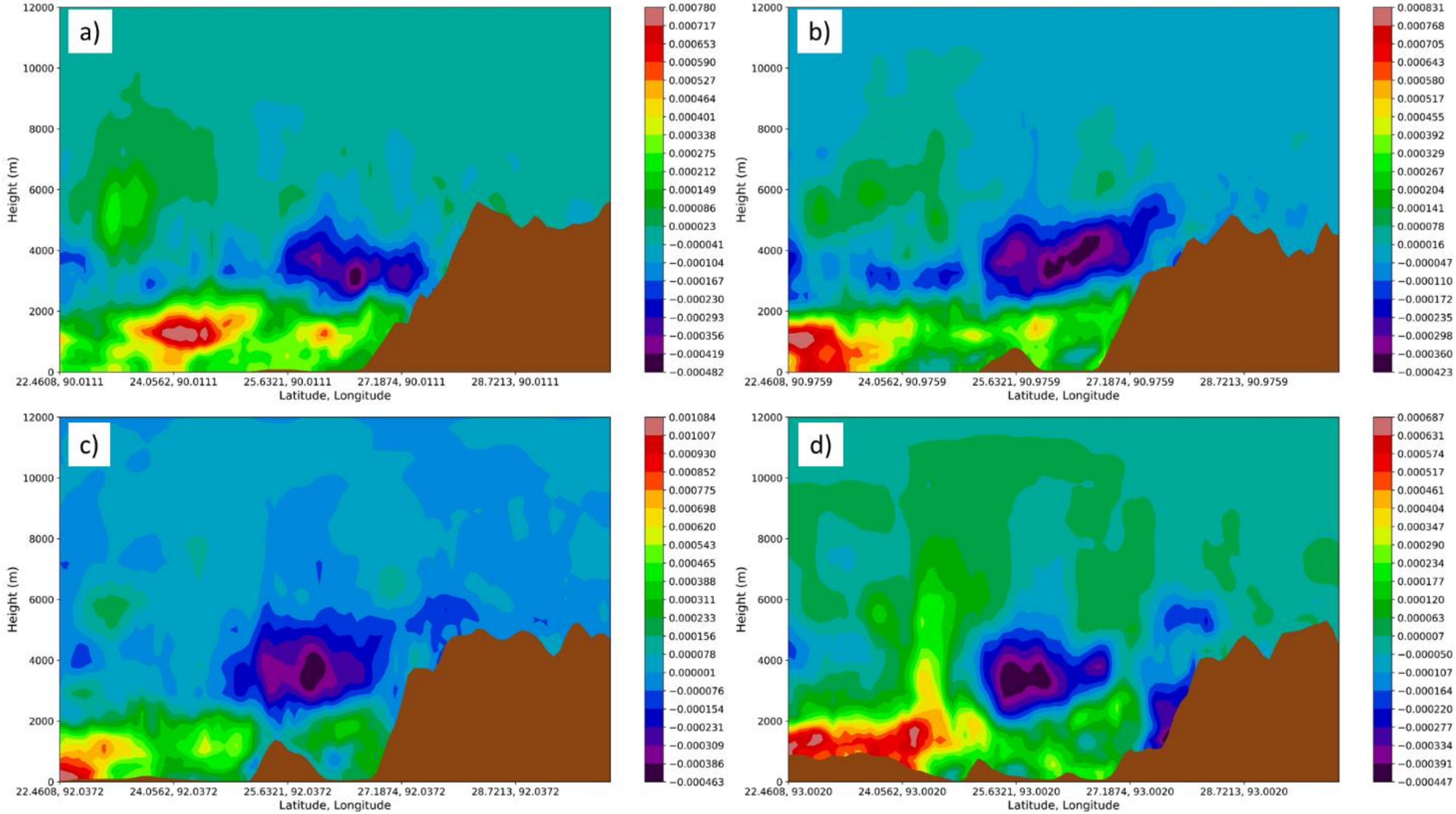

Figure 3.15: Vertical cross-sectional profiles of water vapor mixing ratio (kg kg^{-1}) change between 22.5° and 30° N latitudes and along a) 90° E b) 91° E c) 92° E d) 93° E longitudes

The region-wise quantitative values of short-wave radiation changes are shown in Table 3.5. For the NOR-NOFEED column, radiation changes due to only aerosols were estimated from NOR_{SWDBNC} – $NOFEED_{SWDBNC}$ and also similar for other scenarios. SWDNBC model variables represent clear sky radiation without clouds. Aerosols radiative feedback also caused a reduction in surface incident solar radiation across all regions due to scattering and absorption with a regional mean of -28.22 W m^{-2}, as shown in Table 3.15. With the increase in emissions, radiation values decrease continuously from -11.85 to -32.29 W m^{-2} for region 1 due to increased scattering and absorption and vary similarly for other regions. Radiation reduction is more in the NOR-NOFEED scenario as it includes radiative feedback from all aerosols. This led to decreased sensible heat fluxes and surface evaporation, which may be verified by Figure 3.16.

Table 3.5: Average region-wise change in surface short-wave radiation (W m^{-2}) aerosol radiative feedback and BC absorption

Region	NOR-NOFEED	NOR-NO_BC_ABS	2NOR-NO_BC_ABS	4NOR-NO_BC_ABS
Region 1	-32.69	-11.85	-20.87	-32.29
Region 2	-30.52	-10.74	-19.50	-30.08
Region 3	-18.47	-5.77	-10.57	-15.38
Region 4	-31.21	-10.82	-20.31	-29.00
Mean	-28.22	-9.80	-17.81	-26.69

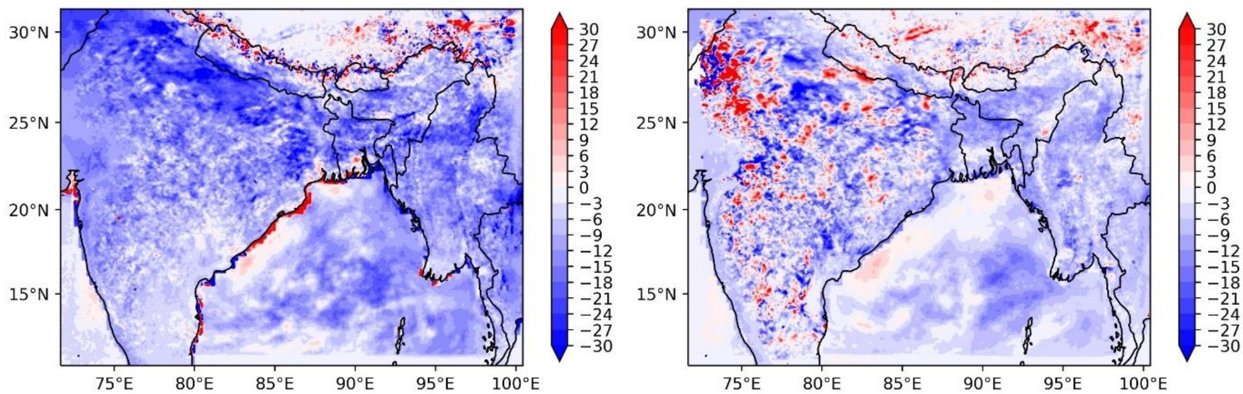

Figure 3.16: Spatial distribution of percentage change in sensible heat flux (left) and upward surface moisture flux (right)

The higher atmospheric level flow over NE India was from the western direction and a simultaneous decrease in moisture was seen over NE India and the western region of NE India, as was seen in Figures 3.13(i, j, k, l). Thus, a decrease in upper-level moisture due to a reduction in surface moisture beyond the west of NE India contributes to a decrease of moisture between 2000 and 4000 m over NE India, which affects the rainfall and clouds over higher terrain areas. High correlation values between cloud fraction and water vapor mixing or moisture at higher altitudes and terrain areas of NE India exist, as shown in Figure 3.17, which also relate the two parameters. Reduction in moisture above 2000 m led to a decrease in clouds and NCR over higher terrain as the Morrison scheme, which is responsible for the NCR, is dependent on moisture availability (Morrison et al., 2009). Moreover, as seen in section 3.3.2, NCR was more dominant, as well as the more affected rainfall.

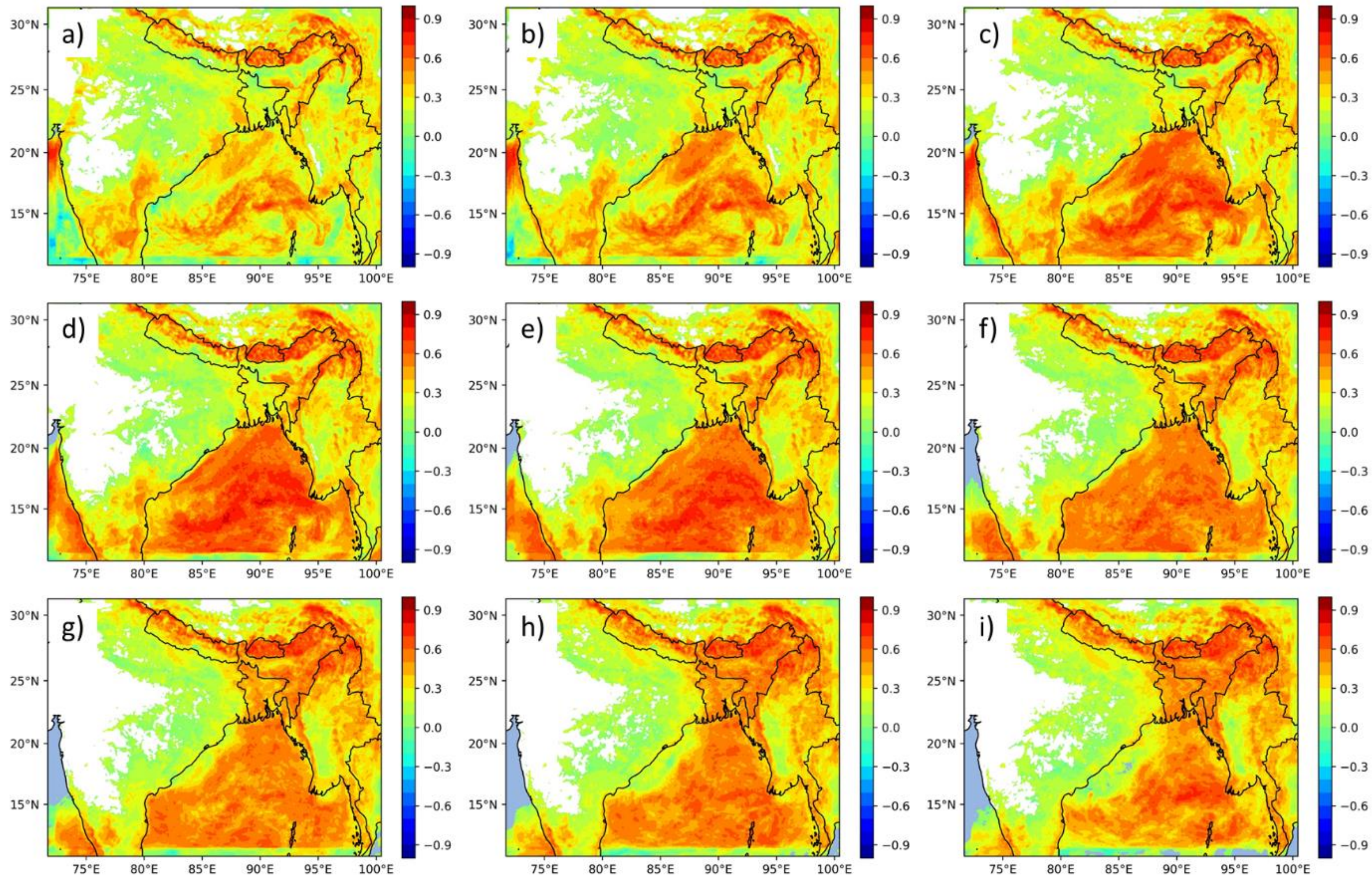

Figure 3.17: Spatial distributions of the correlation coefficient between cloud fraction and water vapor mixing ratio from model level = 6 to 14 shown from figure a to i. Geopotential heights of model levels are provided in Figure 3.18.

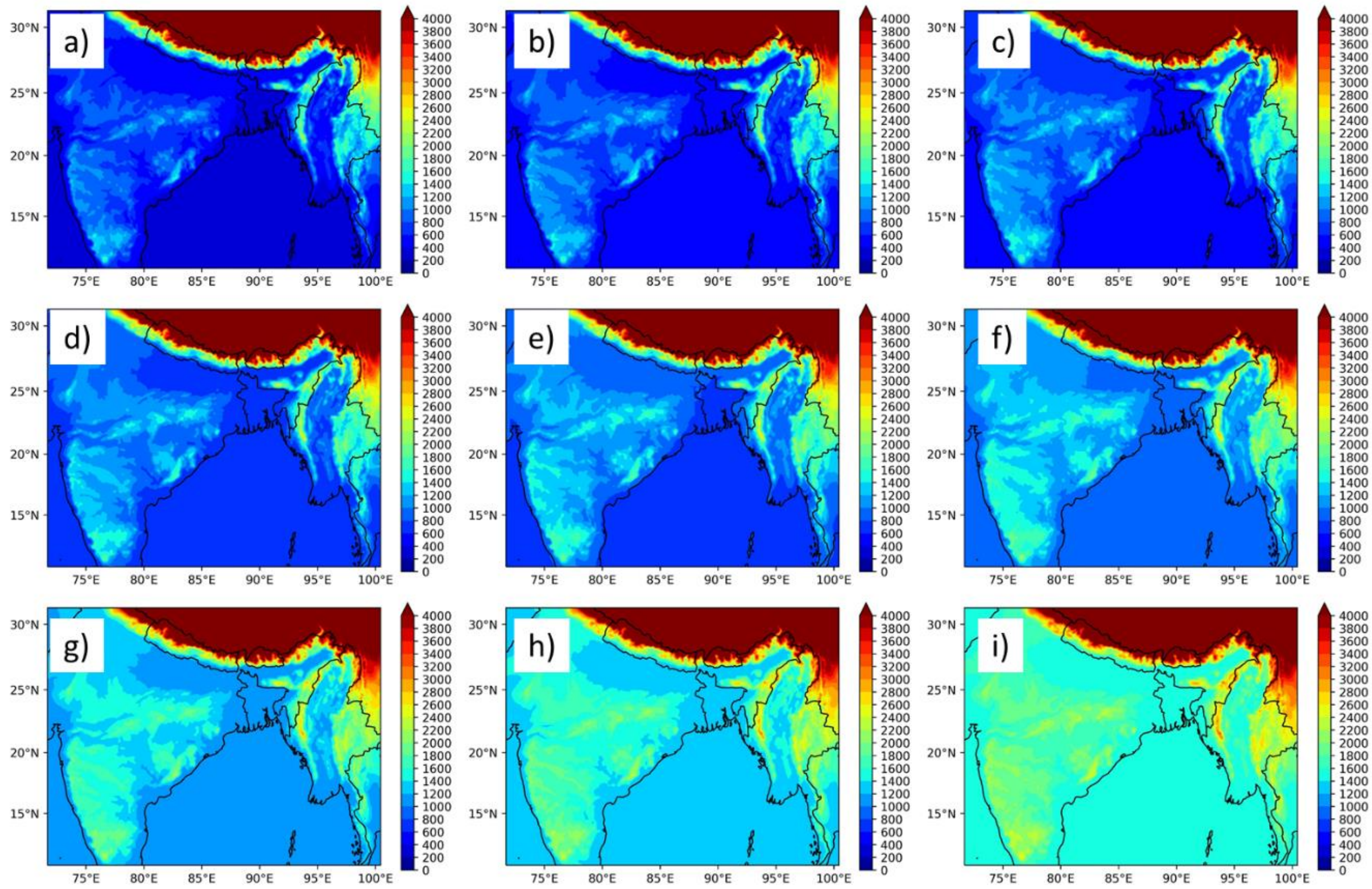

Figure 3.18: Spatial distributions of geopotential heights from model level = 6 to 14 shown from figure a to i

The cross-section profile of temperature change between 22.46° and 30° N latitudes and along the 92.03° E longitude due to radiative feedbacks in Figure 3.19 shows the presence of a layered temperature profile, with temperature increases and decreases occurring alternately. Similar profiles also exist along other longitudes within NE India (figures not shown).

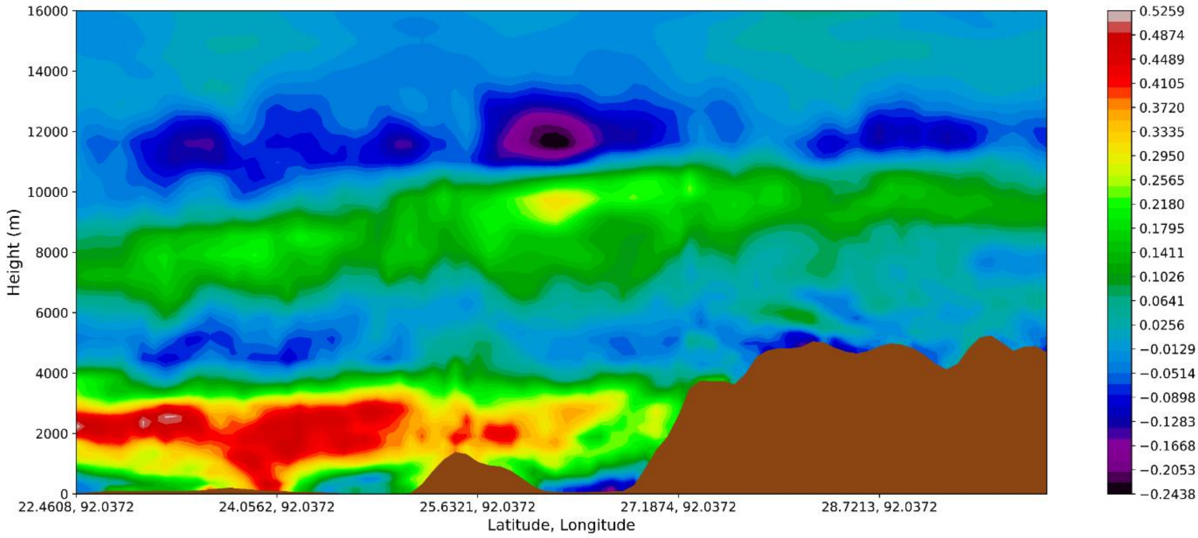

Figure 3.19: Vertical cross-sectional profile of difference in temperature (K) between NOR and NOFEED simulations between 22.46 ° N and 30.0° N latitude and along 92.03° E longitude

Elevated heating is observed below 4000 m with a maximum regional average (average of region 1, 2, 3 and 4) temperature increase of 0.265 K between 1500-1600 m (hereafter referred to as elevated temperature layer). Another elevated heating layer is observed between 6000 m and 10000 m, though its magnitude of temperature increase is less. This heating is due to the presence of absorptive aerosols like BC and dust. Figures 3.20 and 3.21 show cross-sectional profiles of BC and dust concentration between 22.46° and 30° N latitudes and along the 92.03° E longitude.

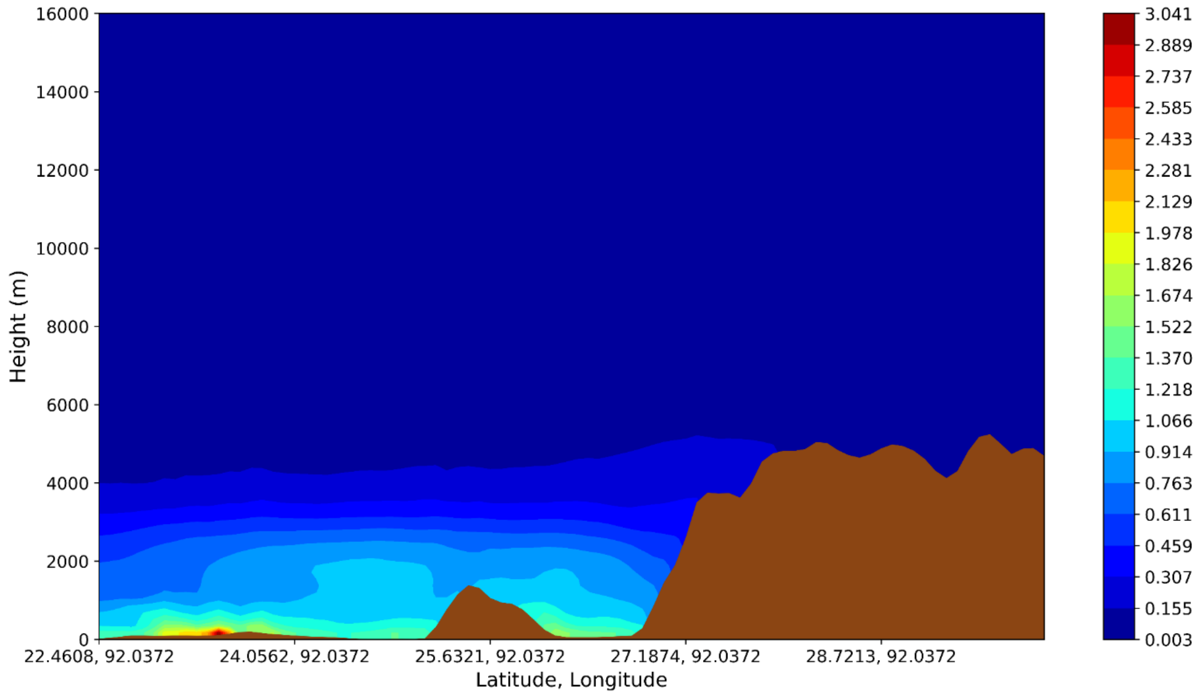

Figure 3.20: Vertical cross-sectional profile of black carbon concentration (μg m^{-3}) between 22.46° and 30.0° N latitudes and along 92.03° E longitude

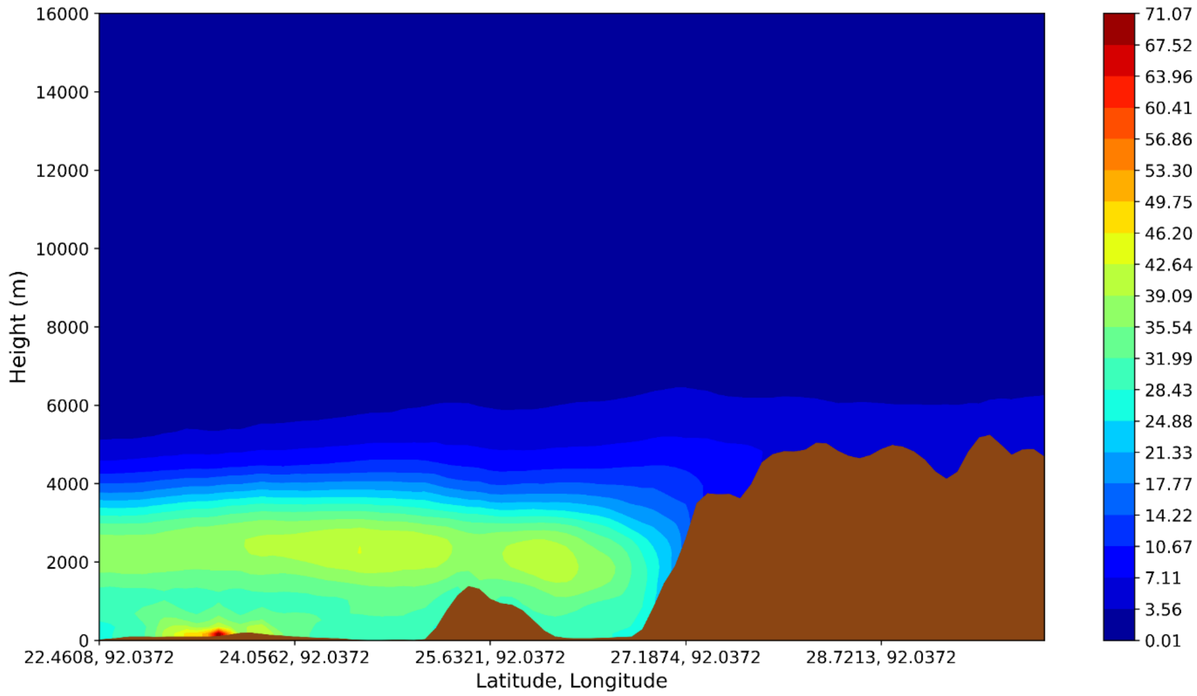

Figure 3.21: Vertical cross-sectional profile of dust concentration (μg m^{-3}) between 22.46° and 30.0° N latitudes and along 92.03° E longitude

Dust had an elevated concentration profile similar, while BC was more concentrated near the surface. Even though BC does not show an elevated concentration profile similar to the dust profile, the similarity between NOR-NOFEED and NOR-NO_BC_ABS profiles below 2000 m in Figure 3.22(a) shows that lower atmosphere heating is mostly contributed by BC and is mostly responsible for the elevated temperature layer.

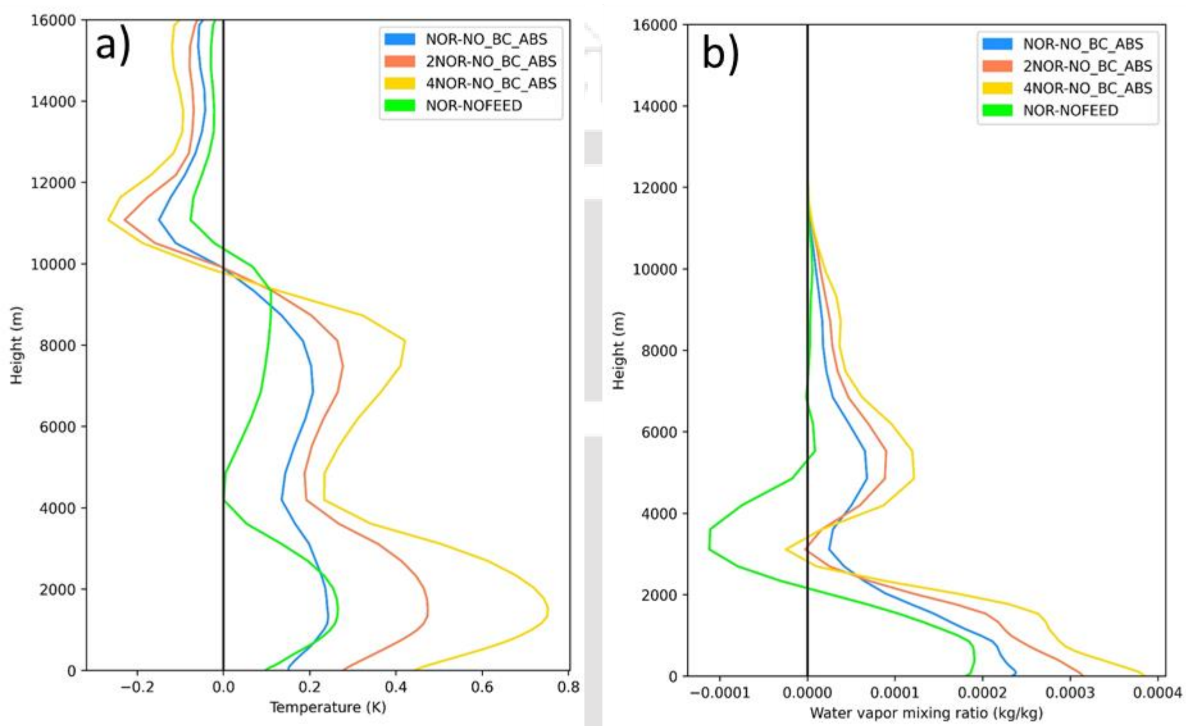

Figure 3.22: Regionally averaged vertical profiles of a) temperature change b) water vapor mixing ratio change, estimated from different simulation combinations

Similar profiles can also be seen for 2NOR-NO_BC_ABS and 4NOR-NO_BC_ABS in Figure 3.22(a), which shows increasing atmospheric heating with increasing emissions of BC. Several studies (Ding et al., 2016; Dong et al., 2017; Wang et al., 2018; Su et al., 2020) have shown that BC is more efficient at absorbing solar radiation and subsequent heating at a higher height, and this can stabilize the atmosphere below leading to increased atmospheric stability and decreased convection and buoyancy for rising of moist air parcel (Koch and Del Genio, 2010; Lohmann and Feichter, 2001; Talukdar et al., 2019). Hence, such elevated heating due to BC can lead to an inversion condition, resulting in increased atmospheric stability and decreased convection. Hence, 2NOR and 4NOR may have an even more stable atmosphere near to the surface compared to NOR. However, considering the whole atmospheric column Figure 3.22(a) showed cooling above 10000 m while heating below it. This is likely to make the atmosphere below 10000 m more unstable, which will facilitate more moisture influx and hence more moisture in the region, as in Figure 3.22(b). With the increase in heating due to an increase in emissions, moisture increase below 2000 m is also seen, which linearly decreases immediately above it between 2000 and 4000 m. This may be due to the increase in atmospheric stability due to the increase in the temperature of the elevated temperature layer, leading to the entrapment of moisture below it. The elevated temperature layer possibly acts as a barrier, restricting upward vertical movement of moisture and thus, moisture decreases immediately above it. With increasing emissions, the moisture profiles also show linearly increasing nature above 4000 m. The decrease between 2000 m and 4000 m and increase above it may also be due to an increased temperature below 2000 m which induces increased instability above it, transferring moisture between 2000 to 4000 m to the upper atmosphere, as can be seen from Figure 3.15 and Figure 3.22(b). Moreover, the increasing BC emissions may have caused increasing surface dimming over the western regions of NE India which also contributed to moisture reduction between 2000 to 4000 m. In addition, reduction in short-wave radiation due to surface dimming and absorption by BC (Ramanathan et al., 2005; Shiogama et al., 2010; Soni et al., 2017), which causes a reduction in sensible heat flux, surface evaporation, turbulence and convection (Yu et al., 2002; Li et al., 2017). This increased atmospheric stability causes a reduction of convective clouds (Habib et al., 2006; Rosenfeld et al., 2008; Gautam et al., 2011; Bollasina et al., 2011; Cherian et al., 2013; Kedia et al., 2014; Kedia et al., 2018). This caused suppression of CR, as CR simulated by the Grell-Freitas scheme is triggered by atmospheric instability (Grell and Freitas, 2014).

However, cloud fraction enhancement was seen at the lower model heights over low terrain areas, especially along the valley, as seen in Figures 3.13(a, b, c, d) where moisture had also increased. Hence, the accumulation of moisture possibly leads to increased clouds and rainfall at lower terrain areas, and hence moisture reduction above 2000 m over lower terrain areas will have a lower effect on rainfall than over higher terrain since most of the rain-forming clouds exist at around 1 km altitude. This can be verified from the regionally averaged vertical profiles of rainwater mixing ratio and cloud fraction in Figures 3.23(a) and 3.23(b), respectively. The increased moisture, especially over lower terrain, leads to increased low-level cloud fraction, especially over these areas.

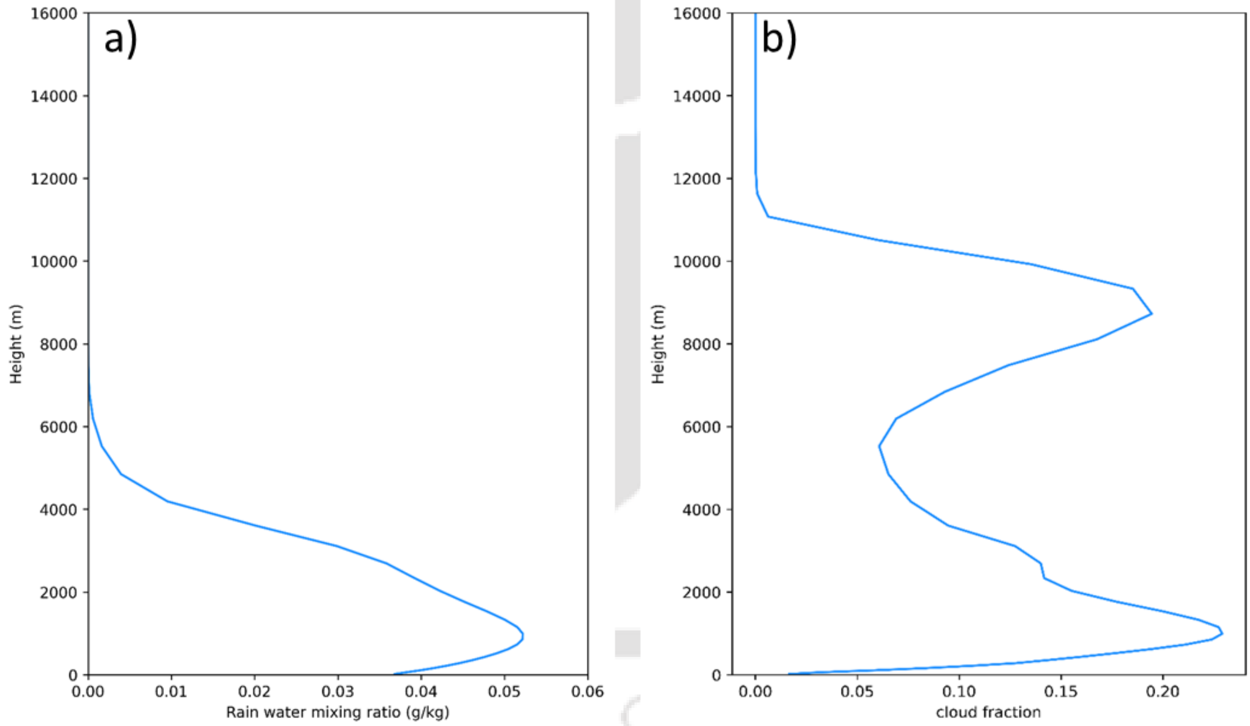

Figure 3.23: Regionally averaged vertical profile of a) rainwater mixing ratio b) cloud fraction from NOR

The question remains, however, if atmospheric heating has any role to play in cloud reduction and rainfall suppression through semi-direct effect. Also, as seen from Figure 3.13, cloud fraction had also reduced at a few low terrain locations, including region 1, although water vapor had increased. This also indicates other processes to be active.

3.3.5 Effect of black carbon absorption

3.3.5.1 Radiation and cloud cover

Table 3.6: Average region-wise change in short-wave radiation due to clouds (W m^{-2})

Region	NOR-NOFEED	NOR-NO_BC_ABS	2NOR-NO_BC_ABS	4NOR-NO_BC_ABS
Region 1	14.79	0.81	10.81	16.48
Region 2	17.09	2.14	4.52	6.06
Region 3	10.94	1.58	2.54	5.61
Region 4	6.87	-5.34	-4.69	3.54
Mean	12.42	-0.20	3.30	7.92

For the NOR-NOFEED column, short-wave radiation changes due to only cloud cover changes were estimated from $NOR_{SWDNBC-SWDNB}$ – $NOFEED_{SWDNBC-SWDNB}$ and accordingly for the other columns. SWDNBC variable was defined before. SWDNB variable represents all-sky radiation with both aerosols and clouds. Aerosol radiative feedbacks also cause a reduction in clouds across all regions, as seen from the positive short-wave radiation values in Table 3.6. Maximum radiation increase is seen in region 2 with a radiation change of 17.09 W m^{-2}. With the increase in BC emissions, a continuous increase in cloud-induced short-wave radiation is seen across all regions, with the maximum increase in region 1. This makes region 1 the most radiatively affected region by BC. Also, maximum suppression of CR rainfall was observed in this region in Figure 3.10(d). This is possibly due to the close proximity with IGP. Dahutia et al. (2018) found the western region of NE India to be most influenced by aerosols due to close proximity to the IGP. Gogoi et al. (2017) found the western NE India region to have the highest radiative forcing due to fossil fuel burning in the IGP. The combined forcing due to aerosol or BC in Table 3.5 and clouds in Table 3.6 across all regions and simulation combinations will come out as negative, indicating increasing surface cooling. For NOR-NOFEED, the regional mean value is -15.79 W m^{-2}. However, the increased short-wave radiation due to cloud fraction reduction may not reach the surface but rather be scattered and absorbed due to increasing BC mass in the atmosphere as a result of increasing emissions. As a result, the increased absorption induces increased atmospheric temperature, as was seen in Figure 3.22(a). The mean temperature increases up to 4 km are 0.20 K, 0.38 K and 0.60 K for NOR-NO_BC_ABS, 2NOR-NO_BC_ABS and 4NOR-NO_BC_ABS, respectively.

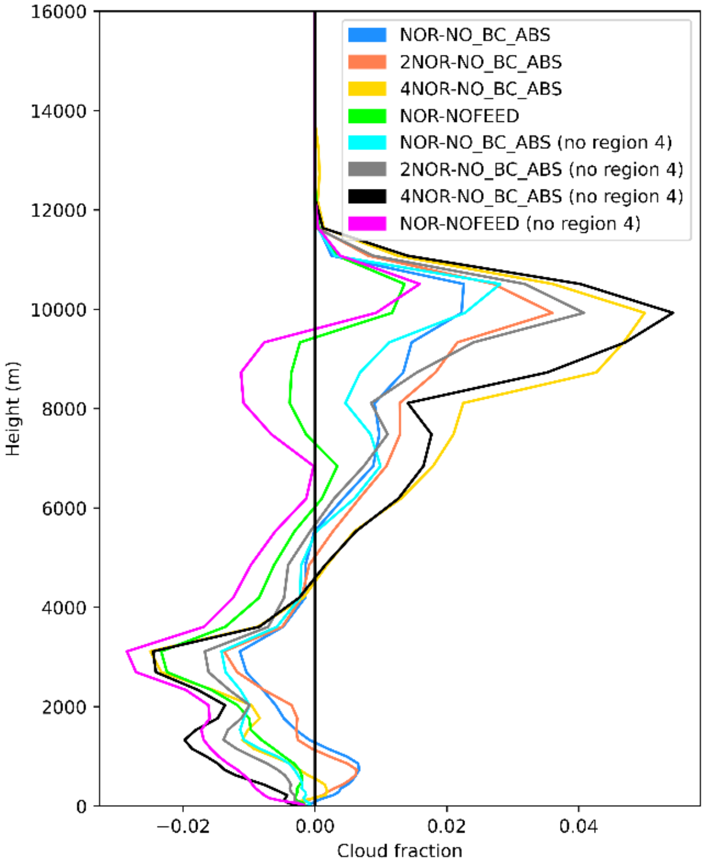

Figure 3.24: Regionally averaged vertical profiles of perturbations in cloud fraction estimated from different simulation combinations

Figure 3.24 shows the NE India regionally averaged vertical cloud fraction perturbation profiles over NE India, both including and excluding region 4. The profiles also show the cloud response to emission changes. An overall decrease in clouds over region is evident in the entire column below 4000 m for the profiles not containing region 4 while vice versa above it. With region 4 included, an increase up to around 1500 m is seen, which is entirely contributed by the southern region, where a significant cloud fraction increase was seen. However, negative values below 1000 m for the profiles not including region 4 are influenced and contributed by higher terrain areas due to the terrain-following nature of the model levels. Thus, the exclusion of the high terrain areas on the northern boundary of region 1 shows an increase below 1000 m (Figure 3.25), which matches with the previous analysis of cloud increase at lower levels in Figures 3.13(a, b, c, d), especially over region 1 while decrease between approximately 1000m and 2000 m.

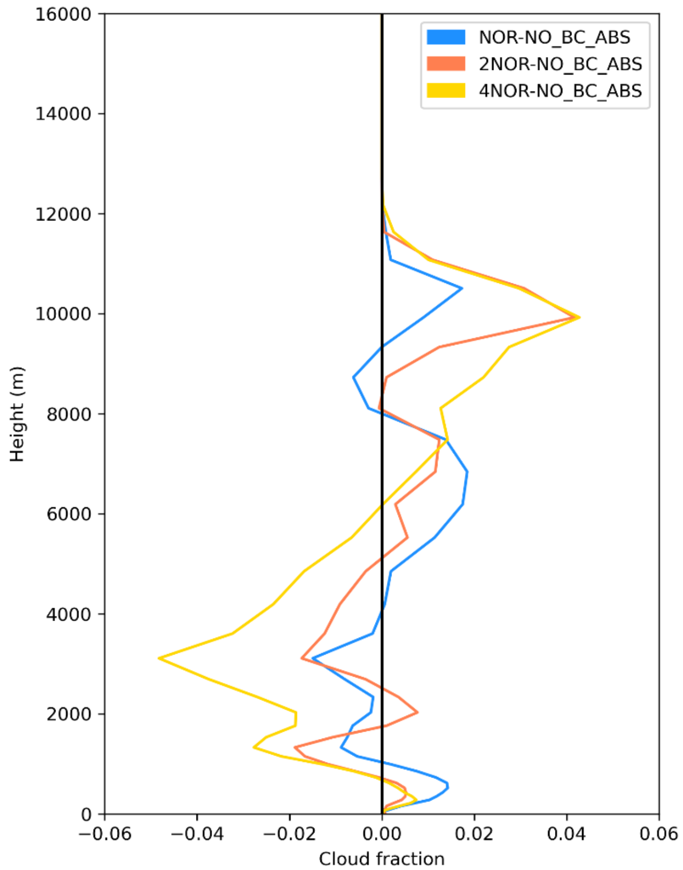

Figure 3.25: Regionally averaged vertical profiles of perturbations in cloud fraction estimated from different simulation combinations in region 1

Thus, the profile also depends on the terrain. However, approximately above 4000 m, an increase in cloud fraction is seen in both figures and is maximum near 10000 m. Also, if the NOR-NO_BC_ABS, 2NOR-NO_BC_ABS and 4NOR-NO_BC_ABS profiles are compared, a linear response of cloud fraction change with emission change is observed, though with opposite nature. Profiles with higher BC emissions show more negative and more positive cloud fraction change below and above 4000 m, respectively. Higher BC heating with higher emissions may be responsible for this. The reason may be due to the transfer of moisture between 2000 m and 4000 m to a higher atmosphere or a decrease in moisture, as discussed before. This was also observed by Koch and Del Genio (2010) and Sarangi et al. (2015) and is due to higher instability in the lower atmosphere causing higher moisture transport to the upper atmosphere and conversion of it to ice-phase hydrometeors which is the constituent of high-level clouds or cirrus clouds. An increase in ice-phase hydrometeor is seen in Figure 3.26, which relates to the finding.

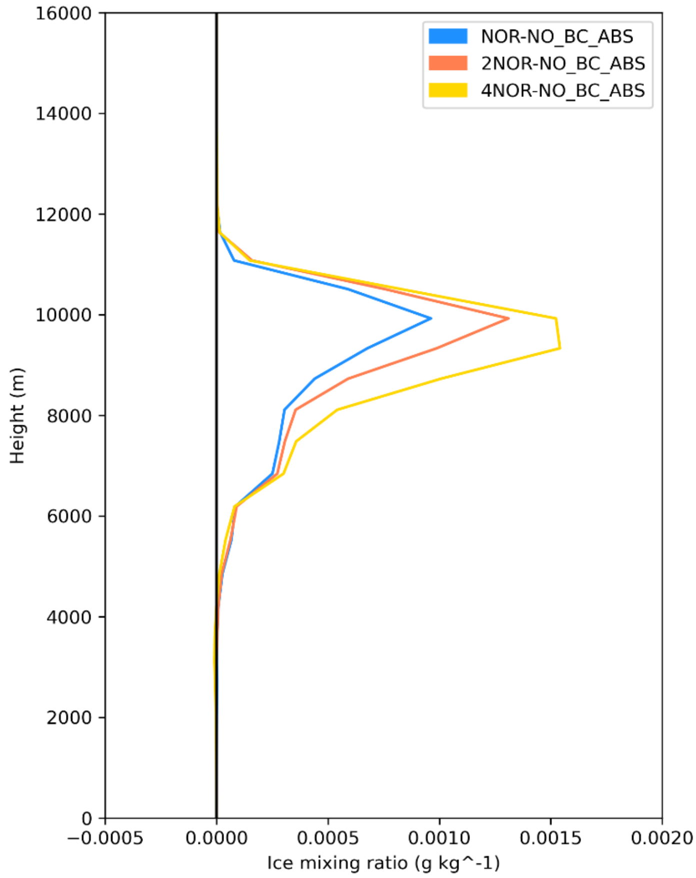

Figure 3.26: Regionally averaged vertical profile of ice-hydrometeor (g kg^{-1})

These cirrus clouds do not affect short-wave radiation as these clouds are transparent to it (Katagiri et al., 2013). Hence, an increase in short-wave radiation was seen in Table 3.6 in spite of the increase in high-level clouds and hence cloud induced solar radiation increased over the region with an increase in BC emissions, increasing the availability of more solar radiation to be absorbed. This possibly led to an increase in near-surface temperature, also seen in Chen et al. (2019) and Yang et al. (2019). The increase in high-level clouds may have further climatic implications.

Another important feature is the bimodal nature of the cloud fraction change profiles (without region 4 in Figure 31) below 4000 m, with one of the modes existing below 2000 m and another between 2000 and 4000 m, both modes indicating cloud decrease. The decrease between 2000 and 4000 m is associated with a decrease in moisture, as discussed before. NOR-NOFEED shows the largest decrease as it includes radiative feedback from all aerosols. The highest decrease in moisture in NOR-NOFEED also matched with the highest decrease in clouds between these heights. However, the mode existing below 2000 m shows cloud decrease even though moisture increase was observed at this height which indicates the presence of another influencing factor. The height of the maximum cloud decrease below 2000 m matches with the height of the highest temperature change, and which also corresponds to emission or temperature increase. Thus, semi-direct effect was active between 1000 m and 2000 m as cloud fraction reduction was seen between these heights. Thus, there are two primary factors that influence cloud fraction: moisture and semi-direct effect. Hence, the increase in short-wave radiation due to cloud change was due to cloud reduction due to moisture decrease and semi-direct effect. The higher altitude heating between 1000 and 2000 m, possibly leading to cloud reduction, can further induce an increase in downwelling solar radiation, allowing the lower-level BC aerosols to absorb more radiation and cause even more heating even at the lower levels, as was observed before.

3.3.5.2 Cloud liquid water path and rainfall

This analysis relates cloud changes with the help of CLWP to rainfall changes over the region since rain water is formed from cloud water.

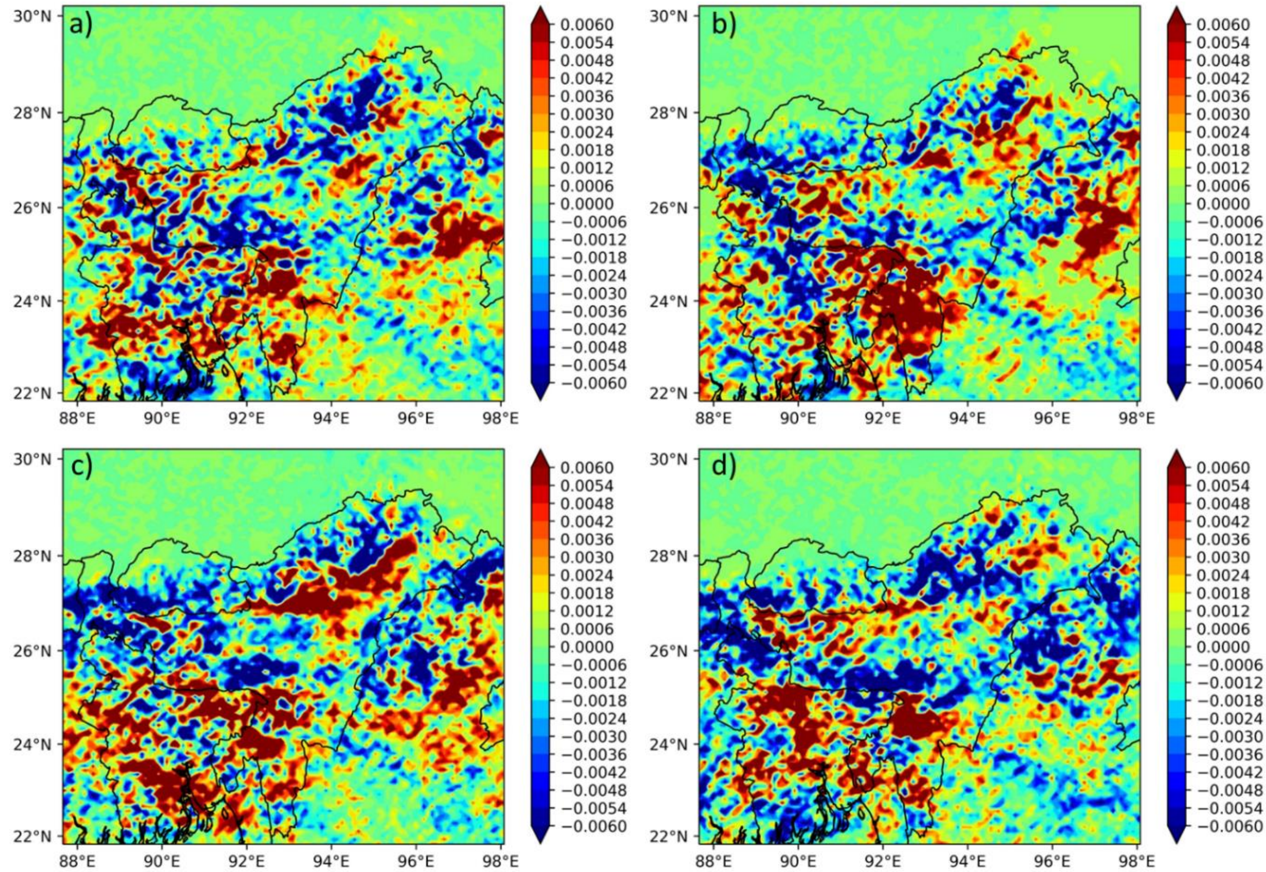

Figure 3.27: Spatial distributions of difference in CLWP (kg m^{-2}) with a) NOR - NO_BC_ABS b) 2NOR - NO_BC_ABS c) 4NOR - NO_BC_ABS d) NOR – NOFEED

Table 3.7: Average region-wise change in cloud liquid water path and rainfall

Region	NOR-NO_BC_ABS	2NOR-NO_BC_ABS	4NOR-NO_BC_ABS
	Cloud liquid water path up to 4 km (kg m^{-2})		
Region 1	-0.0006	-0.0010	-0.0016
Region 2	-0.0007	-0.0005	-0.0007
Region 3	-0.0011	-0.0004	-0.0003
Region 4	0.0017	0.0028	0.0020
	Cloud liquid water path (kg m^{-2}) between 1000 m and 2000 m		
Region 1	-0.0003	-0.00031	-0.0005
Region 2	-0.0003	-0.0002	0.0004
Region 3	-0.0005	-0.0003	-0.0003
Region 4	0.0010	0.0015	0.0012
	Rain water (kg m^{-2}) between 1000 m and 2000 m		
Region 1	-0.0011	-0.0039	-0.0076
Region 2	-0.0027	-0.0026	0.0036
Region 3	-0.0052	-0.0017	0.0036
Region 4	0.0059	0.0103	0.0052
	Rainfall (%)		
Region 1	5.37	2.24	0.92
Region 2	7.72	4.87	17.84
Region 3	1.72	6.68	9.39
Region 4	31.19	40.78	23.98

Figures 3.27(a, b, c) show that with the increase in emissions, the spatial extent and magnitude of negative CLWP values increase (or clouds decrease), but the CLWP decrease was more concentrated over region 1 and the high terrain areas. This may also be seen in Table 3.7, which shows the region-wise average CLWP changes. CLWP was calculated up to 4 km since most of the rainfall was formed within this height, as seen in Figure 3.23(a). Thus, CLWP changes contained the effect of both cloud changes due to moisture and semi-direct effect. Also, region 1 showed the largest decrease in CLWP with increasing BC emissions, ranging from -0.0006 kg m^{-2} to -0.0016 kg m^{-2}. In region 3, opposite distribution is seen due to a drastic increase in clouds at lower terrains. Region 4, shows positive values in all scenarios though decreased in 4NOR-NO_BC_ABS (0.0020 kg m^{-2}) compared to 2NOR-NO_BC_ABS (0.0028 kg m^{-2}). Whether due to moisture reduction or semi-direct effect or both, aerosols lead to CLWP reduction over regions 1, 2 and 3, evident from the negative CLWP under all scenarios.

Higher terrain clouds are mainly affected by moisture while low terrain locations are due to both moisture and semi-direct effect.

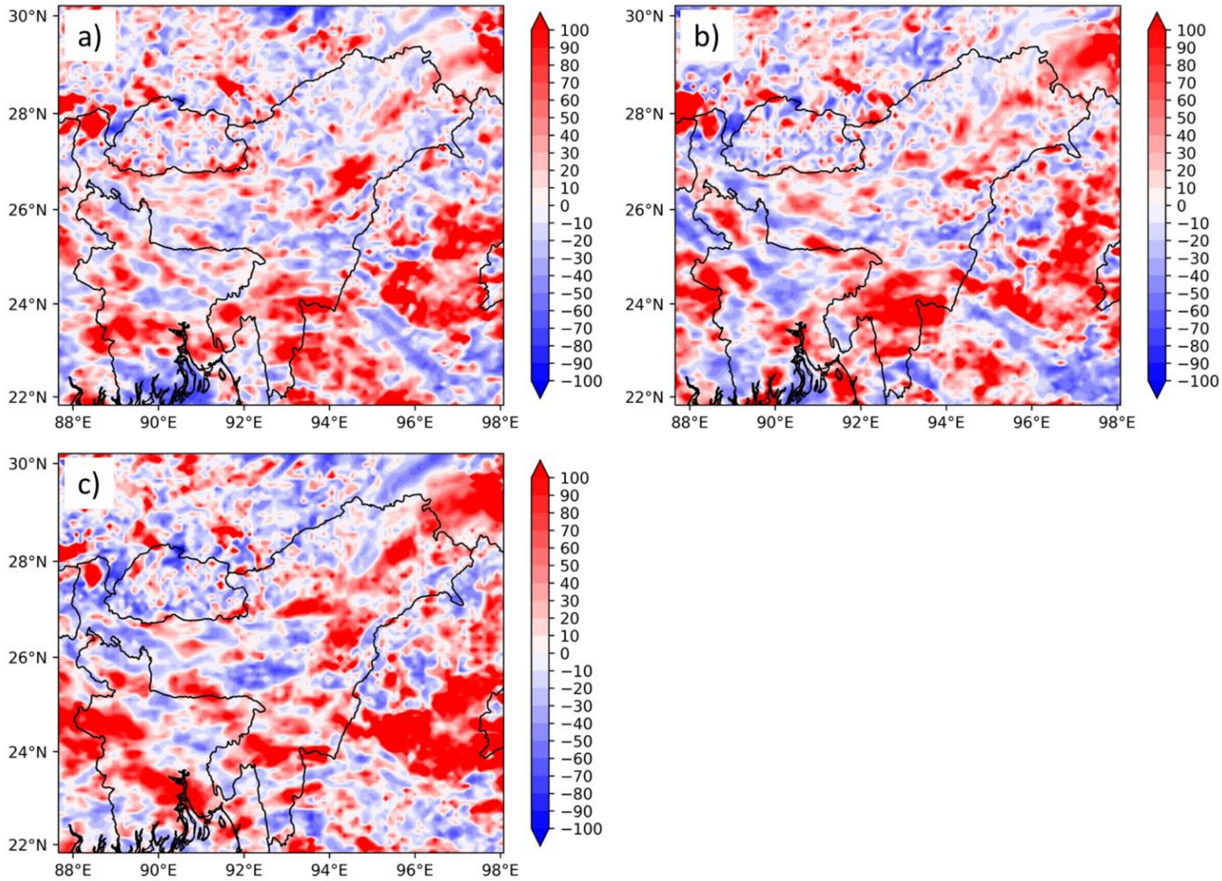

Figure 3.28: Spatial distribution of percentage change in total rainfall with a) NOR - NO_BC_ABS b) 2NOR - NO_BC_ABS c) 4NOR - NO_BC_ABS

The spatial distributions of increases and decreases in CLWP in Figures 3.27(a, b, c) also showed similarity with the corresponding spatial rainfall distribution in Figures 3.28(a, b, c). This shows that an increase or decrease in CLWP also induces similar changes in rainfall. This also proves that BC influences CLWP, which affects rainfall. With the increase in BC emissions, a continuous decrease in the positive value from 5.37 to 0.92% is observed in region 1, which relates well with the continuous decrease in CLWP from -0.0006 to -0.0016 kg m^{-2}. Similarly, region 4 also follows a similar pattern of rainfall and CLWP change. A sudden decrease was seen in both rainfall and CLWP in 4NOR-NO_BC_ABS compared to 2NOR-

NO_BC_ABS in this region. Along with it a drastic increase in cloud-induced solar radiation is seen in Table 3.6. Region 2 and 3 observed increases and became concentrated regions of rainfall and did not show such linear relationships showing the possibility of other processes to be more dominant, or it may be dependent on the spatial extent of the selected region. Since BC evaporates clouds between 1000 m and 2000 m where a sizeable amount of rain was formed, CLWP and rain water produced between these two heights are compared in Table 3.7. CLWP and rain water show close correspondence between them on comparison between NOR-NO_BC_ABS, 2NOR-NO_BC_ABS and 4NOR-NO_BC_ABS, especially over low terrain regions of 1, 2 and 4. Change in CLWP also induces a similar response in the rain water formed between these heights. Also, the percentage rainfall change, shown in Table 3.7 shows similarity with rain water change, especially in regions 1 and 4. Thus, CLWP, rain water and rainfall are possibly related, and hence a decrease in both CLWP and rain water with increasing emissions possibly indicates the effect of semi-direct effect on rainfall formation. BC has been found to decrease CLWP and cloud cover through semi-direct effect in previous studies also (Ackerman et al., 2000; McFarquhar and Wang, 2006; Lindeman et al., 2011; Johnson et al., 2004; Panicker et al., 2014; Hill and Dobbie, 2008; Yoon et al., 2016) and decrease rainfall. Habib et al. (2006) had also found absorbing aerosols to decrease rainfall over eastern India by evaporating clouds. Huang et al. (2014) also found dust-induced heating to cause cloud evaporation and decreased rainfall.

Thus, we can say that there is an interplay between emissions, clouds and rainfall. The increasing emissions lead to an increase in lower-level moisture in all the regions but impact the regions differently. In region 4 where a large rainfall increase is seen due to moisture influx, suddenly rainfall decreased and cloud decrease was also seen. So there exists a threshold emission that impacts that region and influences the rainfall-producing process. The process becomes more clear with further increase in emissions, which is explained in Chapter 5.

3.4 Summary

This simulation study using WRF-Chem examines the aerosol influence on the atmospheric mechanisms responsible for pre-monsoon rainfall over NE India. The study included the radiative effect of all aerosols and the influence of BC absorption on radiation, clouds and rainfall. This is the first of its kind study on atmospheric mechanisms over the NE India region, which also relates clouds and rainfall.

The results showed the prevalence of varied wind flow, which brings moisture into the NE India region from different directions at different atmospheric altitudes that affected the rainfall differently at different terrains heights of the region. Near the surface, wind flows from the south over the Bay of Bengal, while the upper-level flow is from the region west of NE India over the IGP. Aerosol radiative feedbacks tend to increase rainfall, especially over the low terrain areas with a heavy increase on the southern side, while a decrease was observed over the higher terrain. The rainfall suppression dominates over the whole region for more time compared to the enhancement and is seen in both cases of CR and NCR. The increase or decrease in rainfall occurs mainly due to low and high-intensity rainfall. The comparison of the model data with observations also showed the prevalence of rainfall suppression.

The combination of reduced convection, surface evaporation and the presence of a stable atmosphere due to elevated temperature layer leads to the suppression of CR. The atmospheric heating also induced increasing moisture influx into the region, which gets trapped below the elevated temperature layer, resulting in increased cloud fraction and rainfall, especially over lower terrain areas. Above the layer, moisture decreased, which led to cloud reduction and decreased rainfall over higher terrain areas. BC was seen to reduce cloud fraction between 1-2 km altitude through semi-direct effect, and reduced rainfall formation was also seen between these two altitudes. Thus, BC caused a continuous increase in moisture in the region but also decreased low-level clouds between 1 and 2 km. Hence, semi-direct effect is also influential in rainfall suppression. Increasing BC emissions led to a decrease in low-intensity but an increase in high-intensity rainfall. Rainfall was influenced for more time by increasing BC emissions.

Thus, this study describes different atmospheric processes prevalent during the pre-monsoon season over the NE India region and relates them to give a holistic understanding of the aerosol influence on the rainfall-producing atmospheric mechanisms. This study shows that apart from the reasons highlighted in previous studies over this region, another mechanism (semi-direct effect) also exists, affecting clouds and rainfall. However, semi-direct effect needs to be studied in combination and separately with the indirect effect to further verify their contributions to rainfall, which is done in Chapter 4. The study also shows the presence of threshold BC emissions which is studied further in Chapter 5.

Model simulated BC concentrations are found to be lower than observations by a factor of 2 to 6 over India (Bond et al., 2013; Ganguly et al., 2009; Moorthy et al., 2013; Nair et al., 2012). As models underestimate BC concentration due to underestimation in BC emission rates (Gadhavi et al., 2015), the 4NOR scenario may not be an unrealistic scenario, as Govardhan et al. (2019) had to apply a factor of 3 to match observed concentrations. Kumar et al. (2015) found underestimated model simulated BC concentrations over different locations in NE India during pre-monsoon with the EDGAR emission inventory, upon which the CAMS emission inventory is based. Hence, it is likely that CAMS inventory may also incorporate underestimated BC emission rates. Thus, higher emissions scenarios (2NOR and 4NOR) may also represent the more realistic emission scenario instead of NOR for the simulation period, and accordingly, the BC effects will apply.

Chapter 4

4. Comparison of climatic effects of local and transported aerosols

4.1 General

This chapter compares and quantifies the climatic effects of aerosols emitted within NE India and those transported from outside to ascertain their relative impact and decide which region's emissions are more effective in affecting the atmosphere over this region during the pre-monsoon season. The relative impact of local and transported aerosols on the atmospheric physical and dynamical processes is studied, which ultimately affects rainfall. Indirect aerosol effect is also studied and the impacts of direct, semi-direct and indirect aerosol effects are compared to find their relative dominance and importance. Here, transported aerosols include the transported primary aerosols emitted from outside NE India as well as the secondary aerosols formed from the transported emissions. The same goes for local emissions.

4.2 Methodology

4.2.1 Simulation details

The study used the same model along with similar modelling domain and input sources, as for the study in Chapter 3. However, model simulations were only carried out for the month of April 2018 but for a similar duration of 13 days from 7-19 April 2018. Similarly, a 3-day period from 7-9 April 2018 was discarded as spin-up and outputs from 10-19 were used for analysis. The model configuration is also similar with the exception that the simulations with the MOZART-MOSAIC chemistry scheme that supports CCN activation into cloud droplets, or indirect effect are also conducted in this study in addition to direct and semi-direct effect. Descriptions of the simulations are provided in Table 4.1.

Table 4.1: Description of simulations

	Simulation name	Description of simulations
1.	NOR-I	Baseline simulation with all aerosol effects
2.	NOFEED-I	Same as NOR-I but with aerosol radiative effects turned off
3.	NOCHEM	Simulation with no atmospheric chemistry and aerosol effects
4.	No_EMISS_NE	Same as NOR-I but with emissions turned on only outside NE India
5.	Only_EMISS_NE	Same as NOR-I but with emissions turned on only within NE India
6.	No_EMISS_NE_4SO_2	Same as No_EMISS_NE but with 4×SO_2 emissions
7.	No_EMISS_NE_0.25SO_2	Same as No_EMISS_NE but with 0.25×SO_2 emissions
8.	No_EMISS_NE_NOFEED	Same as No_EMISS_NE but with aerosol radiative effects turned off
9.	Only_EMISS_NE_NOFEED	Same as Only_EMISS_NE but with aerosol radiative effects turned off
10.	No_NE_BCI	Same as NOR-I but with BC emissions turned on only outside NE India
11.	Only_NE_BCI	Same as NOR-I but with BC emissions turned on only within NE India
12.	NOR	Baseline simulation with only direct and semi-direct effect
13.	2NOR	Same as NOR but with 2×BC emissions
14.	No_NE_BC	Same as NOR but with BC emissions within NE India region turned off
15.	No_NE_2×BC	Same as No_NE_BC but with 2×BC emissions outside NE India
16.	Only_NE_BC	Same as NOR but with BC emissions turned off outside NE India
17.	Only_NE_2×BC	Same as Only_NE_BC but with 2×BC emissions inside NE India
18.	NOFEED	Same as NOR but with aerosol radiative effects off

All the simulations were conducted with the MOZART-MOSAIC chemistry scheme, except simulation 3, which was purely a meteorology simulation and did not include any atmospheric chemistry and aerosol effects. Moreover, simulations 1 to 11 (except 3), were conducted with the MOZART-MOSAIC chemistry scheme which also supports indirect aerosol effect along with direct and semi-direct effect, while simulations 12 to 18 did not include indirect effect.

The NOR simulation which was used in Chapter 3, is also used in this study. NOR-I is also the baseline simulation run with the baseline emissions as NOR but also includes indirect aerosol effect. No_EMISS_NE had all emissions (biogenic, anthropogenic and dust) disabled within the NE India region bounded by 22° N and 29° N latitudes and 89° E and 97° E longitudes while No_NE_BC and No_NE_BCI only had BC emissions disabled within the same region. Only_EMISS_NE had all emissions disabled outside of the above region along with boundary conditions for all chemical species modified to zero to nullify the transport of emissions from outside the domain and similarly, Only_NE_BC and Only_NE_BCI had BC emissions disabled outside the NE India region with boundary conditions for BC modified to zero. The remaining simulations can be understood from Table 4.1 and their application is better understood from Section 4.2.2 and 4.3.

4.2.2 Separation of aerosol effects

4.2.2.1 Rainfall

The procedure for differentiating the different aerosol effects and their effect-wise impact on rainfall is described below. As per Ghan et al. (2012) and Bauer and Menon (2012), the total aerosol effect is the algebraic sum of direct, indirect and semi-direct effects. Similar approaches were used by Yang et al. (2011).

For aerosol effects due to emissions in the entire modelling region:

NOR-I – NOCHEM = Total aerosol effect = Direct + Semi-direct + Indirect, (5)

Both NOFEED-I and NOR-I includes indirect effect but NOFEED-I does not include aerosol radiative effects. Thus,

NOR-I – NOFEED-I = Direct + Semi-direct effect (6)

Also, since NOFEED-I includes only indirect effect,

NOFEED-I – NOCHEM = Indirect effect (7)

A similar approach was used by Wang et al. (2015).

Similarly, for aerosol effects due to transported emissions only:

No_EMISS_NE – NOCHEM = Direct + Semi-direct + Indirect (8)

No_EMISS_NE – No_EMISS_NE_NOFEED = Direct + Semi-direct effect, (9)

No_EMISS_NE_NOFEED – NOCHEM = Indirect effect, (10)

Similarly, for aerosol effects due to local emissions only:

Only_EMISS_NE – NOCHEM = Direct + Semi-direct + Indirect, (11)

Only_EMISS_NE – Only_EMISS_NE_NOFEED = Direct + Semi-direct effect, (12)

Only_EMISS_NE_NOFEED – NOCHEM = Indirect effect, (13)

NOR-I – NOCHEM gives the total rainfall change due to the total aerosol effect from emissions in the entire region. The rainfall changes due to other aerosol effects due to emissions from the entire domain, local as well as transported aerosols were calculated in a similar way.

4.2.2.2 Radiative forcing

For calculation of RF, the following procedure was used. Net (NET) RF is the sum of the short-wave (SW) and long-wave (LW) RF. The 'SWDNB' model variable represents the SW radiation in the downwelling (DN) direction on the ground surface (B). Similarly, UP represents upwelling, T represents top-of-atmosphere and C represents clear sky, i.e., without clouds. The other radiation variables can be understood by combing these.

Calculation of NET RF due to emissions in the entire domain:

At surface,

$$\text{Net total RF} = \text{NOR-I}_{((SWDNB+LWDNB)-(SWUPB+LWUPB))} - \text{NOCHEM}_{((SWDNB+LWDNB)-(SWUPB+LWUPB))} \quad (14)$$

Net indirect RF = NOFEED-I$_{((SWDNB+LWDNB)-(SWUPB+LWUPB))}$ - NOCHEM$_{((SWDNB+LWDNB)-SWUPB+LWUPB))}$ (15)

Net direct + semi-direct RF = NOR-I$_{((SWDNB+LWDNB)-(SWUPB+LWUPB))}$ – NOFEED-I$_{((SWDNB+LWDNB)-(SWUPB+LWUPB))}$ (16)

Net direct RF = NOR-I$_{((SWDNBC+LWDNBC)-(SWUPBC+LWUPBC))}$ – NOFEED-I$_{((SWDNBC+LWDNBC)-(SWUPBC+LWUPBC))}$ (17)

Net semi-direct RF = (Direct + semi-direct RF) – Net direct RF (18)

At TOA,

Net total RF = NOR-I$_{((SWDNT+LWDNT)-(SWUPT+LWUPT))}$ - NOCHEM$_{((SWDNT+LWDNT)-(SWUPT+LWUPT))}$ (19)

Net indirect RF = NOFEED-I$_{((SWDNT+LWDNT)-(SWUPT+LWUPT))}$ - NOCHEM$_{((SWDNT+LWDNT)-(SWUPT+LWUPT))}$ (20)

Net direct + semi-direct RF = NOR-I$_{((SWDNT+LWDNT)-(SWUPT+LWUPT))}$ – NOFEED-I$_{((SWDNT+LWDNT)-(SWUPT+LWUPT))}$ (21)

Net direct RF = NOR-I$_{((SWDNTC+LWDNTC)-(SWUPTC+LWUPTC))}$ – NOFEED-I$_{((SWDNTC+LWDNTC)-(SWUPTC+LWUPTC))}$ (22)

Net semi-direct RF = (Direct + semi-direct RF) – Net direct RF (23)

Thus, Net atmospheric RF = Total RF$_{TOA}$ – Total RF$_{SURFACE}$ (24)

Similarly, the SW or LW RF was similarly found by using either or SW or LW radiation instead of combined radiations. NOR-I was replaced by No_EMISS_NE or Only_EMISS_NE, while NOFEED was replaced by No_EMISS_NE_NOFEED or Only_EMISS_NE_NOFEED to find contributions of local and transported emissions.

4.2.3 Model evaluation

IOA, RMSE and ME were used as statistical parameters.

4.2.3.1 Evaluation of chemical species

Similar to the NOR simulation evaluated in Chapter 3, NOR-I simulated chemical species were compared against the MERRA2 dataset. Performance statistics for both NOR and NOR-I are shown in Table 4.2 for comparison.

Table 4.2: Statistical evaluation of chemical species. RMSE and ME in µg m^{-3}

		NOR-I – Whole domain	NOR– Whole domain	NOR-I – NE India	NOR – NE India
BC	RMSE	1.12	**0.70**	1.11	**0.64**
	IOA	0.46	**0.51**	0.42	**0.53**
	ME	0.16	0.21	-0.42	**-0.13**
Organic carbon	RMSE	6.24	**4.60**	7.90	**5.44**
	IOA	0.50	0.49	0.42	**0.47**
	ME	0.31	-0.45	-2.95	-2.99
DUST	RMSE	42.91	**38.62**	34.95	**23.90**
	IOA	0.37	**0.39**	0.28	**0.37**
	ME	-19.70	**-16.25**	-26.95	**-16.75**
Sulfate	RMSE	2.58	2.47	4.14	**2.88**
	IOA	0.42	0.40	0.41	**0.46**
	ME	1.14	1.39	-2.17	**-1.01**
Mean of all species	RMSE	13.21	**11.60**	12.03	**8.22**
	IOA	0.44	**0.45**	0.38	**0.46**
	ME	-4.52	**-3.78**	-8.12	**-5.22**

NOR gave a much better overall estimation of all the chemical species throughout the domain with lower RMSE, higher IOA and lower ME compared to NOR-I and is even more evident over NE India. Moreover, the predicted chemical species of nitric oxide (NO), nitrogen dioxide (NO_2), sulfur dioxide (SO_2), $PM_{2.5}$ and PM_{10} were compared against in-situ observations at the cities of Delhi (28.56 °N, 77.11 °E), Kanpur (26.57 °N, 80.32 °E), Patna (25.61 °N, 85.13 °E) and Siliguri (26.69 °N, 88.41 °E), obtained from Central Pollution Control Board, India (https://app.cpcbccr.com/ccr/#/caaqm-dashboard-all/caaqm-landing/caaqm-data-availability). These cities are located along the IGP. It is noteworthy to mention that several datasets pertaining to different locations are available within a city. However, not all locations within a city contained the full data for the required days (10-19 April 2018). Hence only that dataset was considered for evaluation which contained the full data. Performance statistics are given in Table 4.3.

Table 4.3: Model performance statistics for chemical species compared against observation stations. RMSE and ME units in μg m^{-3}

		NOR			NOR-I		
		RMSE	IOA	ME	RMSE	IOA	ME
DELHI	NO	24.82	0.35	-23.28	23.86	0.36	-22.48
	NO_2	30.22	0.17	28.47	35.58	0.14	33.22
	PM_{10}	37.87	0.48	-19.65	73.84	0.37	-47.57
	$PM_{2.5}$	15.72	0.62	-10.12	21.15	0.62	15.14
KANPUR	NO	42.17	0.43	-36.42	42.38	0.43	-36.65
	NO_2	54.22	0.25	-53.52	59.32	0.22	-58.60
	$PM_{2.5}$	24.10	0.48	-20.02	17.70	0.43	-9.34
	SO_2	20.44	0.45	18.49	10.97	0.53	8.90
PATNA	NO	12.18	0.35	-10.69	12.14	0.35	-10.67
	NO_2	8.79	0.55	-0.60	8.49	0.57	0.06
	$PM_{2.5}$	55.62	0.22	-55.28	49.78	0.21	-48.48
SILIGURI	NO	5.77	0.25	-5.64	5.77	0.24	-5.64
	NO_2	14.17	0.42	-9.90	16.94	0.22	-16.76
	PM_{10}	22.28	0.52	-19.53	30.07	0.44	-27.76
	$PM_{2.5}$	14.51	0.52	-12.90	14.27	0.52	-12.94
Mean		25.25	0.40	-15.37	28.15	0.37	-15.97

The performance statistics were better with particulate matter than with gaseous species. Comparatively, the performance was better with MERRA2. The relatively lower performance with in-situ comparison may be due to the grid size as in-situ observations are affected by local emission sources as well the deficiencies in emission inventory. Moreover, NOR performed better than NOR-I here as well.

4.2.3.2 Evaluation of meteorology

The NOR simulation utilised in this study was evaluated in Chapter 3. Similarly, meteorological evaluation of NOR-I w.r.t wind direction, wind speed, temperature and humidity were carried out against surface station datasets, as described in Chapter 3. Performance statistics are provided in Table 4.4.

Table 4.4: Model performance statistics for meteorological parameters

	Bangalore	Delhi	Guwahati	Kolkata	Mumbai	Patna
			Temperature			
RMSE (°K)	2.58	2.23	2.88	4.02	2.61	1.89
IOA	0.91	0.94	0.75	0.79	0.80	0.95
ME (°K)	-2.32	-0.34	-1.97	-3.16	-1.99	-0.74
			Relative humidity			
RMSE (%)	9.33	8.71	11.21	15.68	10.49	11.63
IOA	0.97	0.92	0.79	0.79	0.85	0.91
ME (%)	0.06	0.53	3.09	12.09	3.99	5.98
			Wind speed			
RMSE (m s^{-1})	1.47	1.91	1.84	1.90	1.44	2.11
IOA	0.49	0.59	0.40	0.48	0.83	0.55
ME (m s^{-1})	0.51	-0.22	-0.35	0.07	-0.71	1.22
			Wind direction			
RMSE (°)	44.06	108.48	146.95	64.29	76.91	104.87
IOA	0.79	0.72	0.47	0.43	0.68	0.75
ME (°)	-18.48	10.28	6.07	22.41	14.23	-26.17

As per the criteria of Emery et al. (2001), the NOR-I simulation under predicted temperature showed good performance with wind speed and wind direction but had large RMSE with wind direction, similar to the NOR simulation.

Similarly, simulated rainfall from NOR-I was evaluated against the IMD rainfall dataset of Pai et al. (2014). The inclusion of all aerosol effects greatly improved simulated rainfall performance with NE India regional average IOA: 0.52, ME: 3.72 mm day^{-1}, RMSE: 13.55 mm day^{-1} compared to only considering direct + semi-direct effect in NOR (IOA: 0.40, ME: 9.22 mm day^{-1}, RMSE: 21.26 mm day^{-1}) in Chapter 3. The improvement in performance and decrease in ME show that indirect effect played a major role during this period in controlling and suppressing rainfall. This improvement may relate to observations of Yang et al. (2011). However, Figure 4.1 showing region-wise rainfall statistics showed the southern region or region 4 to contain large errors. The regions may be seen from Figure 4.2(d).

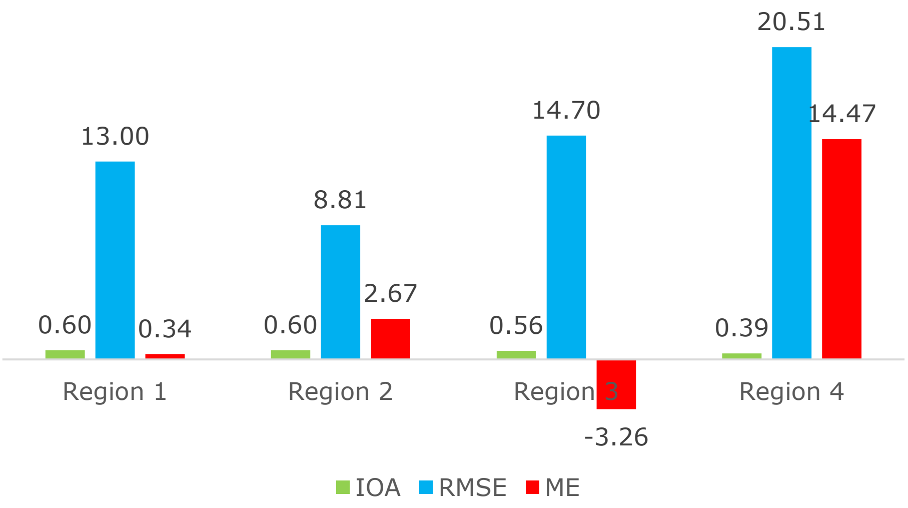

Figure 4.1: Region-wise rainfall evaluation statistics with NOR-I. RMSE and ME in mm day^{-1}

4.3 Results and discussion

4.3.1 PM_{10} spatial and vertical distribution

Figure 4.2 shows the time-averaged spatial distribution of PM_{10} concentration. The NE India region was divided into four regions based on the proximity from the IGP, shown in Figure 4.2(d). Region 1 and region 2 fall along the Brahmaputra River Valley, with region 1 being closest to IGP. Region 3 is mostly a mountainous region and region 4 is the southern region closer to the

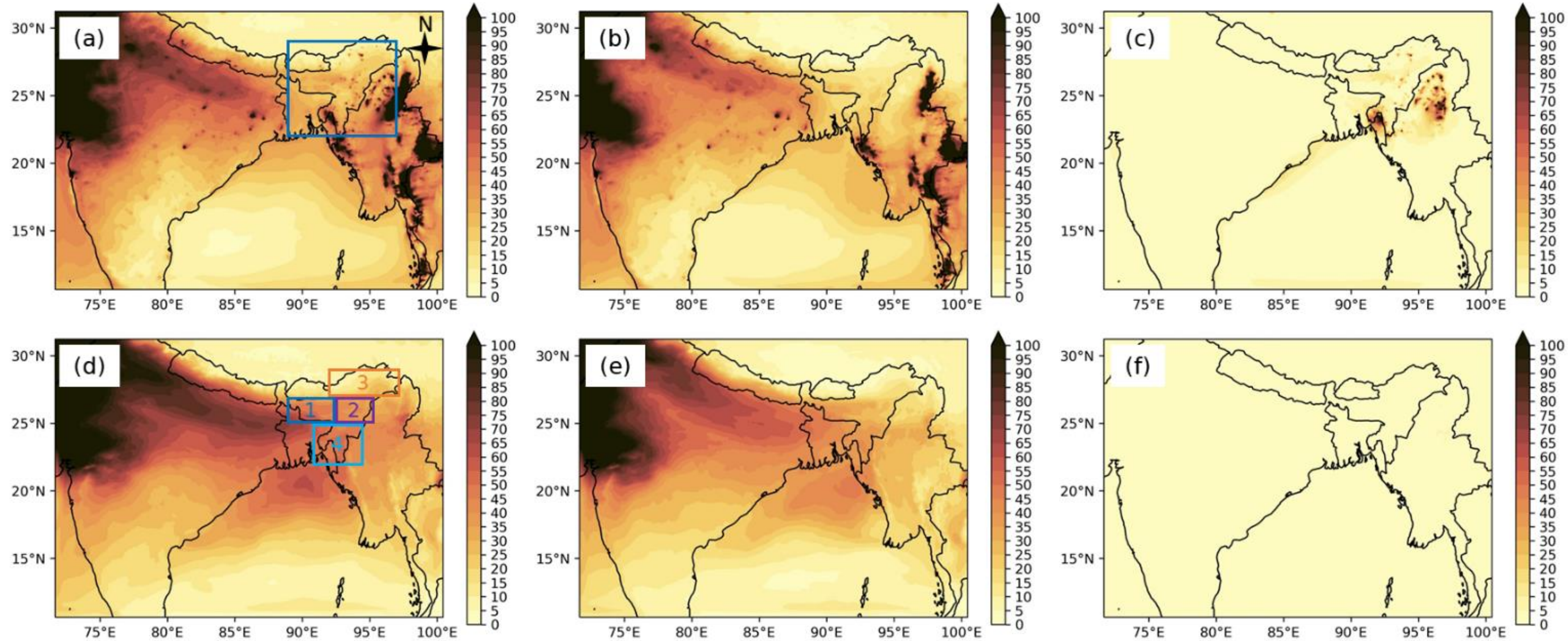

Figure 4.2: Spatial distribution of PM_{10} concentration (μg m^{-3}) in NOR-I, (a, d), No_EMISS_NE (b, e) and Only_EMISS_NE (c, f). Upper row shows distribution at model level 0 (near surface) and the lower row at model level 15

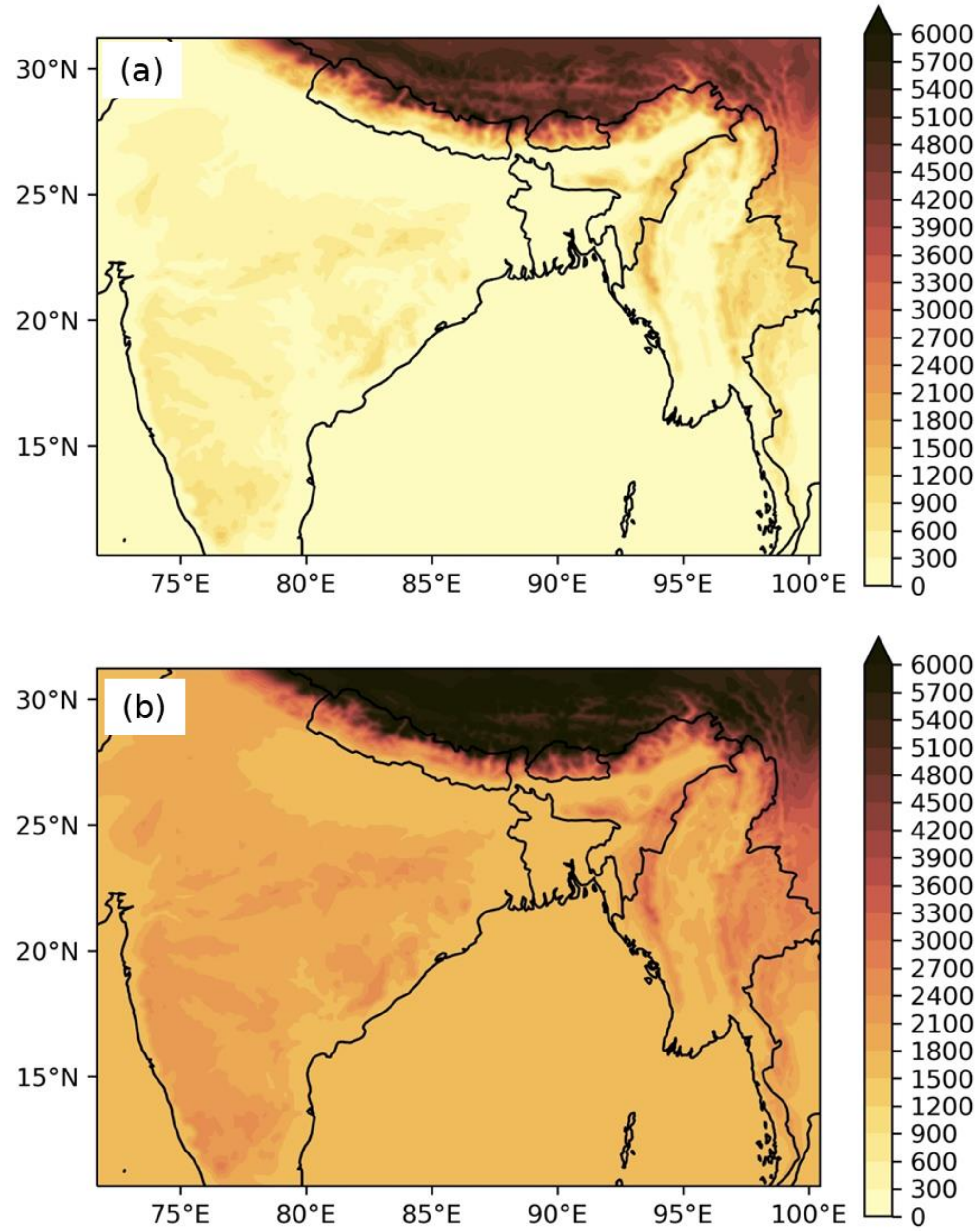

Figure 4.3: Spatial distributions of geopotential heights (m) of model level a) 0 (near surface) b) 15

Table 4.5: Region-wise PM_{10} concentration (µg m^{-3}) in different scenarios at different atmospheric heights

	No_EMISS_NE		Only_EMISS_NE		NOR-I		(No_EMISS_NE/ (No_EMISS_NE + Only_EMISS_NE))*100%	
Model level	0	15	0	15	0	15	0	15
Region 1	18.18	32.67	6.49	1.01	30.25	42.99	73.70	97.00
Region 2	12.78	21.70	6.33	1.14	26.64	33.75	66.86	95.02
Region 3	5.25	7.33	3.43	0.90	12.69	12.39	60.48	89.03
Region 4	21.62	36.01	16.03	0.88	40.12	47.38	57.43	97.62
Average	14.46	24.43	8.07	0.98	27.43	34.13	64.18	96.14

Bay of Bengal. The spatial distribution of geopotential heights of model level 0 and 15 are shown in Figure 4.3, while region-wise concentration values within NE India at the two atmospheric heights are shown in Table 4.5. PM_{10} concentration contours shown in Figure 4.2(a, b, d, e), emanating from IGP and spreading into NE India indicated the transport of aerosols from IGP into NE India. The similarity of these spatial distributions of No_EMISS_NE to the baseline scenario, NOR-I, especially within NE India region inferred that most of the aerosol mass within NE India was contributed by transported aerosols, while PM_{10} emitted or formed over NE India remained mainly confined within the region as shown in Figure 4.2(c), possibly due to the mountainous terrain, as also described in Kundu et al. (2018). Both near the surface and at higher atmosphere (level 15), No_EMISS_NE showed a higher regional average concentration (surface: 14.46 $\mu g\ m^{-3}$, higher atmosphere: 24.43 $\mu g\ m^{-3}$) which was closer to the baseline scenario of NOR-I (surface: 27.43 $\mu g\ m^{-3}$, higher atmosphere: 34.13 $\mu g\ m^{-3}$) compared to the local emission scenario of Only_EMISS_NE (surface: 8.07 $\mu g\ m^{-3}$, higher atmosphere: 0.98 $\mu g\ m^{-3}$). Thus, transported aerosols contributed higher surface PM_{10} concentration (64.18 %) than local emission and contribution from local emissions were negligible at higher atmosphere, as also seen in Figure 4.2(f) and 96.14 % of it was contributed by transported aerosols. The higher concentration in the higher atmosphere was due to transported aerosols developing an elevated PM_{10} profile (Figure 4.4) having a maximum concentration near 2000 m and which shows much greater similarity with the baseline scenario.

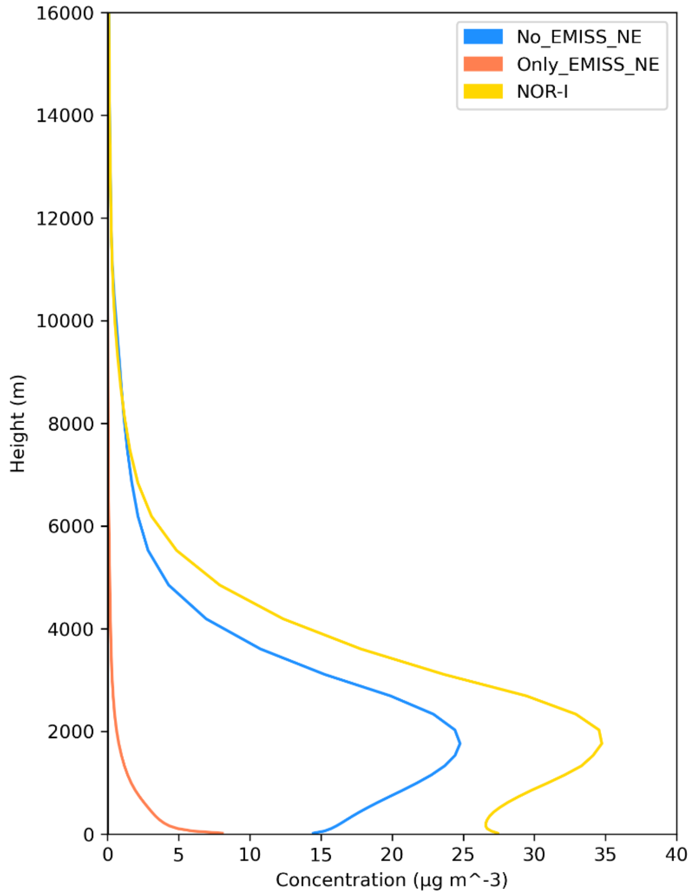

Figure 4.4: Regional average vertical profile of PM_{10} concentration (µg m^{-3}) in different scenarios

The long-range transport and strong convective activity during this season are responsible for the elevated profile (Pathak et al. (2016). Hence, transported aerosols contributed to the bulk of the aerosols over NE India throughout the atmospheric column (93.98 %) indicated by the column integrated PM_{10} mass of 313.97 g m^{-2} (No_EMISS_NE) and 20.08 g m^{-2} (Only_EMISS_NE). NOR-I had column integrated PM_{10} mass of 466.63 g m^{-2}. Further analysis indicated that transported aerosols accounted for >50 % of BC, organic carbon, sulfate, nitrate, ammonium and dust aerosol mass over NE India's atmosphere as the column integrated mass for these species in No_EMISS_NE were 4.55, 19.59, 51.66, 2.20, 13.74 and 207.82 g m^{-2}, respectively, while it was 0.94, 6.51, 1.79, 0.12, 0.56 and 6.60 g m^{-2}, respectively in Only_EMISS_NE. The spatial distribution of column integrated mass of these species can be seen in Figures 4.5, 4.6, 4.7, 4.8, 4.9 and 4.10.

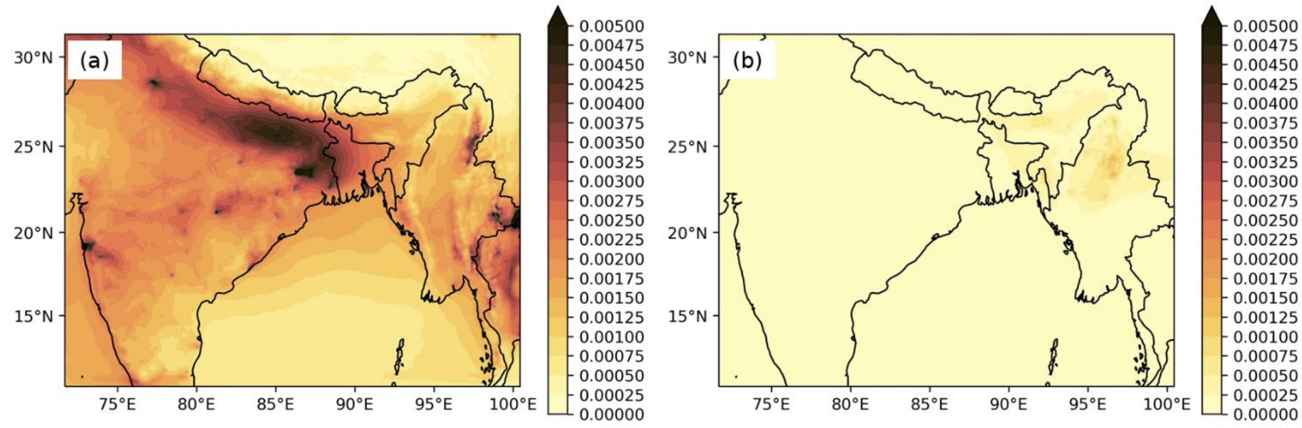

Figure 4.5: Spatial distribution of column integrated BC mass (g m^{-2}) in a) No_EMISS_NE b) Only_EMISS_NE

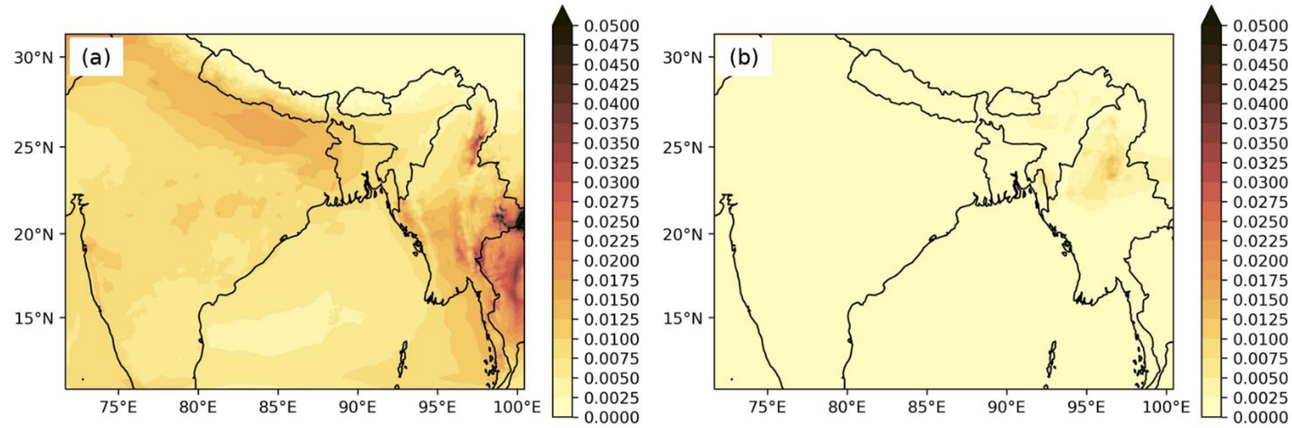

Figure 4.6: Spatial distribution of column integrated organic carbon mass (g m^{-2}) in a) No_EMISS_NE b) Only_EMISS_NE

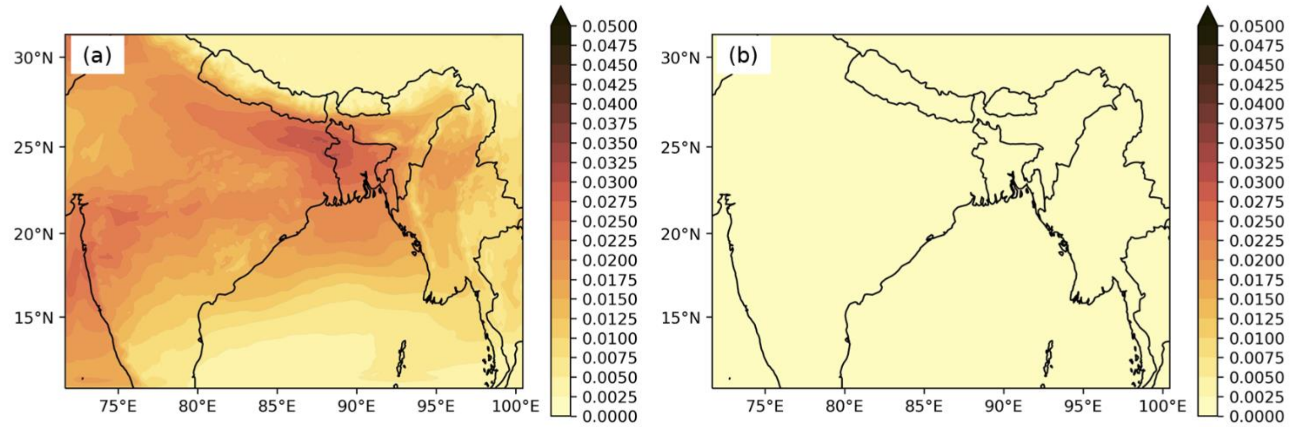

Figure 4.7: Spatial distribution of column integrated sulfate mass (g m^{-2}) in a) No_EMISS_NE b) Only_EMISS_NE

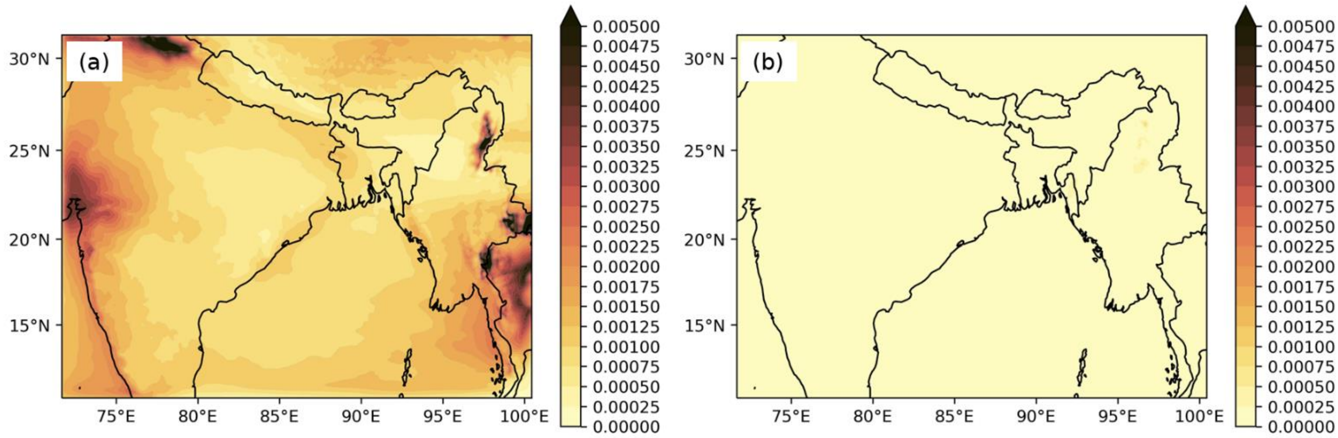

Figure 4.8: Spatial distribution of column integrated nitrate mass (g m^{-2}) in a) No_EMISS_NE b) Only_EMISS_NE

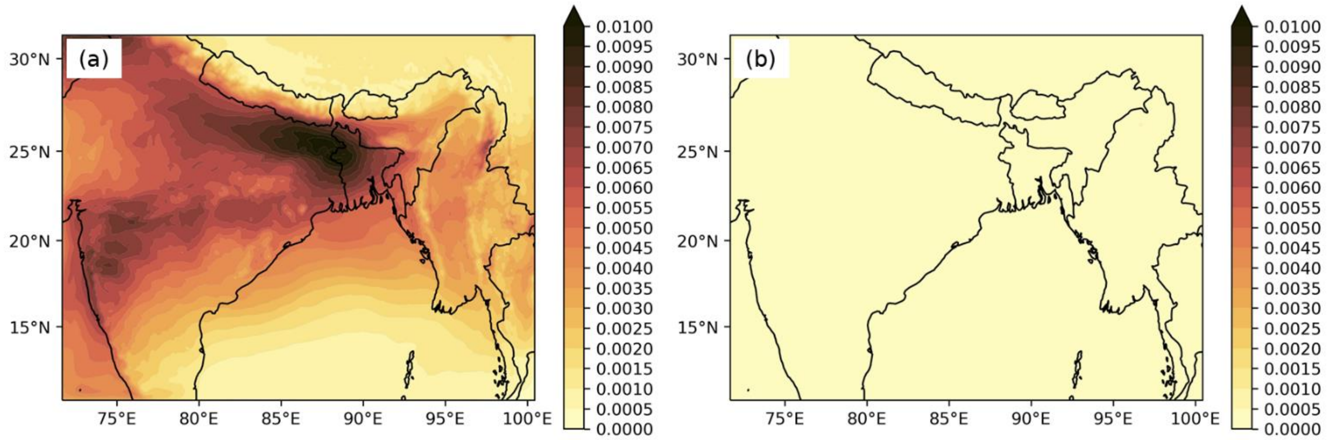

Figure 4.9: Spatial distribution of column integrated ammonium mass (g m^{-2}) in a) No_EMISS_NE b) Only_EMISS_NE

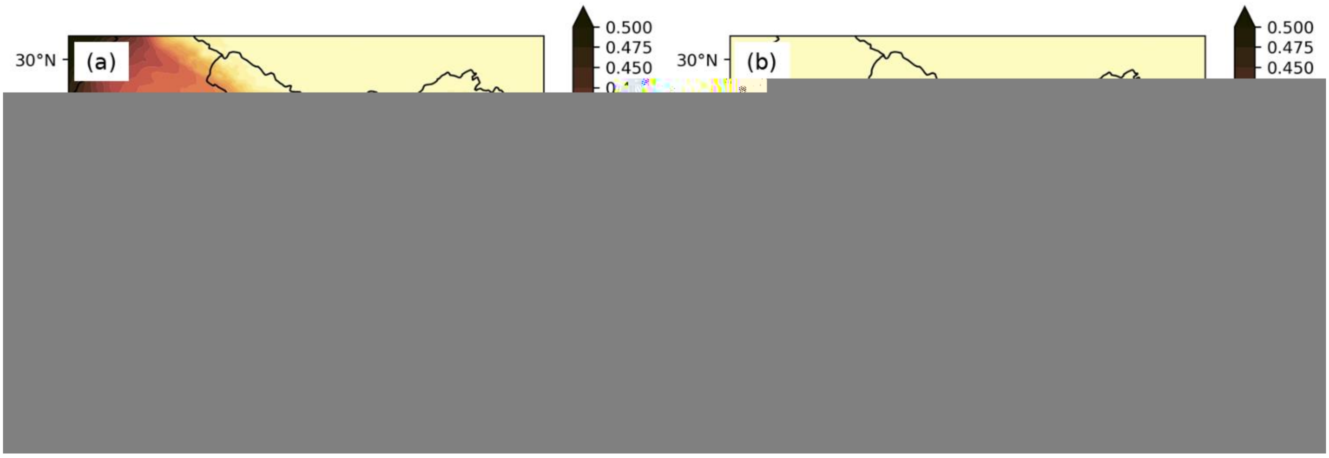

Figure 4.10: Spatial distribution of column integrated dust mass (g m^{-2}) in a) No_EMISS_NE b) Only_EMISS_NE

Region 1, being in close proximity to IGP, as seen in Figure 4.2(d), received maximum near-surface aerosol mass (73.70 %) from transported aerosols, compared to the other regions, followed by region 2 (66.86 %), 3 (60.48 %) and 4 (57.43 %). However, even though No_EMISS_NE and Only_EMISS_NE is the bifurcation of NOR-I into two separate emission regions, the sum of No_EMISS_NE and Only_EMISS_NE column integrated mass as well as concentrations didn't equate to NOR-I values and is always less than it. This indicated the formation of extra aerosol mass due to the interaction of emissions of the two regions.

4.3.2 Aerosol effects of local and transported aerosols on radiative forcing

RF due to different aerosol effects was estimated based on the methodology described in Section 4.2.2.2.

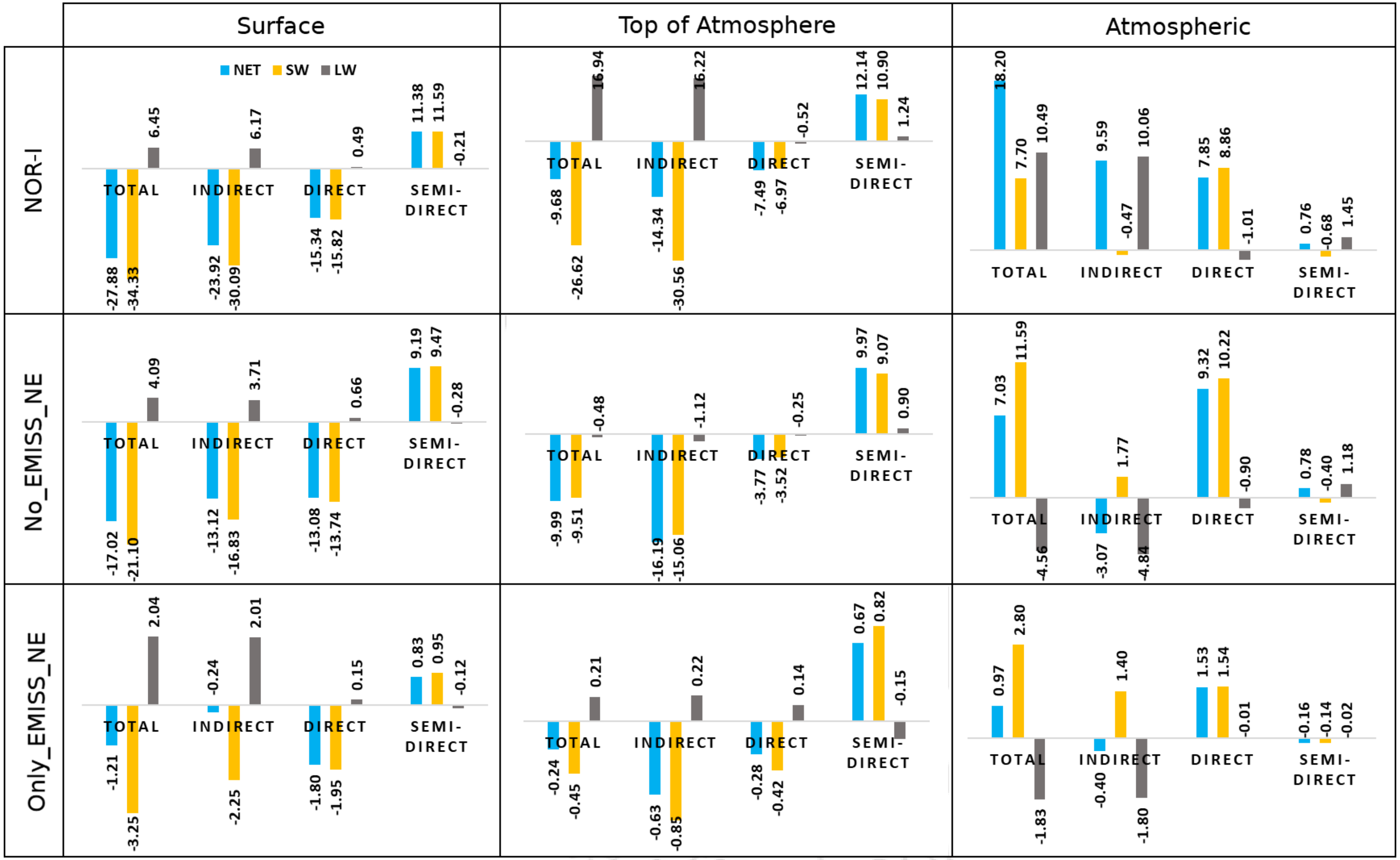

Figure 4.11: NE India regional average RF (W m^{-2}) due to different aerosol effects at NET, SW and LW wavelengths in different emission scenarios

The baseline scenario indicated that direct and indirect aerosol effects caused NET surface and TOA dimming while causing atmospheric heating, as seen in Figure 4.11. This is due to the presence of aerosols that scatter and absorb solar radiation, reducing it at the surface while increasing it at the top of the atmosphere as well as causing atmospheric heating. Net direct surface, TOA and atmospheric RF were -15.34, -7.49 and 7.85 Wm^{-2} and was mainly contributed by SW radiation. Indirect effect had the same effect on solar radiation as the direct effect and was due to the formation of numerous smaller cloud droplets, which has better reflectivity to solar radiation, also known as the 1^{st} indirect effect or Twomey effect (Twomey, 1977). However, positive atmospheric RF (18.20 W m^{-2}) causing atmospheric heating (10.06 W m^{-2}) was mainly caused by LW radiation (16.22 W m^{-2}) at the TOA contributed by indirect effect. This was due to greater cloud cover (Figure 47) at 8 – 10 km which is not seen in the other two scenarios.

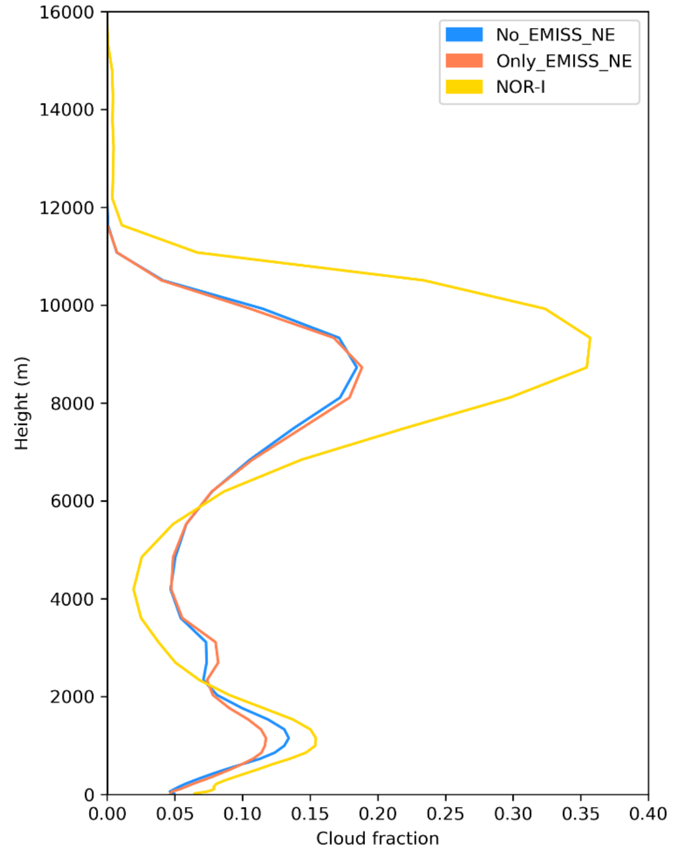

Figure 4.12: Regional average vertical profile of cloud cover in different scenarios

The indirect effect also caused warming at the surface (6.17 W m^{-2}), as it contributed to greater cloud cover (Nandan et al., 2022), causing heating of the surface through LW radiation. The total net surface RF was -27.88 W $m^{-2,}$ out of which -23.92 W m^{-2} or 85.80% was contributed by indirect forcing. Indirect SW forcing (-30.08 W m^{-2}) was almost twice the direct SW forcing (-15.82 W m^{-2}), while semi-direct SW forcing (+11.58 W m^{-2}) was ~75% of the direct forcing. Semi-direct effect showed positive surface RF due to cloud cover reduction. Thus, atmospheric heating and the subsequent evaporation of clouds compensated to a large extent the reduction in solar radiation due to aerosols. The atmospheric RF (0.76 W m^{-2}) due to semi-direct effect was due to LW radiation, which may be due to increased solar radiation at the surface, which released the heat into the atmosphere in the form of LW radiation. However, this value was very small. The indirect RF contributed most to the total surface, TOA and atmospheric RF at both SW and LW wavelengths and hence was found to be the dominant aerosol effect affecting radiation over NE India.

Quantitatively, No_EMISS_NE provided RF values (surface: -17.02 W m^{-2}, TOA: -9.99 W m^{-2} and atmospheric RF: 7.03 W m^{-2}) that were much similar and closer to the baseline scenario (surface: -27.88 W m^{-2}, TOA: -9.68 W m^{-2} and atmospheric RF: 18.20 W m^{-2}) than Only_EMISS_NE (surface: -1.21 W m^{-2}, TOA: -0.24 W m^{-2} and atmospheric RF: 0.97 W m^{-2}). Consequently, the No_EMISS_NE net indirect, direct and semi-direct surface RF values of -13.12, -13.08 and 9.19 W m^{-2} were significantly larger than the corresponding Only_EMISS_NE RF values of -0.24, -1.80 and 0.83 W m^{-2}. A similar conclusion could be inferred at TOA also. Hence transported aerosols were primarily responsible for all the different aerosol effects on radiation over NE India as a greater amount of aerosol mass was contributed by it. Moreover, No_EMISS_NE net direct atmospheric RF (9.32 W m^{-2}) was found to be even higher than the baseline scenario (7.85 W m^{-2}). This indicated that the NE India region contained more scattering aerosols while transported aerosols contained more absorbing aerosols as the difference in the direct atmospheric RF is mainly driven by changes in the TOA RF (-7.49 vs. -3.77 W m^{-2}) than surface RF (-15.34 vs. -13.08 W m^{-2}). Region 1 had the highest direct and semi-direct net surface RF of -20.41 W m^{-2} and 19.20 W m^{-2}, respectively, due to its close proximity to IGP.

4.3.3 Aerosol effects of local and transported aerosols on rainfall

Table 4.6: Changes in total (mm) due to different aerosol effects in different scenarios

		Total aerosol effect	Direct + Semi-direct	Indirect
NOR-I	Region 1	-100.60	-13.21	-87.39
	Region 2	-71.93	-1.34	-70.59
	Region 3	-102.60	-2.49	-100.11
	Total	-275.13	-17.04	-258.09
No_EMISS_NE	Region 1	-29.81	-18.37	-11.44
	Region 2	-21.52	-5.88	-15.64
	Region 3	-21.73	0.30	-22.04
	Total	-73.06	-23.95	-49.11
Only_EMISS_NE	Region 1	-26.81	-6.23	-20.57
	Region 2	2.48	-0.17	2.65
	Region 3	-0.12	-2.01	1.89
	Total	-24.45	-8.42	-16.04

The quantitative changes in regional average rainfall amounts as well as region-wise values over NE India due to the different aerosol effects induced by the aerosols in different scenarios are provided in Table 4.6. Rainfall from region 4 was not considered due to large errors being associated with it. In the baseline scenario (NOR-I), the total aerosol effect caused rainfall suppression in all three regions, with a regional total of -275.13 mm. Reductions in rainfall due to the total aerosol effect was contributed by suppressions due to both direct + semi-direct and indirect effect and was observed in all the considered regions. The highest suppression was observed in region 3 (-102.60 mm), followed by region 1 (-100.60 mm). The role of direct + semi-direct effect was observed to be minimal with a total regional suppression of -17.04 mm while the indirect effect (-258.09 mm) was responsible for almost the whole of the suppression of -275.13 mm. Region 1 observed the highest suppression of -13.21 mm due to direct + semi-direct effect as this region's radiation was highest impacted by these effects.

Direct effect could suppress rainfall by reducing surface evaporation and convection through surface dimming while semi-direct by evaporation of clouds (Talukdar et al., 2019; Lohmann and Feichter, 2001; Habib et al., 2006; Bollasina et al., 2011; Koch and Del Genio, 2010b). However, the surface dimming by indirect effect (-23.92 W m^{-2}) with NOR-I was much larger than the combined direct + semi-direct effect (-3.96 W m^{-2}). Hence the reduction in surface moisture flux due to indirect effect (-6.45×10^{-6} kg m^{-2} s^{-1}) was much greater than due to the combined direct + semi-direct effect (-1.1×10^{-6} kg m^{-2} s^{-1}) and much similar to the reduction due to total aerosol effect (-7.56×10^{-6} kg m^{-2} s^{-1}). This was also observed in the case of No_EMISS_NE. The greater surface dimming of -17.02 W m^{-2} in No_EMISS_NE caused a much higher negative surface moisture flux change of -3.82×10^{-6} kg m^{-2} s^{-1} due to total aerosol effect, mostly contributed by indirect effect (-2.79×10^{-6} kg m^{-2} s^{-1}) compared to direct + semi-direct effect (-1.03×10^{-6} kg m^{-2} s^{-1}). Hence, indirect effect in NOR-I and No_EMISS_NE dominated moisture reduction through the reduction in surface moisture flux over most areas of NE India at both low and high-terrain regions, as seen in Figure 4.13.

However, the direct + semi-direct effect caused an increase of moisture in NOR-I and No_EMISS_NE over most of NE India in spite of a negative surface moisture flux not observed in Only_EMISS_NE. This indicated that direct + semi-direct caused an increase in the transport of moisture from another region, in this case from the Bay of Bengal. The equivalent potential temperature (EPT) profiles in Figure 4.14 compared the atmospheric stability due to different aerosol effects.

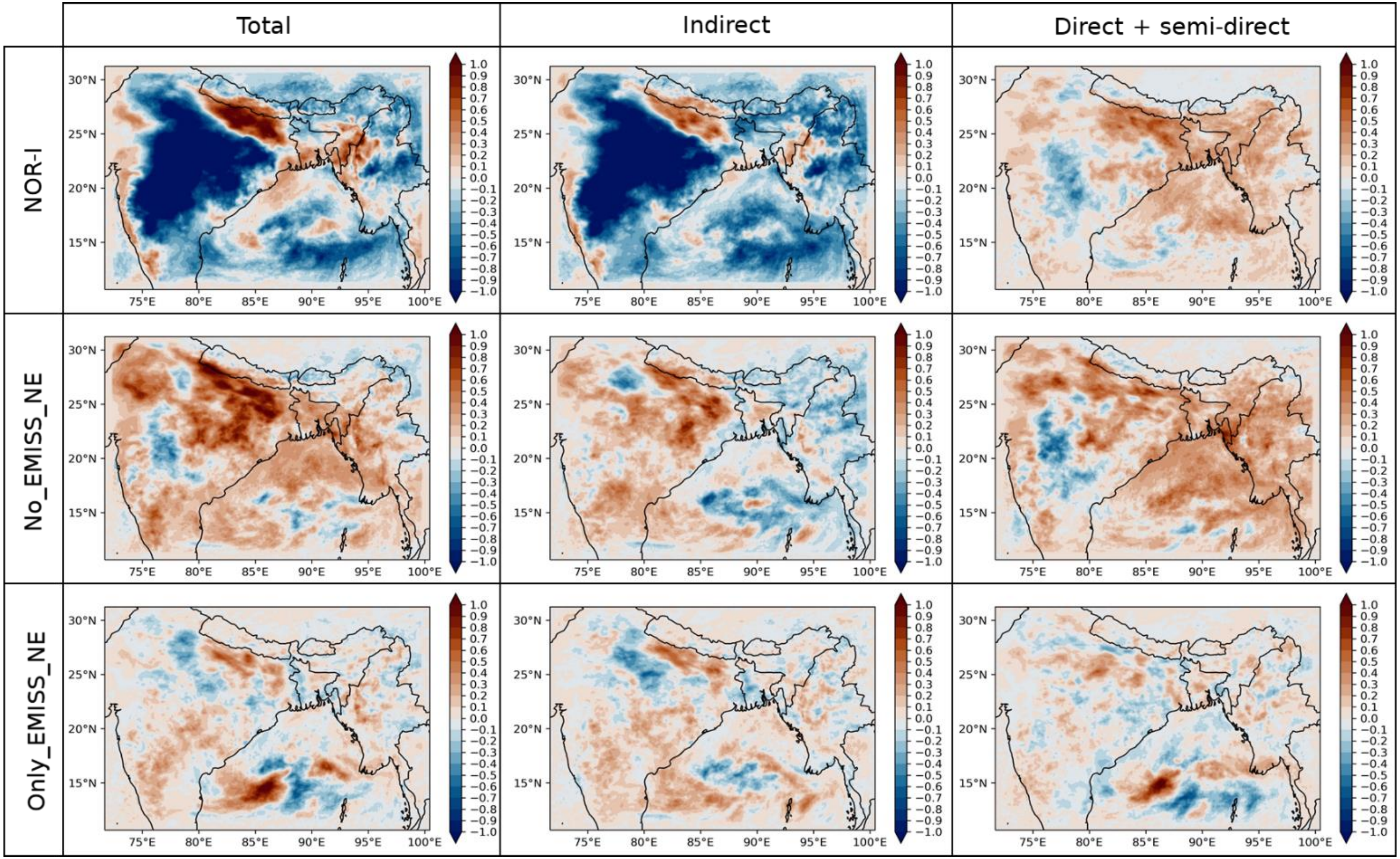

Figure 4.13: Spatial distribution of change in near-surface water vapor mixing ratio (g kg^{-1}) due to total aerosol effect, direct + semi-direct effect and indirect effect

The greater surface dimming due to the indirect effect in No_EMISS_NE caused not only negative surface moisture flux but also a significant increase in atmospheric stability (indicated by increasing value of indirect effect EPT profile with height), reducing convection, which possibly also contributed reduction to rainfall suppression. However, although the direct + semi-direct EPT profile showed increased atmospheric stability below 1 km, but created an overall unstable atmosphere in the lower atmosphere. This instability, primarily caused due to atmospheric heating of BC, created an unstable region over NE India which facilitated the increased transport of moisture from the Bay of Bengal (discussed later). Hence, though the direct effect reduces rainfall by reducing surface moisture flux and convection but also possibly enhances it by transporting moisture. This transported moisture possibly compensated to some extent the rainfall reduction due to a decrease in surface moisture flux, convection and cloud evaporation caused by direct and semi-direct effects. Hence, the rainfall reduction due to direct + semi-direct effect (-17.04 mm) was possibly significantly less than the indirect effect (-258.09 mm). Thus, the effect of direct and indirect effects on dynamics was distinctly different. The EPT profile of the total aerosol effect in No_EMISS_NE also showed an unstable lower atmosphere, supporting moisture transport. A similar explanation could be given for moisture increase due to direct + semi-direct in NOR-I but the increase in atmospheric stability and moisture reduction due to greater surface dimming by its indirect effect was significantly larger, which created an overall stable atmosphere due to the total aerosol effect in NOR-I. The EPT profiles of Only_EMISS_NE showed almost zero perturbation throughout the atmosphere and hence was unable to affect atmospheric stability and cause moisture transport. Thus, the direct + semi-direct effect in Only_EMISS_NE did not show significant moisture change in Figure 4.13. Moreover, the significantly smaller surface dimming (-1.21 W m^{-2}) in Only_EMISS_NE caused a very small but positive change of 8.15×10^{-8} kg m^{-2} s^{-1} due to the total aerosol effect and hence similar moisture change is observed in Figure 4.13. Hence aerosols emitted solely from NE India had negligible capability in affecting moisture through different aerosol effects. Moisture reduction over NE India was much greater due to the indirect effect in No_EMISS_NE compared to Only_EMISS_NE, while moisture increase was much greater in No_EMISS_NE compared to Only_EMISS_NE due to a higher direct + semi-direct effect.

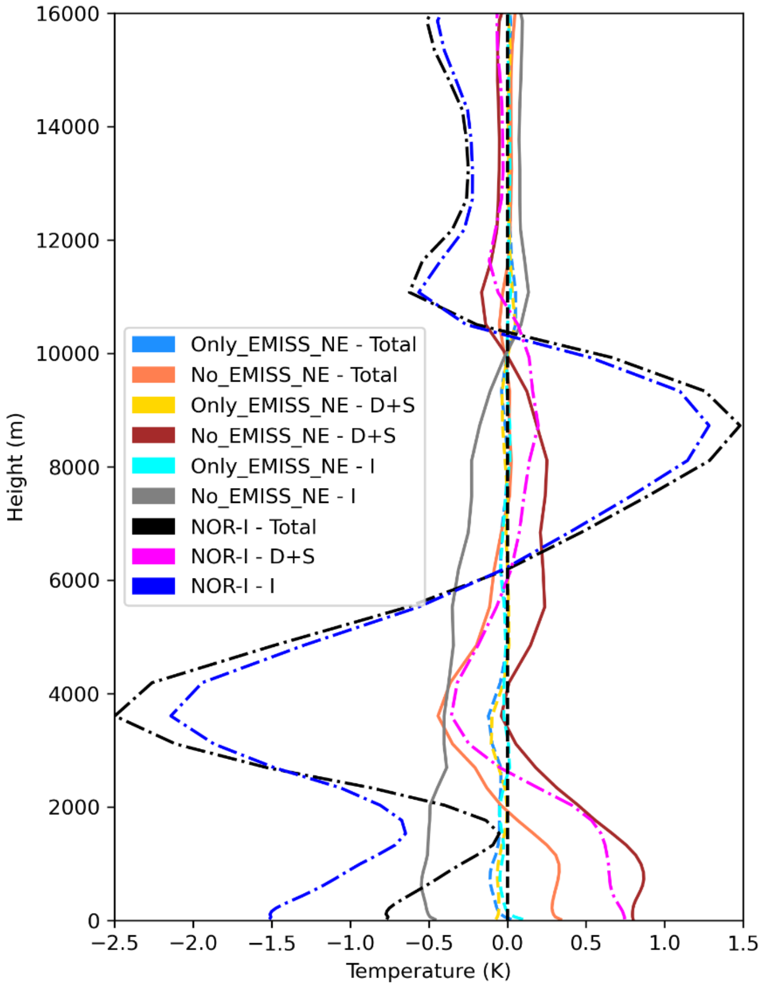

Figure 4.14: Perturbation of EPT (K) due to total aerosol effect (Total), direct + semi-direct (D+S) and indirect (I) aerosol effect in No_EMISS_NE (non-dashed), Only_EMISS_NE (dashed) and NOR-I (dashdot)

Moreover, the positive NE India regional average difference of column integrated CCN number (4.38×10^{10} m^{-2}), cloud droplet number (4.42×10^{13} m^{-2}) and cloudwater (27.93 g m^{-2}), and estimated from No_EMISS_NE – Only_EMISS_NE indicated that transported aerosols had a greater impact through aerosol indirect effect (Zhang et al., 2010). The presence of larger aerosol amounts in the form of CCN affects the cloud lifetime by affecting the conversion from cloudwater to rainwater, thus, to rainfall, thereby suppressing rainfall through the second indirect effect (Cherian et al., 2017; Shiogama et al., 2010). The presence of a large amount of CCN facilitates the condensation of water vapor on numerous CCN particles, producing numerous cloud droplets with smaller radii. This restricts small cloud droplets from growing in size due to a reduction in interaction with other cloud droplets, which affects their conversion to rain droplets, and, thus, to rainfall.

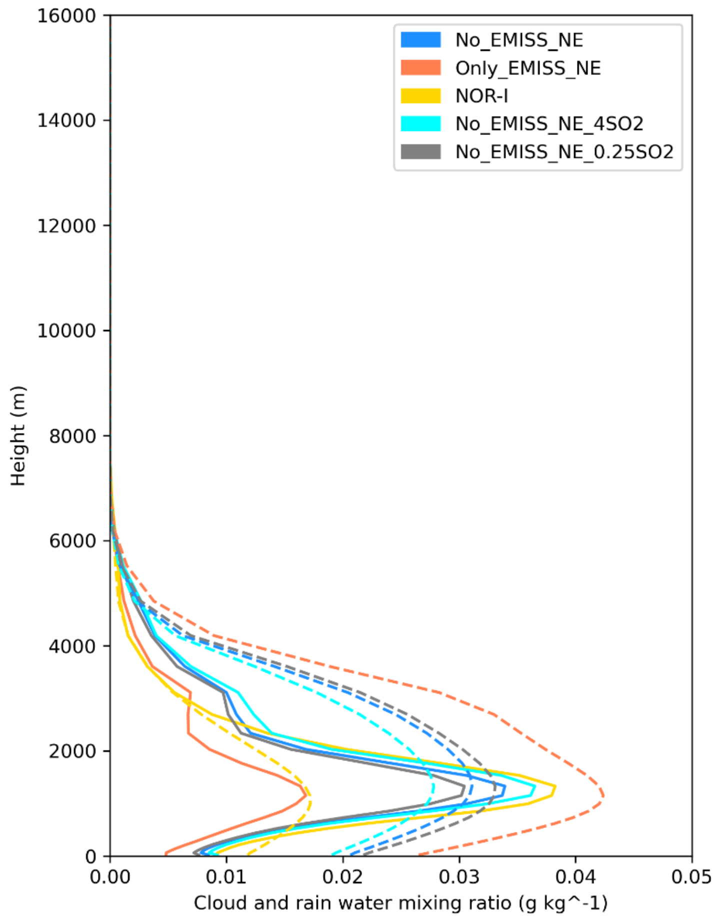

Figure 4.15: NE India regional average vertical profiles of cloudwater mixing ratio (non-dashed) and rainwater mixing ratio (dashed) in different scenarios (g kg^{-1})

Due to more aerosol mass over NE India (Section 4.3.1), NOR-I and No_EMISS_NE had significantly higher cloudwater compared to Only_EMISS_NE, as seen in Figure 4.15.

Consequently, NOR-I and No_EMISS_NE had a significantly lower rainwater mixing ratio than Only_EMISS_NE. Thus, rainfall suppression due to indirect effect was highest in NOR-I, followed by No_EMISS_NE and Only_EMISS_NE. Hence, the combined effect of reduction in moisture, instability and rainfall formation contributed to the reduction in rainfall through indirect and total aerosol effects. This could be a possible key mechanism associated with the decreasing rainfall trend in the region. Reduction of moisture due to the direct effect of aerosols and evaporation of clouds by BC were found to be possible mechanisms in Chapter 3. However, this study shows that the contribution of direct and semi-direct effects was very small compared to the indirect effect. The indirect effect has been found to be the dominant aerosol effect in many studies (Wang et al., 2015; Liu et al., 2016; Makar et al., 2015) and was found to suppress monsoon rainfall over India (Manoj et al., 2012). Aerosol indirect effect is mainly dictated by the warm clouds (Christensen et al., 2016). Thus, the higher cloud cover associated with NOR-I and No_EMISS_NE in the lower atmosphere which affected SW radiation more in section 4.3.2, was due to a greater amount of cloudwater in the lower atmosphere.

Moreover, No_EMISS_NE and Only_EMISS_NE simulations were evaluated against the IMD rainfall dataset and NOR-I simulation to check whether the local or transported aerosols had greater control over the rainfall in NE India. No_EMISS_NE showed better regional average rainfall statistics than Only_EMISS_NE with higher IOA (0.48 vs. 0.47), lower RMSE (18.85 vs. 20.37 mm day^{-1}), and lower ME (6.94 vs. 8.22 mm day^{-1}) on comparing with the IMD rainfall dataset. Also, the simulated rainfall of No_EMISS_NE showed higher rainfall similarity with NOR-I than Only_EMISS_NE with higher IOA (0.65 vs. 0.63), lower RMSE (56.32 vs. 61.92 mm day^{-1}) and lower ME (39.30 vs. 39.81 mm day^{-1}). Hence, No_EMISS_NE showed more similarity with the baseline scenario as well as observed data and had greater control over the region's rainfall.

4.3.4 Role of local and transported BC

In section 4.3.3, the direct effect showed to increase moisture over NE India through an increase in atmospheric instability, caused mainly due to atmospheric heating of BC as observed in Chapter 3. Hence, to negate the effects of the indirect effect on atmospheric dynamics, scenarios in Table 4.1 containing only direct and semi-direct effects were used in this analysis. Moreover, NOR gave a much better performance with BC concentration estimation than when the indirect effect was included (NOR-I). The results from No_EMISS_NE, Only_EMISS_NE, No_NE_BCI and Only_NE_BCI scenarios were compared and related.

4.3.4.1 BC atmospheric distribution

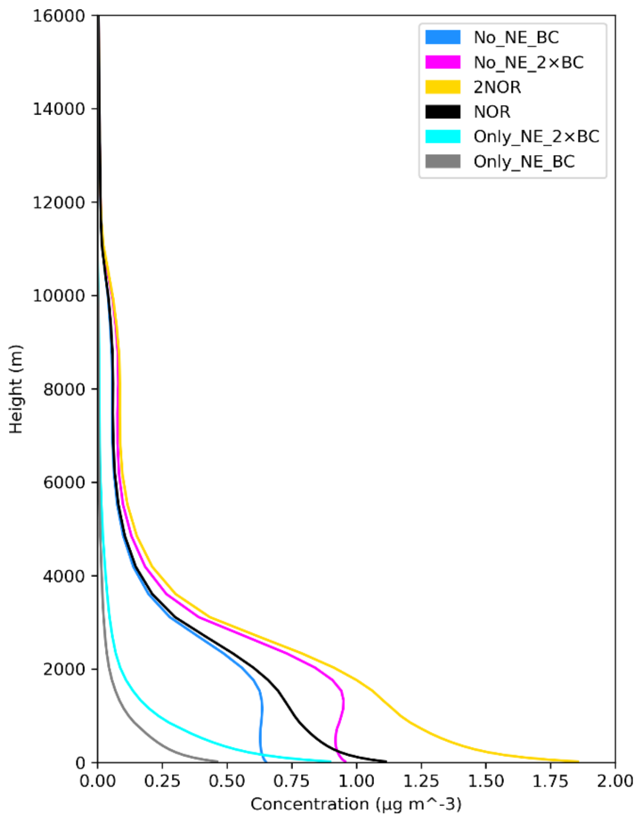

Figure 4.16: Regionally averaged vertical profiles of BC concentration (μg m^{-3}) in different scenarios

The regional average vertical profiles of BC concentration in NOR, 2NOR, No_NE_BC, No_NE_2×BC, Only_NE_BC and Only_NE_2×BC can be seen in Figure 4.16, in which the transported BC and local BC profiles resemble the No_EMISS_NE and Only_EMISS_NE PM_{10} profiles, respectively. In transported BC scenarios, BC was available up to much higher atmospheric height and profiles showed elevated concentration at around 1500 m indicating stronger BC transport at that height. In Only_NE_BC and Only_NE_2×BC, BC was confined near the surface, which decreased continuously and was available only up to half the altitude of transported BC. NOR profile was seen as the combination of Only_NE_BC and No_NE_BC profiles but had greater similarities with the latter. Moreover, IGP was the dominant source of transported BC, as seen in Figure 4.17. Comparing the BC concentration contours in Figure 4.17(a) and 4.17(c) it was observed that BC from the IGP flowed into NE India and thus contributed to BC found over the region, while BC emitted over NE India remained mainly confined within the region. On increasing the BC emissions outside NE India, a greater amount of BC was found to exist over the NE India region, especially over the western region or region 1 as seen in Figure 4.17(b) and a similar conclusion was seen with doubling BC emissions inside NE, as seen from Figure 4.17(d). Thus, region 1 not only received comparatively more BC from the IGP but locally emitted BC was also maximum in this region. The region of Bangladesh also seemed to contribute to BC in region 4 as seen in Figure 4.17(c) and Figure 4.17(d). The break in the concentration contours on the eastern side of regions 2 and 4 in Figure 4.17(c), however indicated that emissions from Myanmar did not contribute to BC over the regions. Even at higher atmosphere levels (Figure 4.18), similar observations were seen. It is noteworthy that emissions from IGP contributed to higher BC concentration over the NE India region than local emissions themselves. As we go even further up (Figure 4.19), very little contribution from local emissions was seen and BC over NE India was entirely contributed by IGP. Also, with increasing height, the region of peak BC concentration shifted from the IGP towards NE India.

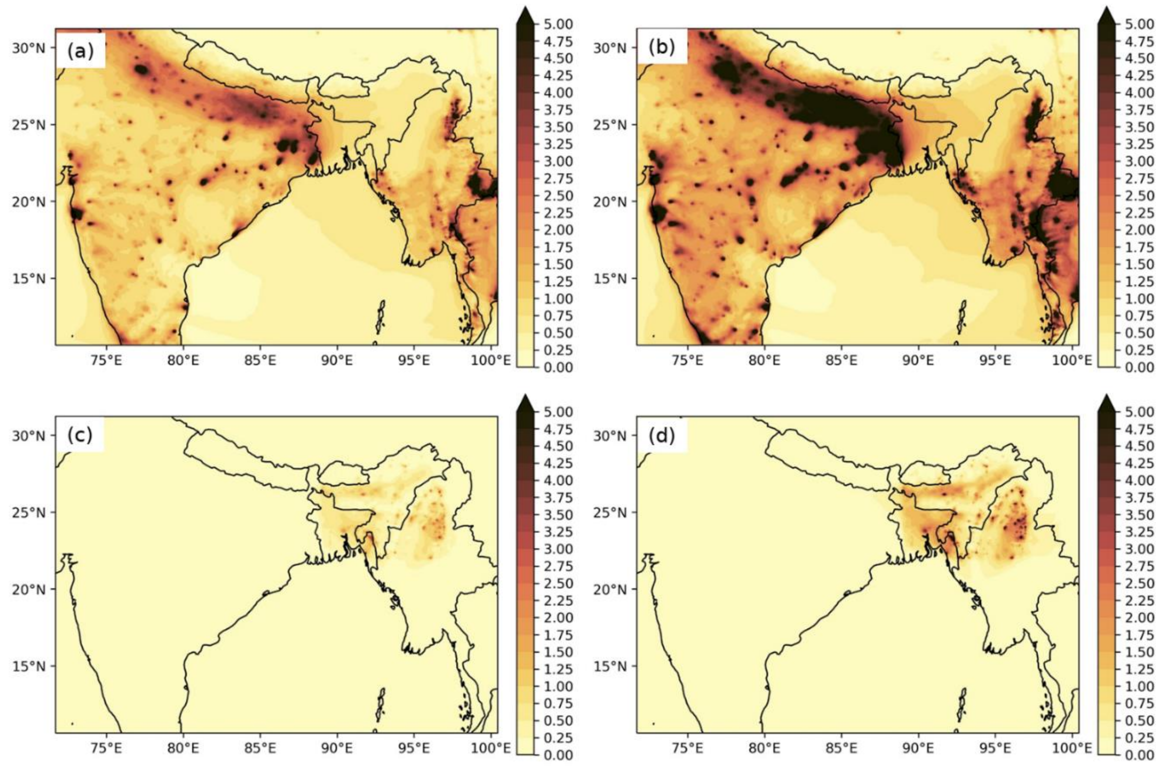

Figure 4.17: Spatial distributions of near surface (model level 0) BC concentration (µg m^{-3}) in a) No_NE_BC b) No_NE_2×BC c) Only_NE_BC d) Only_NE_2×BC

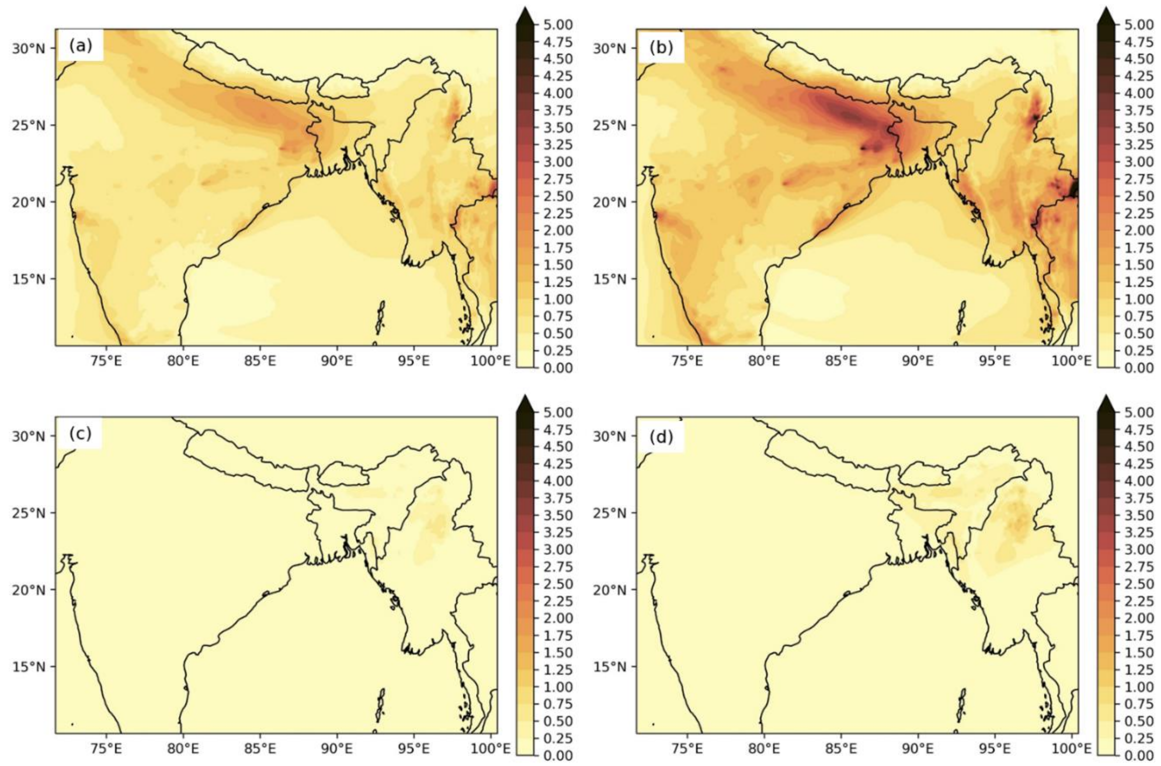

Figure 4.18: Spatial distributions of BC concentration (µg m^{-3}) in a) No_NE_BC b) No_NE_2×BC c) Only_NE_BC d) Only_NE_2×BC level at model level 10

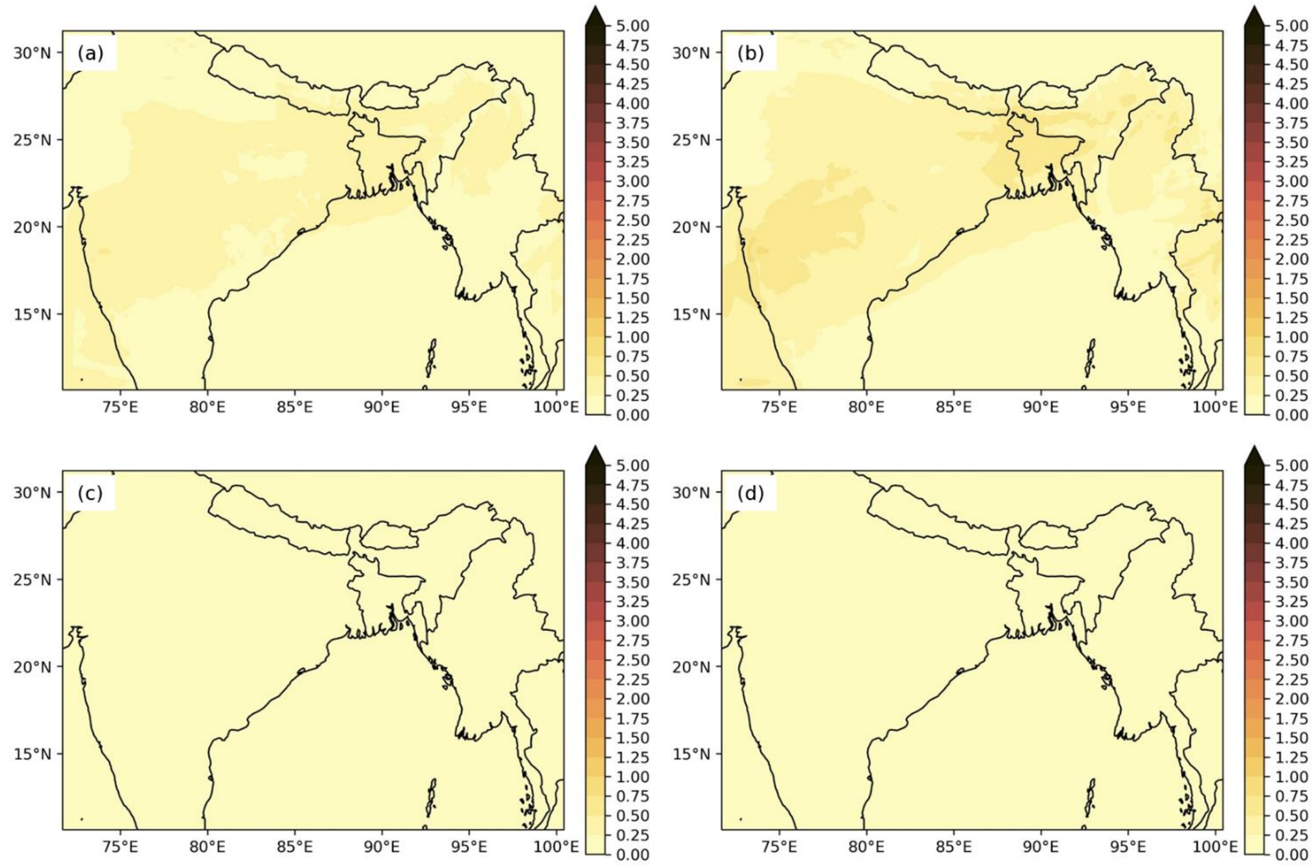

Figure 4.19: Spatial distributions of BC concentration (μg m^{-3}) in a) No_NE_BC b) No_NE_2×BC c) Only_NE_BC d) Only_NE_2×BC at model level 20

Table 4.7: BC concentration (μg m^{-3}) at different model levels under different scenarios

	No_NE_BC (1)	No_NE_2×BC (2)	Only_NE_BC (3)	Only_NE_2×BC (4)	NOR	2NOR	(1) + (3)	(2) + (4)
Level 0								
Region 1	0.90	1.39	0.72	1.39	1.61	2.82	1.62	2.78
Region 2	0.63	0.92	0.39	0.76	1.04	1.69	1.02	1.67
Region 3	0.38	0.50	0.16	0.33	0.53	0.80	0.54	0.82
Region 4	0.69	1.02	0.58	1.12	1.27	2.11	1.27	2.14
Average	**0.65**	**0.96**	**0.46**	**0.90**	**1.11**	**1.85**	**1.11**	**1.85**
Level 10								
Region 1	0.88	1.32	0.24	0.45	1.11	1.79	1.11	1.77
Region 2	0.62	0.92	0.18	0.34	0.81	1.24	0.79	1.26
Region 3	0.35	0.46	0.09	0.18	0.44	0.62	0.44	0.65
Region 4	0.67	1.00	0.16	0.31	0.86	1.34	0.83	1.31
Average	**0.63**	**0.93**	**0.17**	**0.32**	**0.80**	**1.25**	**0.80**	**1.25**
Level 20								
Region 1	0.36	0.52	0.02	0.03	0.38	0.56	0.38	0.55
Region 2	0.28	0.39	0.03	0.06	0.30	0.44	0.31	0.45
Region 3	0.20	0.26	0.03	0.06	0.23	0.32	0.23	0.32
Region 4	0.28	0.39	0.02	0.03	0.29	0.42	0.29	0.42
Average	**0.28**	**0.39**	**0.02**	**0.05**	**0.30**	**0.43**	**0.30**	**0.44**

The quantitative concentration values in different scenarios and at different atmospheric heights is provided in Table 4.7. Transported BC mainly from IGP contributed to a higher regional average (0.65 µg m^{-3}) compared to the local emissions (0.46 µg m^{-3}). Similar results were observed even on doubling the emissions (0.96 µg m^{-3} vs. 0.90 µg m^{-3}). This quantitatively verifies the results observed before. However, the response of concentration to an increase in BC emission rates varied under different scenarios. Doubling the BC emissions from Only_NE_BC to Only_NE_2×BC led to almost double the regional average concentration from 0.46 µg m^{-3} to 0.90 µg m^{-3}, but such response was not seen in the case of No_NE_BC and No_NE_2×BC and a smaller increase of 0.31 µg m^{-3} was observed. This is due to the reason that BC emissions within the NE India region remained within the region as seen in Figure 4.17(c) and 4.17(d) but are transported from other regions in transported BC scenarios. Since No_NE_BC and Only_NE_BC are theoretically a bifurcation of NOR into two separate regions and No_NE_2×BC and Only_NE_2×BC is a bifurcation of 2NOR, the contribution of BC emissions from inside and outside NE region to the BC concentration over NE India was estimated. The bifurcation was also verified by the near-surface regional average concentration of NOR (1.11 µg m^{-3}) exactly matching the sum of No_NE_BC and Only_NE_BC and similar results were observed at higher model levels also. This showed that BC over the NE India region is the sum of BC concentration from local emissions within NE and transported BC and percentage contribution could be found out by dividing the local or transported BC from NOR simulation. A similar analysis was done in Table 4.5, but the sum of local and transported PM_{10} concentration values didn't match with NOR-I. Similar conclusions could be derived for 2NOR and the sum of No_NE_2×BC and Only_NE_2×BC. Near the surface, No_NE_BC and No_NE_2×BC contributed to 58.55 % and 51.89 %, respectively of the BC over the region, and were also responsible for most of the BC in the higher atmosphere as shown in Table 4.7. At level 10 and level 20, the proportion of transported

BC was 78 % and 93 %, respectively and thus, in the higher atmosphere also, most of the BC found was mainly from the IGP. Moreover, since BC emissions within NE India mostly stay within the same region, an increase in emissions within the region may lead to an accumulation of BC over the region due to the mountainous terrain, as discussed before.

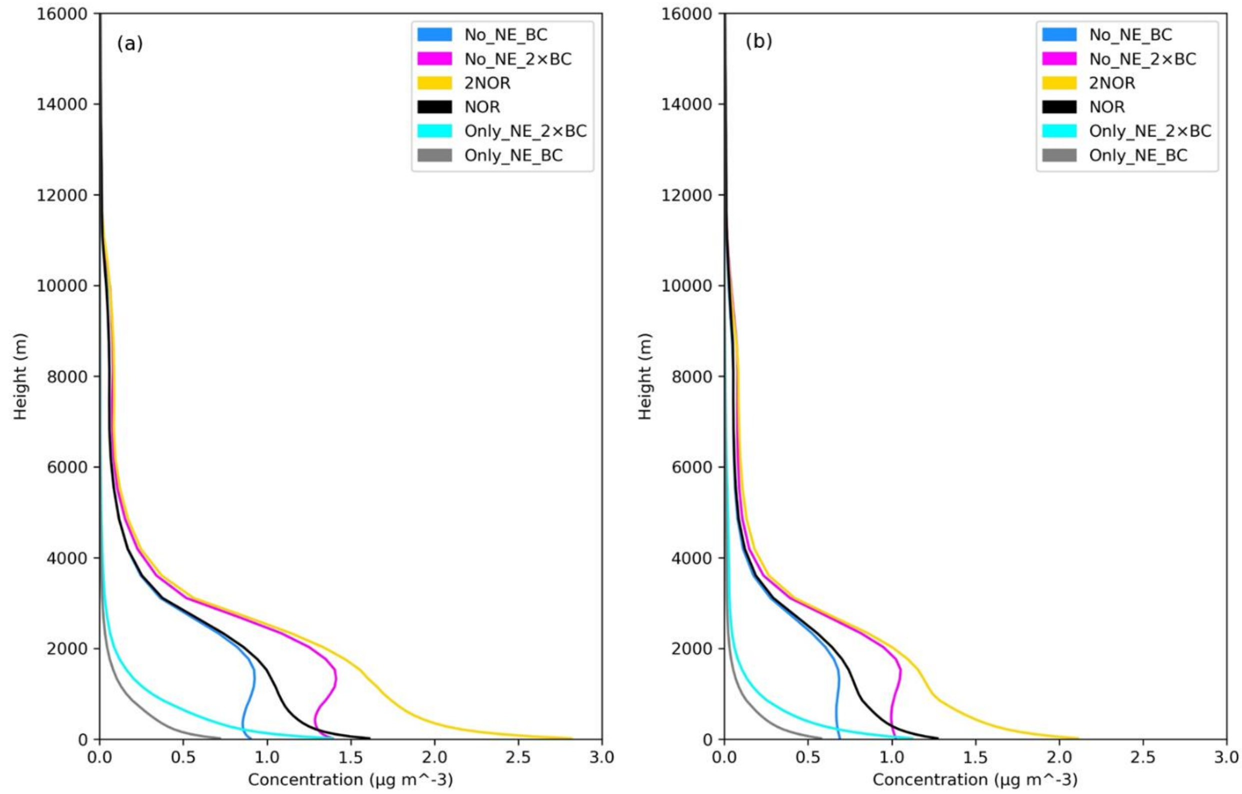

Figure 4.20: Regionally averaged vertical profiles of BC concentration (µg m^{-3}) in a) region 1 b) region 4

Being in closer proximity to the IGP, region 1 experienced stronger BC transport from it, as can be verified from Table 4.7. The transport is even stronger than region 4 which can be verified from Figure 4.20. This is followed by region 2 and region 3. Thus, BC concentration in the regions matched the proximity to IGP.

4.3.4.2 Radiative heating

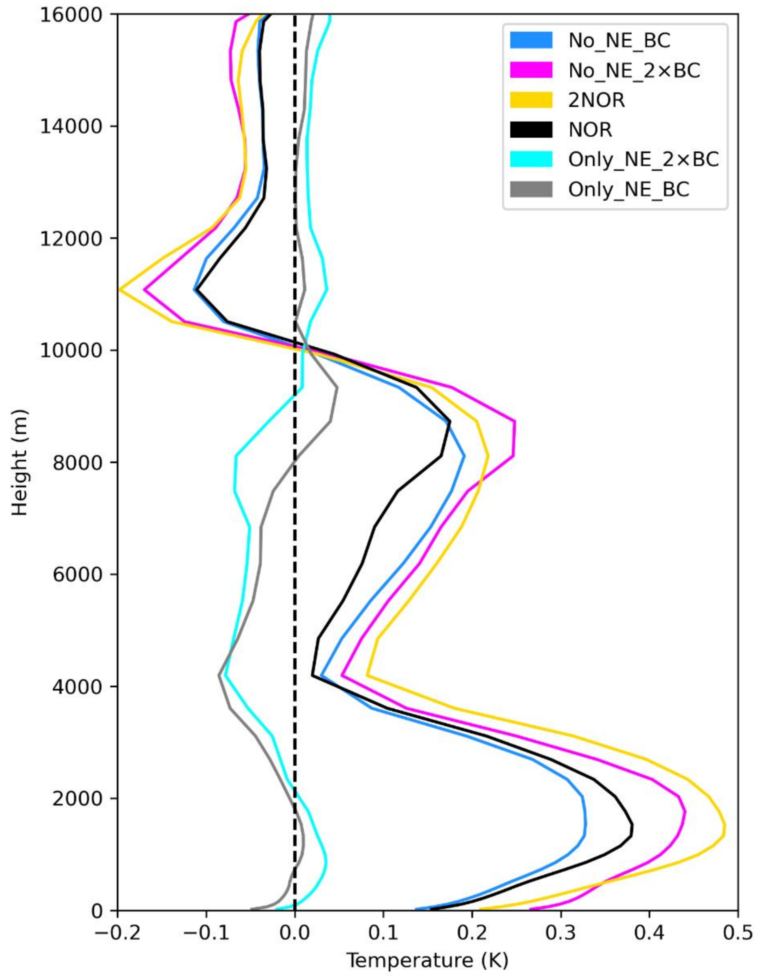

Figure 4.21: Regionally averaged vertical profiles of sensible temperature perturbation (K)

The perturbation in sensible temperature due to different scenarios is provided in Figure 4.21. Each profile each estimated by subtracting the sensible temperature from each of the simulations in the figure from NOFEED simulation. The qualitative similarity between No_NE_BC and NOR profiles and No_NE_2×BC and 2NOR profiles showed that the atmospheric heating was mainly caused by the BC transported from IGP. The increase in sensible temperature occurred mainly in the lower atmosphere. There existed a vast difference between the temperature profiles of local and transported BC. For Only_NE_BC and Only_NE_2×BC profiles, temperature perturbation was considerably less and the profile almost stayed near the zero-perturbation line throughout the atmosphere, while the remaining profiles showed great variation with height. For Only_NE_BC and Only_NE_2×BC profiles, the peaks below 2000 m were closer to the surface, possibly due to the presence of most of the BC near the surface. There existed a certain height difference between the peaks of these BC profiles in Figure 4.16 and the corresponding temperature profiles in Figure 4.21, with temperature peaks existing above concentration peaks. It is possibly related to higher atmospheric heating at higher heights due to more efficient absorption of sunlight, as was discussed in previous studies (Ding et al., 2016; Dong et al., 2017; Wang et al., 2018) Due to the presence of elevated BC concentration for the remaining profiles, elevated heating was also observed for them with positive tendencies below 10 km and cooling above it. The atmospheric heating rate (HR) was estimated using equation 25 as per Liou (1980), and was also used by Kedia et al. (2016) and Bibi et al. (2017).

$$HR = \frac{g}{C_p} \cdot \frac{\Delta F}{\Delta P}, \tag{25}$$

where g is the acceleration due to gravity (9.81 m s^{-2}), C_p is the specific heat capacity of air at constant pressure (1.005 kJ K^{-1} kg^{-1}), ΔF the atmospheric RF and ΔP is the atmospheric pressure (300 hPa) difference between surface and 3 km altitude as most of the BC was present below this height. Moreover, in order to compare the effectiveness of heating by local and transported BC, two parameters, heating efficiency (HE) and heating slope (HS), were defined by equations 26 and 27.

$$HE = \frac{HR}{\text{Column sum of BC concentration within 3 km (CC)}} \tag{26}$$

$$HS = \frac{\Delta HR}{\Delta CC}, \tag{27}$$

HE has units of K day^{-1} μg^{-1} m^3, thus measuring the heating contributed by per unit concentration of BC below 3 km. HE was used to assess the effect of BC vertical distribution on atmospheric heating while HS was used to assess the response of atmospheric heating rate to BC concentration changes and has similar units as HE. CC has units of µg m^{-3}.

Table 4.8: NE India region average values of columnar BC concentration (µg m^{-3}) and atmospheric heating parameters in different scenarios

	No_NE_BC	No_NE_2×BC	Only_NE_BC	Only_NE_2×BC
HR	0.460	0.597	0.123	0.178
CC	12.458	18.391	3.905	7.563
HE	0.037	0.032	0.032	0.024
ΔHE	-0.004		-0.008	
HS	0.023		0.015	

The quantitative values of the parameters are provided in Table 4.8. Only_NE_BC had a regional net average HR of 0.123 K day^{-1} compared to 0.460 K day^{-1} of No_NE_BC. This indicated a 3.73 times higher atmospheric heating rate by transported BC. An increase in local emissions from Only_NE_BC to Only_NE_2×BC caused a small increase in heating rate of 0.055 K day^{-1} compared to the increase of 0.137 K day^{-1} from No_NE_BC to No_NE_2×BC. As per the definition, HE was inversely proportional to CC and this was exactly followed in all regions across all scenarios (Figure 4.22 and 4.23).

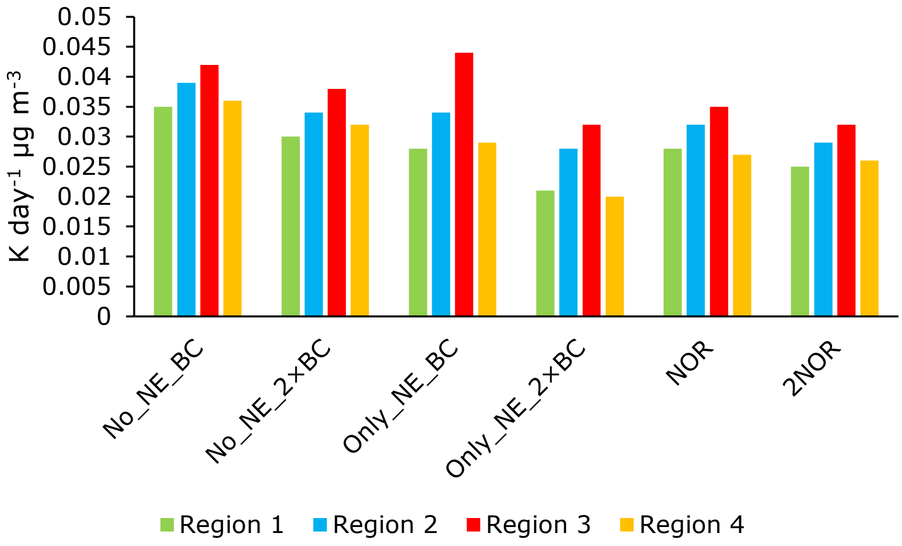

Figure 4.22: Region-wise HE in different scenarios

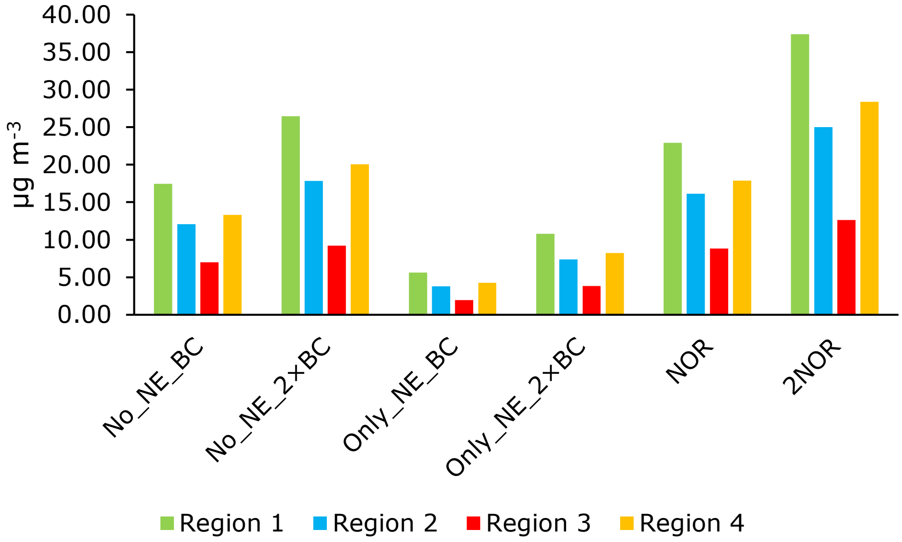

Figure 4.23: Column integrated BC concentration

However, HE was higher in the case of transported BC compared to local BC with values of 0.037 K day^{-1} µg^{-1} m^{3} (No_NE_BC) vs. 0.032 K day^{-1} µg^{-1} m^{3} (Only_NE_BC) and 0.032 K day^{-1} µg^{-1} m^{3} (No_NE_2×BC) vs. 0.024 K day^{-1} µg^{-1} m^{3} (Only_NE_2×BC), even if CC was higher in the case of transported BC. The reason might be that transported BC might have undergone a higher amount of chemical transformation due to higher atmospheric time, leading to a higher lensing effect on the BC core, resulting in enhanced absorption (Liu et al., 2015).

Slater et al. (2022) also found that the HR per unit mass of BC is higher when it is aloft than when near the surface. Also, it was observed that on increasing emissions, the decrease in HE was smaller in the case of transported BC (-0.004 K day^{-1} μg^{-1} m^3) than local BC (-0.008 K day^{-1} μg^{-1} m^3). Hence, with the increase in BC emissions, HE decreased more when BC was more concentrated near the surface than in the atmosphere. HS indicated that atmospheric heating increased at a higher rate of 0.023 K day^{-1} μg^{-1} m^3 with increasing transported BC compared to 0.015 K day^{-1} μg^{-1} m^3. Thus, the increase in transported BC emissions had more impact on atmospheric heating over NE India than when present near the surface with local emissions.

4.3.4.3 Atmospheric stability and moisture

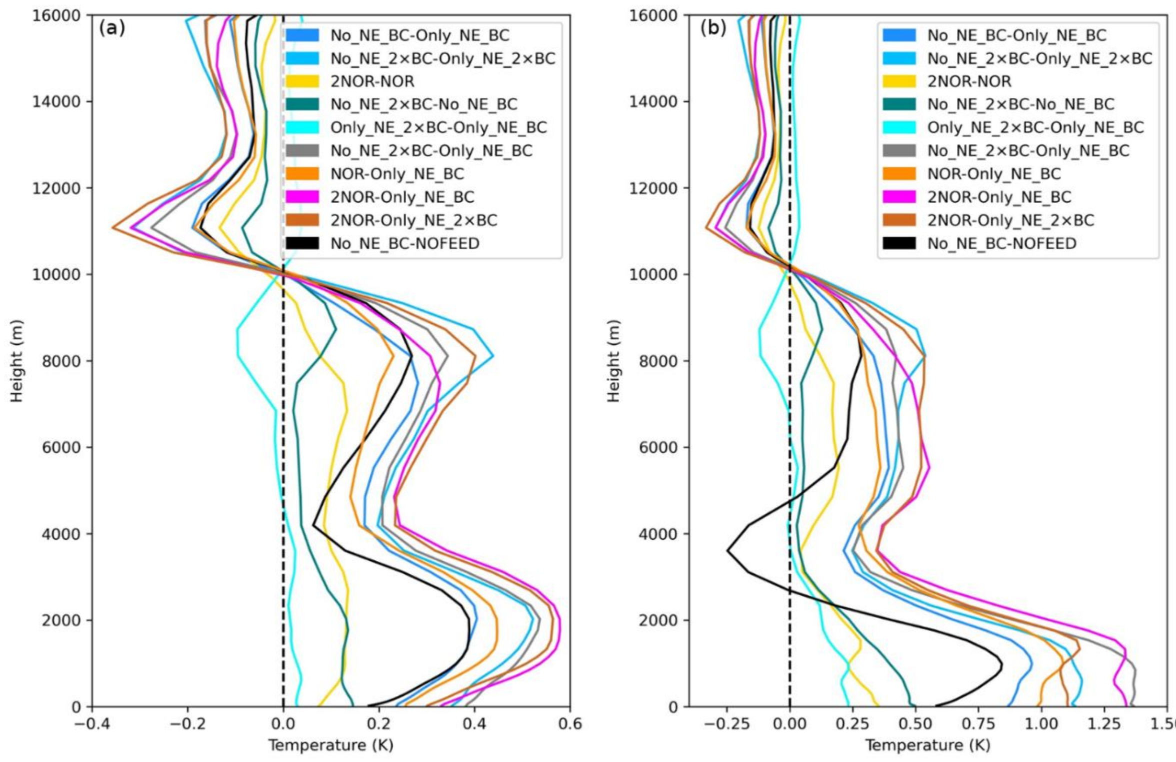

Figure 4.24: Regionally averaged vertical profiles showing perturbations in a) potential temperature (K) b) equivalent potential temperature (K)

Chapter 3, as well as Soni et al. (2018), showed an increased influx of moisture into the region during pre-monsoon due to BC. In order to compare and separate the effects of local and transported BC on atmospheric stability through temperature and moisture, potential temperature (PT) and EPT were estimated. PT estimates atmospheric stability based on temperature, while EPT accounts for both temperature and moisture and is a more realistic parameter. In most of the profiles in both parameters in Figure 4.24(a) and 4.24(b), positive perturbation was observed approximately below 10 km and negative above it which indicated an increase in atmospheric instability and vice-versa for an increase in atmospheric stability. (Zhao et al., 2011). The positive perturbations below 10 km varied with height and were most profound in the profiles No_NE_BC – Only_NE_BC, No_NE_2×BC – Only_NE_2×BC and No_NE_2×BC – Only_NE_BC, each of which was estimated from the difference between a transported BC scenario and local BC scenario. These profiles showed similarity with the corresponding profiles of NOR – Only_NE_BC, 2NOR – Only_NE_2×BC and 2NOR – Only_NE_BC in both the parameters, indicating that they were closer to the normal atmospheric scenario. The positive perturbations were, however, comparatively smaller with 2NOR – NOR, No_NE_2×BC – No_NE_BC and Only_NE_2×BC – Only_NE_BC in both the parameters, each pair being the same scenario with only a difference in emission rates. This shows that BC atmospheric distribution played an important role in instability. The Only_NE_2×BC – Only_NE_BC profile not only showed a smaller increase in instability than No_NE_2×BC – No_NE_BC profile but also contributed to the smallest increase in instability in both the parameters. Thus, transported BC and an increase in transported BC emissions led to higher atmospheric instability than local BC. However, there occurred a region of increased stability from the ground surface to the first peak of transported BC profiles at approximately 1000 m, indicated by increasing temperature with height. Thus, transported BC may also be responsible for air quality scenarios over NE India by creating a stable boundary layer.

Moreover, EPT profiles showed higher positive perturbations and hence higher instability compared to the corresponding PT profiles with values exceeding 1.25 K. The positive difference or additional instability between the corresponding profiles of Figure 4.24(a) and 4.24(b) was due to moisture. The difference also indicated that moisture contributed even more to the instability than BC.

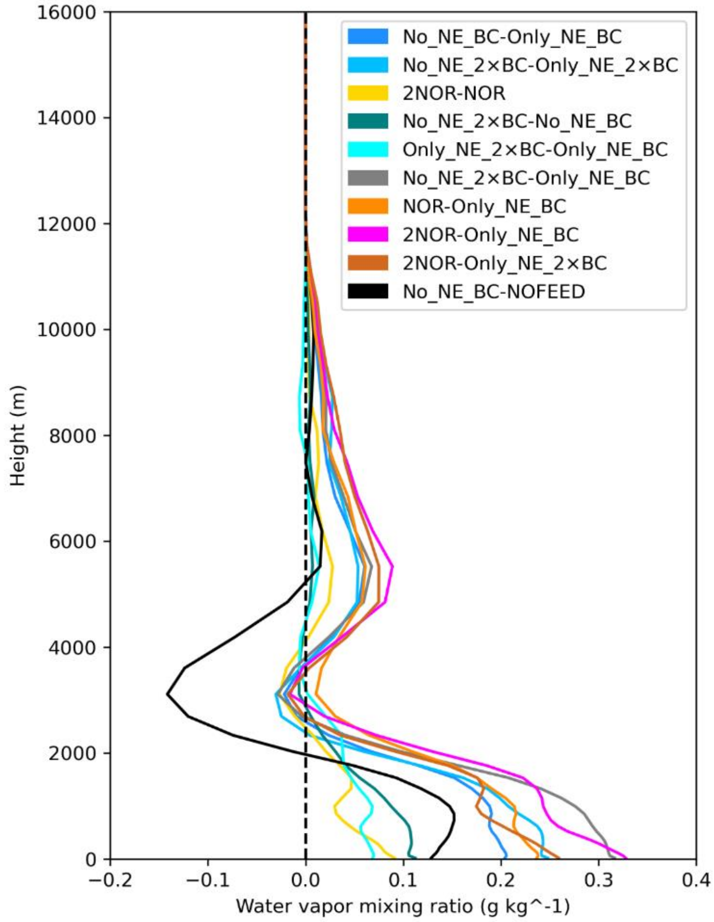

Figure 4.25: Regionally averaged vertical profiles showing perturbations in water vapor mixing ratio (g kg^{-1})

The peaks for EPT existed closer to the surface due to most of the moisture also remaining near the surface, as shown in Figure 4.25. The close qualitative and quantitative similarity between No_NE_BC – NOFEED, No_NE_BC – Only_NE_BC and NOR – Only_NE_BC profiles in Figure 4.24(a) showed that aerosol radiative effect due to transported BC was intricately linked with the PT profile and the positive perturbations in each of these profiles were also closely linked with BC. This was also seen in Figure 4.24(b), but since it also included the effect of moisture, larger differences were seen.

BC, whether transported or emitted locally, caused a positive perturbation in moisture at least below 2 km altitude, as seen in Figure 4.25. The perturbation was much larger in profiles that had a combination of transported and local BC scenarios and which had higher transported BC emissions and followed a pattern similar to PT and EPT. This links BC, instability and moisture in the region, i.e., higher transported BC caused higher instability which brought a higher amount of moisture which would possibly again cause higher instability. It was the same for scenarios that included indirect effect, as can be observed from the similarities of the No_NE_BCI – Only_NE_BCI (Figure 4.26) and No_NE_BC – Only_NE_BC profile in Figure 4.25.

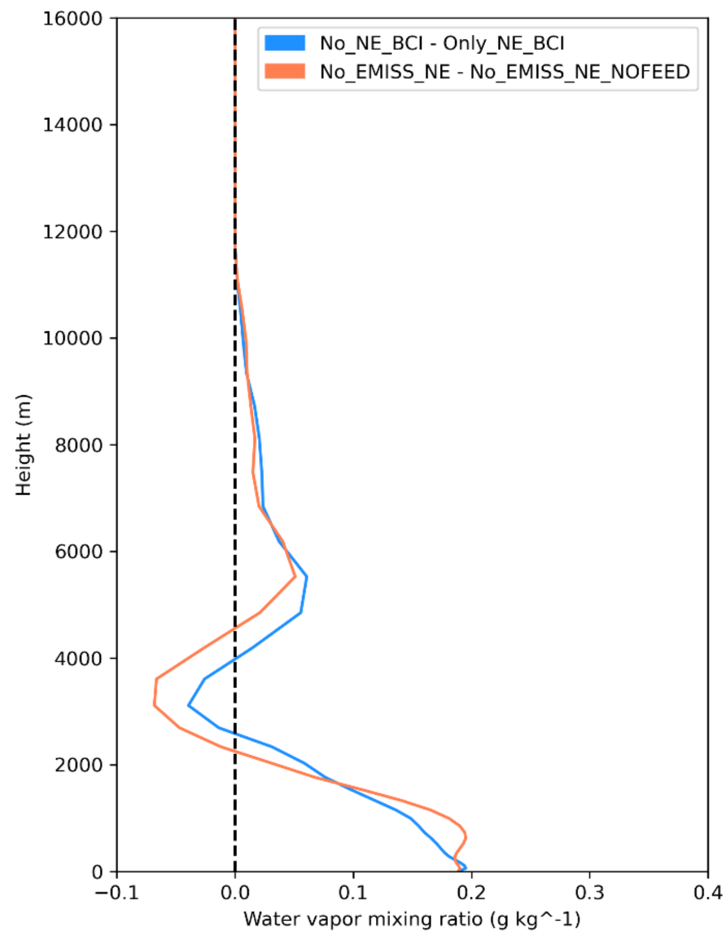

Figure 4.26: Regionally averaged vertical profiles of water vapor mixing ratio (g kg^{-1}) perturbations

The higher moisture with transported BC scenarios was due to higher moisture flux caused by it over the Bay of Bengal compared to local BC and can be verified from Figure 4.27. Consequently, No_NE_BC (33.95 kg m^{-2}) and No_NE_2×BC (34.15 kg m^{-2}) had higher region average precipitable water vapor than Only_NE_BC (33.49 kg m^{-2}) and Only_NE_2×BC (33.64 kg m^{-2}). Hence transported BC in Section 4.3.3 was primarily responsible for transporting moisture from the Bay of Bengal by affecting the atmospheric dynamics. The mechanism is similar to the "heat pump" model by Lau et al. (2006).

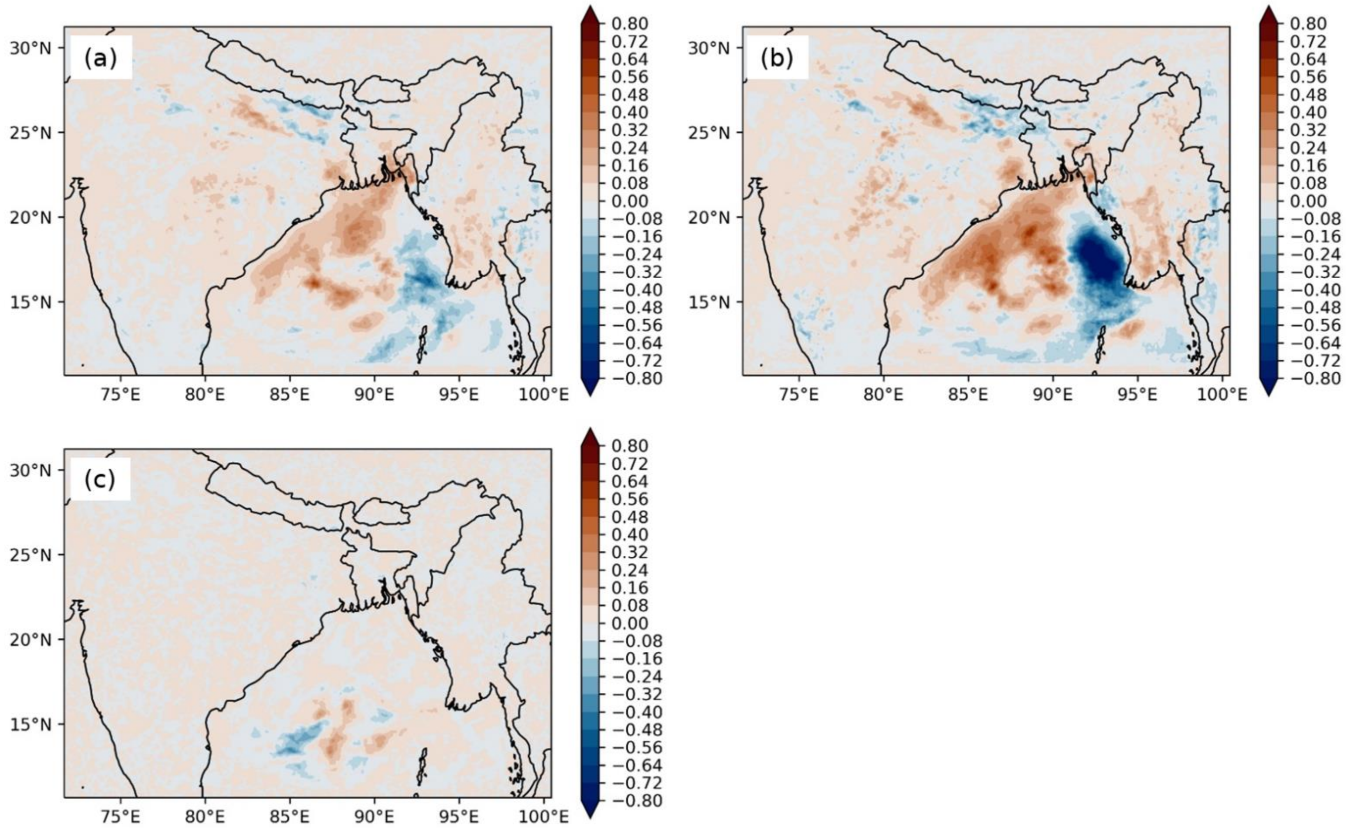

Figure 4.27: Spatial distributions of change in moisture flux (g s^{-1} m^{-2}) in a) No_NE_BC – Only_NE_BC b) No_NE_2×BC – Only_NE_BC c) Only_NE_2×BC – Only_NE_BC near surface

Furthermore, the similarity of No_EMISS_NE – Only_EMISS_NE profile with No_NE_BCI – Only_NE_BCI in Figure 4.26 inferred that the direct radiative effect of transported BC was responsible for the moisture increase in Figure 4.13. Hence, No_NE_BCI caused a higher rainfall of 36.26 mm than Only_NE_BCI, as seen in Figure 4.28. The relation of increased rainfall due to an increase in moisture was also observed in Kedia et al. (2016). The increase is mostly in region 1, 4 and the upper part of the Brahmaputra valley.

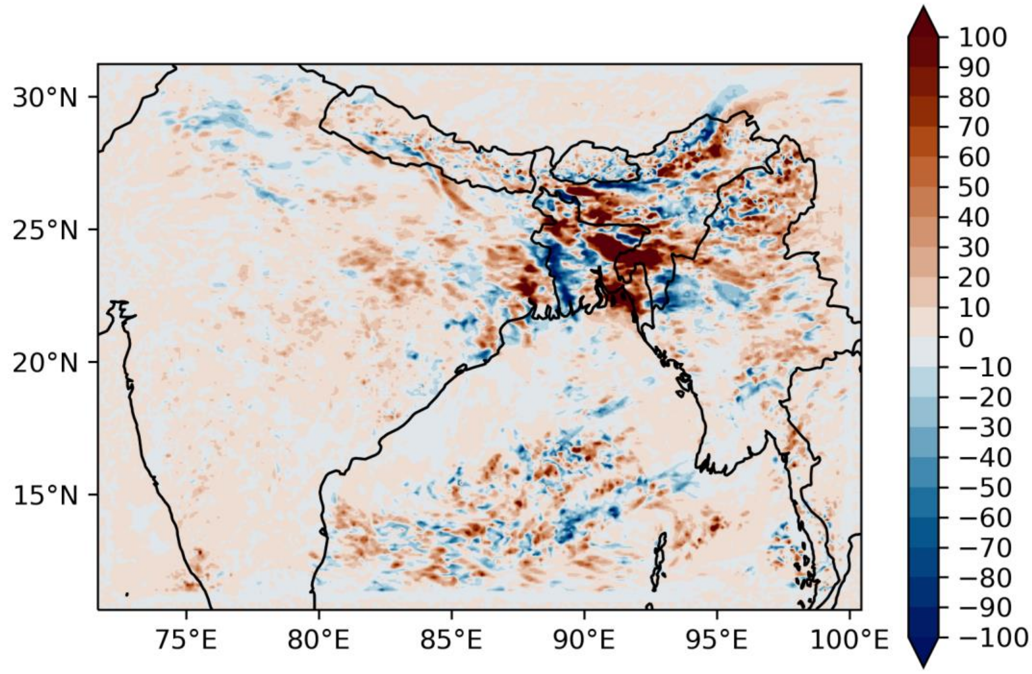

Figure 4.28: Spatial distributions of change in rainfall (mm) in No_NE_BCI – Only_NE_BCI

So, doesn't BC suppress rainfall through indirect aerosol effect? Aged BC also contributes as CCN (Lambe et al., 2015), contributing to indirect aerosol effect but the difference in the column average CCN concentration over NE India was small with 2122 cm^{-3} in No_NE_BCI and 2175 cm^{-3} in Only_NE_BCI, though it was observed previously that transported BC concentration was much higher than local BC over NE India. Hence, it indicated that BC didn't contribute much as CCN. Kristjánsson (2002) also observed BC contributes only marginally to indirect effect. Moreover, a lower value of CCN with No_NE_BCI may be related to the suppression of CCN activation due to BC, as observed over Central India (Nair Jayachandran et al., 2020), as transported BC had higher BC concentration. Thus, the positive effect on rainfall by transported BC was primarily due to the greater change in dynamics than the cloud modifications causing suppression. Enhancement of CCN number concentration generally leads to enhancement of indirect aerosol effect (Yu et al., 2013) but the difference in CCN was very small. Rather, the increase in moisture, caused by the increase in atmospheric instability possibly condensed on a relatively smaller number of CCN particles promoting larger cloud droplets which enhanced rainfall. This indicated that the higher transported BC emissions didn't contribute to rainfall suppression through indirect aerosol, but rather counteracted the suppression of rainfall due to the indirect effect of other aerosol species. The rainfall enhancement was due to an increase in moisture, contributed by the transported fraction of BC, as explained in Section 4.3.4.3. Moreover, rainfall suppression was also more due to transported aerosols, mainly contributed by indirect effect (Table 4.6).

4.3.5 Role of sulfate aerosol

Also, among the non-absorbing aerosols, sulfate aerosol is an important contributor to CCN and indirect effect (Kristjánsson, 2002). Its concentration was found to be the highest among non-absorbing aerosols and most of its mass over NE India was found to be transported (Sect. 4.3.1). Concentration profiles can be seen from Figure 4.29.

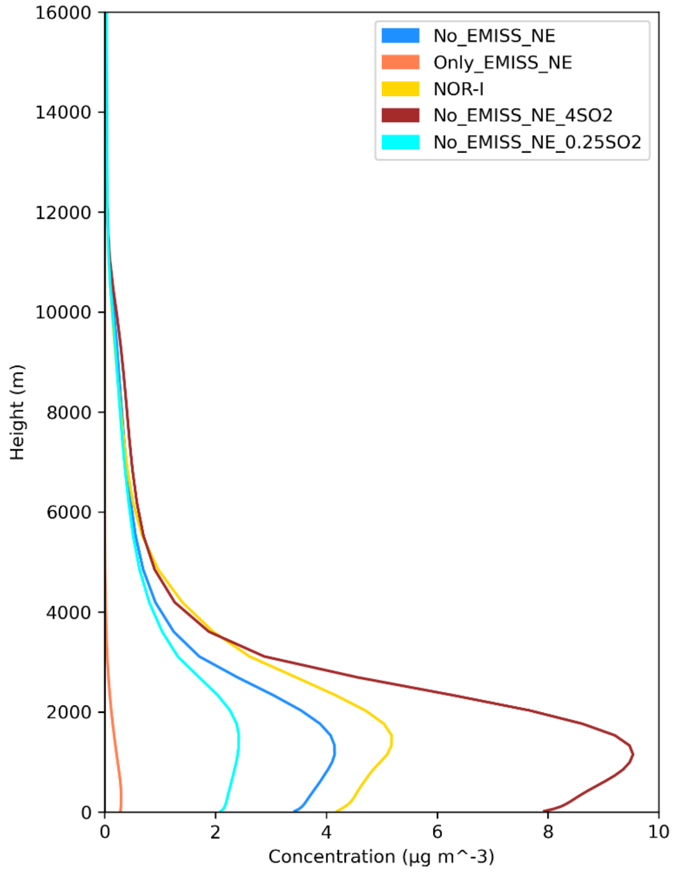

Figure 4.29: Regional average vertical profile of sulfate aerosol concentration (µg m^{-3}) in different scenarios

Hence, the response of rainfall over NE India was checked by increasing (No_EMISS_NE_4SO₂) and decreasing (No_EMISS_NE_0.25SO₂) SO_2 emissions outside NE India and compared against the baseline transported scenario (No_EMISS_NE) since sulfate is mainly formed within the atmosphere by oxidation of SO_2 (Wang et al., 2021). No_EMISS_NE_4SO₂ caused an increase in column average CCN concentration to 3524 cm^{-3} compared to 1753 cm^{-3} in No_EMISS_NE, while No_EMISS_NE_0.25SO₂ showed a decrease (1390 cm^{-3}). Thus, changes in transported SO_2 emissions showed a significant response to CCN and hence to indirect effect. The increase in SO_2 emissions with No_EMISS_NE_4SO₂ caused an increase in cloudwater mixing ratio compared to No_EMISS_NE, as seen in Figure 4.15, while its decrease also caused a decrease. Thus, No_EMISS_NE_4SO₂ and No_EMISS_NE_0.25SO₂ had lower and higher rainwater mixing ratios, respectively, compared to No_EMISS_NE. Consequently, No_EMISS_NE_4SO_2 had higher rainfall suppression and gave lesser rainfall (-22.23 mm) compared to No_EMISS_NE_0.25SO_2. Spatial distribution is shown in Figure 4.30 which shows mainly negative change over the region. Thus, an increase in non-absorbing transported aerosol caused rainfall suppression through indirect effect. Hence, we can say that the under the influence of different aerosol effects that reduce surface moisture evaporation by surface dimming, the moisture transported from the Bay of Bengal by the influence of BC transported from IGP remains the primary source of rainfall. However, the supposed rainfall is suppressed by the aerosols emanating from the IGP.

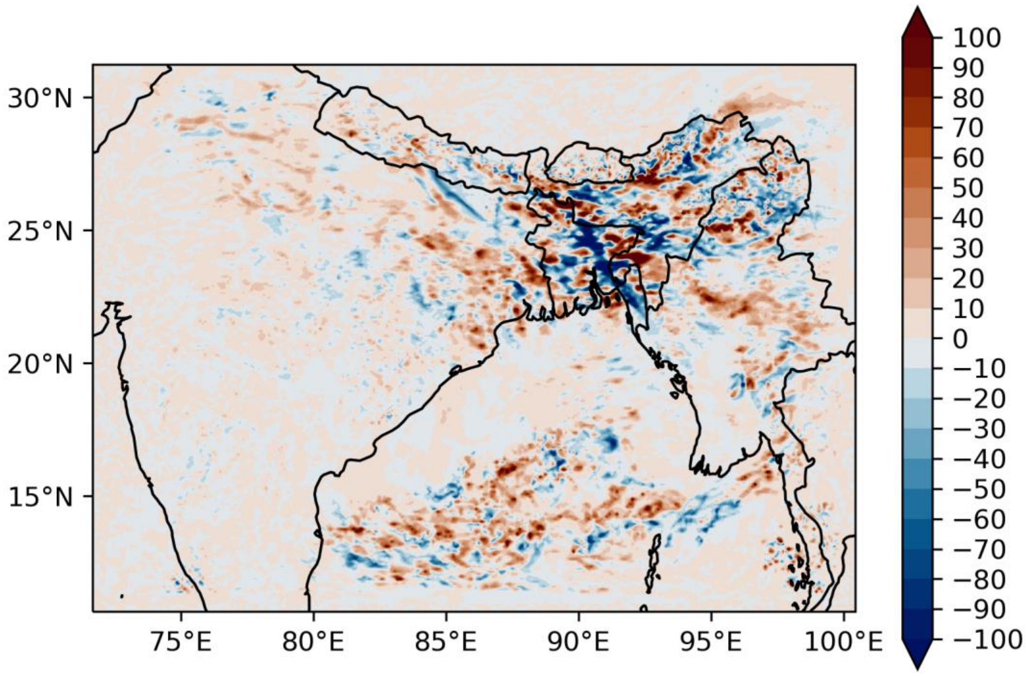

Figure 4.30: Spatial distributions of change in rainfall (mm) in No_EMISS_NE_4SO_2 – No_EMISS_NE_0.25SO_2

The indirect effect was observed to be the dominant aerosol effect for suppressing rainfall. However, with an increase in BC, suppression of rainfall due to direct and semi-direct effects through surface processes (surface moisture flux, convection) and cloud evaporation as well as due to indirect aerosol effect (atmospheric stability, surface moisture flux and cloud to rainwater conversion) becomes comparatively weaker mechanisms than the direct effect of radiative heating by BC, enhancing rainfall through the transport of moisture. Moisture transported by BC remain the one and only source for rainfall over NE India. All other aerosol processes reduce moisture. However, the increase in transported SO_2 emissions also caused further suppression of rainfall. Hence, an increase in transported aerosols of an absorbing aerosol (BC) and a non-absorbing aerosol (sulfate), both being a contributor to CCN, exerted different impacts on rainfall and hence most likely controls the enhancement and suppression of pre-monsoon rainfall over NE India, thus counteracting each other. However, since decreasing rainfall trend has been observed, the impacts of the indirect aerosol effect could be dominant. Here, the response of only one non-absorbing aerosol (sulfate) was checked and possibly had contributions from other similar species also. Other non-absorbing aerosol species like nitrate also contribute to indirect aerosol effect (Wang et al., 2010; Zaveri et al., 2021) which may contribute to rainfall suppression as sulfate.

4.4 Summary

Transported aerosols, primarily from IGP, were found to be responsible for the bulk of the aerosol mass (93.98 %) over NE India while contributing 64.18 % of near-surface PM_{10} concentration, thus primarily responsible for air pollution as climatic impacts over the region during pre-monsoon season. The climatic impacts, both w.r.t. RF as well as rainfall, were dominated by the indirect aerosol effect. The impacts of the indirect aerosol effects of transported aerosols were much higher in affecting radiation (-13.12 W m^{-2} vs. -0.24 W m^{-2} at the surface, 7.30 W m^{-2} vs. 0.97 W m^{-2} in the atmosphere) as well as suppressing rainfall (-49.11 mm vs. -16.04 mm) compared to local emissions. The greater surface dimming by transported aerosols caused a higher negative change in surface moisture flux (-3.82×10^{-6} kg m^{-2} s^{-1} vs. 8.15×10^{-8} kg m^{-2} s^{-1}) as well as higher aerosol mass reduced cloudwater to rainwater conversion, both of which contributed to higher rainfall suppression. Transported aerosols caused 4.42×10^{13} m^{-2} higher cloud droplets than local emissions. The atmospheric instability due to the direct + semi-direct effect and indirect effect of transported aerosols were found to be contradictory and caused an increase and decrease, respectively. The direct effect of transported aerosols, though also caused negative surface moisture flux over NE India (-1.03×10^{-6} kg m^{-2} s^{-1}), however, increased moisture over NE India, increasing moisture flux over the Bay of Bengal. Further analysis showed that transported BC was more efficient in atmospheric heating over NE India and together with the higher transported BC mass, an increase in its emissions caused higher atmospheric instability over the region, which brought more moisture from the Bay of Bengal. The increased moisture further contributed to higher instability. Hence, the rainfall suppression caused through the different atmospheric processes by direct, semi-direct and indirect effects were nullified. The direct effect of BC thus overpowered the other rainfall-suppressing processes. Indirect aerosol effect and radiative heating were the main rainfall-controlling factors. Hence, changes in emissions of aerosols or chemical species contributing to these processes will possibly contribute to rainfall suppression and enhancement over NE India. Moreover, rainfall simulated with transported aerosols was found to be more similar to the IMD observation datasets as well as the baseline emission scenario, indicating its possible greater influence in the real-world scenario.

The study shows that the atmospheric transport of emissions from IGP to NE India has a significant impact on NE India's atmosphere during pre-monsoon and the impacts are even greater than the emissions within the NE India region.

Chapter 5

5.Direct aerosol effect of black carbon on rainfall intensity

5.1 General

The analysis in the previous chapters showed that transported BC emissions increases rainfall over NE India through direct radiative effect. This chapter analyses the response of rainfall intensity with increase in BC emissions. The chapter also analyses whether the semi-direct effect has any role or do rainfall increases indefinitely with an increase in BC emissions, as semi-direct effect cause cloud evaporation which reduces rainfall. This compliments the findings of Chapter 3.

5.2 Methodology

The model, model inputs, modelling domains, model configuration and simulation period in this study is similar to Chapter 3 and 4. The list of simulations that were used is given in table 5.1.

Table 5.1: Description of simulations

	Simulation name	**Description of simulations**
1.	NOR-I	Baseline simulation
2.	4NOR-I	Same as NOR-I but with 4×BC emissions
3.	8NOR-I	Same as NOR-I but with 8×BC emissions
4.	NOFEED-I	Same as NOR-I but with no aerosol radiative effects
5.	4NOFEED-I	Same as NOFEED-I but with 4×BC emissions
6.	8NOFEED-I	Same as NOFEED-I but with 8×BC emissions
7.	NOR	Same as NOR-I but without indirect effect
8.	2NOR	Same as NOR but with 2×BC emissions
9.	4NOR	Same as NOR but with 4×BC emissions
10.	NO_BC_ABS	Same as NOR but with BC absorption turned off
11.	No_NE_BCI	Same as NOR-I but with BC emissions turned on only outside NE India
12.	Only_NE_BCI	Same as NOR-I but with BC emissions turned on only within NE India

The NOR-I simulation utilized in Chapter 4 are also used in this study. 4NOR-I and 8NOR-I have 4 and 8 times the BC emission rates, respectively, compared to NOR-I. NOFEED-I, 4NOFEED-I and 8NOFEED-I are similar to NOR-I, 4NOR-I and 8NOR-I, but with aerosol radiative effects turned off. Simulations 7, 8, 9 and 10 are the same as that in Chapter 3. Simulations 11 and 12 are the same as that used in Chapter 4. The direct and semi-direct and were separated using a similar methodology as in Chapter 4.

$$\text{NOR-I} - \text{NOFEED-I} = \text{Direct} + \text{Semi-direct effect} \quad (28)$$

$$\text{4NOR-I} - \text{4NOFEED-I} = \text{Direct} + \text{Semi-direct effect} \quad (29)$$

$$\text{8NOR-I} - \text{8NOFEED-I} = \text{Direct} + \text{Semi-direct effect} \quad (30)$$

The BC emissions in Chapter 3 go up to 4×, here it goes up to 8×.

5.3 Results and discussion

As pointed out in Chapter 3 also, simulated rainfall is of two types: grid-scale or NCR contributed by the transport of moisture from water bodies and sub-grid scale or CR, caused by rising thermals. NCR is controlled by the microphysics scheme, while CR by the cumulus scheme. The division of NE India into sub-regions is the same as that in Chapter 4. The total of the region average CR amounts is shown in Table 5.2 while for NCR in Table 5.3. Moreover, the total rainfall values in both tables have been classified into different intensities of rainfall as per IMD (https://mausam.imd.gov.in/imd_latest/contents/pdf/pubbrochures/Heavy%20Rainfall%20Warning%20Services.pdf). The intensities are as follows. Light: up to 1 cm hr^{-1}, moderate: 1-2 cm hr^{-1}, intense: 2-3 cm hr^{-1}, very intense: 3-5 cm hr^{-1}, extremely intense: 5-10 cm hr^{-1} and cloud burst: >10 cm hr^{-1}. The rainfall occurring under each intensity (cm hr^{-1}) has been summed up to give the total rainfall amount under each intensity (mm).

Table 5.2: Classification of CR into different intensities (mm)

	Total	Low	Moderate	Intense	Very intense	Extreme intense	Cloud burst
NOR-I	322.03	314.61	7.42	0.00	0.00	0.00	0.00
4NOR-I	312.59	307.54	5.06	0.00	0.00	0.00	0.00
8NOR-I	311.58	305.86	5.72	0.00	0.00	0.00	0.00

Table 5.3: Classification of NCR into different intensities (mm)

	Total	Low	Moderate	Intense	Very intense	Extreme intense	Cloud burst
NOR-I	268.00	183.28	52.26	19.40	11.37	1.70	0.00
4NOR-I	304.55	190.71	64.41	28.92	17.34	3.18	0.00
8NOR-I	290.69	188.48	60.65	25.86	14.37	1.32	0.00

Table 5.4: Change in total and intensity-wise NCR due to changes in direct effect of BC (mm)

	Total	Low	Moderate	Intense	Very intense	Extreme intense	Cloud burst
4NOR-I - NOR-I	34.36	4.54	15.04	8.41	4.94	1.43	0.00
8NOR-I - 4NOR-I	-20.19	-0.52	-7.67	-5.38	-6.11	-0.50	0.00

Table 5.2 shows that CR contributes slightly higher rainfall than NCR in Table 5.3 over NE India across all simulation scenarios. However, CR in all scenarios except NOR-I remained between 311.58 mm and 322.03 mm and was much less sensitive to the change in emissions than NCR. A lesser effect on CR was also seen in Chapter 3. NCR increased from 268.00 mm in NOR-I to 304.55 mm in 4NOR-I. Thus, NCR varied significantly between the simulations compared to CR. Also, most of the CR occurred under low intensity and there was none to very little rainfall in the other intensities across all scenarios. Moreover, CR decreased with an increase in BC emissions. NCR, on the other hand, occurred even with extreme intensity and showed perturbation with the change in emissions. Moreover, BC affects rainfall by transporting moisture through direct effect, which is an NCR type. Hence, direct effect on NCR is mainly studied in this study. Moreover, Table 5.4 shows that due to the direct radiative effect, NCR increased by 34.36 mm over the region from NOR-I to 4NOR-I, while it decreased by -20.19 mm with a further increase from 4NOR-I to 8NOR-I. Thus, the increase in rainfall due to the increased moisture transport from the Bay of Bengal is not a monotonic phenomenon but reverses after a particular level of BC emissions. Here the level is found to be between 4× to 8×BC emissions.

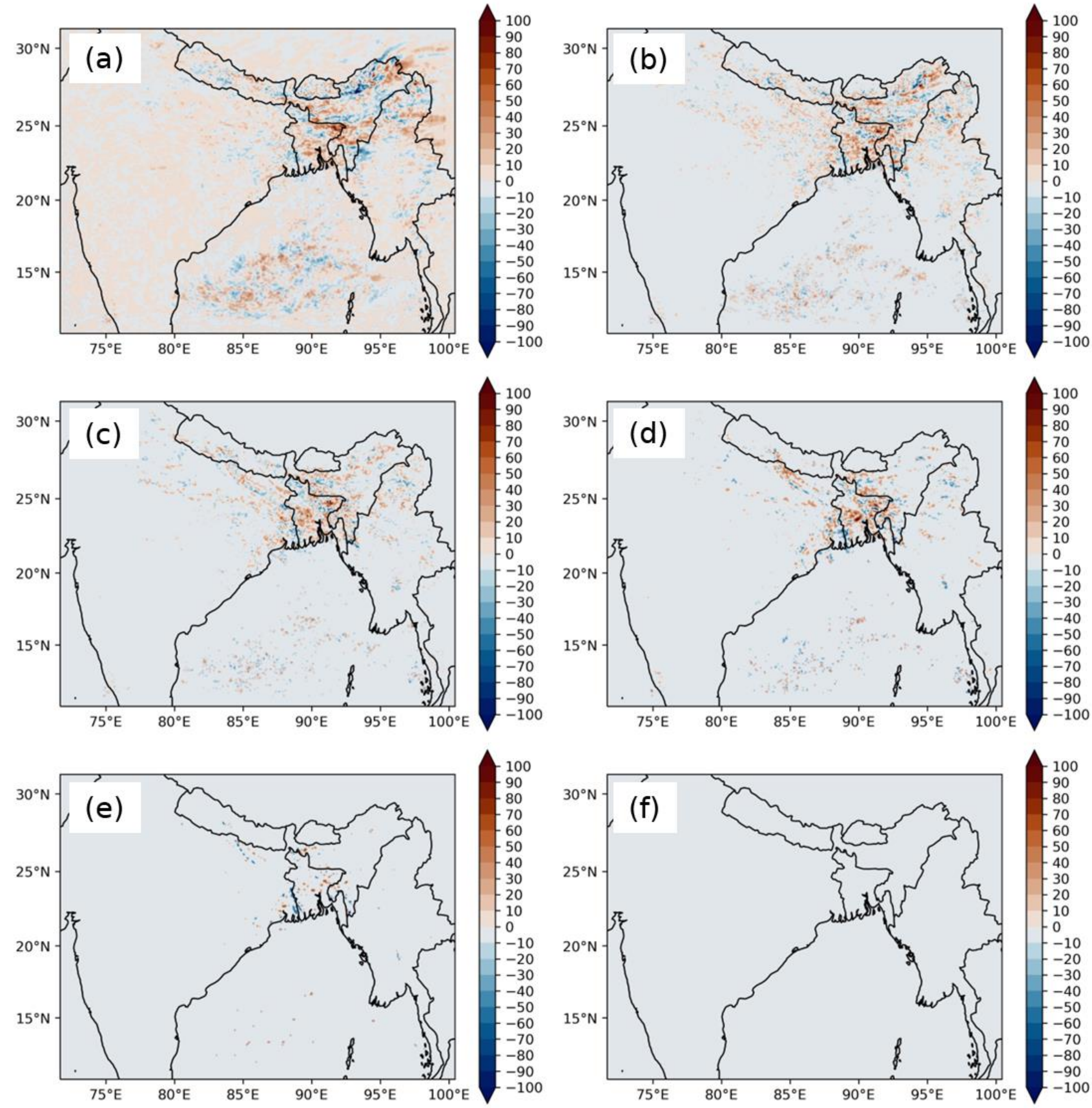

Figure 5.1: Spatial distribution of intensity-wise change in NCR (mm) from 4NOR-I – NOR-I a) low b) moderate c) intense d) very intense e) extreme intense d) cloud burst intense due to direct effect of BC

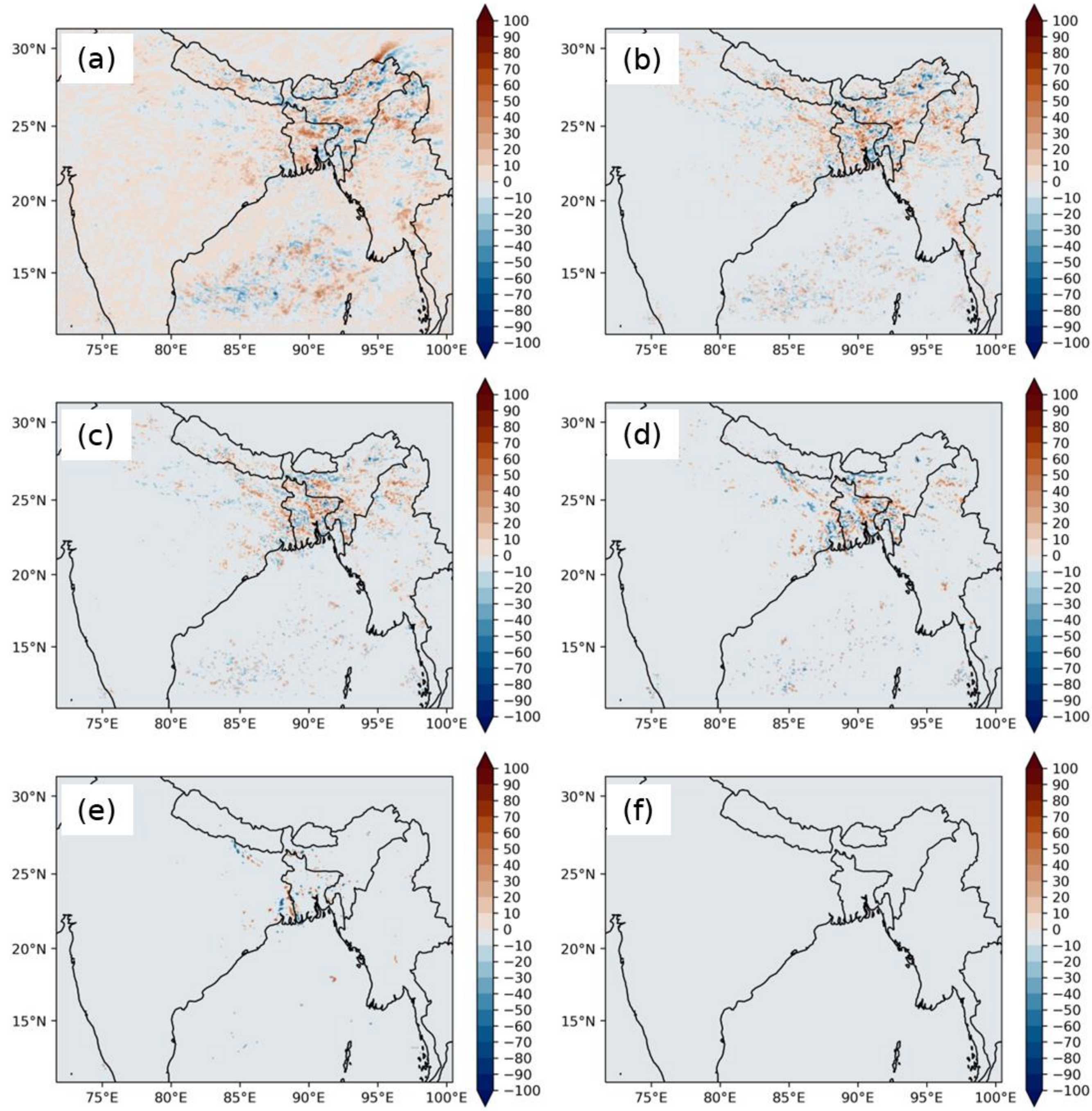

Figure 5.2: Spatial distribution of intensity-wise change in NCR (mm) from 8NOR-I – 4NOR-I a) low b) moderate c) intense d) very intense e) extreme intense d) cloud burst intense due to direct effect of BC

Table 5.5: Region-wise and intensity-wise changes in NCR (mm) due to direct effect of BC

	Low	Moderate	Intense	Very intense	Extreme intense	Cloud burst	Total
4NOR-I – NOR-I							
Region 1	7.95	7.47	2.74	2.95	0.90	0.00	22.01
Region 2	-8.30	-0.27	0.57	0.12	0.10	0.00	-7.79
Region 3	-1.04	2.64	1.30	-0.22	0.11	0.00	2.79
Region 4	5.94	5.21	3.80	2.08	0.32	0.00	17.35
8NOR-I – 4NOR-I							
Region 1	-4.21	-5.08	-5.06	-6.00	0.15	0.00	-20.20
Region 2	7.84	3.37	2.16	0.68	-0.05	0.00	13.99
Region 3	-3.40	-4.00	-2.37	-0.86	-0.20	0.00	-10.84
Region 4	-0.75	-1.96	-0.10	0.07	-0.40	0.00	-3.14

Figure 5.1 and 5.2 shows the spatial distribution of intensity-wise change in rainfall due to direct effect of BC in 4NOR-I – NOR-I and 8NOR-I – 4NOR-I, respectively and the region-wise values are provided in Table 5.5. It can be seen from Figure 5.1 that changes in BC emissions affects mainly the rainfall over NE India and the increase in rainfall in 4NOR-I – NOR-I mainly occurs over region 1, 3 and 4, as also seen from the total in Table 5.5. An increase in rainfall with low-intensity rainfall mainly occurred along the Brahmaputra River valley and similar results are seen for moderate, intense and very intense intensities. However, rainfall increased through all intensities in region 1 and 4, while rainfall reduction through particular intensities were observed for region 2 and 3. Thus, region 1 and 4 were the most affected region, experiencing extreme rainfall with a total increase of 22.01 mm and 17.35 mm, respectively. A slight increase of 2.79 mm was observed for region 3, mainly contributed by the low-intensity rainfall in the upper part of the Brahmaputra River valley. Region 2 observed

a decrease with a value of -7.79 mm. Further verification is provided by the NOR, 4NOR and 8NOR simulations from Chapter 3, which only included the direct and semi-direct effects.

Table 5.6: Region-wise percentage of time rainfall change occurs under a particular rainfall intensity

	Region 1						
Rainfall intensity (mm hr^{-1})	0-5	5-10	≥10	- 0-5	- 5-10	≤ -10	0 (no change)
NOR-NO_BC_ABS	19.92	4.07	16.44	19.88	4.23	16.40	19.06
2NOR-NO_BC_ABS	19.32	4.28	17.21	19.71	4.27	16.80	18.41
4NOR-NO_BC_ABS	18.90	4.24	17.10	20.31	4.34	16.93	18.18
	Region 2						
NOR-NO_BC_ABS	21.48	4.12	14.04	21.57	4.07	13.07	21.65
2NOR-NO_BC_ABS	20.97	4.49	14.81	21.12	3.87	13.00	21.74
4NOR-NO_BC_ABS	20.37	4.30	16.01	21.00	3.99	13.12	21.21
	Region 3						
NOR-NO_BC_ABS	19.53	3.66	14.69	21.48	3.63	15.54	21.47
2NOR-NO_BC_ABS	19.71	3.74	15.24	21.36	3.57	15.16	21.22
4NOR-NO_BC_ABS	18.38	3.51	15.82	22.01	3.59	15.40	21.29
	Region 4						
NOR-NO_BC_ABS	25.82	4.37	17.64	18.66	3.22	13.69	16.60
2NOR-NO_BC_ABS	25.49	4.34	19.88	18.27	3.15	13.45	15.42
4NOR-NO_BC_ABS	25.21	4.28	18.97	19.52	3.27	14.26	14.49

Table 5.6 shows the percentage of time rainfall change occurs under a particular intensity. The intensities used are as discussed in Chapter 3, since the simulations are from Chapter 3. Considering the positive changes (0-5, 5-10 and ≥ 10 mm hr^{-1} columns), it can be seen that with the increase in emissions, low-intensity rainfall decreases and high-intensity rainfall increases in general. Moderate-intensity rainfall increased with 2NOR but again decreased with 4NOR. The decrease in low-intensity rainfall may be that it is caused by smaller cloud droplets, which evaporate easily with increasing atmospheric temperature. Most of the high-intensity rainfall enhancement changes occur in region 4, followed by region 1 as also seen in this chapter. The increasing atmospheric temperature induced by the increased absorption by BC was responsible for this, as the difference between the simulations in Table 5.6 represents the absorption. Thus, the increase in BC caused high-intensity rainfall along with the increase in

its duration. It was observed in Chapter 3 that the increase in BC emissions caused an increase in high level-clouds due to an increase in the ice hydrometeor. However, besides ice, the increase in BC absorption also caused an increase in the formation of snow and graupel hydrometeors, as observed in Figure 5.3. The possible reasons for this are that with an increase in black carbon concentrations, an increase in moisture was also seen. Increased black carbon also increases atmospheric instability over the region, which facilitates the transfer of more moisture to the upper atmosphere, which facilitates the formation of ice, snow and graupel hydrometeors. Melting of graupel hydrometeor can also produce higher-intensity rainfall. The increase in cloud cover near 10 km contributed by ice is a possible validation of this. This conclusion is based on the study by Li et al. (2011) and Sarangi et al. (2015).

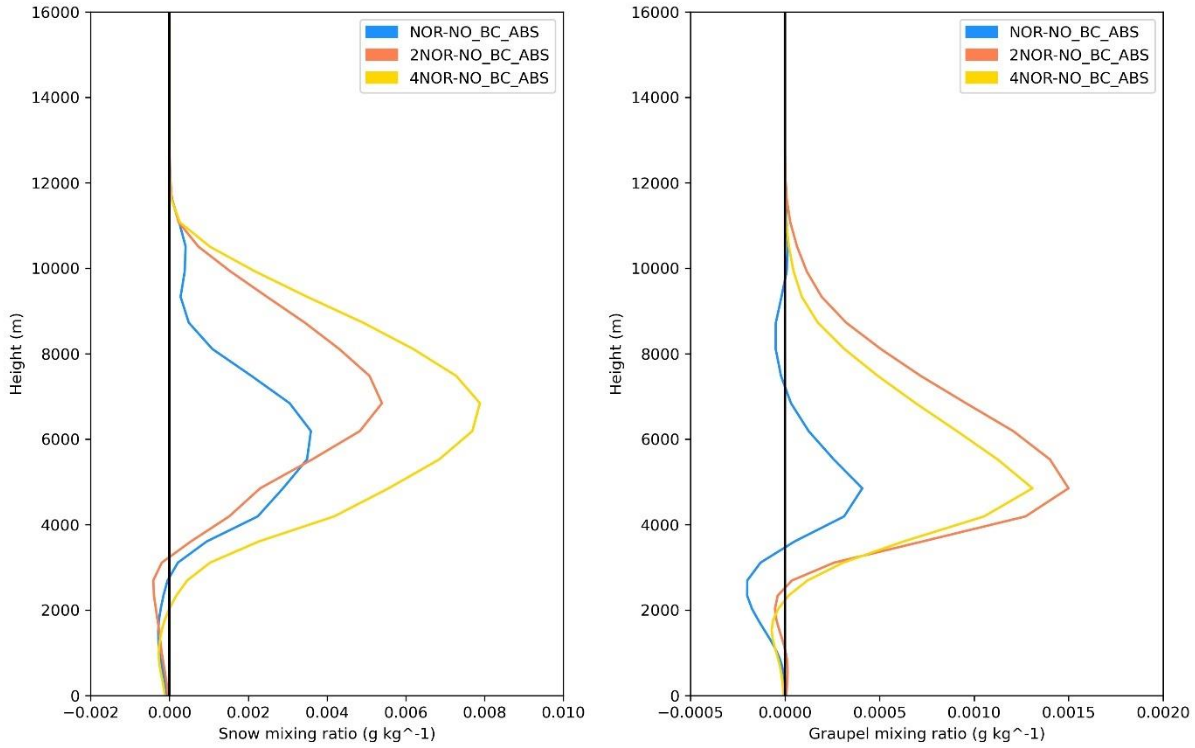

Figure 5.3: Regionally averaged vertical profile of snow hydrometeor (left) and graupel hydrometeor (right)

Thus this explains the high-intensity rainfall mechanism by direct effect of BC. For the negative changes (- 0-5, - 5-10 and ≤ -10 mm/hr columns), all rainfall intensities are suppressed for less duration with 2NOR in general, compared to NOR and 4NOR. Also, it can be seen from the last column that with the increase in BC emissions and associated atmospheric heating, BC influences rainfall for more amount of time. Similar plots as in Figure 5.3 were also observed for NOR-I, 4NOR-I and 8NOR-I, as shown in Figure 5.4, which infers that the increase in BC absorption are responsible for such impacts. Thus, similar mechanisms also occurred with the inclusion of indirect effects also in NOR-I, 4NOR-I and 8NOR-I. This could be an additional process for high-intensity rainfall, apart from the increase in moisture below 2000 m. However, the significantly smaller difference between the 4NOR-I and 8NOR-I profiles compared to NOR-I and 4NOR-I profiles need further investigation.

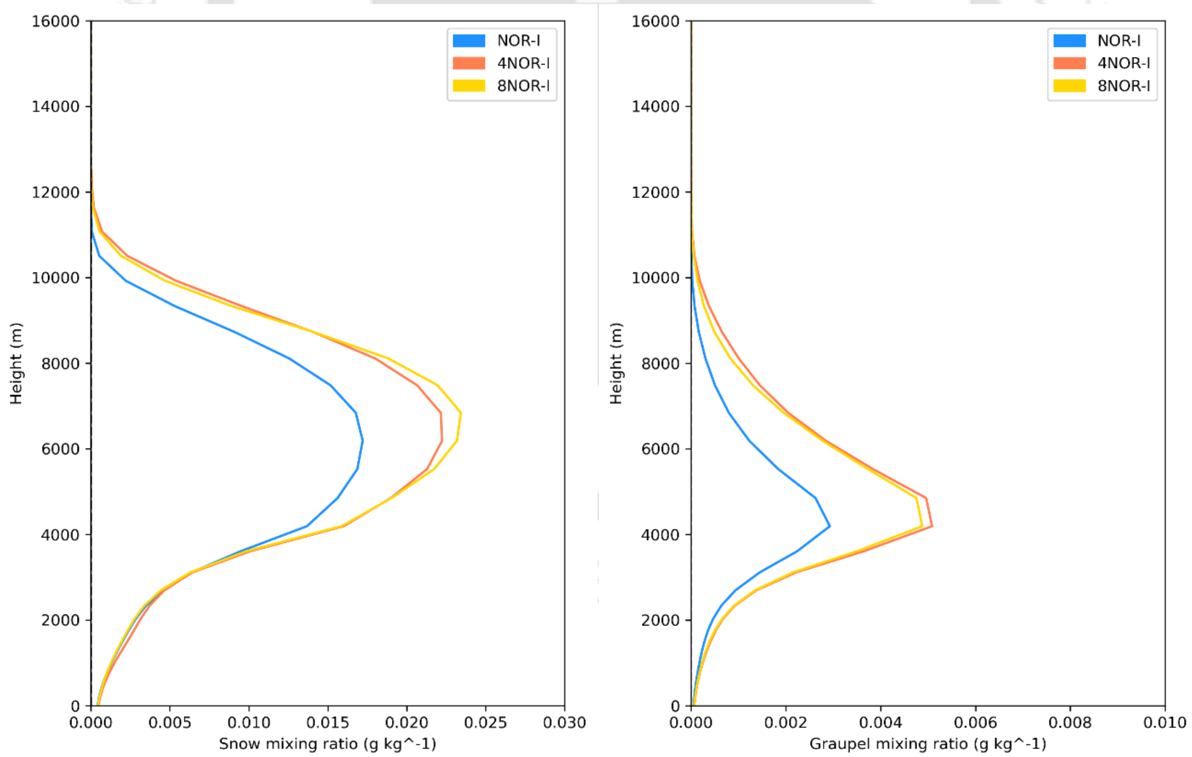

Figure 5.4: Regionally averaged vertical profile of snow hydrometeor (left) and graupel hydrometeor (right) in NOR-I, 4NOR-I and 8NOR-I

Moreover, intensity-wise rainfall difference estimated from No_NE_BCI – Only_NE_BCI show positive values which implied that the transported BC, primarily from IGP was responsible for the increase in rainfall through different intensities. The spatial distribution is shown in Figure 5.5. Increase of 11.83 mm, 7.37 mm, 6.92 mm, 5.95 mm and 0.95 mm was observed for low, moderate, intense, very intense and extreme intense rainfall, caused by transported BC and hence show similar conclusions as was observed for 4NOR-I – NOR-I. This concluded that transported BC was responsible for the high-intensity rainfall over NE India.

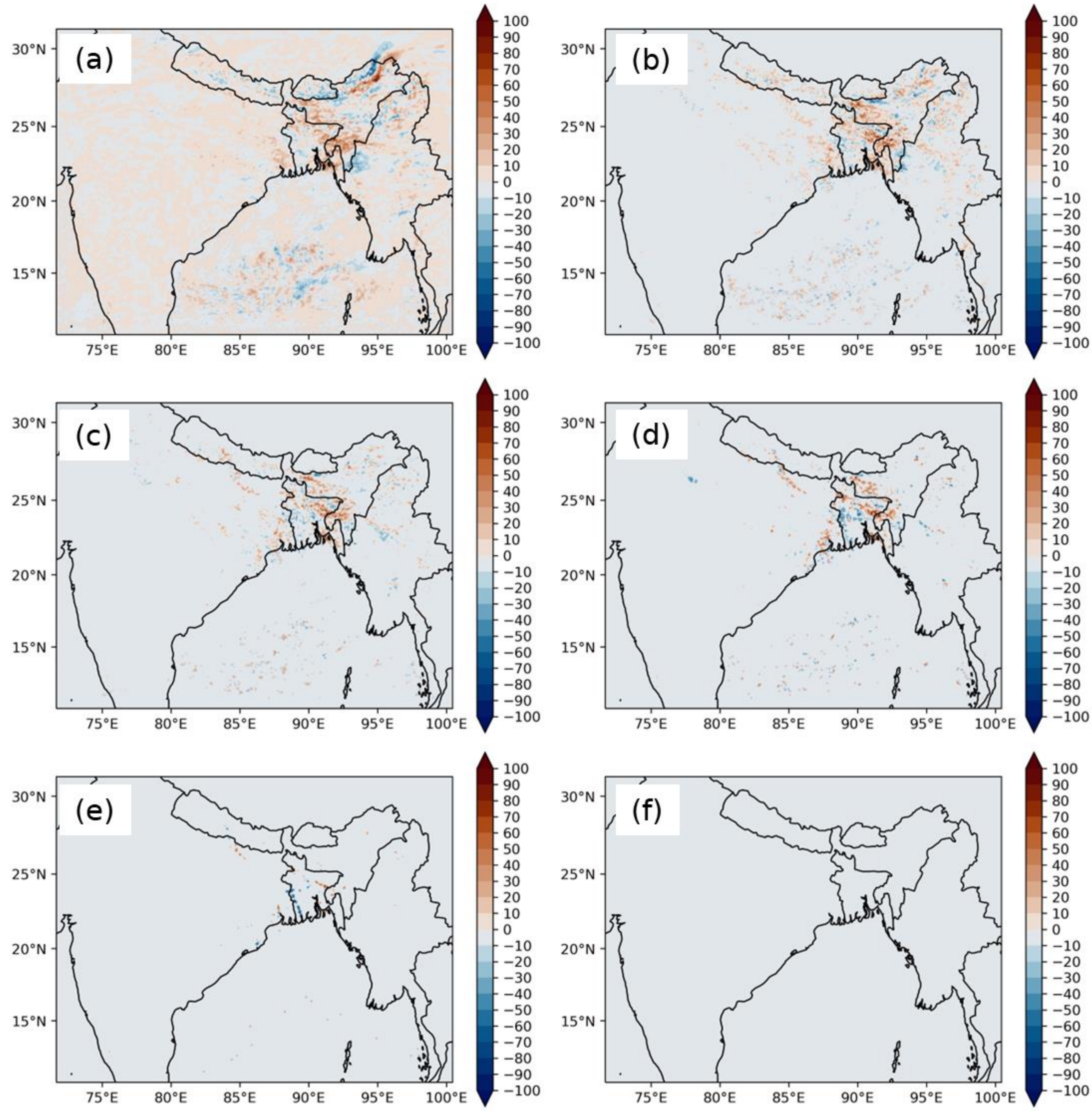

Figure 5.5: Spatial distribution of intensity-wise change in NCR (mm) from No_NE_BCI – Only_NE_BCI a) low b) moderate c) intense d) very intense e) extreme intense d) cloud burst intense

However, as we move from 4NOR-I – NOR-I to 8NOR-I – 4NOR-I, contrasting results were observed. The regions (1, 3 and 4) which had observed positive total rainfall, became negative with values of -20.20 mm, -10.84 mm and -3.14 mm for region 1, 3 and 4, respectively. The reduction occurred through a reduction in all or most of the intensities. Region 2, on the contrary, showed a positive change of 13.99 mm. This is also observed from Figure 5.2 and Table 5.5. The conclusion regarding the spatial distribution of the intensities is opposite to Figure 66. However, in both cases, region 1 was the common region and responded strongly to the change in emissions. The reasons for the increase are described in the previous chapters. However, this chapter shows that rainfall can become negative and ultimately contribute to suppression. The decrease was partly due to a continuous decrease in transported moisture between 2000-4000 m, as shown in Figure 5.6. Thus, the change in the intensities is related to moisture availability.

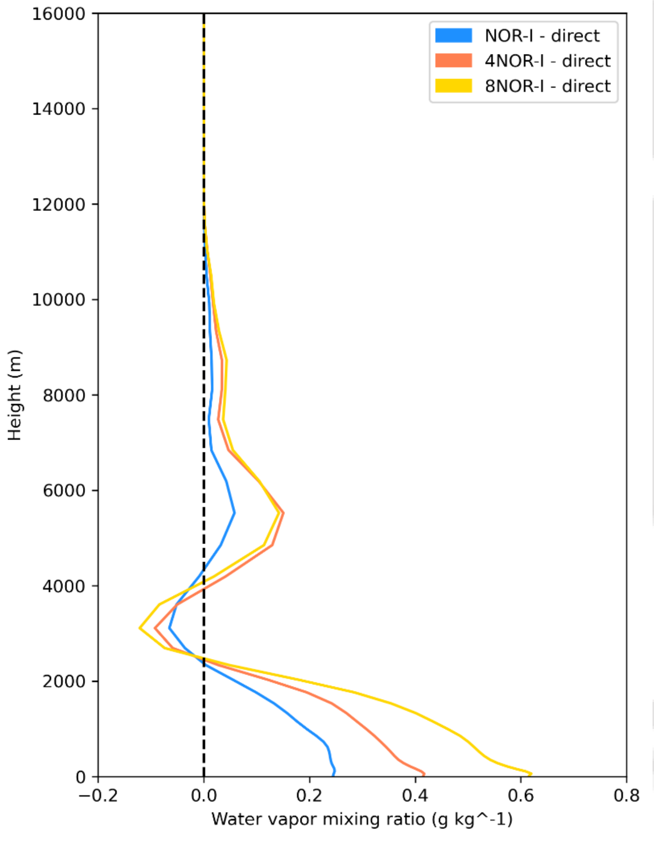

Figure 5.6: Regional average vertical profiles of water vapor mixing ratio (g kg^{-1}) due to direct effect in different scenarios

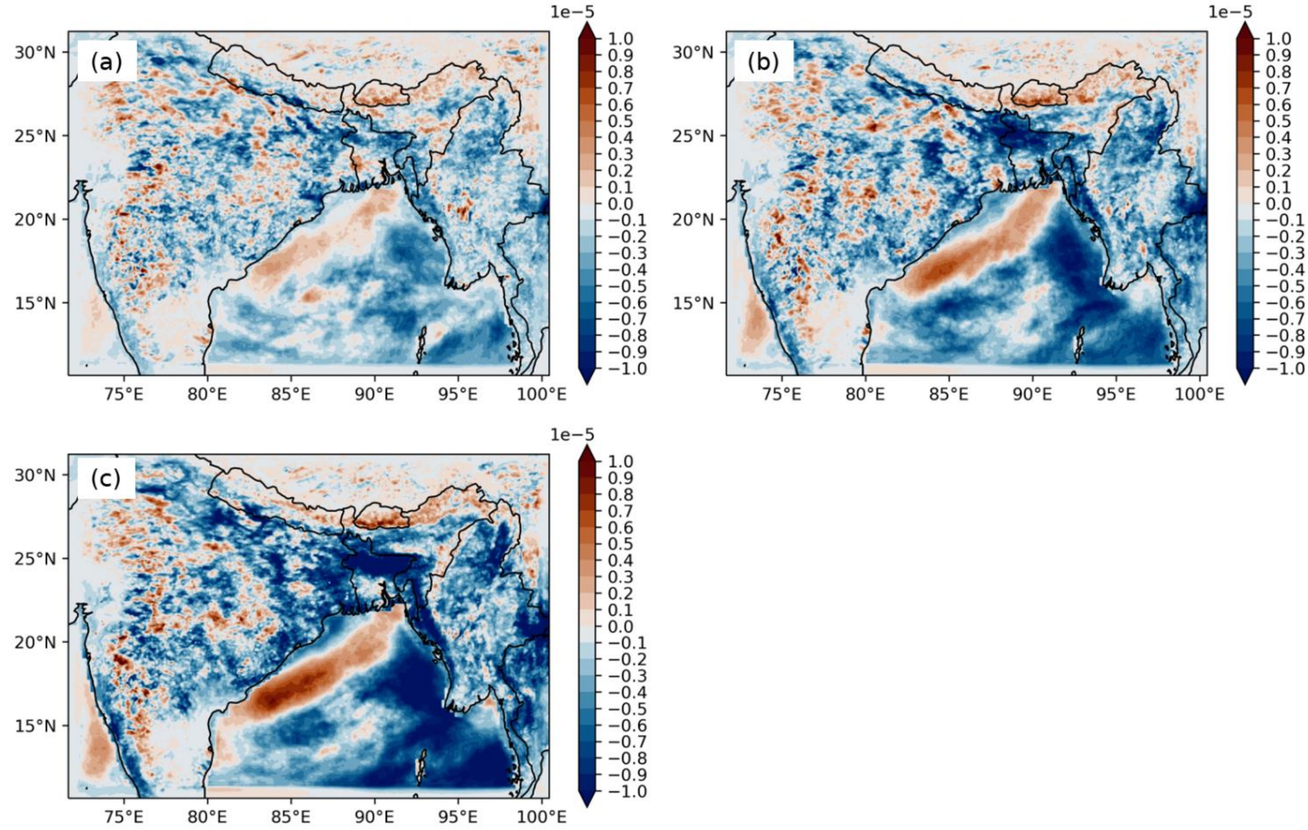

Figure 5.7: Spatial distribution of change in surface moisture due to direct effect in a) NOR-I b) 4NOR-I c) 8NOR-I

The successive moisture decrease between 2000-4000 m was due to successive decreases in surface moisture flux over North and Central India region, as shown in Figure 5.7, due to surface cooling. Quantitatively, the values are -1.59×10^{-6}, -1.83×10^{-6} and -2.58×10^{-6} kg m^{-2} s^{-1} for NOR-I, 4NOR-I and 8NOR-I, respectively. The positive values over the higher terrain of NE India are due to the reduction of moisture causing a decrease in clouds which have a positive effect on surface radiation and on the surface moisture flux. This would accompany the rainfall suppression caused by the indirect effect of non-absorbing aerosols. However, successive increase is seen over the Bay of Bengal.

Moreover, the moisture decrease was accompanied by cloud evaporation due to semi-direct effect, as explained in Chapter 3. The semi-direct net surface RF shows a continuous increase with the increase in BC emissions, as seen in Figure 5.8. The increase was mostly over region 1, where a maximum rainfall decrease was observed. The regional NE India average RF values due to semi-direct effect for NOR-I, 4NOR-I and 8NOR-I were 11.38, 14.47 and 16.21 W m^{-2}.

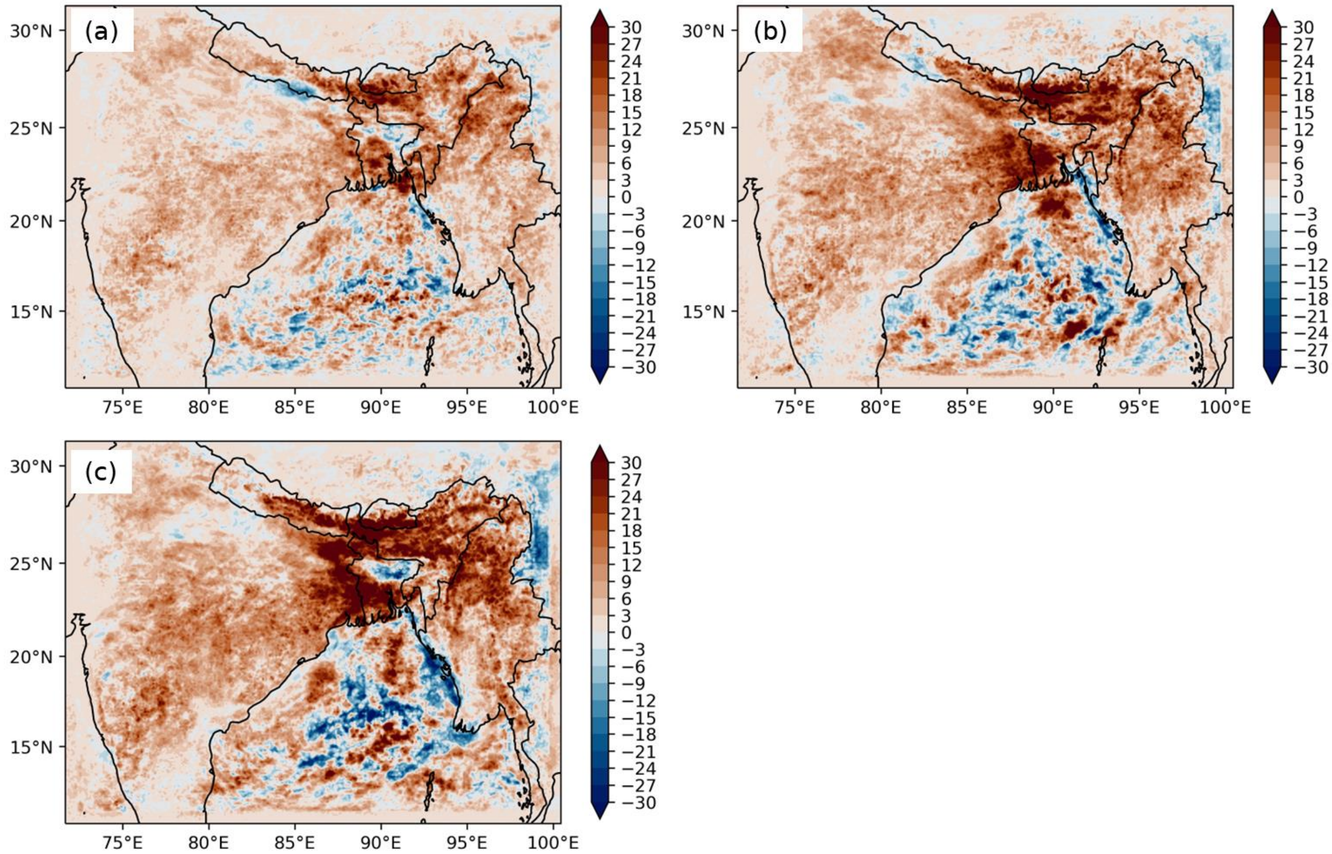

Figure 5.8: Spatial distribution of semi-direct RF in a) NOR-I b) 4NOR-I c) 8NOR-I

Thus, cloud evaporation and subsequent decrease in rainfall possibly were active across all three scenarios, but the influence of other effects on mechanisms influencing moisture availability had a greater effect on rainfall. Thus, a decrease in moisture and cloud evaporation both played a role in reducing rainfall intensity. This adds to the conclusions of Chapter 3.

5.4 Summary

The study shows the relevance of another region, i.e., the North and Central part of India, apart from the Bay of Bengal, that contributes to moisture and, subsequently, rainfall over NE India during the pre-monsoon season. Hence, any negative influence on this region, whether through

BC or any other aerosol will also have a negative impact on the rainfall over NE India. Thus, it is not necessary for aerosols to be transported to NE India to affect its rainfall. The mere presence of it leading to surface dimming and subsequent reduction in surface moisture flux over North and Central Part of India will reduce rainfall over NE India. However, there is an exception in that the presence of greater and greater amount of BC increases moisture flux over the Bay of Bengal but is reduced over North and Central Part of India. An increase in BC caused an increase in low, moderate and intense rainfall along the Brahmaputra River valley. However, most of the high-intensity rainfall increase was observed over the western and southern parts of NE India. The western region was most affected by emissions changes. Both the increase in high-intensity rainfall and duration was observed to be caused by transported BC. Apart from the increase in high-intensity rainfall due to the increase in moisture, the formation of ice-phase hydrometeors was also seen and could also add to the high-intensity rainfall. Thus, it may contribute to the observed increase in high-intensity rainfall events over NE India. However, the study also finds that rainfall that increase in BC emissions does not cause a continuous increase in rainfall, but a threshold BC level was found to exist between 4-8 times the BC emissions. Hence all aerosol effects ultimately cause rainfall suppression. Thus, apart from the indirect aerosol effect, the direct effect of BC also ultimately caused a rainfall decrease. The increase and decrease in rainfall, along with the corresponding increase and decrease in intensities, seemed to be controlled by moisture availability. Cloud evaporation and its subsequent negative effect on rainfall and rainfall intensity was always active but the ultimate impact on rainfall was dominated by other processes.

Chapter 6

6. Comparison and evaluation of planetary boundary layer parametrization schemes

6.1 General

This study compares and evaluates the applicability of six planetary boundary layer (PBL) parametrization schemes over the NE India region through numerical simulations of the WRF model. This study is also done as the simulated meteorological parameters were not very accurate, as seen in previous chapters. Hence, the performance is checked by using a finer resolution (3 km) in place of 10 km in WRF-Chem. This study helps to decide which PBL scheme gives better prediction for meteorology, while the PBL comparison in Chapter 3 was with respect to prediction of chemical species. Moreover, the analysis is extended to the monsoon season also to check whether similar or different PBL schemes are suitable as both these seasons are rainfall periods for this region. Also, PBL scheme suitability analysis has not been conducted for this region before. The best schemes considering different combinations of meteorological parameters were evaluated and thus will also help to choose a suitable PBL scheme for meteorological predictions in this region.

6.2 Methodology

6.2.1 Model configuration and simulation details

WRF model is one of the most widely used meteorological models used for forecasting and research. The Advanced Research WRF (ARW) core of the WRF model v4.2.1 (Skamarock et al. 2019) was used in this study. The model configuration is given in Table 6.1. The model configuration is similar to that used in the previous chapters but without atmospheric chemistry.

Table 6.1: Model configuration

Domain size: d01	231 × 197 × 35
d02	247 × 211 × 35
d03	349 × 311 × 35
Grid size (km)	27 (d01), 9 (d02), 3 (d03)
Time step (s)	120 (d01), 40 (d02), 10 (d03)
Cumulus scheme	Grell-Freitas (d01 and d02 only) (Grell and Freitas 2014)
Microphysics	Morrison double moment (Morrison et al. 2009)
SW and LW radiation	RRTMG (Iacono et al. 2008)
Land surface model	NOAH (Tewari et al. 2004)
Initial and boundary conditions	ERA5 Reanalysis (Hersbach et al., 2020)

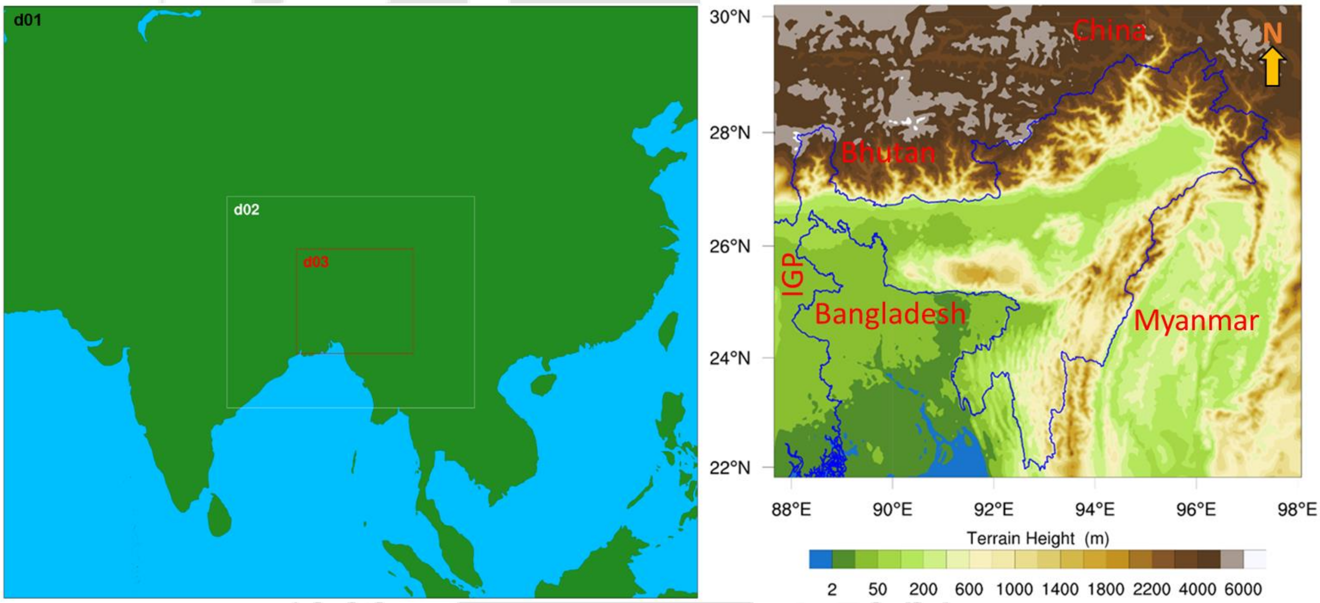

Figure 6.1: Modelling domains (left); d03 domain (right)

The difference exists in the domain configuration, which are shown in Table 6.1 and Figure 6.1. The configuration used an outer domain (d01) and two nested domains (d02 and d03). The area of study is the NE region of India covered by domain 3 (d03) at 3 km grid size, enclosed by the blue line. The study area has a highly varying topography with the Himalayas in the North and in the North-East, along with hill ranges, plain areas and river valleys. Domain d03 is bordered by Bhutan and China on the North, Myanmar on the East, Bangladesh on the South and the IGP on the West. The 3 km resolution was selected as this resolution is used by the IMD for operational forecasting. The simulations were carried out for one month of pre-monsoon (April) and monsoon (July) with hourly model outputs. The model was run from 16 March 2018 to 30 April 2018 for pre-monsoon and 15 June 2018 to 31 July 2018. The initial 15 days for each season were considered as spin-up duration and hence the model outputs from d03 from 1 April to 30 April for pre-monsoon and 1 July to 31 July for monsoon were considered for analysis. Six one-month-long simulations were conducted with three non-local schemes (ACM2, YSU and HONG) and three local schemes (QNSE, MYJ and MYNN3) in each season. Altogether, 12 simulations were carried out with six PBL schemes. An updated land cover dataset, MCD12Q1 (Sulla-Menashe and Friedl, 2018) for 2018, was implemented. Along with the conventional way of evaluating PBL schemes with the major weather parameters individually, this study also evaluates on the basis of different combinations of weather parameters to ascertain their applicability in the region.

6.2.2 Observational data

For evaluating the performance of the model, several types of meteorological data have been used for different model variables. The 2 m temperature, 2 m relative humidity, 10 m wind speed and direction model variables were compared with surface datasets (https://mesonet.agron.iastate.edu/sites/locate.php). The site collects meteorological data from airport sites. Vertical profiles of sensible temperature, relative humidity, wind speed and wind direction were compared with radiosonde data from the Department of Atmospheric Science, University of Wyoming (http://weather.uwyo.edu/upperair/sounding.html). The above observation data pertains to the Lokpriya Gopinath Bordoloi International Airport, Assam (26.10° N, 91.58° E) within d03 named GH. Rainfall was analysed with IMD datasets (https://www.imdpune.gov.in/cmpg/Griddata/Rainfall_25_Bin.html.) by Pai et al. (2014).

The statistical parameters used to evaluate the performances of the different PBL schemes were: ME, IOA, RMSE, mean absolute error (MAE), normalised mean error (NME) and normalised RMSE (NRMSE), depending on the meteorological parameter and the analysis type. While deciding the best schemes, more priority was given to the error terms (RMSE, NRMSE) and IOA than error terms (ME, MAE, NME) as in Moya-Álvarez et al. (2020).

6.3 Results and discussion

6.3.1 Temperature and relative humidity

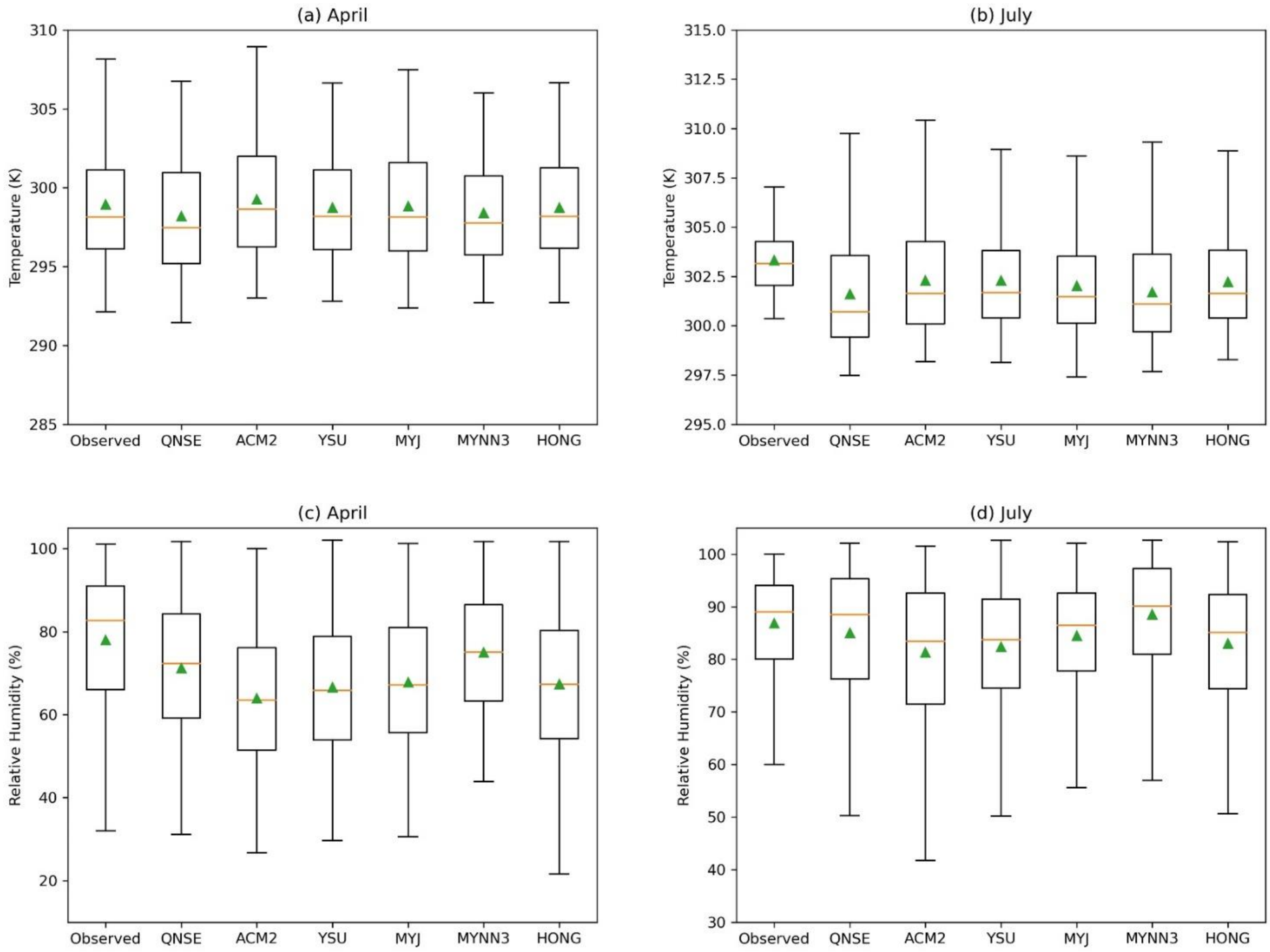

Figure 6.2: Comparison of observed 2 m temperature in (a) April, (b) July and 2 m relative humidity in (c) April, (d) July with the schemes

The positively skewed distributions of simulated 2 m temperatures were similar to the observed distribution in April but not in July, as seen in Figures 6.2(a) and 6.2(b). This shows that the majority of the observed data was well predicted by the schemes in April, but not in July. Most of the observations in July lay between 302 K and 304 K, which none of the schemes could predict, thus giving significantly lower mean temperatures. In April, the MYJ scheme provided a temperature variation most similar to the observed. QNSE had the most predictions in the lower ranges and the lowest predicted temperature among all the schemes that contributed to it predicting the lowest mean temperature. Though the inter-quartile range (IQR) is similar to the observed for MYNN3, it predicted significantly fewer higher temperatures which contributed to it being the second coldest PBL scheme. ACM2 has a larger IQR with higher values and highest minimum and maximum values compared to all the schemes as well as the observations, thus making it the warmest PBL scheme in April. MYJ and ACM2 distributions are quite similar, but MYJ made more predictions on the colder side. HONG and YSU were similar in predictions. In July, a similar conclusion followed. QNSE and MYNN3, though they predicted some higher temperatures compared to some schemes, have most of the predictions on the colder side. ACM2 again had a majority of the predictions on the warmer side. HONG and YSU performed quite similarly. Overall, it can be observed that model predictions with all the schemes show quite a variation, contrary to the observations. With respect to the distribution, the non-local schemes performed better, especially YSU and HONG.

The simulated 2 m relative humidity showed a near-normal distribution in April while being negatively skewed in July, as seen in Figures 6.2(c) and 6.2(d). The values associated with the IQR also show that most of the predictions lie between 50% and 85% in April but achieved higher values in July and thus were closer to the observations. In April, the range of predictions made by QNSE, YSU and MYJ was similar to the observed but had most of the predicted values on the dry side. However, the driest predictions were made by ACM2, thus showing the smallest mean relative humidity among all the schemes. MYNN3 scheme predicted a higher percentage of high humidity values than the rest of the schemes and couldn't predict dry atmospheric conditions, with a minimum value being around 45% while it was about 32% for the observations. This made its mean humidity value closer to the observed than any other PBL scheme. The performance of schemes improved in July. ACM2 and HONG show a wide range of humidity both in April and July. MYNN3 had the best range compared to the observed in July, though it made more predictions on the wetter side. Both the humidity plots show a similar sequence of mean humidity values in both months.

Table 6.2 shows the model performance statistics of 2 m temperature and 2 m relative humidity. The results from Figure 6.2 are evident in the ME of both temperature and relative humidity. In April, all schemes had negative temperature ME with the exception of ACM2 having a positive ME of 0.31 K. The ME increased further in July and all schemes simulated a colder atmosphere. QNSE and MYNN3 simulated the coldest atmospheres in both April and July. The average ME values show that overall, a colder atmosphere was simulated by local schemes, while non-local schemes, though also simulated colder temperatures, had lesser ME. The least ME was shown by the ACM2 scheme with an average value of -0.36 K for both months. The IOA values ranged between 0.78 and 0.92 for all the schemes in both months, but the values were much better in April, ranging between 0.90 and 0.92. In July, it ranged from 0.78 to 0.81. The highest IOA values for 2 m temperature were obtained for ACM2 for both months separately as well as the averaged value for both months. With the exception of YSU and HONG, all other schemes showed degradation in RMSE values. The biggest increase was seen for ACM2, which increased from 1.87 K in April to 2.09 K in July. The local schemes, especially MYNN3 and QNSE have RMSE values on the higher side in both months compared to the other schemes with averaged values of 2.15 K and 2.30 K. If the preferable RMSE value of 2.0 K, IOA > 0.7 and ME ±0.5 K proposed by Emery et al. (2001) is considered, ACM2 and MYJ scheme can be considered to be the best scheme for simulating temperature in April, while YSU and HONG sit on the borderline due to their slightly higher RMSE values. MYNN3 performance was also similar to YSU and HONG but had a slightly larger ME.

Table 6.2: Model performance statistics for 2 m temperature and 2 m relative humidity

PBL scheme	QNSE		YSU		ACM2		MYNN3		MYJ		HONG		Recommended scheme
	April	July	April	July	April	July	April	July	April	July	April	July	
2m temperature													
ME (K)	-0.76	-1.72	-0.21	-1.03	0.31	-1.04	-0.56	-1.63	-0.13	-1.31	-0.20	-1.11	April: ACM2 and MYJ July: YSU Both months: ACM2
Average	-1.24		-0.62		-0.36		-1.09		-0.72		-0.65		
IOA	0.90	0.78	0.90	0.81	0.92	0.81	0.90	0.78	0.91	0.80	0.90	0.81	
Average	0.84		0.85		0.86		0.84		0.85		0.85		
RMSE (K)	2.20	2.40	2.05	2.00	1.87	2.09	2.05	2.25	1.97	2.13	2.06	2.01	
Average	2.30		2.02		1.98		2.15		2.05		2.03		
2m relative humidity													
ME (%)	-6.77	-1.82	-11.39	-4.48	-14.08	-5.51	-3.04	1.73	-10.18	-2.36	-10.64	-3.81	April: MYNN3 July: MYNN3 Both months: MYNN3
Average	-4.29		-7.93		-9.79		-.0.65		-6.27		-7.22		
IOA	0.82	0.80	0.75	0.74	0.76	0.74	0.85	0.80	0.79	0.76	0.78	0.73	
Average	0.81		0.74		0.75		0.82		0.77		0.75		
RMSE (%)	13.46	9.17	16.70	10.13	17.38	10.94	11.39	8.16	15.20	9.21	15.87	10.30	
Average	11.31		13.41		14.16		9.77		12.20		13.08		

In July, all schemes passed the IOA criteria but had either large or borderline RMSE values. YSU can be considered the performing scheme if all three statistical parameters were considered in July. When both months' averaged statistics were considered, ACM2 was the best performing. The differences in the 2 m temperature may be related to the cloud cover simulated by the different schemes. ACM2 simulates less cover, which allows more solar radiation and hence has higher temperatures (Xie et al. 2012).

The model performance of relative humidity in July showed a significant improvement compared to April w.r.t model ME and RMSE though the IOA degraded slightly. Negative ME, though present in both months, decreased significantly in July. All the schemes had a negative ME in April, with ACM2 having a maximum of -14.08%. The local schemes were seen to have less ME, with MYNN3 producing the best results. The same can be said for the month of July, but with MYNN3 overpredicting slightly. In both months, MYNN3 has the best statistics w.r.t all three parameters. ACM2 simulated the driest atmosphere with an average ME of -9.79% and the largest RMSE value of 14.16%. If the acceptance criteria of IOA > 0.7, RMSE < 20% and ME < 10% were considered as used by Gunwani and Mohan (2017), the model have performed satisfactorily in July and only ME of YSU, ACM2, MYJ, HONG being slightly higher in April. The high ME, especially in April by most schemes, was probably caused by high vertical mixing, which supports the transport of more moisture to the upper atmosphere (Braun and Tao 2000). Different parametrizations of vertical mixing affect the vertical mixing extent and hence the moisture availability (Sathyanadh et al. 2017).

Thus, it can be summarized that the model performed differently with respect to the two different meteorological variables in both months. The performance of the model was better with respect to temperature in the pre-monsoon, while it was better for relative humidity in the monsoon. Generally, it is seen that local schemes performed better with relative humidity while the temperature was better simulated by non-local schemes. Though a scheme might be relatively better performing, its inadequacies are highlighted with the box plots.

The monthly averaged diurnal profiles of 2 m temperature and 2 m relative humidity are shown in Figure 6.3. In April, all the schemes overestimated temperature between the 6^{th} hour of the day (6 a.m. local time) to around 12 p.m. noon, as shown in Figure 6.3(a). After the 14^{th} hour, however, most of the schemes began to underestimate, and this underestimation process continued until the next day at 6 a.m., except for ACM2, which was able to produce a profile similar to the observed. QNSE scheme simulated the coldest nights with the largest negative ME from around the 18^{th} hour of the day (6 p.m. local time) to 6 a.m. This was also observed in Boadh et al. (2016). Between the 15^{th} and 18^{th} hour, a rapid reduction in temperature was observed with all the schemes, which stabilised a little after the latter. On average, MYNN3 simulated the coldest temperatures between the 12^{th} and 15^{th} hour, which is generally the peak solar insolation period of the day. The large ME from Table 26 in July are evident from the profile in Figure 6.3(b). The model underestimated the temperature almost throughout the day. The ME pattern was similar to April but greater in magnitude. The colder temperatures, especially during the evening and night, might be due to excessive mixing. This was also observed in Hariprasad et al. (2014). Sathyanadh et al. (2017) also observed a similar phenomenon and attributed it to a negative ME in incoming longwave radiation.

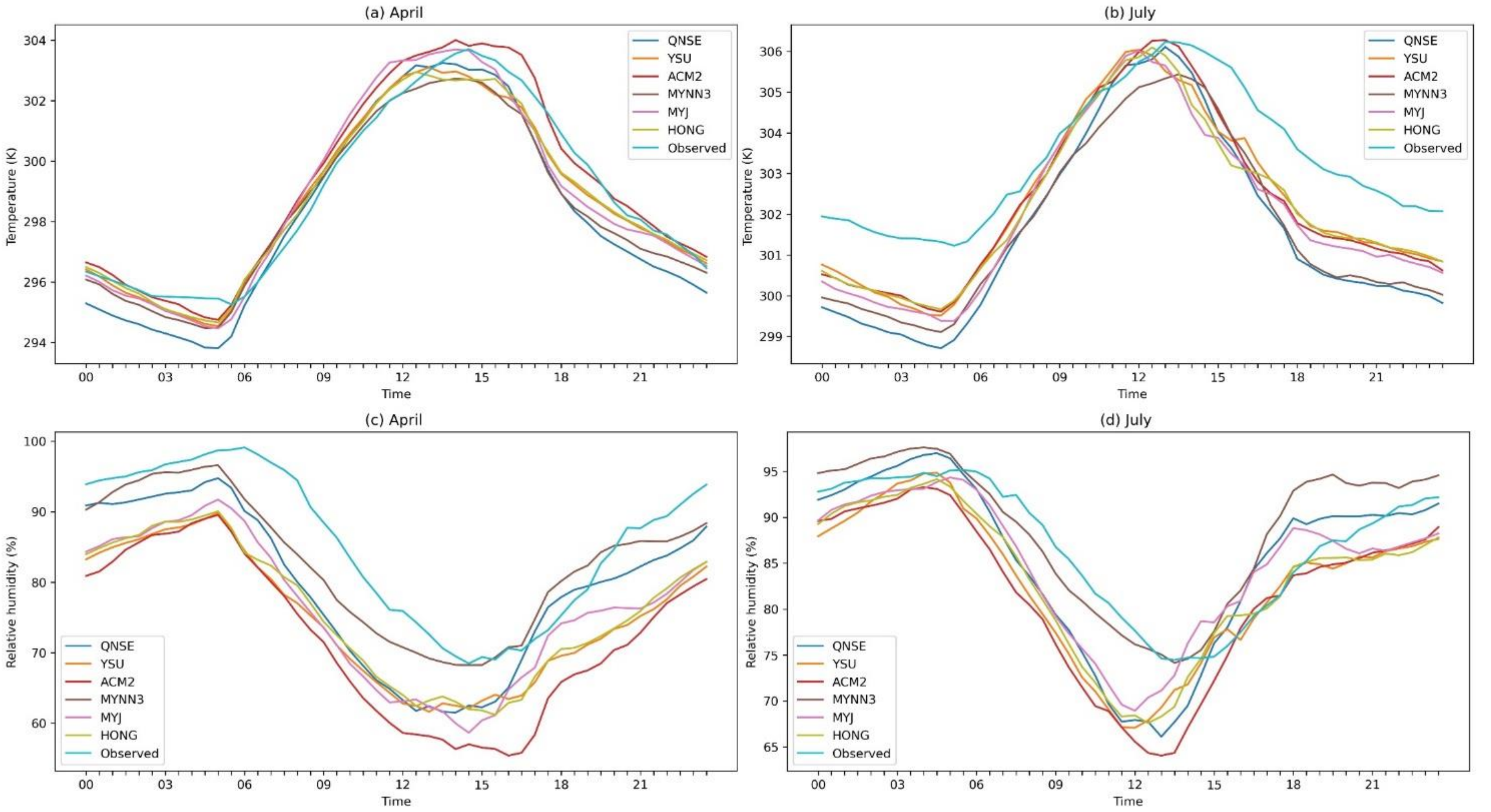

Figure 6.3: Monthly averaged diurnal profiles of 2 m temperature in (a) April, (b) July and 2 m relative humidity in (c) April, (d) July

The humidity profile during April in Figure 6.3(c) was underestimated by all the schemes, though MYNN3 produced a better profile. The dry ME associated with all the schemes and the largest ME by ACM2 was also observed by Hariprasad et al. (2014). The non-local schemes especially have significant negative ME throughout the day, which is also evident from Table 6.2 as well as Figure 6.2(c). The July profile in Figure 6.3(d) shows that most of the schemes except MYNN3 reached a minimum at around 12:30 p.m., while the observed profile had a minimum at around 2 p.m., similar to the observed. In terms of ME, the simulated profiles are much closer to the observed, especially after the 15th hour (3 p.m. local time) to 6 a.m. in the morning, but a large negative ME still exists from 6 a.m. till 2 p.m. excepting MYNN3. MYNN3, however, shows a larger ME in the evening at the 18th hour.

The vertical profiles of meteorological parameters showing the underlying condition of the atmosphere at that instant of time were used to evaluate the model's capability to define the atmosphere's vertical structure. Such profiles pertaining to 00 UTC, 1 April 2018 and 00 UTC, 1 July 2018, are shown for sensible temperature and relative humidity at GH in Figures 6.4 and 6.5 and are compared with observations from the radiosonde data at 00 UTC, which corresponds to 5:30 a.m. local time, which is an early morning period. The plots show that the model was able to match the pattern of the observed profiles. However, discrepancies do exist, especially near the surface.

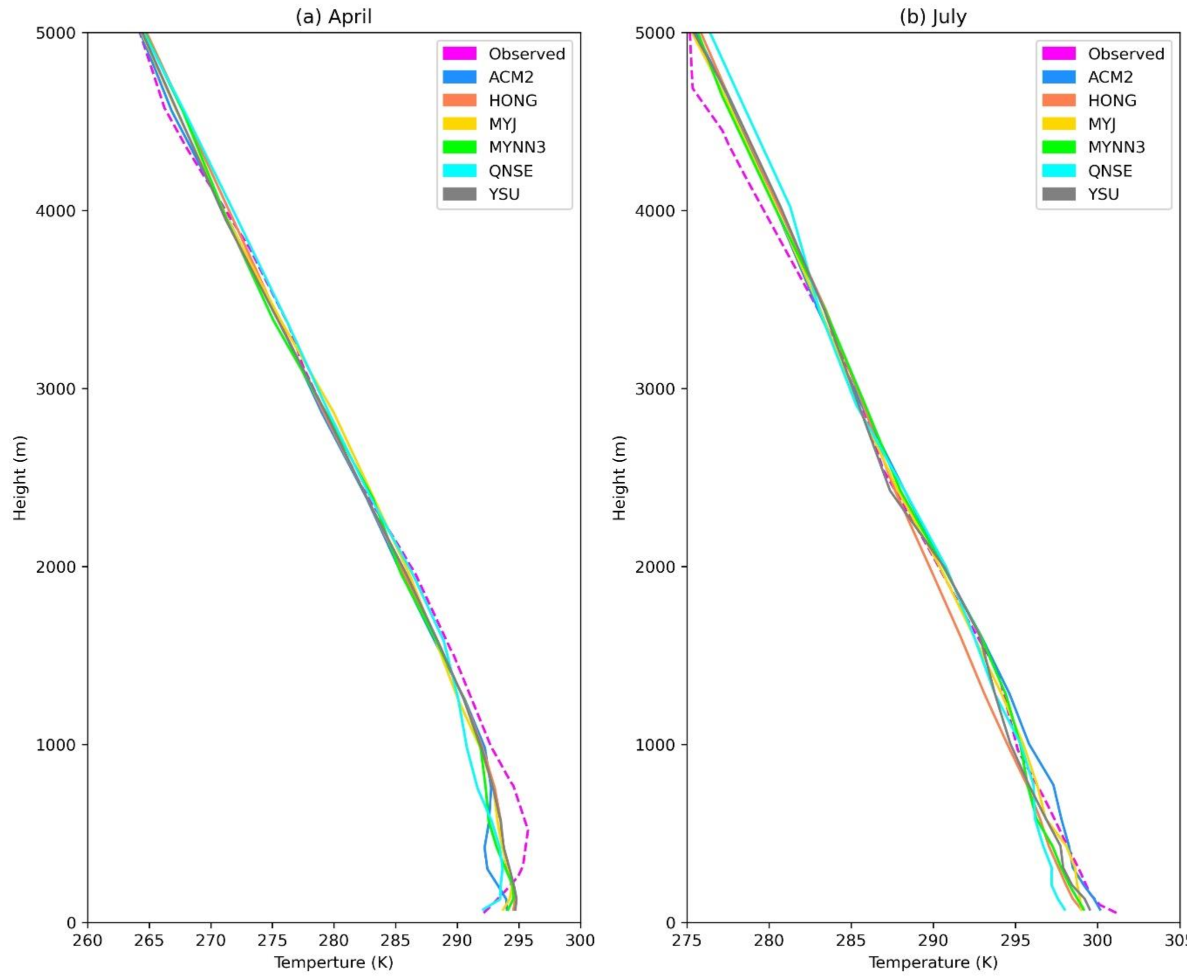

Figure 6.4: Comparison of sensible temperature profiles in (a) April and (b) July at GH

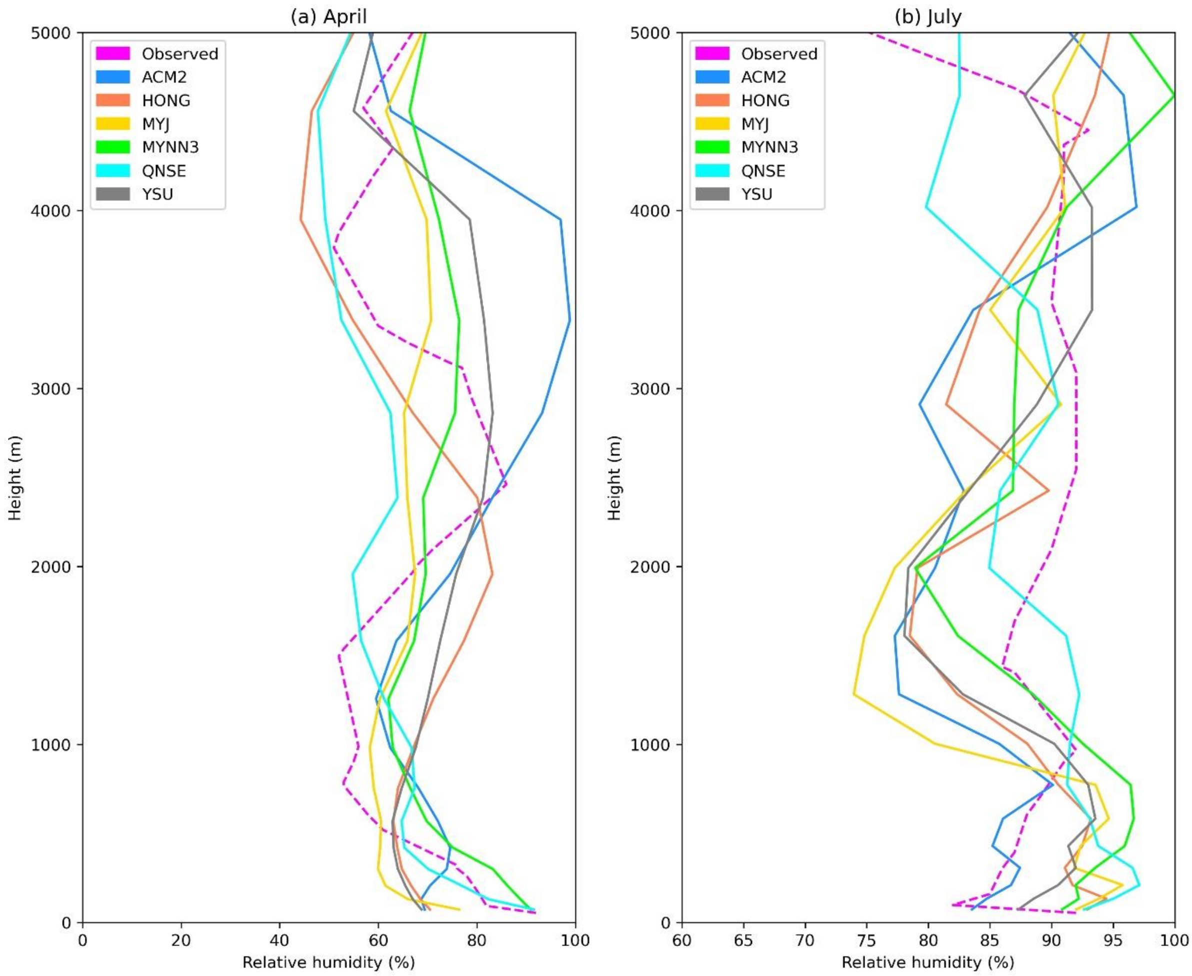

Figure 6.5: Comparison of relative humidity profiles in (a) April and (b) July at GH

6.3.2 Wind speed and wind direction

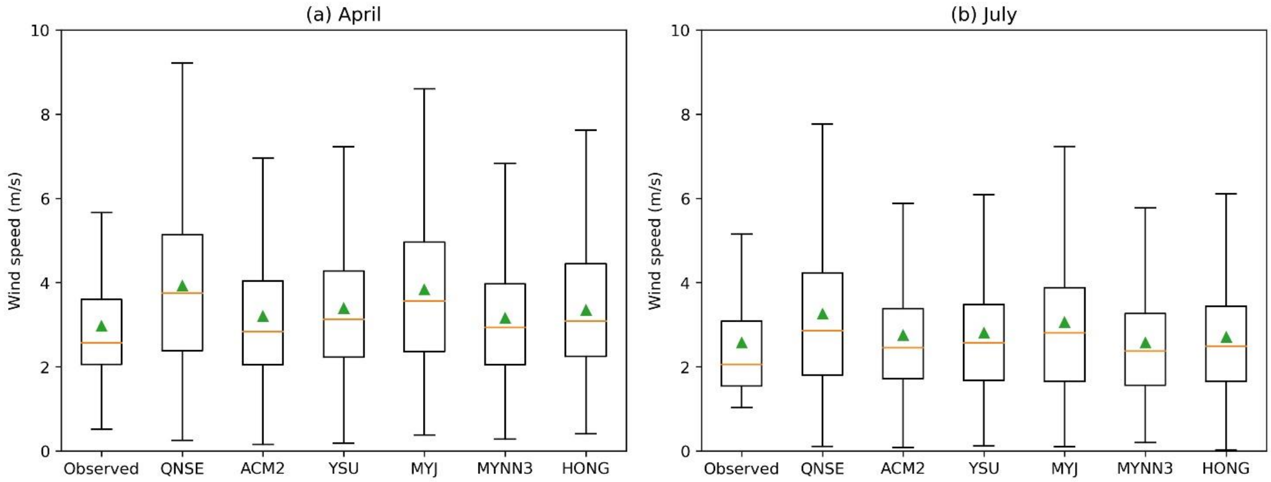

Figure 6.6: Comparison of 10 m wind speed in (a) April and (b) July

Boxplots for 10 m wind speed in Figure 6.6(a) and Figure 6.6(b) show that QNSE and MYJ simulated relatively higher wind speeds in both seasons and with larger errors, also reported in Hariprasad et al. (2014). This is reflected in the highest ME and RMSE values in Table 6.3.

Table 6.3: Performance statistics for wind speed

	QNSE		YSU		ACM2		MYNN3		MYJ		HONG		Recommended scheme
	April	July	April	July	April	July	April	July	April	July	April	July	
ME (m/s)	0.96	0.69	0.43	0.23	0.24	0.18	0.19	0.00	0.87	0.48	0.38	0.14	April: HONG
Average	0.83		0.33		0.21		0.09		0.68		0.26		July: MYNN3 and YSU
IOA	0.52	0.53	0.50	0.60	0.51	0.51	0.44	0.56	0.53	0.54	0.56	0.57	
Average	0.53		0.55		0.51		0.50		0.54		0.57		
RMSE (m/s)	2.27	2.02	1.94	1.61	1.93	1.75	1.97	1.55	2.16	1.90	1.78	1.65	Both months: HONG
Average	2.15		1.78		1.84		1.76		2.03		1.72		

The observed mean wind speed was lower in July compared to April, and this was also reflected by all the schemes, as also seen in Figure 6.6. The ME also decreased in July, and along with it, a decrease in RMSE was also seen across all the schemes. The pattern of the ranges and the mean values remained similar in both months. The wind speed range was more closely simulated by MYNN3 in both cases. According to Emery et al. (2001), ME should be ±0.5 m/s, IOA > 0.6 and RMSE should be within 2.0 m/s for wind speed. The ME was positive in both months, indicating the model always produced higher 10 m mean wind speeds. This was also reported in previous studies (Roux et al. 2009; Hariprasad et al. 2014; Madala et al. 2015). MYNN3, however, had the least ME in both months but had the least IOA in April. IOA is lower than the recommended value with most of the schemes in both months, but HONG in April and YSU in July have better IOA values. Also, it has been observed that July IOA values are equal to or better than April values. HONG in April and MYNN3, YSU in July performed relatively better. HONG could be considered the best scheme for both months combined, as it has the highest average IOA and least RMSE.

Table 6.4: Performance statistics for wind direction

	QNSE		YSU		ACM2		MYNN3		MYJ		HONG		Recommended scheme
	April	July	April	July	April	July	April	July	April	July	April	July	
ME (degrees)	-21.93	22.96	-14.74	4.88	3.91	6.96	-16.21	2.02	-15.58	5.35	-7.87	13.09	April: MYNN3
MAE (degrees)	22.44		9.81		5.43		9.11		10.46		10.48		
IOA	0.52	0.59	0.60	0.62	0.58	0.64	0.63	0.63	0.58	0.57	0.59	0.67	July: HONG
Average	0.56		0.61		0.61		0.63		0.58		0.63		
RMSE (degrees)	78.23	68.11	70.76	65.5	72.77	64.33	68.93	65.46	72.72	68.36	71.15	61.48	Both months: HONG
Average	73.17		68.13		68.55		67.19		70.54		66.31		

However, the performance of the model with respect to 10 m wind direction shows high RMSE values to be present with all the schemes in both months, as seen in Table 6.4. Large RMSE values have also been seen in previous studies (Carvalho et al. 2014; Dzebre and Adaramola 2020). Carvalho et al. (2014) observed that WRF produced large RMSE values at lower wind speeds, which decreased with increasing speeds. The reason for this could also be the terrain representation in the model. Thus, the performance regarding wind directions is required to be studied further in future studies. In April, the model produced an anti-clockwise ME with most schemes, while vice-versa in July. However, relatively MYNN3 and HONG produced the best results in April and July, respectively. HONG also produced the best results for both months. Good performance with MYNN3 was also observed by Dzebre and Adaramola (2020).

Similar to temperature and relative humidity, wind speed and wind direction at GH and are compared with observations from the radiosonde data in Figures 6.7 and 6.8. The plots show that the model is able to match the overall vertical profiles of wind speed and wind direction.

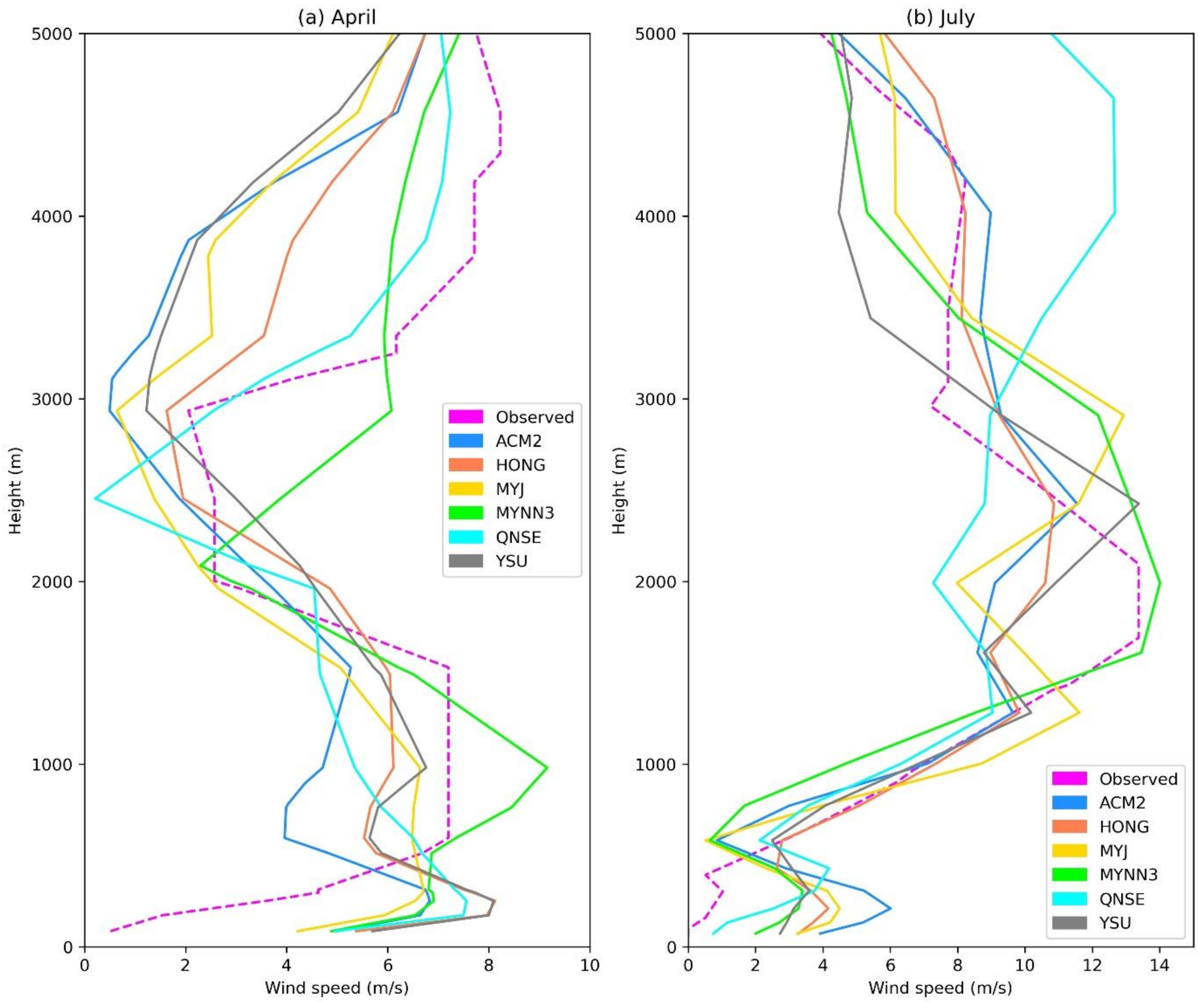

Figure 6.7: Comparison of wind speed profiles in (a) April and (b) July at GH

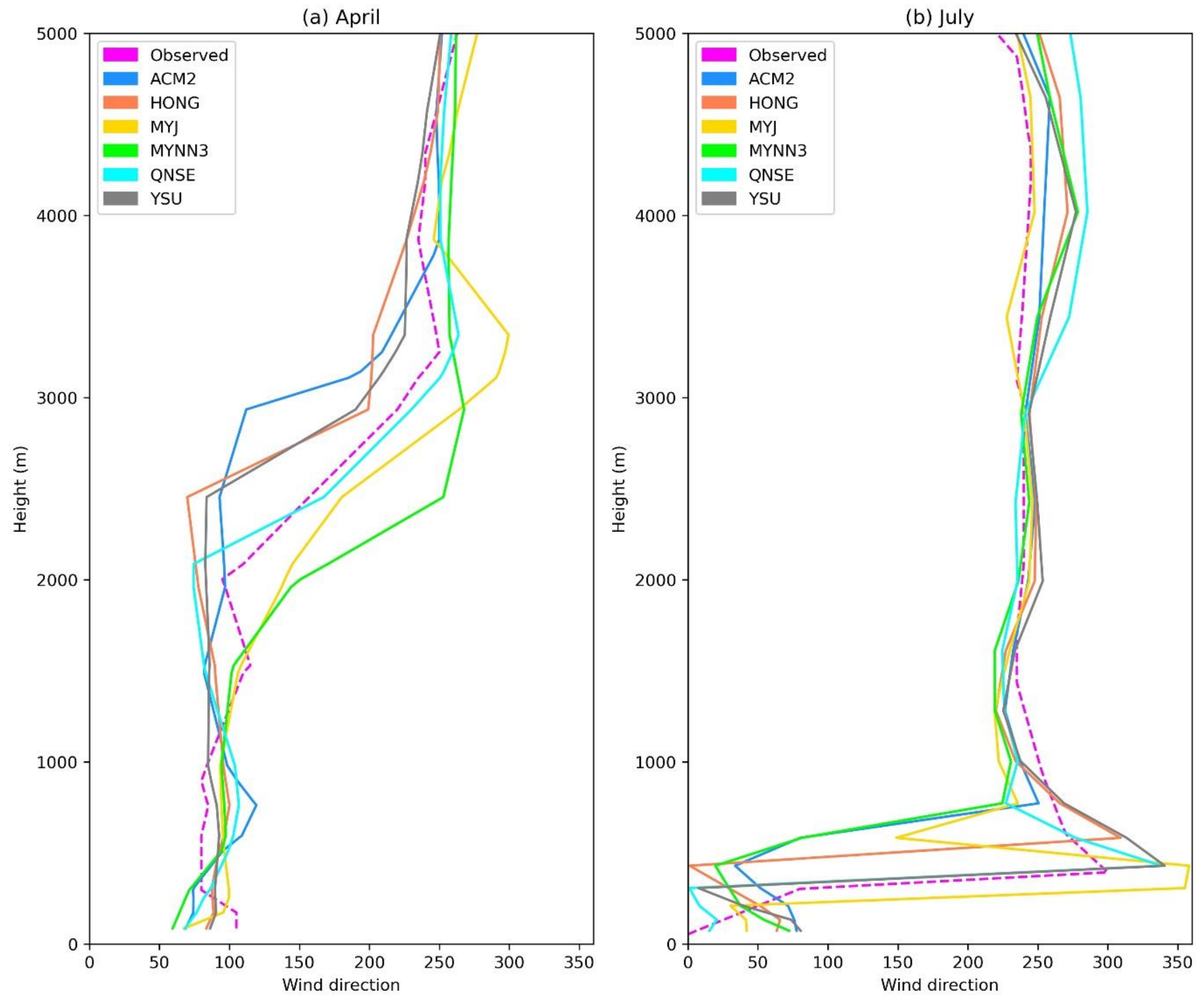

Figure 6.8: Comparison of wind direction profiles in (a) April and (b) July at GH

6.3.3 Rainfall

The rainfall performance statistics are shown in Table 6.5. The rainfall performance is comparatively better in April than in July with lower ME and RMSE and higher IOA. All the schemes overestimated rainfall over the region, except ACM2 in April. HONG performed the best in April (ME: 0.37 mm day^{-1}, IOA: 0.48 and RMSE: 11.99 mm day^{-1}) while MYJ in July (ME: 3.95 mm day^{-1}, IOA: 0.42 and RMSE: 24.39 mm day^{-1}) as well as both the months combined (ME: 2.164 mm day^{-1}, IOA: 0.451 and RMSE: 18.198 mm day^{-1}). Madala et al. (2014) also found MYJ to better capture rainfall events better during a severe thunderstorm event in Gadanki, India in April 2011. Moya-Álvarez et al. (2020) adjudged MYNN3 as the

Table 6.5: Performance statistics for rainfall

	QNSE		YSU		ACM2		MYNN3		MYJ		HONG		Recommended scheme
	April	July	April	July	April	July	April	July	April	July	April	July	
ME (mm/day)	0.51	4.62	0.37	4.14	-0.49	2.47	0.73	4.65	0.37	3.95	0.37	4.44	April: HONG
Average MAE	2.570		2.258		1.486		2.693		2.164		2.408		July: MYJ
IOA	0.47	0.41	0.48	0.42	0.46	0.39	0.48	0.40	0.47	0.42	0.48	0.42	
Average	0.443		0.455		0.430		0.446		0.451		0.455		
RMSE (mm/day)	11.85	25.19	12.18	24.53	11.88	25.24	12.30	25.44	12.00	24.39	11.99	24.84	Both months: MYJ
Average	18.526		18.356		18.564		18.872		18.198		18.420		

best PBL scheme for simulating rainfall at a complex terrain in the mountainous region in the central Andes of Peru, but this study showed different results.

6.3.4 Combined performance of PBL schemes

We come across situations where an overall better scheme is required to be selected considering all the meteorological parameters. This is especially relevant with chemical transport models for multi-month time periods. In such situations, PBL schemes are generally not varied between the different time periods. Table 6.6 shows the combined average statistical values considering relative humidity, temperature, wind speed and rainfall. The statistics from wind direction evaluation were not used. These would help to select a scheme when either temperature and relative humidity is a priority or when an overall better scheme with all variables is required. The values are shown for each month as well as combined for both months. NMAE value for a particular scheme shows what is the overall ME with a particular scheme, considering either two or all four parameters. NRMSE can be described similarly, which represents the overall error. The normalisation of the statistical parameters helps to overcome the units associated with different meteorological parameters. Since IOA values are already unitless, values are the average of the values shown in previous tables. For April, HONG had the overall best statistics (NMAE: 0.081, IOA: 0.681 and NRMSE: 2.441), while YSU (NMAE: 0.107, IOA: 0.645 and NRMSE: 0.680) had the best statistics in July. Thus, HONG and YSU predicted the meteorology better in April and July, respectively. When both months were considered, HONG was the best scheme (NMAE: 0.092, IOA: 0.658 and NRMSE: 1.566). Hence, HONG can be used for both the pre-monsoon and monsoon seasons.

Table 6.6: Combined statistics of temperature, relative humidity, wind speed and rainfall

	QNSE	YSU	ACM2	MYNN3	MYJ	HONG	Recommended scheme
	April						
NMAE	0.124	0.088	0.085	0.056	0.121	0.081	April: HONG
IOA	0.678	0.658	0.664	0.669	0.677	0.681	
NRMSE	2.449	2.492	2.438	2.500	2.472	2.441	
	July						July: YSU
NMAE	0.153	0.107	0.077	0.086	0.123	0.102	
IOA	0.631	0.645	0.613	0.637	0.631	0.634	
NRMSE	0.731	0.680	0.710	0.687	0.703	0.691	
	April and July combined						Both months: HONG
NMAE	0.139	0.098	0.081	0.071	0.122	0.092	
IOA	0.655	0.651	0.639	0.653	0.654	0.658	
NRMSE	1.590	1.586	1.574	1.593	1.587	1.566	

6.3.5 Comparison of model performance between WRF and WRF-Chem

Table 6.7: Comparison of model performance statistics for different meteorological parameters in WRF and WRF-Chem simulations

		WRF	WRF-Chem
Temperature	RMSE (°K)	2.05	2.88
	IOA	0.90	0.75
	ME (°K)	-0.56	-1.97
Relative humidity	RMSE (%)	11.39	11.21
	IOA	0.85	0.79
	ME (%)	-3.04	3.09
Wind speed	RMSE (m s^{-1})	1.97	1.84
	IOA	0.44	0.40
	ME (m s^{-1})	0.19	-0.35
Wind direction	RMSE (°)	68.93	146.95
	IOA	0.63	0.47
	ME (°)	-16.21	6.07
Rainfall	RMSE (mm day^{-1})	12.30	13.55
	IOA	0.48	0.52
	ME (mm day^{-1})	0.73	3.72

Table 6.7 shows the performance statistics of NOR-I simulation with WRF-Chem and the WRF simulation. Only the MYNN3 statistics from the WRF simulation are considered since the WRF-Chem simulations were mainly run with MYNN3. Except for rainfall, the performance statistics for the remaining parameters are for the Guwahati meteorological station. For rainfall, the whole NE region was compared. All meteorological parameters show significant

improvement, especially with temperature and wind direction. However, the rainfall IOA with NOR-I was higher. Thus, simulations including all aerosol effects with a fine resolution may yield better performance as it was seen in Chapter 4 that the inclusion of indirect effect greatly improved rainfall performance.

6.4 Summary

This study compares and evaluates the ACM2, MYJ, HONG, MYNN3, QNSE and YSU planetary boundary layer parametrization schemes with the WRF model in the NE region of India. The study intended to assess the performance and suitability of the schemes in the pre-monsoon and monsoon seasons in this complex terrain and heavy rainfall region. Evaluations were made for major weather parameters of temperature, relative humidity, wind speed, wind direction, and rainfall.

In general, non-local schemes performed better with temperature, while local schemes performed better with relative humidity estimation. ACM2 was the best scheme for 2 m temperature, while MYNN3 performed best with relative humidity. Non-local produced large ME with humidity in April. Rainfall performance was better with the HONG scheme in April and MYJ in July as well as in both months together. Though the performance of schemes varied with parameters and season, considering the combined statistics of multiple parameters, YSU and HONG are good schemes for this region. MYNN3 also performed well with most of the weather parameters separately. HONG performed well with the wind parameters. The better performances might be related with higher instability and hence better mixing produced by these schemes. This study also provides results based on combined statistics of multiple parameters, in which HONG was found to be a suitable scheme. Thus, this study provides an up-to-date evaluation of the PBL schemes with the WRF model in this region. With the exception of relative humidity, a different scheme was found to be more suitable for monsoon than the one found suitable for pre-monsoon. This underlines the requirement for such studies. Moreover, compared to the meteorological evaluation in previous chapters, the increase in resolution does show an increase in model performance. The inclusion of atmospheric chemistry along with a finer resolution may further increase the performance, especially with rainfall. This study also shows that different PBL schemes give more accurate predictions for chemical species and meteorology in Chapter 3 and 6, respectively. This implies that a PBL scheme which give best results with chemical species (MYNN3) might not give the best performance with meteorology prediction. Hence, different PBL schemes are to be employed according to the objective of the study, whether chemical species or meteorology is more important or a single PBL scheme can be used according to the combined performance of chemical species and meteorology.

Chapter 7

7. Findings and conclusions

7.1 General Summary

The findings of this study can play a significant role in the preparation and implementation of policies and regulations. The research explains how aerosols affect the pre-monsoon rainfall mechanisms over NE India. The study finds IGP to be a significant source of emissions, the control of which would lead to a significant reduction in air pollution as well as climatic impacts over NE India. The emissions released within NE India were found to have a significantly lower impact w.r.t both aspects. The lower atmospheric flow towards NE India enhanced moisture transport from the Bay of Bengal due to the increase in atmospheric instability caused by transported BC from IGP. This increased moisture over the lower terrain areas of NE India, which enhanced rainfall in these areas. Thus, though the direct effect reduced moisture by decreasing moisture flux from the surface through surface dimming in the whole domain, but also compensated it through transport from the Bay of Bengal, and thus also compensated the rainfall. However, the upper atmospheric flow was from over North and Central India which carried moisture as well as aerosols from IGP into NE India. Thus, apart from the Bay of Bengal, the study also found North and Central India to significantly impact rainfall over NE India, and hence changes in characteristics of this region will also impact rainfall over NE India. Hence, the reduction in surface moisture due to surface dimming by both direct and indirect effect reduced moisture availability at higher heights which reduced rainfall over the higher terrain areas of NE India. The impact of the indirect effect was found to be significantly greater and also reduced rainfall through the increase in atmospheric stability and modification of the clouds. Reduction in rainfall through semi-direct effect occurred by evaporating clouds, especially over the western region of NE India. Cloud evaporation and subsequent reduction in rainfall were always active, but its impact was lower than the rainfall changes caused by the other aerosol effects. However, the direct radiative effects of BC on rainfall did not increase but reduced gradually with an increase in BC emissions. Hence, there existed a threshold of BC emissions and concentration, after which BC also started causing rainfall suppression. The presence of large amounts of moisture through direct effect caused high-intensity rainfall over the region affecting mostly the western and southern regions of NE India. Figure 7.1 briefly summarises the climatic impacts of transported aerosols while Figure 7.2 summarises the mechanisms. Moreover, MYNN3 best simulated the dispersion of chemical species in pre-monsoon with WRF-Chem. However, the improvement in grid size at 3 km with WRF showed improvement in the prediction of meteorological parameters compared to 10 km with WRF-Chem and found HONG and YSU schemes to be more accurate during pre-monsoon and monsoon seasons, respectively and hence can be used for weather prediction.

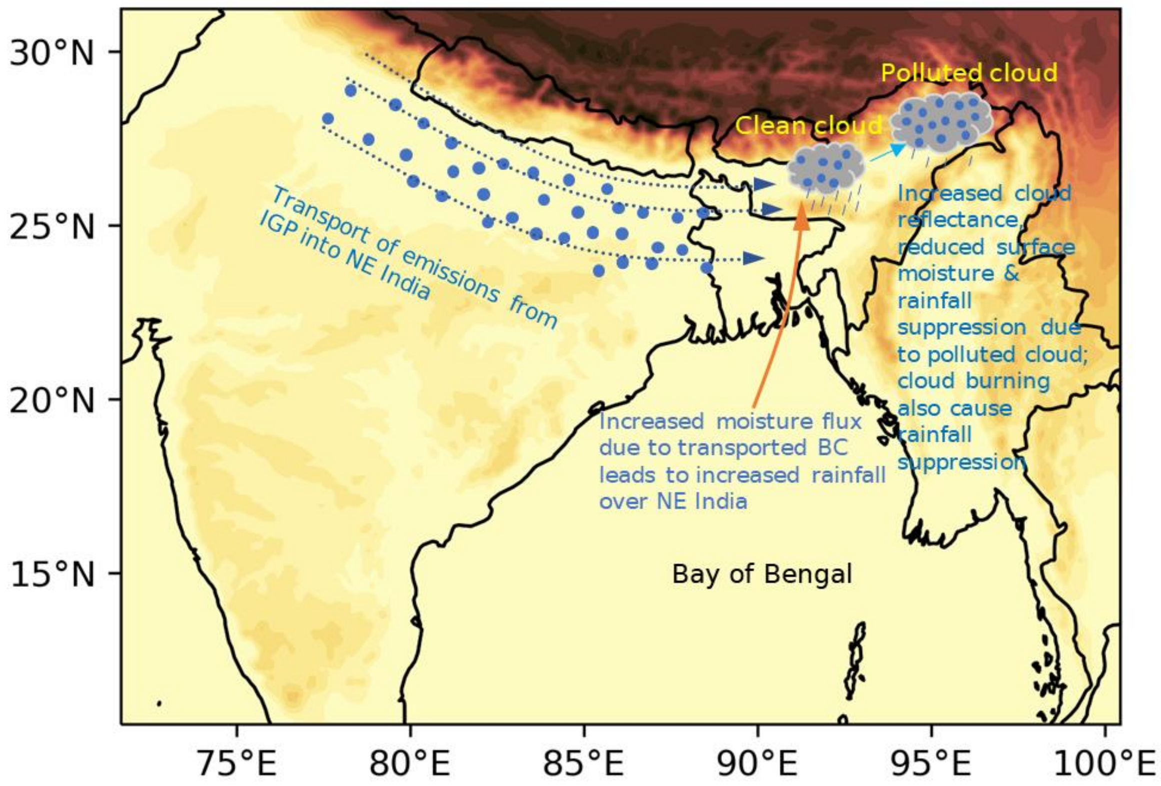

Figure 7.1: Climatic impacts of transported emissions from the IGP over NE India

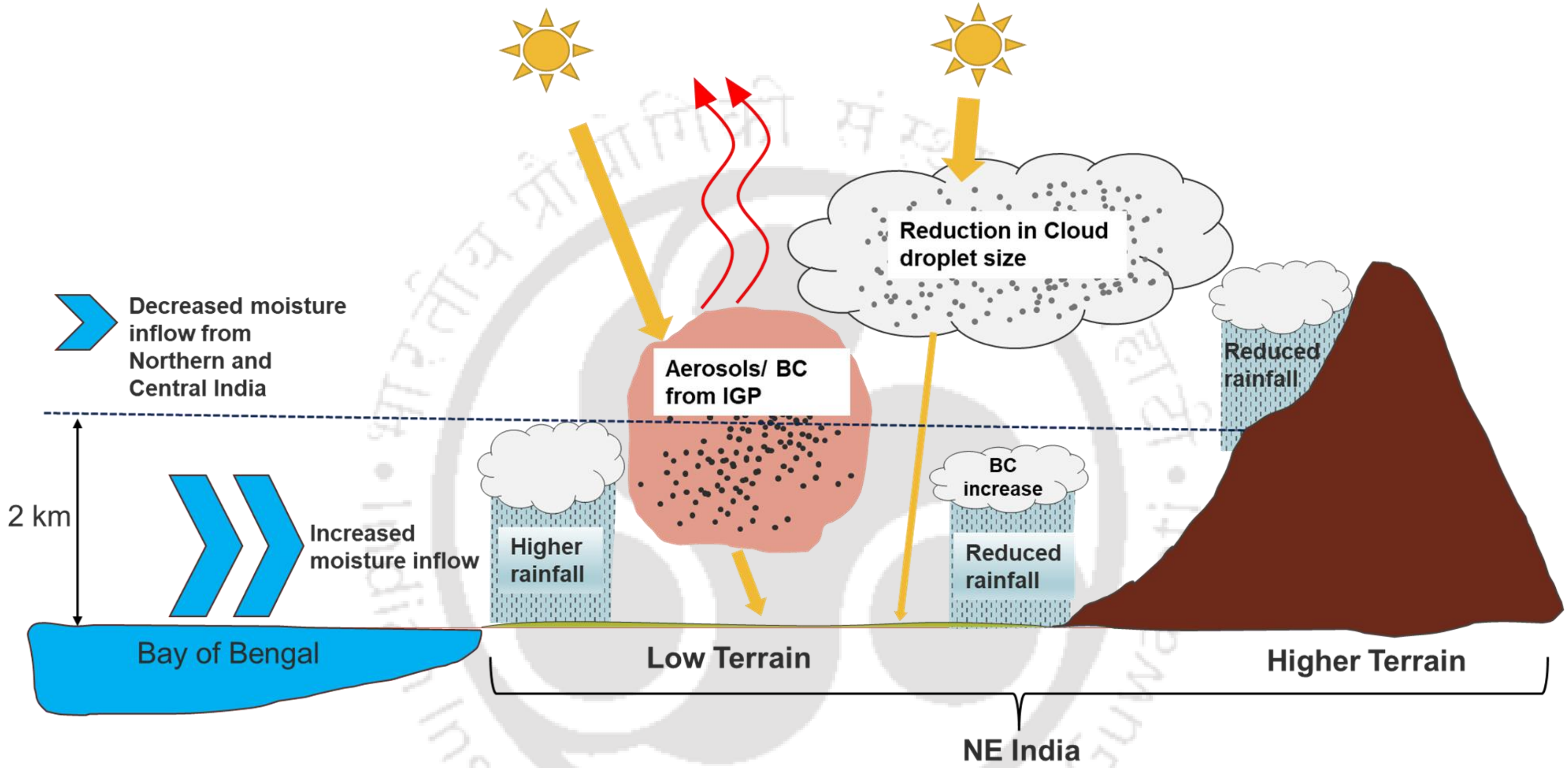

Figure 7.2: Summary of mechanisms affecting rainfall over NE India

7.2 Key findings

1. Two regions - the Bay of Bengal and the North and Central regions of India contributed to the moisture necessary for rainfall over NE India.
2. The wind flow in the lower atmosphere transported moisture from the Bay of Bengal, while the upper-atmospheric flow transported moisture from the North and Central regions of India.
3. The increase in BC increased the moisture transported from the Bay of Bengal but reduced the moisture transported from the North and Central regions of India due to the increasing direct effect of BC.
4. The increasing amounts of BC caused successively increased instability over NE India, which facilitated a greater amount of moisture transport from the Bay of Bengal through the lower atmospheric wind flow.
5. The presence of an increasing amount of BC caused surface dimming over North and Central regions of India which reduced surface moisture evaporation and thus decreased the moisture transported through upper-atmospheric flow.
6. The increase in BC increased rainfall over lower terrain areas but reduced rainfall over higher terrain areas.
7. Cloud evaporation through semi-direct effect was also found to reduce rainfall by evaporating clouds, mainly over the western and southern areas of NE India.
8. A threshold limit of BC was found to exist between 4-8 times the baseline BC emissions, the exceedance of which also caused BC to suppress rainfall through the combined effect of moisture reduction and cloud evaporation through semi-direct effect.

9. The presence of a greater amount of BC was found to increase high-intensity rainfall, both in amount and duration, caused by the increasing instability and subsequent moisture availability.
10. The presence of a greater amount of BC was found to increase ice-phase hydrometeors.
11. The indirect aerosol effect on rainfall and radiative forcing was much greater than the direct and semi-direct effect.
12. Indirect effect caused significantly higher rainfall suppression than direct and semi-direct effects through a combined effect of surface moisture reduction, increased atmospheric stability and modification of clouds.
13. The quantity of BC, organic carbon, sulfate, nitrate, ammonium and dust aerosol, mainly transported from the IGP, was much higher than that emitted from within NE India.
14. Transported aerosols were found to contribute to most of the near-surface PM_{10} concentration and in the higher atmosphere over NE India and thus also contributed significantly to the air pollution over the region.
15. The climatic effects of the transported aerosols were found to be much greater than the emissions from within NE India, both with respect to radiative forcing and rainfall. Transported aerosols caused higher rainfall suppression over NE India through all the aerosol effects.
16. Transported emissions showed greater control over the rainfall in NE India than local emissions.
17. BC primarily transported from the IGP was found to have higher heating capacity than locally emitted BC and was responsible for the increased atmospheric instability over NE India and increased moisture flux over the Bay of Bengal.

18. Changes in the emissions of transported BC caused a higher impact on atmospheric heating over NE India than local emissions.
19. Transported BC was also responsible for the increase in rainfall and higher rainfall intensity over the NE India region, while the increase in transported SO_2 emissions also caused suppression of rainfall.
20. The impact of BC on rainfall suppression through indirect effect was non-existent.
21. The western region of NE India was most affected by aerosols due to its close proximity to the IGP.
22. MYNN3 scheme was found to be the most accurate for predicting chemical species during the pre-monsoon season.
23. In terms of meteorology, ACM2 and MYJ schemes were found best for predicting temperature in pre-monsoon while YSU in monsoon. MYNN3 was the most accurate for predicting relative humidity during both seasons. HONG was found to be the best for predicting wind speed in pre-monsoon, while MYNN3 and YSU in July. MYNN3 showed the highest accuracy in predicting wind direction during pre-monsoon, while it was HONG in July. Rainfall was also best simulated by Hong in pre-monsoon, while monsoon rainfall was best predicted by MYJ.
24. HONG was the most accurate scheme in pre-monsoon considering all the meteorological parameters, while for monsoon, it was YSU. Moreover, HONG showed the best performance considering both seasons.
25. Significant improvement in the simulation of meteorological parameters was observed over Guwahati with the decrease in grid size.
26. The use of simulations including all the aerosol effects with a fine grid size gave better rainfall forecasts in the pre-monsoon season, as aerosol loading is high during this season.

7.3 Key conclusions

1. The aerosol effects exerted by the aerosols primarily transported from the IGP have a significant role in the decreasing rainfall trend over NE India.
2. BC increases rainfall initially but ultimately contributes to rainfall suppression.
3. BC may also have a role in high-intensity rainfall over NE India.
4. Controlling and regulating the emissions in the IGP can significantly improve the air quality as well as the climatic impacts over NE India.
5. The use of a chemistry model such as WRF-Chem with a fine resolution may yield even better rainfall predictions.

7.4 Limitations

1. Due to computational limitations, the simulations with WRF-Chem could only be conducted at 10 km resolution and for a period of 13 days.
2. Finer resolution and longer duration simulations could add further details.
3. Improvement of emission inventories could provide better results.
4. Indirect aerosol effects may be underestimated as Liu et al. (2016) report that the aerosol activation parametrization in WRF-Chem by Abdul-Razzak and Ghan (2002) underestimates aerosol activation. Moreover, indirect aerosol effect is not coupled with convective clouds and convective rainfall.

7.5 Future Scope

This study can be extended to other seasons also to find out the region of emissions that has greater influence on air pollution and climatic impacts over NE India during those seasons. Also, as this study only covered the effect of BC on the atmosphere over NE India in a detailed manner, it can be extended to other aerosol species. This will help to find anthropogenic aerosol species that have greater climatic and air pollution impact on NE India during the different seasons, which would help to design interventions to control their emissions. The above studies may be conducted using WRF-Chem with a finer grid resolution to provide better predictions of the atmosphere. This in addition may also reduce the uncertainty associated with the non-coupling of indirect aerosol with convective rainfall by treating smaller clouds as non-convective clouds. Moreover, higher intensity rainfall by indirect effect should can also be studied on local scales.

References

Abdul-Razzak, H., Ghan, S.J., 2002. A parameterization of aerosol activation 3. Sectional representation. J. Geophys. Res. Atmos. 107, 1–6. https://doi.org/10.1029/2001jd000483

Ackerman, A.S., Toon, O.B., Stevens, D.E., Heymsfield, A.J., Ramanathan, V., Welton, E.J., 2000. Reduction of tropical cloudiness by soot. Science (80-.). 288, 1042–1047. https://doi.org/10.1126/science.288.5468.1042

Albrecht, B.A., 1989. Aerosols, cloud microphysics, and fractional cloudiness. Science (80-.). 245, 1227–1230. https://doi.org/10.1126/science.245.4923.1227

Andreae, M.O., Crutzen, P.J., 1997. Atmospheric Aerosols : Biogeochemical Sources and Role in Atmospheric Chemistry 276.

Angevine, W.M., 2005. An integrated turbulence scheme for boundary layers with shallow cumulus applied to pollutant transport. J. Appl. Meteorol. 44, 1436–1452. https://doi.org/10.1175/JAM2284.1

Babu, S.S., Moorthy, K.K., Manchanda, R.K., Sinha, P.R., Satheesh, S.K., Vajja, D.P., Srinivasan, S., Kumar, V.H.A., 2011. Free tropospheric black carbon aerosol measurements using high altitude balloon: Do BC layers build their own homes up in the atmosphere? Geophys. Res. Lett. 38, 1–6. https://doi.org/10.1029/2011GL046654

Bagtasa, G., Cayetano, M.G., Yuan, C.S., Uchino, O., Sakai, T., Izumi, T., Morino, I., Nagai, T., Macatangay, R.C., Velazco, V.A., 2019. Long-range transport of aerosols from East and Southeast Asia to northern Philippines and its direct radiative forcing effect. Atmos. Environ. 218, 117007. https://doi.org/10.1016/j.atmosenv.2019.117007

Baklanov, A., Schlünzen, K., Suppan, P., Baldasano, J., Brunner, D., Aksoyoglu, S., Carmichael, G., Douros, J., Flemming, J., Forkel, R., Galmarini, S., Gauss, M., Grell, G., Hirtl, M., Joffre, S., Jorba, O., Kaas, E., Kaasik, M., Kallos, G., Kong, X., Korsholm, U., Kurganskiy, A., Kushta, J., Lohmann, U., Mahura, A., Manders-Groot, A., Maurizi, A., Moussiopoulos, N., Rao, S.T., Savage, N., Seigneur, C., Sokhi, R.S., Solazzo, E., Solomos, S., Sørensen, B., Tsegas, G., Vignati, E., Vogel, B., Zhang, Y., 2014a. Online coupled regional meteorology chemistry models in Europe: Current status and prospects. Atmos. Chem. Phys. 14, 317–398. https://doi.org/10.5194/acp-14-317-2014

Baklanov, A., Schlünzen, K., Suppan, P., Baldasano, J., Brunner, D., Aksoyoglu, S., Carmichael, G., Douros, J., Flemming, J., Forkel, R., Galmarini, S., Gauss, M., Grell, G., Hirtl, M., Joffre, S., Jorba, O., Kaas, E., Kaasik, M., Kallos, G., Kong, X., Korsholm, U., Kurganskiy, A., Kushta, J., Lohmann, U., Mahura, A., Manders-Groot, A., Maurizi, A., Moussiopoulos, N., Rao, S.T., Savage, N., Seigneur, C., Sokhi, R.S., Solazzo, E., Solomos, S., Sørensen, B., Tsegas, G., Vignati, E., Vogel, B., Zhang, Y., 2014b. Online coupled regional meteorology chemistry models in Europe: Current status and prospects. Atmos. Chem. Phys. 14, 317–398. https://doi.org/10.5194/acp-14-317-2014

Banks, R.F., Tiana-Alsina, J., Baldasano, J.M., Rocadenbosch, F., Papayannis, A., Solomos, S., Tzanis, C.G., 2016. Sensitivity of boundary-layer variables to PBL schemes in the WRF model based on surface meteorological observations, lidar, and radiosondes during the HygrA-CD campaign. Atmos. Res. 176–177, 185–201. https://doi.org/10.1016/j.atmosres.2016.02.024

Barman, N., Gokhale, S., 2019. Urban black carbon - source apportionment, emissions and long-range transport over the Brahmaputra River Valley. Sci. Total Environ. 693, 1–14. https://doi.org/10.1016/j.scitotenv.2019.07.383

Bauer, S.E., Menon, S., 2012. Aerosol direct, indirect, semidirect, and surface albedo effects from sector contributions based on the IPCC AR5 emissions for preindustrial and present-day conditions. J. Geophys. Res. Atmos. https://doi.org/10.1029/2011JD016816

Bhat, M.A., Romshoo, S.A., Beig, G., 2022. Characteristics, source apportionment and long-range transport of black carbon at a high-altitude urban centre in the Kashmir valley, North-western Himalaya. Environ. Pollut. 305, 119295. https://doi.org/10.1016/j.envpol.2022.119295

Bibi, S., Alam, K., Chishtie, F., Bibi, H., Rahman, S., 2017. Observations of black carbon aerosols characteristics over an urban environment: Radiative forcing and related implications. Sci. Total Environ. 603–604, 319–329. https://doi.org/10.1016/j.scitotenv.2017.06.082

Boadh, R., Satyanarayana, A.N.V., Rama Krishna, T.V.B.P.S., Madala, S., 2016. Sensitivity of PBL schemes of the WRF-ARW model in simulating the boundary layer flow parameters for their application to air pollution dispersion modeling over a tropical station. Atmosfera 29, 61–81. https://doi.org/10.20937/ATM.2016.29.01.05

Bollasina, M.A., Ming, Y., Ramaswamy, V., 2011. Anthropogenic aerosols and the weakening of the south asian summer monsoon. Science (80-.). 334, 502–505. https://doi.org/10.1126/science.1204994

Bonasoni, P., Laj, P., Marinoni, A., Sprenger, M., Angelini, F., Arduini, J., Bonafè, U., Calzolari, F., Colombo, T., Decesari, S., Di Biagio, C., Di Sarra, A.G., Evangelisti, F., Duchi, R., Facchini, M.C., Fuzzi, S., Gobbi, G.P., Maione, M., Panday, A., Roccato, F., Sellegri, K., Venzac, H., Verza, G.P., Villani, P., Vuillermoz, E., Cristofanelli, P., 2010. Atmospheric Brown Clouds in the Himalayas: First two years of continuous observations at the Nepal Climate Observatory-

Pyramid (5079 m). Atmos. Chem. Phys. 10, 7515–7531. https://doi.org/10.5194/acp-10-7515-2010

Bond, T.C., Bergstrom, R.W., 2006. Light absorption by carbonaceous particles: An investigative review. Aerosol Sci. Technol. 40, 27–67. https://doi.org/10.1080/02786820500421521

Bond, T.C., Doherty, S.J., Fahey, D.W., Forster, P.M., Berntsen, T., Deangelo, B.J., Flanner, M.G., Ghan, S., Kärcher, B., Koch, D., Kinne, S., Kondo, Y., Quinn, P.K., Sarofim, M.C., Schultz, M.G., Schulz, M., Venkataraman, C., Zhang, H., Zhang, S., Bellouin, N., Guttikunda, S.K., Hopke, P.K., Jacobson, M.Z., Kaiser, J.W., Klimont, Z., Lohmann, U., Schwarz, J.P., Shindell, D., Storelvmo, T., Warren, S.G., Zender, C.S., 2013. Bounding the role of black carbon in the climate system: A scientific assessment. J. Geophys. Res. Atmos. 118, 5380–5552. https://doi.org/10.1002/jgrd.50171

Braham, J.R.R., 1974. Cloud Physics of Urban Weather Modification—A Preliminary Report. Bull. Am. Meteorol. Soc.

Braun, S.A., Tao, W.K., 2000. Sensitivity of high-resolution simulations of Hurricane Bob (1991) to planetary boundary layer parameterizations. Mon. Weather Rev. 128, 3941–3961. https://doi.org/10.1175/1520-0493(2000)129<3941:SOHRSO>2.0.CO;2

Brooks, J., Allan, J.D., Williams, P.I., Liu, D., Fox, C., Haywood, J., Langridge, J.M., Highwood, E.J., Kompalli, S.K., O'Sullivan, D., Babu, S.S., Satheesh, S.K., Turner, A.G., Coe, H., 2019a. Vertical and horizontal distribution of sub-micron aerosol chemical composition and physical characteristics across Northern India, during the pre-monsoon and monsoon seasons. Atmos. Chem. Phys. Discuss. 1–31. https://doi.org/10.5194/acp-2018-1109

Brooks, J., Liu, D., Allan, J.D., Williams, P.L., Haywood, J., Highwood, E.J., Kompalli, S.K., Babu, S.S., Satheesh, S.K., Turner, A.G., Coe, H., 2019b. Black carbon physical and optical properties across northern India during pre-monsoon and monsoon seasons. Atmos. Chem. Phys. 19, 13079–13096. https://doi.org/10.5194/acp-19-13079-2019

Carvalho, D., Rocha, A., Gómez-Gesteira, M., Silva Santos, C., 2014. WRF wind simulation and wind energy production estimates forced by different reanalyses: Comparison with observed data for Portugal. Appl. Energy 117, 116–126. https://doi.org/10.1016/j.apenergy.2013.12.001

Chakrabarty, R.K., Garro, M.A., Wilcox, E.M., Moosmller, H., 2012. Strong radiative heating due to wintertime black carbon aerosols in the Brahmaputra River Valley. Geophys. Res. Lett. 39, 1–5. https://doi.org/10.1029/2012GL051148

Chapman, E.G., Gustafson, W.I., Easter, R.C., Barnard, J.C., Ghan, S.J., Pekour, M.S., Fast, J.D., 2009. Coupling aerosol-cloud-radiative processes in the WRF-Chem model: Investigating the radiative impact of elevated point sources. Atmos. Chem. Phys. 9, 945–964. https://doi.org/10.5194/acp-9-945-2009

Chatterjee, A., Adak, A., Singh, A.K., Srivastava, M.K., Ghosh, S.K., Tiwari, S., Devara, P.C.S., Raha, S., 2010. Aerosol chemistry over a high altitude station at northeastern Himalayas, India. PLoS One 5. https://doi.org/10.1371/journal.pone.0011122

Chaudhuri, S., Middey, A., 2013. Disparity in the characteristic of thunderstorms and associated lightning activities over dissimilar terrains. Meteorol. Atmos. Phys. 119, 151–161. https://doi.org/10.1007/s00703-012-0226-4

Chaudhury, A.S., Nikhil, V.A., Gokhale, S., 2022. Black carbon in different climatic seasons of the Brahmaputra River Valley of Northeast India – Field measurements at two different heights and analysis. Atmos. Pollut. Res. 13, 101327. https://doi.org/10.1016/j.apr.2022.101327

Chawala, P., Priyan R, S., SM, S.N., 2023. Climatology and landscape determinants of AOD, SO2 and NO2 over Indo-Gangetic Plain. Environ. Res. 220, 115125. https://doi.org/10.1016/j.envres.2022.115125

Chen, B.L.Z.H.M., Wang, S.L.T.J., Liu, L.J.Z.H.N., Chen, M.X.P.L., 2019. The direct effects of black carbon aerosols from different source sectors in East Asia in summer 5293–5310. https://doi.org/10.1007/s00382-019-04863-5

Chen, Y., Chen, S., Zhao, D., Li, J., Bi, H., Lou, G., Guan, Y., 2022. The role of boundary layer height in India on transboundary pollutions to the Tibetan Plateau. Sci. Total Environ. 837, 155816. https://doi.org/10.1016/j.scitotenv.2022.155816

Cherian, R., Quaas, J., Salzmann, M., Tomassini, L., 2017. Black carbon indirect radiative effects in a climate model. Tellus, Ser. B Chem. Phys. Meteorol. 69, 1–10. https://doi.org/10.1080/16000889.2017.1369342

Cherian, R., Venkataraman, C., Quaas, J., Ramachandran, S., 2013. GCM simulations of anthropogenic aerosol-induced changes in aerosol extinction, atmospheric heating and precipitation over India. J. Geophys. Res. Atmos. 118, 2938–2955. https://doi.org/10.1002/jgrd.50298

Choudhury, G., Tyagi, B., Krishna Vissa, N., Singh, J., Sarangi, C., Nand Tripathi, S., Tesche, M., 2020a. Aerosol-enhanced high precipitation events near the Himalayan foothills. Atmos. Chem. Phys. 20, 15389–15399. https://doi.org/10.5194/acp-20-15389-2020

Choudhury, G., Tyagi, B., Vissa, N.K., Singh, J., Sarangi, C., Tripathi, S.N., Tesche, M., 2020b. Aerosol-induced high precipitation events near the Himalayan foothills. Atmos. Chem. Phys. 1–

17. https://doi.org/10.5194/acp-2020-440

Christensen, M.W., Chen, Y.C., Stephens, G.L., 2016. Aerosol indirect effect dictated by liquid clouds. J. Geophys. Res. 121, 14636–14650. https://doi.org/10.1002/2016JD025245

Cohen, A.E., Cavallo, S.M., Coniglio, M.C., Brooks, H.E., 2015. A review of planetary boundary layer parameterization schemes and their sensitivity in simulating southeastern U.S. cold season severe weather environments. Weather Forecast. 30, 591–612. https://doi.org/10.1175/WAF-D-14-00105.1

Crippa, M., Guizzardi, D., Muntean, M., Schaaf, E., Dentener, F., DeAardenne, J.A. Van, Monni, S., Doering, U., Olivier, J.G.J., Pagliari, V., 2018. Gridded emissions of air pollutants for the period 1970–2012 within EDGAR v4.3.2. Earth Syst. Sci. Data 10, 1987–2013. https://doi.org/10.5194/essd-10-1987-2018

Cuchiara, G.C., Li, X., Carvalho, J., Rappenglück, B., 2014. Intercomparison of planetary boundary layer parameterization and its impacts on surface ozone concentration in the WRF/Chem model for a case study in houston/texas. Atmos. Environ. 96, 175–185. https://doi.org/10.1016/j.atmosenv.2014.07.013

Dahutia, P., Pathak, B., Bhuyan, P.K., 2019. Vertical distribution of aerosols and clouds over north-eastern South Asia: Aerosol-cloud interactions. Atmos. Environ. 215, 116882. https://doi.org/10.1016/j.atmosenv.2019.116882

Dahutia, P., Pathak, B., Bhuyan, P.K., 2018a. Aerosols characteristics, trends and their climatic implications over northeast india and adjoining South Asia. Int. J. Climatol. 38, 1234–1256. https://doi.org/10.1002/joc.5240

Dahutia, P., Pathak, B., Bhuyan, P.K., 2018b. Aerosols characteristics, trends and their climatic implications over northeast india and adjoining South Asia. Int. J. Climatol. 38, 1234–1256. https://doi.org/10.1002/joc.5240

Dash, S.K., Jenamani, R.K., Kalsi, S.R., Panda, S.K., 2007. Some evidence of climate change in twentieth-century India. Clim. Change 85, 299–321. https://doi.org/10.1007/s10584-007-9305-9

Davies, J., 2014. Aerosol in the Atmosphere [WWW Document]. URL https://allaboutaerosol.wordpress.com/aerosol-in-the-atmosphere/ (accessed 3.23.19).

Devara, P.C.S., Manoj, M.G., 2013. Aerosol-cloud-precipitation interactions: A challenging problem in regional environment and climate research. Particuology 11, 25–33. https://doi.org/10.1016/j.partic.2012.07.006

Dhar, P., De, B.K., Banik, T., Gogoi, M.M., Babu, S.S., Guha, A., 2017. Atmospheric aerosol radiative forcing over a semi-continental location Tripura in North-East India: Model results and ground observations. Sci. Total Environ. 580, 499–508. https://doi.org/10.1016/j.scitotenv.2016.11.200

Ding, A.J., Huang, X., Nie, W., Sun, J.N., Kerminen, V.M., Petäjä, T., Su, H., Cheng, Y.F., Yang, X.Q., Wang, M.H., Chi, X.G., Wang, J.P., Virkkula, A., Guo, W.D., Yuan, J., Wang, S.Y., Zhang, R.J., Wu, Y.F., Song, Y., Zhu, T., Zilitinkevich, S., Kulmala, M., Fu, C.B., 2016. Enhanced haze pollution by black carbon in megacities in China. Geophys. Res. Lett. 43, 2873–2879. https://doi.org/10.1002/2016GL067745

Dong, Z., Li, Z., Yu, X., Cribb, M., Li, X., Dai, J., 2017. Opposite long-term trends in aerosols between low and high altitudes: A testimony to the aerosol-PBL feedback. Atmos. Chem. Phys. 17, 7997–8009. https://doi.org/10.5194/acp-17-7997-2017

Dzebre, D.E.K., Adaramola, M.S., 2020. A preliminary sensitivity study of Planetary Boundary Layer parameterisation schemes in the weather research and forecasting model to surface winds in coastal Ghana. Renew. Energy 146, 66–86. https://doi.org/10.1016/j.renene.2019.06.133

Emery, C., Tai, E., Yarwood, G., 2001. Enhanced Meteorological Modeling and Performance Evaluation for Two Texas Ozone Episodes. Env. Int. Corp. 235.

Emmons, L.K., Walters, S., Hess, P.G., Lamarque, J.F., Pfister, G.G., Fillmore, D., Granier, C., Guenther, A., Kinnison, D., Laepple, T., Orlando, J., Tie, X., Tyndall, G., Wiedinmyer, C., Baughcum, S.L., Kloster, S., 2010. Description and evaluation of the Model for Ozone and Related chemical Tracers, version 4 (MOZART-4). Geosci. Model Dev. 3, 43–67. https://doi.org/10.5194/gmd-3-43-2010

Fadnavis, S., Sabin, T.P., Roy, C., Rowlinson, M., Rap, A., Vernier, J.P., Sioris, C.E., 2019. Elevated aerosol layer over South Asia worsens the Indian droughts. Sci. Rep. 9, 1–11. https://doi.org/10.1038/s41598-019-46704-9

Fan, J., Zhang, R., Tao, W.K., Mohr, K.I., 2008. Effects of aerosol optical properties on deep convective clouds and radiative forcing. J. Geophys. Res. Atmos. 113, 1–16. https://doi.org/10.1029/2007JD009257

Fast, J.D., Gustafson, W.I., Easter, R.C., Zaveri, R.A., Barnard, J.C., Chapman, E.G., Grell, G.A., Peckham, S.E., 2006. Evolution of ozone, particulates, and aerosol direct radiative forcing in the vicinity of Houston using a fully coupled meteorology-chemistry-aerosol model. J. Geophys. Res. Atmos. 111, 1–29. https://doi.org/10.1029/2005JD006721

Gadhavi, H.S., Renuka, K., Ravi Kiran, V., Jayaraman, A., Stohl, A., Klimont, Z., Beig, G., 2015. Evaluation of black carbon emission inventories using a Lagrangian dispersion model - A case study over southern India. Atmos. Chem. Phys. 15, 1447–1461. https://doi.org/10.5194/acp-15-1447-2015

Ganguly, D., Ginoux, P., Ramaswamy, V., Winker, D.M., Holben, B.N., Tripathi, S.N., 2009. Retrieving the composition and concentration of aerosols over the Indo-Gangetic basin using CALIOP and AERONET data. Geophys. Res. Lett. 36, 1–5. https://doi.org/10.1029/2009GL038315

Gautam, R., Hsu, N.C., Tsay, S.C., Lau, K.M., Holben, B., Bell, S., Smirnov, A., Li, C., Hansell, R., Ji, Q., Payra, S., Aryal, D., Kayastha, R., Kim, K.M., 2011. Accumulation of aerosols over the Indo-Gangetic plains and southern slopes of the Himalayas: Distribution, properties and radiative effects during the 2009 pre-monsoon season. Atmos. Chem. Phys. 11, 12841–12863. https://doi.org/10.5194/acp-11-12841-2011

Ghan, S.J., Liu, X., Easter, R.C., Zaveri, R., Rasch, P.J., Yoon, J.H., Eaton, B., 2012a. Toward a minimal representation of aerosols in climate models: Comparative decomposition of aerosol direct, semidirect, and indirect radiative forcing. J. Clim. 25, 6461–6476. https://doi.org/10.1175/JCLI-D-11-00650.1

Ghan, S.J., Liu, X., Easter, R.C., Zaveri, R., Rasch, P.J., Yoon, J.H., Eaton, B., 2012b. Toward a minimal representation of aerosols in climate models: Comparative decomposition of aerosol direct, semidirect, and indirect radiative forcing. J. Clim. 25, 6461–6476. https://doi.org/10.1175/JCLI-D-11-00650.1

GMAO, 2015. MERRA-2 tavg1_2d_aer_Nx: 2d,1-Hourly,Time-averaged,Single-Level,Assimilation,Aerosol Diagnostics V5.12.4, Greenbelt, MD, USA, Goddard Earth Sciences Data and Information Services Center (GES DISC) [WWW Document]. Glob. Model. Assim. Off. https://doi.org/10.5067/KLICLTZ8EM9D

Gogoi, M.M., Babu, S.S., Moorthy, K.K., Bhuyan, P.K., Pathak, B., Subba, T., Chutia, L., Kundu, S.S., Bharali, C., Borgohain, A., Guha, A., Kumar De, B., Singh, B., Chin, M., 2017a. Radiative effects of absorbing aerosols over northeastern India: Observations and model simulations. J. Geophys. Res. 122, 1132–1157. https://doi.org/10.1002/2016JD025592

Gogoi, M.M., Babu, S.S., Moorthy, K.K., Bhuyan, P.K., Pathak, B., Subba, T., Chutia, L., Kundu, S.S., Bharali, C., Borgohain, A., Guha, A., Kumar De, B., Singh, B., Chin, M., 2017b. Radiative effects of absorbing aerosols over northeastern India: Observations and model simulations. J. Geophys. Res. 122, 1132–1157. https://doi.org/10.1002/2016JD025592

Gogoi, M.M., Bhuyan, P.K., Moorthy, K.K., 2009. An In ves ti ga tion of Aero sol Size Dis tri bu tion Prop er ties at Dibrugarh : North-East ern India 20, 521–533.

https://doi.org/10.3319/TAO.2008.06.11.01(A)An

Govardhan, G., Nanjundiah, R.S., Satheesh, S.K., Krishnamoorthy, K., Kotamarthi, V.R., 2015. Performance of WRF-chem over indian region: Comparison with measurements. J. Earth Syst. Sci. 124, 875–896. https://doi.org/10.1007/s12040-015-0576-7

Govardhan, G., Satheesh, S.K., Moorthy, K.K., Nanjundiah, R., 2019. Simulations of Black Carbon Over Indian Region: Improvements and Implications of Diurnality in Emissions. Atmos. Chem. Phys. Discuss. 1–25. https://doi.org/10.5194/acp-2019-152

Granier, C., Darras, S., Denier van der Gon, H., Doubalova, J., Elguindi, N., Galle, B., Gauss, M., Guevara, M., Jalakanen, J.-P., Kuenen, J., Liousse, C., Quack, B., Simpson, D., Sinderlova, K., 2019. The Copernicus Atmosphere Monitoring Service global and regional emissions (April 2019 version). https://doi.org/10.24380/d0bn-kx16

Grell, G.A., Freitas, S.R., 2014. A scale and aerosol aware stochastic convective parameterization for weather and air quality modeling. Atmos. Chem. Phys. 14, 5233–5250. https://doi.org/10.5194/acp-14-5233-2014

Grell, G.A., Peckham, S.E., Schmitz, R., McKeen, S.A., Frost, G., Skamarock, W.C., Eder, B., 2005. Fully coupled "online" chemistry within the WRF model. Atmos. Environ. 39, 6957–6975. https://doi.org/10.1016/j.atmosenv.2005.04.027

Guenther, A., Karl, T., Harley, P., Wiedinmyer, C., Palmer, P.I., Geron, C., 2006. and Physics Estimates of global terrestrial isoprene emissions using MEGAN (Model of Emissions of Gases and Aerosols from Nature) 3181–3210.

Guha, A., De, B.K., Dhar, P., Banik, T., Chakraborty, M., Roy, R., Choudhury, A., Gogoi, M.M., Babu, S.S., Moorthy, K.K., 2015. Seasonal Characteristics of Aerosol Black Carbon in Relation to Long Range Transport over Tripura in Northeast India. Aerosol Air Qual. Res. 15, 786–798. https://doi.org/10.4209/aaqr.2014.02.0029

Gunwani, P., Govardhan, G., Jena, C., Yadav, P., Kulkarni, S., Debnath, S., Pawar, P. V., Khare, M., Kaginalkar, A., Kumar, R., Wagh, S., Chate, D., Ghude, S.D., 2023. Sensitivity of WRF/Chem simulated PM2.5 to initial/boundary conditions and planetary boundary layer parameterization schemes over the Indo-Gangetic Plain. Environ. Monit. Assess. 195, 560. https://doi.org/10.1007/s10661-023-10987-3

Gunwani, P., Mohan, M., 2017. Sensitivity of WRF model estimates to various PBL parameterizations in different climatic zones over India. Atmos. Res. 194, 43–65. https://doi.org/10.1016/j.atmosres.2017.04.026

Gunwani, P., Sati, A.P., Mohan, M., Gupta, M., 2020. Assessment of physical parameterization schemes in WRF over national capital region of India. Meteorol. Atmos. Phys. 133, 399–418. https://doi.org/10.1007/s00703-020-00757-y

Habib, G., Venkataraman, C., Chiapello, I., Ramachandran, S., Boucher, O., Shekar Reddy, M., 2006. Seasonal and interannual variability in absorbing aerosols over India derived from TOMS: Relationship to regional meteorology and emissions. Atmos. Environ. 40, 1909–1921. https://doi.org/10.1016/j.atmosenv.2005.07.077

Hariprasad, K.B.R.R., Srinivas, C. V., Singh, A.B., Vijaya Bhaskara Rao, S., Baskaran, R., Venkatraman, B., 2014. Numerical simulation and intercomparison of boundary layer structure with different PBL schemes in WRF using experimental observations at a tropical site. Atmos. Res. 145–146, 27–44. https://doi.org/10.1016/j.atmosres.2014.03.023

Hersbach, H., Bell, B., Berrisford, P., Hirahara, S., Horányi, A., Muñoz-Sabater, J., Nicolas, J., Peubey, C., Radu, R., Schepers, D., Simmons, A., Soci, C., Abdalla, S., Abellan, X., Balsamo, G., Bechtold, P., Biavati, G., Bidlot, J., Bonavita, M., De Chiara, G., Dahlgren, P., Dee, D., Diamantakis, M., Dragani, R., Flemming, J., Forbes, R., Fuentes, M., Geer, A., Haimberger, L., Healy, S., Hogan, R.J., Hólm, E., Janisková, M., Keeley, S., Laloyaux, P., Lopez, P., Lupu, C., Radnoti, G., de Rosnay, P., Rozum, I., Vamborg, F., Villaume, S., Thépaut, J.N., 2020. The ERA5 global reanalysis. Q. J. R. Meteorol. Soc. 146, 1999–2049. https://doi.org/10.1002/qj.3803

Hill, A.., Dobbie, S., 2008. The impact of aerosols on non-precipitating marine stratocumulus. II: The semi-direct effect. Q. J. R. Meteorol. Soc. 134, 1155–1165. https://doi.org/10.1002/qj.277

Hoesly, R.M., Smith, S.J., Feng, L., Klimont, Z., Janssens-Maenhout, G., Pitkanen, T., Seibert, J.J., Vu, L., Andres, R.J., Bolt, R.M., Bond, T.C., Dawidowski, L., Kholod, N., Kurokawa, J.I., Li, M., Liu, L., Lu, Z., Moura, M.C.P., O'Rourke, P.R., Zhang, Q., 2018. Historical (1750-2014) anthropogenic emissions of reactive gases and aerosols from the Community Emissions Data System (CEDS). Geosci. Model Dev. 11, 369–408. https://doi.org/10.5194/gmd-11-369-2018

Hong, S.-Y., Noh, Y., Dudhia, J., 2006. A New Vertical Diffusion Package with an Explicit Treatment of. Mon. Weather Rev. 134, 2318–2341.

Huang, J., Wang, T., Wang, W., Li, Z., Yan, H., 2014. Climate effects of dust aerosols over East Asian arid and semiarid regions. Nature 11398–11416. https://doi.org/10.1002/ 2014JD021796

Iacono, M.J., Delamere, J.S., Mlawer, E.J., Shephard, M.W., Clough, S.A., Collins, W.D., 2008. Radiative forcing by long-lived greenhouse gases: Calculations with the AER radiative transfer models. J. Geophys. Res. Atmos. https://doi.org/10.1029/2008JD009944

Jain, S.K., Kumar, V., 2012. Trend analysis of rainfall and temperature data for India. Curr. Sci. 102, 37–49.

Jain, S.K., Kumar, V., Saharia, M., 2013. Analysis of rainfall and temperature trends in northeast India. Int. J. Climatol. 33, 968–978. https://doi.org/10.1002/joc.3483

Janjić, Z.I., 2001. Nonsingular Implementation of the Mellor-Yamada Level 2 . 5 Scheme in the NCEP Meso model, National Centers for Encironmental Prediction, Office Note #437 1–61.

Johnson, B.T., Shine, K.P., Forster, P.M., 2004. The semi-direct aerosol effect: Impact of absorbing aerosols on marine stratocumulus. Q. J. R. Meteorol. Soc. 130, 1407–1422. https://doi.org/10.1256/qj.03.61

Kant, S., Panda, J., Gautam, R., 2019. A seasonal analysis of aerosol-cloud-radiation interaction over Indian region during 2000–2017. Atmos. Environ. 201, 212–222. https://doi.org/10.1016/j.atmosenv.2018.12.044

Kant, S., Panda, J., Rao, P., Sarangi, C., Ghude, S.D., 2021. Study of aerosol-cloud-precipitation-meteorology interaction during a distinct weather event over the Indian region using WRF-Chem. Atmos. Res. 247, 105144. https://doi.org/10.1016/j.atmosres.2020.105144

Katagiri, S., Hayasaka, T., Shimizu, A., Matsui, I., Nishizawa, T., Sugimoto, N., Takamura, T., 2013. Long term analysis of cirrus clouds' effects on shortwave and longwave radiation derived from data acquired by ground-based and satellite-borne observations. AIP Conf. Proc. 1531, 492–495. https://doi.org/10.1063/1.4804814

Kedia, S., Cherian, R., Islam, S., Das, S.K., Kaginalkar, A., 2016. Regional simulation of aerosol radiative effects and their influence on rainfall over India using WRFChem model. Atmos. Res. 182, 232–242. https://doi.org/10.1016/j.atmosres.2016.07.008

Kedia, S., Das, S.K., Islam, S., Hazra, A., Kumar, N., 2019. Aerosols impact on the convective and non-convective rain distribution over the Indian region: Results from WRF-Chem simulation. Atmos. Environ. 202, 64–74. https://doi.org/10.1016/j.atmosenv.2019.01.020

Kedia, S., Kumar, R., Islam, S., Sathe, Y., Kaginalkar, A., 2018. Radiative impact of a heavy dust storm over India and surrounding oceanic regions. Atmos. Environ. 185, 109–120. https://doi.org/10.1016/j.atmosenv.2018.05.005

Kedia, S., Ramachandran, S., Holben, B.N., Tripathi, S.N., 2014. Quantification of aerosol type, and sources of aerosols over the Indo-Gangetic Plain. Atmos. Environ. 98, 607–619. https://doi.org/10.1016/j.atmosenv.2014.09.022

Koch, D., Bauer, S.E., Del Genio, A., Faluvegi, G., McConnell, J.R., Menon, S., Miller, R.L., Rind, D., Ruedy, R., Schmidt, G.A., Shindell, D., 2011. Coupled aerosol-chemistry-climate twentieth-century transient model investigation: Trends in short-lived species and climate responses. J. Clim. 24, 2693–2714. https://doi.org/10.1175/2011JCLI3582.1

Koch, D., Del Genio, A.D., 2010a. Black carbon semi-direct effects on cloud cover: Review and synthesis. Atmos. Chem. Phys. 10, 7685–7696. https://doi.org/10.5194/acp-10-7685-2010

Koch, D., Del Genio, A.D., 2010b. Black carbon semi-direct effects on cloud cover: Review and synthesis. Atmos. Chem. Phys. 10, 7685–7696. https://doi.org/10.5194/acp-10-7685-2010

Konwar, M., Parekh, A., Goswami, B.N., 2012. Dynamics of east-west asymmetry of Indian summer monsoon rainfall trends in recent decades. Geophys. Res. Lett. 39, 1–6. https://doi.org/10.1029/2012GL052018

Koren, I., Kaufman, Y.J., Rosenfeld, D., Remer, L.A., Rudich, Y., 2005. Aerosol invigoration and restructuring of Atlantic convective clouds. Geophys. Res. Lett. 32, 1–4. https://doi.org/10.1029/2005GL023187

Krishnamohan, K.S., Modak, A., Bala, G., 2021. Effects of local and remote black carbon aerosols on summer monsoon precipitation over india. Environ. Res. Commun. 3. https://doi.org/10.1088/2515-7620/AC18D1

Kristjánsson, J.E., 2002. Studies of the aerosol indirect effect from sulfate and black carbon aerosols. J. Geophys. Res. Atmos. 107, 1–19. https://doi.org/https://doi.org/10.1029/2001JD000887

Kumar, M., Parmar, K.S., Kumar, D.B., Mhawish, A., Broday, D.M., Mall, R.K., Banerjee, T., 2018. Long-term aerosol climatology over Indo-Gangetic Plain: Trend, prediction and potential source fields. Atmos. Environ. 180, 37–50. https://doi.org/10.1016/j.atmosenv.2018.02.027

Kumar, P., Beig, G., Sahu, S.K., Yadav, R., Maji, S., Singh, V., Bamniya, B.R., 2023. Development of a high-resolution emissions inventory of carbonaceous particulate matters and their growth during 2011–2018 over India. Atmos. Environ. 303, 119750. https://doi.org/10.1016/j.atmosenv.2023.119750

Kumar, R., Barth, M.C., Pfister, G.G., Nair, V.S., Ghude, S.D., Ojha, N., 2015. What controls the seasonal cycle of black carbon aerosols in India? J. Geophys. Res. Atmos. 120, 1–17. https://doi.org/10.1002/2014JD022650.Received

Kumar, V., Jain, S.K., Singh, Y., 2010. Analyse des tendances pluviométriques de long terme en Inde. Hydrol. Sci. J. 55, 484–496. https://doi.org/10.1080/02626667.2010.481373

Kundu, S.S., Borgohain, A., Barman, N., Devi, M., Raju, P.L.N., 2018. Spatial Variability and Radiative Impact of Aerosol along the Brahmaputra River Valley in India: Results from a

Campaign. J. Environ. Prot. (Irvine,. Calif). 09, 405–430. https://doi.org/10.4236/jep.2018.94026

Lamarque, J.F., Emmons, L.K., Hess, P.G., Kinnison, D.E., Tilmes, S., Vitt, F., Heald, C.L., Holland, E.A., Lauritzen, P.H., Neu, J., Orlando, J.J., Rasch, P.J., Tyndall, G.K., 2012. CAM-chem: Description and evaluation of interactive atmospheric chemistry in the Community Earth System Model. Geosci. Model Dev. 5, 369–411. https://doi.org/10.5194/gmd-5-369-2012

Lambe, A.T., Ahern, A.T., Wright, J.P., Croasdale, D.R., Davidovits, P., Onasch, T.B., 2015. Oxidative aging and cloud condensation nuclei activation of laboratory combustion soot. J. Aerosol Sci. 79, 31–39. https://doi.org/10.1016/j.jaerosci.2014.10.001

Lau, K.M., Kim, M.K., Kim, K.M., 2006. Asian summer monsoon anomalies induced by aerosol direct forcing: The role of the Tibetan Plateau. Clim. Dyn. 26, 855–864. https://doi.org/10.1007/s00382-006-0114-z

Lee, H.J., Jo, Y.J., Kim, S., Kim, D., Kim, J.M., Choi, D., Jo, H.Y., Bak, J., Park, S.Y., Jeon, W., Kim, C.H., 2022. Transboundary aerosol transport process and its impact on aerosol-radiation-cloud feedbacks in springtime over Northeast Asia. Sci. Rep. 12, 1–10. https://doi.org/10.1038/s41598-022-08854-1

Lesins, G., Chylek, P., Lohmann, U., 2002. A study of internal and external mixing scenarios and its effect on aerosol optical properties and direct radiative forcing. J. Geophys. Res. Atmos. 107, AAC 5-1-AAC 5-12. https://doi.org/10.1029/2001jd000973

Li, Z., Guo, J., Ding, A., Liao, H., Liu, J., Sun, Y., Wang, T., Xue, H., Zhang, H., Zhu, B., 2017. Aerosol and boundary-layer interactions and impact on air quality. Natl. Sci. Rev. 4, 810–833. https://doi.org/10.1093/nsr/nwx117

Li, Z., Niu, F., Fan, J., Liu, Y., Rosenfeld, D., Ding, Y., 2011. Long-term impacts of aerosols on the vertical development of clouds and precipitation. Nat. Geosci. 4, 888–894. https://doi.org/10.1038/ngeo1313

Lindeman, J.D., Boybeyi, Z., Gultepe, I., 2011. An examination of the aerosol semi-direct effect for a polluted case of the ISDAC field campaign. J. Geophys. Res. Atmos. https://doi.org/10.1029/2011JD015649

Liou, K.N., 1980. An Introduction to Atmospheric Radiation.

Liu, S., Aiken, A.C., Gorkowski, K., Dubey, M.K., Cappa, C.D., Williams, L.R., Herndon, S.C., Massoli, P., Fortner, E.C., Chhabra, P.S., Brooks, W.A., Onasch, T.B., Jayne, J.T., Worsnop, D.R., China, S., Sharma, N., Mazzoleni, C., Xu, L., Ng, N.L., Liu, D., Allan, J.D., Lee, J.D., Fleming, Z.L., Mohr, C., Zotter, P., Szidat, S., Prévôt, A.S.H., 2015. Enhanced light absorption by mixed source black and brown carbon particles in UK winter. Nat. Commun. 6. https://doi.org/10.1038/ncomms9435

Liu, X.Y., Zhang, Y., Zhang, Q., He, K. Bin, 2016. Application of online-coupled WRF/Chem-MADRID in East Asia: Model evaluation and climatic effects of anthropogenic aerosols. Atmos. Environ. 124, 321–336. https://doi.org/10.1016/j.atmosenv.2015.03.052

Lohmann, U., Feichter, J., 2005. Atmospheric Chemistry and Physics Global indirect aerosol effects: a review. Atmos. Chem. Phys 5, 715–737.

Lohmann, U., Feichter, J., 2001. Can the direct and semi-direct aerosol effect compete with the indirect effect on a global scale? Geophys. Res. Lett. 28, 159–161. https://doi.org/10.1029/2000GL012051

Lu, Z., Zhang, Q., Streets, D.G., 2011. Sulfur dioxide and primary carbonaceous aerosol emissions in China and India, 1996-2010. Atmos. Chem. Phys. 11, 9839–9864. https://doi.org/10.5194/acp-11-9839-2011

Madala, S., Satyanarayana, A.N.V., Rao, T.N., 2014. Performance evaluation of PBL and cumulus parameterization schemes of WRF ARW model in simulating severe thunderstorm events over Gadanki MST radar facility - Case study. Atmos. Res. 139, 1–17. https://doi.org/10.1016/j.atmosres.2013.12.017

Madala, S., Satyanarayana, A.N.V., Srinivas, C. V., Kumar, M., 2015. Mesoscale atmospheric flow-field simulations for air quality modeling over complex terrain region of Ranchi in eastern India using WRF. Atmos. Environ. 107, 315–328. https://doi.org/10.1016/j.atmosenv.2015.02.059

Makar, P.A., Gong, W., Milbrandt, J., Hogrefe, C., Zhang, Y., Curci, G., Žabkar, R., Im, U., Balzarini, A., Baró, R., Bianconi, R., Cheung, P., Forkel, R., Gravel, S., Hirtl, M., Honzak, L., Hou, A., Jiménez-Guerrero, P., Langer, M., Moran, M.D., Pabla, B., Pérez, J.L., Pirovano, G., San José, R., Tuccella, P., Werhahn, J., Zhang, J., Galmarini, S., 2015. Feedbacks between air pollution and weather, Part 1: Effects on weather. Atmos. Environ. 115, 442–469. https://doi.org/10.1016/j.atmosenv.2014.12.003

Manoj, M.G., Devara, P.C.S., Joseph, S., Sahai, A.K., 2012. Aerosol indirect effect during the aberrant Indian Summer Monsoon breaks of 2009. Atmos. Environ. 60, 153–163. https://doi.org/10.1016/j.atmosenv.2012.06.007

McFarquhar, G.M., Wang, H., 2006. Effects of aerosols on trade wind cumuli over the Indian Ocean: Model simulations. Q. J. R. Meteorol. Soc. 132, 821–843. https://doi.org/10.1256/qj.04.179

Menon, S., Hansen, J., Nazarenko, L., Luo, Y., 2002. Climate effects of black carbon aerosols in China and India. Science (80-.). 297, 2250–2253. https://doi.org/10.1126/science.1075159

Ming, Y., Ramaswamy, V., Persad, G., 2010. Two opposing effects of absorbing aerosols on global-mean precipitation. Geophys. Res. Lett. https://doi.org/10.1029/2010GL042895

Mitchell, J.M., 1971. The Effect of Atmospheric Aerosols on Climate with Special Reference to Temperature near the Earth's Surface. J. Appl. Meteorol. https://doi.org/10.1175/1520-0450(1971)010<0703:teoaao>2.0.co;2

Moffet, R.C., Prather, K.A., 2009. In-situ measurements of the mixing state and optical properties of soot with implications for radiative forcing estimates. Proc. Natl. Acad. Sci. 106, 11872–11877. https://doi.org/10.1073/pnas.0900040106

Mohan, M., Bhati, S., 2011. Analysis of WRF Model Performance over Subtropical Region of Delhi, India. Adv. Meteorol. 2011, 1–13. https://doi.org/10.1155/2011/621235

Mohan, M., Gupta, M., 2018. Sensitivity of PBL parameterizations on PM10 and ozone simulation using chemical transport model WRF-Chem over a sub-tropical urban airshed in India. Atmos. Environ. 185, 53–63. https://doi.org/10.1016/j.atmosenv.2018.04.054

Mondal, A., Khare, D., Kundu, S., 2015. Spatial and temporal analysis of rainfall and temperature trend of India. Theor. Appl. Climatol. 122, 143–158. https://doi.org/10.1007/s00704-014-1283-z

Mondal, A., Lakshmi, V., Hashemi, H., 2018. Intercomparison of trend analysis of Multisatellite Monthly Precipitation Products and Gauge Measurements for River Basins of India. J. Hydrol. 565, 779–790. https://doi.org/10.1016/j.jhydrol.2018.08.083

Moorthy, K.K., Beegum, S.N., Srivastava, N., Satheesh, S.K., Chin, M., Blond, N., Babu, S.S., Singh, S., 2013. Performance evaluation of chemistry transport models over India. Atmos. Environ. 71, 210–225. https://doi.org/10.1016/j.atmosenv.2013.01.056

Morrison, H., Thompson, G., Tatarskii, V., 2009. Impact of cloud microphysics on the development of trailing stratiform precipitation in a simulated squall line: Comparison of one- and two-moment schemes. Mon. Weather Rev. 137, 991–1007. https://doi.org/10.1175/2008MWR2556.1

Moya-Álvarez, A.S., Estevan, R., Kumar, S., Flores Rojas, J.L., Ticse, J.J., Martínez-Castro, D., Silva, Y., 2020. Influence of PBL parameterization schemes in WRF_ARW model on short - range precipitation's forecasts in the complex orography of Peruvian Central Andes. Atmos. Res. 233, 104708. https://doi.org/10.1016/j.atmosres.2019.104708

Nabat, P., Somot, S., Mallet, M., Sevault, F., Chiacchio, M., Wild, M., 2014. Direct and semi-direct aerosol radiative effect on the Mediterranean climate variability using a coupled regional climate system model. Clim. Dyn. 44, 1127–1155. https://doi.org/10.1007/s00382-014-2205-6

Nair Jayachandran, V., Nair Suresh Babu, S., Vaishya, A., Gogoi, M.M., Nair, V.S., Krishnakumari Satheesh, S., Krishna Moorthy, K., 2020. Altitude profiles of cloud condensation nuclei characteristics across the Indo-Gangetic Plain prior to the onset of the Indian summer monsoon. Atmos. Chem. Phys. 20, 561–576. https://doi.org/10.5194/acp-20-561-2020

Nair, V.S., Babu, S.S., Gogoi, M.M., Moorthy, K.K., 2016. Large-scale enhancement in aerosol absorption in the lower free troposphere over continental India during spring. Geophys. Res. Lett. 43, 11,453-11,461. https://doi.org/10.1002/2016GL070669

Nair, V.S., Babu, S.S., Manoj, M.R., Moorthy, K.K., Chin, M., 2017. Direct radiative effects of aerosols over South Asia from observations and modeling. Clim. Dyn. 49, 1411–1428. https://doi.org/10.1007/s00382-016-3384-0

Nair, V.S., Solmon, F., Giorgi, F., Mariotti, L., Babu, S.S., Moorthy, K.K., 2012. Simulation of South Asian aerosols for regional climate studies. J. Geophys. Res. Atmos. 117, 1–17. https://doi.org/10.1029/2011JD016711

Nakanishi, M., Niino, H., 2006. An improved Mellor–Yamada level-3 model: its numerical stability and application to a regional prediction of advection fog. Boundary-Layer Meteorol. 119, 397–407. https://doi.org/10.1007/s10546-005-9030-8

Nandan, R., Ratnam, M.V., Kiran, V.R., Naik, D.N., 2022. Aerosol-cloud interaction in water clouds observed using ground-based, in-situ, and satellite-based observations over an Indian continental region. Atmos. Res. 280, 106436. https://doi.org/10.1016/j.atmosres.2022.106436

Nenes, A., Conant, W.C., Seinfeld, J.H., 2002. Black carbon radiative heating effects on cloud microphysics and implications for the aerosol indirect effect 2. Cloud microphysics. J. Geophys. Res. Atmos. 107, AAC 24-1-AAC 24-11. https://doi.org/10.1029/2002jd002101

Ojha, N., Naja, M., Singh, K.P., Sarangi, T., Kumar, R., Lal, S., Lawrence, M.G., Butler, T.M., Chandola, H.C., 2012. Variabilities in ozone at a semi-urban site in the Indo-Gangetic Plain region: Association with the meteorology and regional processes. J. Geophys. Res. Atmos. 117, 1–19. https://doi.org/10.1029/2012JD017716

Ojha, N., Sharma, A., Kumar, M., Girach, I., Ansari, T.U., Sharma, S.K., Singh, N., Pozzer, A., Gunthe, S.S., 2020. On the widespread enhancement in fine particulate matter across the Indo-Gangetic Plain towards winter. Sci. Rep. 10, 1–9. https://doi.org/10.1038/s41598-020-62710-8

Pai, D.S., Sridhar, L., Rajeevan, M., Sreejith, O.P., Satbhai, N.S., Mukhopadhyay, B., 2014. Development of a new high spatial resolution (0.25° × 0.25°) long period (1901-2010) daily gridded rainfall data set over India and its comparison with existing data sets over the region. Mausam 65, 1–18.

Panda, J., Sharan, M., 2012. Influence of land-surface and turbulent parameterization schemes on regional-scale boundary layer characteristics over northern India. Atmos. Res. 112, 89–111. https://doi.org/10.1016/j.atmosres.2012.04.001

Panicker, A.S., Pandithurai, G., Safai, P.D., Dipu, S., Prabha, T. V., Konwar, M., 2014. Observations of black carbon induced semi direct effect over Northeast India. Atmos. Environ. 98, 685–692. https://doi.org/10.1016/j.atmosenv.2014.09.034

Panicker, A.S., Pandithurai, G., Safai, P.D., Prabha, T. V., 2016. Indirect forcing of black carbon on clouds over northeast India. Q. J. R. Meteorol. Soc. 142, 2968–2973. https://doi.org/10.1002/qj.2878

Pathak, B., Kalita, G., Bhuyan, K., Bhuyan, P.K., Moorthy, K.K., 2010. Aerosol temporal characteristics and its impact on shortwave radiative forcing at a location in the northeast of India 115, 1–14. https://doi.org/10.1029/2009JD013462

Pathak, B., Subba, T., Dahutia, P., Bhuyan, P.K., Moorthy, K.K., Gogoi, M.M., Babu, S.S., Chutia, L., Ajay, P., Biswas, J., Bharali, C., Borgohain, A., Dhar, P., Guha, A., De, B.K., Banik, T., Chakraborty, M., Kundu, S.S., Sudhakar, S., Singh, S.B., 2016. Aerosol characteristics in north-east India using ARFINET spectral optical depth measurements. Atmos. Environ. 125, 461–473. https://doi.org/10.1016/j.atmosenv.2015.07.038

Pleim, J.E., 2007. A combined local and nonlocal closure model for the atmospheric boundary layer. Part I: Model description and testing. J. Appl. Meteorol. Climatol. 46, 1383–1395. https://doi.org/10.1175/JAM2539.1

PTI, 2022. Studies Suggest Increase in Extreme Rainfall Events, Rising Trend of Black Carbon Concentration in Northeast [WWW Document]. URL https://www.news18.com/news/india/studies-suggest-increase-in-extreme-rainfall-events-rising-trend-of-black-carbon-concentration-in-northeast-6573931.html (accessed 5.2.22).

Rahul, P.R.C., Bhawar, R.L., Ayantika, D.C., Panicker, A.S., Safai, P.D., Tharaprabhakaran, V., Padmakumari, B., Raju, M.P., 2014. Double blanket effect caused by two layers of black carbon aerosols escalates warming in the Brahmaputra River Valley. Sci. Rep. 4, 1–7. https://doi.org/10.1038/srep03670

Rai, D., Pattnaik, S., 2019. Evaluation of WRF planetary boundary layer parameterization schemes for simulation of monsoon depressions over India. Meteorol. Atmos. Phys. 131, 1529–1548. https://doi.org/10.1007/s00703-019-0656-3

Raju, A., Parekh, A., Chowdary, J.S., Gnanaseelan, C., 2015. Assessment of the Indian summer monsoon in the WRF regional climate model. Clim. Dyn. 44, 3077–3100. https://doi.org/10.1007/s00382-014-2295-1

Ramachandran, S., Rupakheti, M., Lawrence, M.G., 2020. Black carbon dominates the aerosol absorption over the Indo-Gangetic Plain and the Himalayan foothills. Environ. Int. 142, 105814. https://doi.org/10.1016/j.envint.2020.105814

Ramanathan, V., Carmichael, G., 2008. Global and regional climate changes due to black carbon. Nat. Geosci. 1, 221–227. https://doi.org/10.1038/ngeo156

Ramanathan, V., Chung, C., Kim, D., Bettge, T., Buja, L., Kiehl, J.T., Washington, W.M., Fu, Q., Sikka, D.R., Wild, M., 2005a. Atmospheric brown clouds: Impacts on South Asian climate and hydrological cycle. Proc. Natl. Acad. Sci. 102, 5326–5333. https://doi.org/10.1073/pnas.0500656102

Ramanathan, V., Chung, C., Kim, D., Bettge, T., Buja, L., Kiehl, J.T., Washington, W.M., Fu, Q., Sikka, D.R., Wild, M., 2005b. Atmospheric brown clouds: Impacts on South Asian climate and hydrological cycle. Proc. Natl. Acad. Sci. U. S. A. 102, 5326–5333. https://doi.org/10.1073/pnas.0500656102

Rana, A., Jia, S., Sarkar, S., 2019. Black carbon aerosol in India: A comprehensive review of current status and future prospects. Atmos. Res. 218, 207–230. https://doi.org/10.1016/j.atmosres.2018.12.002

Romatschke, U., Houze, R.A., 2011. Characteristics of precipitating convective systems in the South Asian monsoon. J. Hydrometeorol. 12, 3–26. https://doi.org/10.1175/2010JHM1289.1

Rosenfeld, D., 2012. Suppression of rain and snow by urban air pollution. Science (80-.). 287, 1793–1796. https://doi.org/10.1126/science.287.5459.1793

Rosenfeld, D., 2006. Aerosol-cloud interactions control of earth radiation and latent heat release budgets. Space Sci. Rev. 125, 149–157. https://doi.org/10.1007/s11214-006-9053-6

Rosenfeld, D., Lohmann, U., Raga, G.B., O'Dowd, C.D., Kulmala, M., Fuzzi, S., Reissell, A., Andreae, M.O., 2008. Flood or drought: How do aerosols affect precipitation? Science (80-.). 321, 1309–1313. https://doi.org/10.1126/science.1160606

Roux, G., Liu, Y., Monache, L.D., Sheu, R.-S., Warner, T.T., 2009. Verification of high resolution WRF-RTFDDA surface forecasts over mountains and plains. Proc. 10th WRF Users' Work. 20–23.

Sadavarte, P., Venkataraman, C., 2014. Trends in multi-pollutant emissions from a technology-linked inventory for India: I. Industry and transport sectors. Atmos. Environ. 99, 353–364. https://doi.org/10.1016/j.atmosenv.2014.09.081

Sarangi, C., Tripathi, S.N., Tripathi, S., Barth, M.C., 2015. Aerosol-cloud associations over gangetic basin during a typical monsoon depression event using WRF-Chem simulation. J. Geophys. Res. 120, 10,974-10,995. https://doi.org/10.1002/2015JD023634

Sarkar, C., Roy, A., Chatterjee, A., Ghosh, S.K., Raha, S., 2019. Factors controlling the long-term (2009–2015) trend of PM 2.5 and black carbon aerosols at eastern Himalaya, India. Sci. Total Environ. 656, 280–296. https://doi.org/10.1016/j.scitotenv.2018.11.367

Sathyanadh, A., Prabha, T. V., Balaji, B., Resmi, E.A., Karipot, A., 2017. Evaluation of WRF PBL parameterization schemes against direct observations during a dry event over the Ganges valley. Atmos. Res. 193, 125–141. https://doi.org/10.1016/j.atmosres.2017.02.016

Shi, L., Zhu, A., Huang, L., Yaluk, E., Gu, Y., Wang, Y., Wang, S., Chan, A., Li, L., 2021. Impact of the planetary boundary layer on air quality simulations over the Yangtze River Delta region, China. Atmos. Environ. 263. https://doi.org/10.1016/j.atmosenv.2021.118685

Shin, H.H., Hong, S.Y., 2015. Representation of the subgrid-scale turbulent transport in convective boundary layers at gray-zone resolutions. Mon. Weather Rev. 143, 250–271. https://doi.org/10.1175/MWR-D-14-00116.1

Shin, H.H., Hong, S.Y., 2011. Intercomparison of Planetary Boundary-Layer Parametrizations in the WRF Model for a Single Day from CASES-99. Boundary-Layer Meteorol. 139, 261–281. https://doi.org/10.1007/s10546-010-9583-z

Shiogama, H., Emori, S., Takahashi, K., Ogura, T.N., Nozawa, T., Takemura, T., 2010. Emission scenario dependency of precipitation on global warming in the MIROC3.2 model. J. Clim. 23, 2404–2417. https://doi.org/10.1175/2009JCLI3428.1

Shrestha, R.K., Connolly, P.J., Gallagher, M.W., 2017. Sensitivity of WRF Cloud Microphysics to Simulations of a Convective Storm Over the Nepal Himalayas. Open Atmos. Sci. J. 11, 29–43. https://doi.org/10.2174/1874282301711010029

Sindhwani, R., Goyal, P., 2014. Assessment of traffic-generated gaseous and particulate matter emissions and trends over Delhi (2000-2010). Atmos. Pollut. Res. 5, 438–446. https://doi.org/10.5094/APR.2014.051

Singh, P., Sarawade, P., Adhikary, B., 2020. Transport of black carbon from planetary boundary layer to free troposphere during the summer monsoon over South Asia. Atmos. Res. 235, 104761. https://doi.org/10.1016/j.atmosres.2019.104761

Singh, S., Gokhale, S., 2021. Source apportionment and light absorption properties of black and brown carbon aerosols in the Brahmaputra River valley region. Urban Clim. 39, 100963. https://doi.org/10.1016/j.uclim.2021.100963

Singh, V., Singh, S., Biswal, A., Kesarkar, A.P., Mor, S., Ravindra, K., 2020. Diurnal and temporal changes in air pollution during COVID-19 strict lockdown over different regions of India. Environ. Pollut. 266, 115368. https://doi.org/10.1016/j.envpol.2020.115368

Sinha, P., Nageswararao, M.., Dash, G.P., Nair, A., Mohanty, U.C., 2019. Pre-monsoon rainfall and surface air temperature trends over India and its global linkages.pdf. Meteorol. Atmos. Phys. 1005–1018. https://doi.org/doi.org/10.1007/s00703-018-0621-6

Skamarock, W.C., Klemp, J.B., Dudhia, J., Gill, D.O., Zhiquan, L., Berner, J., Wang, W., Powers, J.G., Duda, M.G., Barker, D.M., Huang, X.-Y., 2019. A Description of the Advanced Research WRF Model Version 4. NCAR Tech. Note NCAR/TN-475+STR 145. https://doi.org/10.5065/1dfh-6p97

Slater, J., Coe, H., Mcfiggans, G., Tonttila, J., Romakkaniemi, S., 2022. The effect of BC on aerosol – boundary layer feedback : potential implications for urban pollution episodes 2937–2953.

Solutions, C. for C. and E., 2010. What is black carbon? [WWW Document]. URL https://www.c2es.org/document/what-is-black-carbon/ (accessed 11.9.18).

Soni, P., Nand, S., Rajesh, T., 2017a. Radiative effects of black carbon aerosols on Indian monsoon : a study using WRF-Chem model. https://doi.org/10.1007/s00704-017-2057-1

Soni, P., Tripathi, S.N., Srivastava, R., 2018. Radiative effects of black carbon aerosols on Indian monsoon: a study using WRF-Chem model. Theor. Appl. Climatol. 132, 115–134. https://doi.org/10.1007/s00704-017-2057-1

Soni, P., Tripathi, S.N., Srivastava, R., 2017b. Radiative effects of black carbon aerosols on Indian monsoon: a study using WRF-Chem model. Theor. Appl. Climatol. 132, 115–134. https://doi.org/10.1007/s00704-017-2057-1

Stull, R.B., 1988. An introduction to boundary layer meteorology. An Introd. to Bound. layer Meteorol. https://doi.org/10.1007/978-94-009-3027-8

Su, T., Li, Z., Li, C., Li, J., Han, W., Shen, C., Tan, W., Wei, J., Guo, J., 2020. The significant impact of aerosol vertical structure on lower atmosphere stability and its critical role in aerosol-planetary boundary layer (PBL) interactions. Atmos. Chem. Phys. 20, 3713–3724. https://doi.org/10.5194/acp-20-3713-2020

Subba, T., Pathak, B., Gogoi, M.M., Ajay, P., Dahutia, P., Chakraborty, A., Bhuyan, P.K., 2023.

Observations on the decadal variability of aerosol in eastern Himalayan foothills: Evidence of an anthropologically induced positive shift. Atmos. Environ. 299, 119638. https://doi.org/10.1016/j.atmosenv.2023.119638

Sukoriansky, S., Galperin, B., Perov, V., 2005. Application of a new spectral theory of stably stratified turbulence to the atmospheric boundary layer over sea ice. Boundary-Layer Meteorol. 117, 231–257. https://doi.org/10.1007/s10546-004-6848-4

Sulla-Menashe, D., Friedl, M.A., 2018. User Guide to Collection 6 MODIS Land Cover (MCD12Q1 and MCD12C1) Product 1–18. https://doi.org/10.5067/MODIS/MCD12Q1

Takemura, T., Uchida, T., 2011. Global Climate Modeling of Regional Changes in Cloud, Precipitation, and Radiation Budget Due to the Aerosol Semi-Direct Effect of Black Carbon. Sola 7, 181–184. https://doi.org/10.2151/sola.2011-046

Talukdar, S., Venkat Ratnam, M., Ravikiran, V., Chakraborty, R., 2019. Influence of Black Carbon Aerosol on the Atmospheric Instability. J. Geophys. Res. Atmos. 124, 5539–5554. https://doi.org/10.1029/2018JD029611

Tewari, M., Chen, F., Wang, W., Dudhia, J., LeMone, M.A., Mitchell, K., Ek., M., Gayno, G., Weigel, J., Cuenca, R.H., 2004. Implementation and verification of the unified NOAH land surface model in the WRF model. 20th Conf. Weather Anal. Forecast. Conf. Numer. Weather Predict. 11–15. https://doi.org/10.1007/s11269-013-0452-7

Tiwari, S., Kumar, R., Tunved, P., Singh, S., Panicker, A.S., 2016. Significant cooling effect on the surface due to soot particles over Brahmaputra River Valley region, India: An impact on regional climate. Sci. Total Environ. 562, 504–516. https://doi.org/10.1016/j.scitotenv.2016.03.157

Tripathi, S.N., Dey, S., Tare, V., Satheesh, S.K., 2005. Aerosol black carbon radiative forcing at an industrial city in northern India. Geophys. Res. Lett. 32, 1–4. https://doi.org/10.1029/2005GL022515

Twomey, S., 1977. The influence of pollution on the shortwave albedo of clouds. J. Atmos. Sci. 1149–1152117. https://doi.org/doi.org/10.1175/1520-0469(1977)034<1149:TIOPOT>2.0.CO;2

Vinay Kumar, P., Venkateswara Naidu, C., 2020. Is Pre-monsoon Rainfall Activity Over India Increasing in the Recent Era of Global Warming? Pure Appl. Geophys. 177, 4423–4442. https://doi.org/10.1007/s00024-020-02471-7

Wallace, J.M., Hobbs, P. V., 2006. Atmospheric Science An Introductory Survey, Second. ed. Elsevier Inc.

Wang, C., 2013. Impact of anthropogenic absorbing aerosols on clouds and precipitation: A review of recent progresses. Atmos. Res. 122, 237–249. https://doi.org/10.1016/j.atmosres.2012.11.005

Wang, K., Hattori, S., Lin, M., Ishino, S., Alexander, B., Kamezaki, K., Yoshida, N., Kang, S., 2021. Isotopic constraints on atmospheric sulfate formation pathways in the Mt. Everest region, southern Tibetan Plateau. Atmos. Chem. Phys. 21, 8357–8376. https://doi.org/10.5194/acp-21-8357-2021

Wang, K., Zhang, Y., Yahya, K., Wu, S.Y., Grell, G., 2015. Implementation and initial application of new chemistry-aerosol options in WRF/Chem for simulating secondary organic aerosols and aerosol indirect effects for regional air quality. Atmos. Environ. 115, 716–732. https://doi.org/10.1016/j.atmosenv.2014.12.007

Wang, T., Li, S., Shen, Y., Deng, J., Xie, M., 2010. Investigations on direct and indirect effect of nitrate on temperature and precipitation in China using a regional climate chemistry modeling system. J. Geophys. Res. Atmos. 115, 1–13. https://doi.org/10.1029/2009JD013264

Wang, Y., Vogel, J.M., Lin, Y., Pan, B., Hu, J., Liu, Y., Dong, X., Jiang, J.H., Yung, Y.L., Zhang, R., 2018. Aerosol microphysical and radiative effects on continental cloud ensembles. Adv. Atmos. Sci. 35, 234–247. https://doi.org/10.1007/s00376-017-7091-5

Wang, Y., Zheng, X., Dong, X., Xi, B., Wu, P., Logan, T., Yung, Y.L., 2020. Impacts of long-range transport of aerosols on marine-boundary-layer clouds in the eastern North Atlantic. Atmos. Chem. Phys. 20, 14741–14755. https://doi.org/10.5194/acp-20-14741-2020

Wang, Z., Huang, X., Ding, A., 2018. Dome effect of black carbon and its key influencing factors: A one-dimensional modelling study. Atmos. Chem. Phys. 18, 2821–2834. https://doi.org/10.5194/acp-18-2821-2018

Wang, Z., Xue, L., Liu, J., Ding, K., Lou, S., Ding, A., Wang, J., Huang, X., 2022. Roles of Atmospheric Aerosols in Extreme Meteorological Events: a Systematic Review. Curr. Pollut. Reports 8, 177–188. https://doi.org/10.1007/s40726-022-00216-9

Warner, T.W., 2011. Numerical Weather and Climate Prediction.

Wiedinmyer, C., Akagi, S.K., Yokelson, R.J., Emmons, L.K., 2010. The Fire INventory from NCAR (FINN) – a high resolution global model to estimate the emissions from open burning. Geosci. Model Dev. Discuss. 3, 2439–2476. https://doi.org/10.5194/gmdd-3-2439-2010

Xie, B., Fung, J.C.H., Chan, A., Lau, A., 2012. Evaluation of nonlocal and local planetary boundary layer schemes in the WRF model. J. Geophys. Res. Atmos. 117, 1–26. https://doi.org/10.1029/2011JD017080

Yang, Q., Gustafson, W.I., Fast, J.D., Wang, H., Easter, R.C., Morrison, H., Lee, Y.N., Chapman, E.G., Spak, S.N., Mena-Carrasco, M.A., 2011. Assessing regional scale predictions of aerosols, marine stratocumulus, and their interactions during VOCALS-REx using WRF-Chem. Atmos. Chem. Phys. 11, 11951–11975. https://doi.org/10.5194/acp-11-11951-2011

Yang, Y., Smith, S., Wang, H., Mills, C., Rasch, P., 2019. Variability, timescales, and non-linearity in climate responses to black carbon emissions. Atmos. Chem. Phys. Discuss. 1–44. https://doi.org/10.5194/acp-2018-904

Yoon, J.H., Rasch, P.J., Wang, H., Vinoj, V., Ganguly, D., 2016. The role of carbonaceous aerosols on short-term variations of precipitation over North Africa. Atmos. Sci. Lett. 17, 407–414. https://doi.org/10.1002/asl.672

Yu, F., Ma, X., Luo, G., 2013. Anthropogenic contribution to cloud condensation nuclei and the first aerosol indirect climate effect. Environ. Res. Lett. 8. https://doi.org/10.1088/1748-9326/8/2/024029

Yu, H., Liu, S.C., Dickinson, R.E., 2002. Radiative effects of aerosols on the evolution of the atmospheric boundary layer. J. Geophys. Res. Atmos. 107. https://doi.org/10.1029/2001jd000754

Zanis, P., 2009. A study on the direct effect of anthropogenic aerosols on near surface air temperature over Southeastern Europe during summer 2000 based on regional climate modeling. Ann. Geophys. 27, 3977–3988. https://doi.org/10.5194/angeo-27-3977-2009

Zaveri, R.A., Easter, R.C., Fast, J.D., Peters, L.K., 2008. Model for Simulating Aerosol Interactions and Chemistry (MOSAIC). J. Geophys. Res. Atmos. 113, 1–29. https://doi.org/10.1029/2007JD008782

Zaveri, R.A., Easter, R.C., Singh, B., Wang, H., Lu, Z., Tilmes, S., Emmons, L.K., Vitt, F., Zhang, R., Liu, X., Ghan, S.J., Rasch, P.J., 2021. Development and Evaluation of Chemistry-Aerosol-Climate Model CAM5-Chem-MAM7-MOSAIC: Global Atmospheric Distribution and Radiative Effects of Nitrate Aerosol. J. Adv. Model. Earth Syst. 13, 1–24. https://doi.org/10.1029/2020MS002346

Zhang, Y., Wen, X.Y., Jang, C.J., 2010. Simulating chemistry-aerosol-cloud-radiation-climate feedbacks over the continental U.S. using the online-coupled Weather Research Forecasting Model with chemistry (WRF/Chem). Atmos. Environ. 44, 3568–3582. https://doi.org/10.1016/j.atmosenv.2010.05.056

Zhao, C., Liu, X., Leung, L.R., Hagos, S., 2011. Radiative impact of mineral dust on monsoon precipitation variability over West Africa. Atmos. Chem. Phys. 11, 1879–1893.

https://doi.org/10.5194/acp-11-1879-2011

Zhao, C., Liu, X., Leung, L.R., Johnson, B., McFarlane, S.A., Gustafson, W.I., Fast, J.D., Easter, R., 2010. The spatial distribution of mineral dust and its shortwave radiative forcing over North Africa: Modeling sensitivities to dust emissions and aerosol size treatments. Atmos. Chem. Phys. 10, 8821–8838. https://doi.org/10.5194/acp-10-8821-2010

List of Publications

Refereed International journals

1. Barman, N., Gokhale, S., 2023. Transported aerosols regulate the pre-monsoon rainfall over north-east India : a WRF-Chem modelling study. Atmos. Chem. Phys. 6197–6215. https://doi.org/doi.org/10.5194/acp-23-6197-2023 [IF:7.197]

2. Barman, N., Gokhale, S., 2022. Aerosol influence on the pre-monsoon rainfall mechanisms over North-East India: A WRF-Chem study. Atmos. Res. 268, 106002. https://doi.org/10.1016/j.atmosres.2021.106002 [IF:5.965]

3. Barman, N., Gokhale, S., 2019. Urban black carbon - source apportionment, emissions and long-range transport over the Brahmaputra River Valley. Sci. Total Environ. 693, 1–14. https://doi.org/10.1016/j.scitotenv.2019.07.383 [IF:10.754]

4. Barman, N., Gokhale, S., 2023. Evaluation of planetary boundary layer parametrization schemes over north-east India [under review Dynamics of Oceans and Atmospheres]

5. Barman, N., Gokhale, S., 2023. The role of planetary boundary layer parametrizations on aerosol transport, its transformation and radiative properties [under review JGR Atmospheres]

Conference:

1. Barman, N., Gokhale, S., 2022. Transported black carbon dominates radiative effects over North East India during pre-monsoon season. *National Conference on Climate Change: Science and Technology Innovation, Tezpur University*, December 15-16.